

**MINERAL BINDING PEPTIDES BY PHAGE  
DISPLAY: EXPERIMENTAL AND  
BIOINFORMATICS STUDIES**

VEERANJANEYULU THOTA

A thesis submitted in partial fulfilment of the requirements of Nottingham  
Trent University for the degree of Doctor of Philosophy

January 2019

This work is the intellectual property of the author. You may copy up to 5% of this work for private study, or personal, non-commercial research. Any re-use of the information contained within this document should be fully referenced, quoting the author, title, university, degree level and pagination. Queries or requests for any other use, or if a more substantial copy is required, should be directed in the first instance to the owner of the Intellectual Property Rights.

## Abstract

Phage display has attracted a great deal of interest in the identification of peptides specific to nanomaterials revealing distinctive binding behaviour. Though significant progress has been made in selecting and screening of biomolecule binding peptides, the accuracy of molecular recognition for inorganic materials is still challenging due to the limitations of phage display libraries and biopanning process. The study presented in this thesis is aimed at isolating mineral binding peptides by phage display and verifying them experimentally and/ or bioinformatically; exploring the role of electrostatic/ non-electrostatic interactions in the aqueous phase and the factors responsible for the adsorption or desorption of peptide or phage from the mineral surface.

Firstly, silica binding peptides LPVRLDW, NDLMNRA, GQSEKHL and GASESYL have been identified using the phage display technique by varying experimental conditions including pH, detergent, washing and elution buffers to remove unique 7-mer peptide binding phages from amorphous hydrophilic silica nanoparticles via disruption of the molecular interactions between the phage attached peptides and the nanoparticles. A repanning method reported here, has experimentally reproduced the majority of the initially discovered silica binders; alongside identifying/ recovering additional peptide sequences HYIDFRW, KIAVIST and YSLKQYQ that may have been overlooked in the routine approach to biopanning. Secondly, an alternative three step elution method reported here, has eluted and recovered most target silica binders including ADIRHIK in the early panning rounds and removed the phage clones that are bound to silica by hydrophobic, hydrogen bonding and electrostatic attractions or repulsions; as opposed to one specific buffer being used for all panning rounds including elution steps in traditional biopanning experiments. Also, the phage clones that resist detection to single elution step have been eluted in the other successive elution steps, thereby recovering and improving the elution procedure for silica surfaces. In addition, these three different elution buffers have eluted phage clones that are interaction or charge specific subject to change in the elution buffer pH condition. The experimental results demonstrate that this sequential three step elution process was able to isolate tightly bound target silica binders in one or two biopanning rounds than the more typical four to five; thereby reducing biopanning rounds, cost and effort. Moreover, the bioinformatic analysis to cross check the authenticity/ quality of target binders has been reported.

Furthermore, selected silica binding peptides isolated from phage display experiments were synthesized by a solid phase peptide synthesis approach and peptide-silica interactions explored *in vitro*, using quantitative and qualitative techniques. The fluorometric analysis of these peptides revealed that the peptide adsorption to silica surfaces would have more than one type of interactions (i.e. electrostatic/ hydrophobic/ H-bonding and Van der Waals) and could be influenced by the experimental conditions. More significantly, an increase in binding activity to negatively charged silica nanoparticles was noticed for the peptides (HYIDFRW, KIAVIST and YSLKQYQ) modified with an amide (NH<sub>2</sub>) group as opposed to a carboxyl group at the C-terminal end; driving an increase in overall charge or pI of the peptides. Insights from the studies presented may provide valuable information for designing and engineering of silica directed constructs for a range of biomedical and nanotechnological applications.

## **Dedication**

I dedicate this thesis to my family, Anjamma Thota, Narayanarao Burri, Srinivasarao Thota, Anjaneya prasad Thota, Adilakshmi Thota, Bijol Bakhai, Bharat Kumar Bakhai, Pratima Bakhai and friends for their selfless support, affection and encouragement at every moment.

Also, it is dedicated in the memory of my father, Venkateshwarlu Thota whose blessing and teachings have always guided me. This is in your ever-loving memory.

*“We should not give up and we should not allow the problem to defeat us”*

- Dr. A.P.J. Abdul Kalam

## **Acknowledgements**

Firstly, I take this occasion to convey my deep thanks and profound regards to my supervisor Professor Carole C. Perry for giving me this research opportunity, her excellent support, invaluable guidance, and continuous inspiration throughout my stay at NTU for almost 6 years. The blessings, help and constant guidance given by her time to time shall carry me a long way in the journey of life. Also, I would like to express my sincere gratitude to my assistant supervisor Dr. David J Belton for his valuable direction and useful suggestions over the years. I am very grateful to my collaborators from US Air Force Office of Scientific Research (AFOSR) for funding this PhD research project FA9550-13-1-0040 and for the valuable advice from Dr. Rajesh R. Naik and Dr. Joseph M. Slocik during our annual meetings. I want to thank Angie Belchers group (Massachusetts Institute of Technology, USA) for checking the peptide sequences against their computationally designed phage library databases.

Special thanks to those who have contributed somehow or other to this project, Dr. Valeria Puddu for providing fully characterised 82 nm sized silica nanoparticles, Dr. Graham Hickman for his assistance specifically for analysing the peptides by mass spectrometry, Mr. Daniel Oliver for his support in carrying out TEM analysis and Dr. Anna Solá Rabadá for her help in writing the silica part together for review paper. I would like to extend my special thanks to Dr. Marion Limo, Mr. Zayd Westcott and Dr. Estefania Boix for their support in sharing review paper work, never-ending meetings and all the fun.

Also, I take this opportunity to thank all my and other lab mates Dr. Mithun Parambath, Dr. Matthew Nicklin, Mrs Robyn Plowright, Miss Monika Michaelis, Dr. Igor Efimov, Dr Victor Volkov, Miss Aneeqa Fayyaz, Miss Sophie Prentice, Miss Elisa Tonoli, Mr. Joseph Chemmarappally and Miss Divya Nagarajan for their friendliness, cooperation, brainstorming discussions and information provided by them in their respective fields. I am very happy for their help and fun during my time.

Personally, I would like extent my warm and heartiest regards to my parents, siblings and close friends for their never-ending love, blessings and prayers in all my life. I am very grateful and appreciate Bijol Bakhai for her indefinite love, endless support, continuous encouragement and for staying and sharing all fun with me during happy and difficult times of life. I also extend my humble regards to Naresh Sampara who has helped me immensely.

# Table of contents

<b>Abstract</b> .....	<b>iii</b>
<b>Dedication</b> .....	<b>iv</b>
<b>Acknowledgements</b> .....	<b>v</b>
<b>Table of contents</b> .....	<b>vi</b>
<b>Glossary</b> .....	<b>x</b>
<b>List of Figures</b> .....	<b>xiii</b>
<b>List of Tables</b> .....	<b>xx</b>
<b>Chapter 1 : Introduction</b> .....	<b>25</b>
1.1 Overview of Combinatorial Phage Display Technologies .....	26
1.1.1 Phage display and biopanning process .....	27
1.1.2 M13 Phage structure and life cycle .....	30
1.1.3 Phage display libraries.....	36
1.2 Overview of Silica (SiO <sub>2</sub> ) .....	39
1.2.1 Silica synthesis and chemistry .....	39
1.2.2 Silica biomolecule interactions and their applications .....	43
1.3 Combinatorial Display Process on Nanomaterial Surfaces .....	48
1.4 Applications of Inorganic Material Binding Peptides .....	49
1.5 Motivation of Project and Objectives .....	56
<b>Chapter 2 : Instrumentation and Experimental Section</b> .....	<b>58</b>
2.1 Materials and Methods.....	59
2.1.1 Materials.....	59
2.1.1.1 Heptapeptide phage display peptide library (Ph.D. <sup>TM</sup> -7).....	59
2.1.1.2 <i>E. coli</i> host strain (K12 ER2738) .....	59
2.1.1.3 Silica nanoparticles .....	59
2.1.1.4 Phage display reagents .....	60
2.1.1.4.1 Washing buffers .....	60
2.1.1.4.2 Elution buffers.....	61
2.1.1.4.3 Culture media .....	61
2.1.1.4.4 Other stock solutions .....	62
2.1.1.4.5 Peptide synthesis reagents.....	62
2.1.1.4.6 Peptide characterization reagents .....	63
2.1.1.4.7 Reagents used for binding studies .....	63
2.1.2 Methods .....	64

2.1.2.1	Phage Display Process.....	64
2.1.2.1.1	Biopanning technique and protocol.....	64
2.1.2.1.2	Phage titering and blue-white screening.....	71
2.1.2.1.3	Plaque amplification.....	73
2.1.2.1.4	Phage DNA purification (Modified procedure).....	74
2.1.2.1.5	Purity testing of phage DNA using a NanoDrop spectrophotometer.....	74
2.1.2.1.6	DNA sequencing and analysis.....	75
2.1.2.2	Bioinformatics.....	77
2.1.2.3	Optimised Biopanning Method and Elution Strategies.....	80
2.1.2.4	Repanning Experiments.....	83
2.1.2.5	Selection of Single Phage Clones for Binding Studies.....	84
2.1.2.6	Synthesis and Characterization of Silica Binding Peptides and Nanoparticles.....	85
2.1.2.6.1	Solid phase peptide synthesis (SPPS).....	87
2.1.2.6.2	High performance liquid chromatography (HPLC).....	90
2.1.2.6.3	Matrix-assisted laser desorption ionization time-of-flight (MALDI-TOF) mass spectrometry.....	92
2.1.2.7	Silica-Peptide Binding studies.....	94
2.1.2.7.1	Fluorescence spectroscopy.....	94
2.1.2.7.2	Raman spectroscopy.....	97
2.1.2.7.3	Transmission electron microscopy (TEM).....	98
<b>Chapter 3 : Selection and Screening of Silica Binding Peptides by Phage Display Process...</b>		<b>101</b>
3.1	Introduction.....	101
3.2	Materials and Methods.....	105
3.2.1	Materials.....	105
3.2.2	Methods.....	105
3.2.2.1	Phage display protocol.....	105
3.2.2.2	Relative binding affinity method.....	105
3.2.2.3	Bioinformatics searching.....	105
3.2.2.4	Silica-peptide interaction studies.....	105
3.3	Results and Discussion.....	106
3.3.1	Silica binders identified from initial (traditional) biopanning.....	106
3.3.2	Repanning to check the reproducibility of silica binders identified in 3.3.1.....	111
3.3.3	Relative binding affinity experiment to evaluate phage binding to silica.....	114
3.3.4	Prediction and bioinformatics analysis of silica binders: Comparison studies	116

3.3.5	Assessment of silica-peptide interactions .....	125
3.3.5.1	Fluorometric quantification of peptide adsorbed to silica .....	125
3.3.5.2	Raman spectroscopy for probing peptide-silica interactions .....	130
3.4	Conclusion.....	133
<b>Chapter 4 : Isolation of Silica Binders by Optimised Biopanning Method and Bioinformatics</b>		<b>136</b>
.....		
4.1	Introduction .....	136
4.2	Materials and Methods.....	142
4.2.1	Materials.....	142
4.2.2	Methods.....	142
4.2.2.1	Phage display protocol .....	142
4.2.2.2	Relative binding affinity method.....	142
4.2.2.3	Bioinformatics searching .....	142
4.3	Results and Discussion.....	143
4.3.1	Silica binders isolated from optimised biopanning method.....	144
4.3.2	Experiment to check the optimised biopanning process 4.3.1 .....	152
4.3.3	Relative binding affinity assay to assess phage binding to silica.....	155
4.3.4	Bioinformatics analysis to check authenticity of target binders .....	156
4.4	Conclusion.....	164
<b>Chapter 5 : Interaction studies of silica binding peptides / phages with silica nanoparticles</b>		<b>167</b>
.....		
5.1	Introduction .....	167
5.2	Materials and Methods.....	171
5.2.1	Materials.....	171
5.2.2	Methods.....	171
5.2.2.1	Fluorescamine protein quantification assay.....	171
5.2.2.2	TEM to visualise the binding of phage peptides to silica .....	171
5.3	Results and Discussion.....	172
5.3.1	Selection of SiBPs for experimental binding studies .....	172
5.3.2	Fluorometric quantification of peptide adsorbed to silica by fluorescamine .....	176
5.3.2.1	Effect of C-terminal group on binding to silica .....	180
5.3.3	TEM to probe silica- phage peptide interactions .....	184
5.4	Conclusions .....	189
<b>Chapter 6 : Overall conclusions and future work .....</b>		<b>192</b>
.....		
6.1	Summary of the thesis.....	192
6.2	Future directions .....	197
<b>Appendices .....</b>		<b>200</b>



<b>Publications .....</b>	<b>209</b>
<b>References .....</b>	<b>212</b>

## Glossary

Ag	Silver
Al <sub>2</sub> O <sub>3</sub>	Aluminum oxide
APTES	(3-Aminopropyl) triethoxysilane
Au	Gold
BDB	Biopanning data base
Boc	t-butyloxycarbonyl
°C	Celsius (temperature)
CdS	Cadmium sulfide
Cu <sub>2</sub> O	Cuprous oxide
DCC	N,N-dicyclohexyl-carbodiimide
ddNTPs	Dideoxy nucleotide triphosphates
DIEA	N,N-diisopropylethylamine
DLS	Dynamic light scattering
DMF	N, N-dimethylformamide
dNTPs	Deoxynucleotide triphosphate
DNA	Deoxyribo Nucleic Acid
DODT	3,6-Dioxa-1,8-octanedithiol
EDTA	Ethylenediamine tetra acetic acid
<i>E. coli</i>	<i>Escherichia Coli</i>
EM Stain 336	Uranyl Acetate Alternative
Fe <sub>2</sub> O <sub>3</sub>	Iron oxide
Fmoc	9-fluorenylmethoxycarbonyl
GaAs	Gallium arsenic
GaN	Gallium nitride
HPLC	High-performance liquid chromatography
IOBPs	Inorganic binding peptides
IPTG	Isopropyl β-D-1 thiogalactopyranoside

IrO <sub>2</sub>	Iridium oxide
MALDI-TOF	Matrix-assisted laser desorption ionization time-of-flight
MgCl <sub>2</sub>	Magnesium chloride
MTES	Methyltriethoxysilane
mg	Milligram
NaCl	Sodium chloride
NaI	Sodium Iodide
NaN <sub>3</sub>	Sodium azide
NH <sub>2</sub>	Amide
NMP	N-methyl-2-pyrrolidone
NPs	Nanoparticles
PBS	Phosphate buffer saline
PEG	Polyethylene glycol
PEG-8000	Polyethylene glycol
Ph.D.7	Phage Display 7 mer (heptapeptides) library
Ph.D.12	Phage Display 12 mer (dodecapeptide) library
Pt	Platinum
R1A	Round 1 amplified eluate
RNA	Ribo Nucleic Acid
SBPs	Solid binding peptides
Si(OH) <sub>4</sub>	Orthosilicic acid
SiBPs	Silica binding peptides
SiO <sub>2</sub>	Silicon dioxide
Si-OH	Silanols
Si-O-Si	Siloxane bonds
SPPS	Solid phase peptide synthesis
TBS	Tris buffer saline
TBST	Tris buffer saline Tween 20

TEA	Triethylamine
TEM	Transmission electron microscopy
TEOS	Tetraethyl orthosilicate
TFA	Trifluoroacetic acid
TiO <sub>2</sub>	Titanium oxide
TIS	Thianisole
X-gal	5-Bromo-4-chloro-3-indolyl β D galactopyranoside
ZnO	Zinc oxide
ZnS	Zinc sulfide
μl	Microliter

## List of Figures

<b>Figure 1.1. Typical phage/ cell surface display and biopanning process used for selecting polypeptide sequences that have binding affinity to given inorganic substrates. Image reprinted<sup>66</sup>.</b> .....	29
Figure 1.2: Diagrammatic representation of M13 bacteriophage genome and the location of genes. Image adapted from ref <sup>84</sup> .....	31
Figure 1.3: Schematic representation of the structure of filamentous phage (wild versus engineered) and their coat proteins (right). Image adapted <sup>84</sup> .....	33
<b>Figure 1.4. Schematic representation of silica formation pathways from Si(OH)<sub>4</sub> or orthosilicic acid through to dimers, oligomers, particles and sols. Also, biomolecules are shown to act at any stage of the silica formation. Image adapted<sup>94</sup>.</b> .....	40
<b>Figure 1.5. Silica surface consisting of different types of silanol groups and their chemistry. Image reprinted<sup>119</sup>.</b> .....	42
Figure 1.6. Proposed interaction mechanisms involved at the silica-biomolecule interface A) Mechanism proposed for alkoxysilane catalytic hydrolysis by silicatein active sites (serine and histidine) reprinted with permission <sup>123</sup> . B) competitive protein exchange occurring upon the fluoro-silica during cell culture in serum supplemented medium reprinted with permission <sup>122</sup> . C) type of interactions occurring at the silica-peptide interface of phage displayed peptides reprinted with permission <sup>4,10</sup> .....	44
<b>Figure 1.7: Schematic representation of Silica-biomolecule interactions and their applications. Figure adapted from<sup>132</sup>.</b> .....	45
<b>Figure 1.8: Specific applications of silica-biomolecule attachment reported:</b> (A) mesoporous silica nanoparticles acting as delivery vehicles carrying potential drugs, peptides and proteins reprinted with permission from <sup>133</sup> . (B) controlled silica biomineralization process using peptide equipped TMV (tobacco mosaic virus) as templates reprinted with permission from <sup>134</sup> .....	46
<b>Figure 1.9: Specific applications of silica-biomolecule attachment reported:</b> (A) Silica mineralisation induced by DNA liquid crystals reprinted with permission from <sup>135</sup> and (B) enzyme immobilization in silica nanospheres via attaching to cobalt coated resin by affinity binding where agarose beads (○), Co <sup>2+</sup> coated agarose beads (◐), his-tagged peptide (—), enzyme (■) and silica nanospheres (■) reprinted with permission from <sup>136</sup> .....	47
Figure 1.10: Schematic representation of different types of combinatorial display approaches such as phage display, bacterial surface display, yeast surface display, ribosome display, mRNA or cDNA display and rational design used for selecting and screening of inorganic material <sup>12</sup> .....	49
<b>Figure 1.11. Schematic representation of solid binding peptides as molecular linkers to link solid materials like nanoparticles and to a wide range of biomolecules such as antigens, antibodies, peptides, proteins, enzymes and functional peptide motifs. Image reproduced<sup>11</sup>.</b> .....	50

Figure 1.12: Schematic representation of inorganic material binding peptides and applications.....	51
<b>Figure 2.1. Typical working principle of biopanning affinity process, selection and screening of material binding peptides using peptide phage libraries.</b> Image reproduced with permission from Springer 2006 <sup>57</sup> .....	65
Figure 2.2. Diagrammatic representation of biopanning process and steps involved. ....	68
<b>Figure 2.3. Illustration depicting the normal dNTPs and fluorescently tagged ddNTPs and their mechanism in DNA synthesis.</b> Panel A shows the structures of normal deoxy nucleotide with hydroxyl (OH) group and dideoxy nucleotide without hydroxyl group (H) at 3' carbon sugar ring. Panel B show how the extension of DNA strand synthesis happens upon addition of deoxy nucleotides (dATP, dCTP, dGTP, and dTTP) while the growing chain terminates with the attachment of dideoxy nucleotides (ddATP, ddCTP, ddGTP, and ddTTP) to the 3' end. Image adapted from Applied Biosystems manual <sup>210</sup> . ....	75
<b>Figure 2.4. Schematic representation of cycle of events that occur in cycle sequencing technology.</b> A) Process of denaturation, annealing, extension and termination forming DNA fragments in thermal cycler B) Electrophoresis separation of fluorescently tagged DNA fragments based on molecular weight. Image adapted from Applied Biosystems manual <sup>210</sup> .....	76
<b>Figure 2.5. An example of the sequencing data obtained from Eurofins (top) and how the peptide TVNFKLY has been interpreted (bottom) and identified.</b> .....	77
<b>Figure 2.6. A screen shot showing the result obtained for peptide GQSEKHL using MimoDB search, Blast, Scan and TUPredict tools.</b> .....	78
<b>Figure 2.7. Diagrammatic representation of optimised biopanning method by exploring elution strategies.</b> A separate second batch (Lot: 0221501) of M13 Ph.D.-7 phage display library (#E8100S) has been used for performing the optimised biopanning method. The optimised biopanning process presents 2 elution approaches (each differ from the traditional biopanning method of Chapter 3) used for Chapter 4: Approach 1 differs from the traditional biopanning method as each mentioned buffers (Gly-HCl, pH-2.2; MgCl <sub>2</sub> , pH-6.1; TEA, pH-11) are used consecutively one after other for each screening (biopanning) round, as appose to one specific buffer being used for all rounds in traditional biopanning and repanning experiments (chapter 3); Approach 2 only used the same Glycine-HCl elution buffer but at varying pH's (i.e. Gly-HCl of pH-2.2; pH-7; pH-11). However, for verifying this optimised elution based biopanning experiments, further panning was done by taking the mixture of amplified library attained by mixing together the already amplified phage libraries that were obtained from the biopanning round 1 of previous separate experiments (Table 2.2) via using Lot 1(Lot: 0211212) of Ph.D.-7 phage display library. ....	80
<b>Figure 2.8. Schematic representation of repanning method.</b> The amplified phages obtained from different biopanning experiments where a small number of sequences screened were mixed together to verify the reproducibility of previously identified peptide sequences.....	84
<b>Figure 2.9. General principle and scheme of solid phase peptide synthesis via Fmoc chemistry.</b> First, the N $\alpha$ - protected C-terminal amino acid is anchored to the	

insoluble solid supported resin with the help of linker. Subsequently, the desired peptide will be assembled by elongating the length of the peptide chain by a cycle of repetitive chemical steps involving 1) deblocking of the temporary Fmoc protecting amino acid group 2) activation of carboxy group of new incoming amino acid 3) coupling. Once the chosen peptide length is achieved, the unwanted resin and side chain protecting groups will be removed by performing final deprotection and cleavage steps. Later, these cleaved and deprotected free peptides will be washed and purified. Image reproduced from Sigma Aldrich website..... 88

**Figure 2.10. Illustration depicting the instrumentation principle and working mechanism of HPLC..... 90**

**Figure 2.11. Illustration describing the principle and mechanism of MALDI-TOF mass spectrometry..... 92**

**Figure 2.12. Illustration depicting the working principle of absorption and fluorescence spectroscopies and fluorescamine binding mechanism to proteins.** a) Jablonski diagram depicting the mechanism of absorption and fluorescence emissions including their electronic and vibrational transitions of a molecule and the transition between them <sup>267</sup>. b) Reaction mechanism of fluorescamine and primary amine groups of terminal amino acids <sup>268</sup>..... 94

**Figure 2.13. Schematic representation of fluorescamine assay protocol used for preparing samples. .... 96**

**Figure 2.14. Working principle of Raman spectroscopy.** Raman scattering is based on the frequency of incident and scattered radiations upon laser hitting the sample forcing the sample to vibrate forming Rayleigh, anti-stokes and stokes Raman spectrum. Image adapted from HORIBA Scientific webinar <sup>278</sup>..... 97

**Figure 2.15. Diagrammatic representation of TEM working principle and mechanism** a) The schematic outline of a TEM b) A ray diagram from the diffraction mechanism in TEM. Image adapted from <sup>279,282</sup>. .... 99

**Figure 3.1. Comparison of functional amino acid groups distributed specific to elution buffer.** All the phage clones identified from panning experiments 1-4 (Glycine-HCl, pH-2.2), 5 (MgCl<sub>2</sub>, pH-6.1) and 6 (Triethylamine, pH-11) are considered while plotting the pie diagrams.....110

**Figure 3.2. Binding ratio (bound/input) of each of the 15 different phage clones to silica nanoparticles.** The relative binding affinity of the phage clones isolated from both initial and repanning experiments was determined by titer assay at pH-7.5. The asterisk (\*) indicates the phage clones displayed most frequently (abundantly observed) and repeated in the screening rounds 3-5. The sequences QQTNWSL, QLAVAPS and VGSYLG I were identified in more than one experiment but not repeated so often. The M13KE (wild type) phage with no random peptides displayed on pIII coat protein was chosen as a main control. In addition, the phage clones GTGSQAS, ETALIAA and SQTFTSD were randomly picked as they found only once in either of the initial and repanning experiments. The assay was repeated twice for each phage clone and the explained phage amounts were arithmetically averaged. The errors bars indicate the standard error obtained from the two separate experimental repeats.....115

**Figure 3.3. Multiple sequence alignment of silica binders.** All the silica binding peptides used for generating this figure were isolated from three sets of biopanning experiments. A total of 77 dissimilar sequences were chosen and analysed. An identified consensus peptide sequence (VSTPLLA) from the multiple sequence alignment was also highlighted and shown. The sequence alignment was generated by using the freely available MSA viewer (<https://toolkit.tuebingen.mpg.de/#/tools/alnviz>) from the Max Planck Institute website. Label indicate the position and number of the peptide sequences. The small logo (figure) that is present on top of the 'label' indicate the number of times the amino acids have appeared in that specific position. The larger the size of the amino acid the higher the times the amino acid have appeared in that specific position of the peptide sequences. For example, the amino acid V (valine) was the most frequently observed residue (14 times), followed by S (serine, 12 times) as second, Q (glutamine, 8 times) and so on in the first position of all the 77 silica binders. Thus, V (valine) has appeared larger in the first column followed by second bigger S (serine) and so on.....119

**Figure 3.4. Adsorption behaviour of peptides on the surface of hydrophilic silica nanoparticles at pH-7.5.** The y-axis represents the amount of peptide adsorbed to silica in mM, while the x-axis shows the initial peptide concentration or peptide added in mM. The theoretical 100% peptide adsorption is shown in black dotted line. The error bars represent the standard deviation error calculated as a result of the assay being repeated in triplicate. Based on the above data, the binding order of the peptides was ranked as KIAVIST>LPVRLDW> NDLMNRA> GQSEKHL and GASESYL.....127

**Figure 3.5. Raman spectrum of amino acids identified in LPVRLDW peptide.** A strong signal has been noticed for Tryptophan (W) at 756 cm<sup>-1</sup> and 1010 cm<sup>-1</sup>.....131

**Figure 3.6. Raman spectrum showing the LPVRLDW peptide alone, silica alone and when peptide adsorbed to silica particularly for the aromatic amino acid tryptophan.** Asterick \* represents the silica bands found at around 440, 732 and 1390 cm<sup>-1</sup>. A) Symmetric benzene/pyrrole in-phase breathing mode of Trp at 756 cm<sup>-1</sup> B) Indole ring vibration with NH bending mode of Trp 880 cm<sup>-1</sup> C) Symmetric benzene/pyrrole out-of-phase breathing mode of Trp at 1012 cm<sup>-1</sup> D) Pyrrole C2-C3 stretching mode of Trp found at 1551 cm<sup>-1</sup>. .....132

**Figure 3.7. Raman spectra obtained from different samples of peptide (LPVRLDW) and silica.** Five different samples such as peptide alone, silica alone, peptide adsorbed to silica (solid powered and dried pellet from solution) and the dried peptide-silica pellet obtained from the fluorescamine assay showing the variation and shifts in the Raman spectra. Asterick \* represents the silica bands found at around 440, 732 and 1390 cm<sup>-1</sup>. .....132

**Figure 4.1. Schematic representation of different types of elution methods.** a) Chemical elution: The non-specific or weakly bound phage are first washed away, and the remaining strongly bound phage are eluted by low or high pH or high salt buffer b) Physical elution: The strongly bound phage is eluted either by using sonication or ultrasound or with a combination a) and b). c) Enzymatic elution: enzymes (such as trypsin or protease) are used to cleave phage bodies at specific sites (capsid or scFv).



Only the immobilized phage bound to the bait (target material or antigen) will be eluted. Any non-specific phages present will be marginalized during several panning rounds. d) Competitive elution: high concentration target antigen is introduced to elute bound phage, with the material binding phage still bound to surface.....137

**Figure 4.2. Schematic representation of peptide/ phage adsorption or desorption onto silica nanoparticle surface and intrinsic bias during biopanning due to pH or charge. Image adapted<sup>4</sup>.....141**

**Figure 4.3. Distribution of functional aminoacids of silica binders eluted from three step elution (optimised biopanning) process.** All the phage clones identified from first and second panning rounds (Table 4.1) using three different elution buffers for each panning round were considered while plotting the pie diagrams.....147

**Figure 4.4. Charge based distribution of peptides eluted in Table 4.2.** The percentage of peptides eluted was calculated by taking the net charge (at pH-7) values for all the peptides (Table 4.2) eluted in three elution buffers separately. For example, A total of 56, 53 and 57 peptide sequences were identified from first (Gly-HCl, pH-2.2), second (MgCl<sub>2</sub>, pH-6.1) and third elution steps counting both panning rounds (R1A and R2A). Out of 56 sequences from first elution, 35, 13 and 8 sequences, showed net positive charge, neutral and net negative charge values. Then dividing the 35/56\*100 will give 63% of peptides eluted in the first elution step using Gly-HCl, pH-2.2, displayed net positive charge. The same calculation were repeated to get other values.....150

**Figure 4.5: Percentage of hydrophobic v/s hydrophilic and amine containing side groups present in selected silica binding peptides mentioned in Table 4.3.** The percentage of functional amine groups calculated by considering amino acids containing amine groups at side chain or N-terminus of the peptide. ....151

**Figure 4.6. Binding ratio (bound/input) of each of the 14 different phage clones to silica nanoparticles.** The relative binding affinity of the phage clones isolated from three step elution process (11 phage clones) and repanning experiment (2 phage clones) was determined by titer assay at pH-7.5. The asterisk (\*) indicates the phage clones displayed most frequently (abundantly observed) and repeated in the first and second screening rounds. The assay was repeated twice for each phage clone and the explained phage amounts were arithmetically averaged. The errors bars indicate the standard error from the two separate experimental repeats. ....155

**Figure 4.7. Prediction of probability of target unrelated peptides or target binders.** The probability values for silica binders were generated using TUP predict tool (<http://immunet.cn/bdb/index.php/site/tools?type=TUPredict>) from BDB or MimoDB database and plotted. Silica binders identified from A) Lot 1 library (initial biopanning and repanning methods) and B) Lot 2 library (optimised biopanning process) were analysed to check the probability of silica binders to non-targets. In addition, the silica binders identified from C) previous studies were also checked for comparison <sup>4,10</sup>. An asterisk (\*) indicate the sequences appeared as tight binders to silica in experimental phage display. From the analysis, the sequences appeared to be likely silica binders and target unrelated peptides were highlighted in blue and red colours.....159

**Figure 4.8. Multiple sequence alignment of silica binders isolated from two different master lots (aliquots) of library.** The silica binding peptides used for generating these two figures were isolated from two different lots (Lot 1: 0211212 and Lot 2: 0221501) of same library. A total of 77 (Lot 1) and 47 (Lot 2) dissimilar sequences were chosen and analysed. The identified consensus peptide sequences (ADLSVTS and VSTPLLA) from the multiple sequence alignment was highlighted and shown. The sequence alignment was generated by using the freely available MSA viewer (<https://toolkit.tuebingen.mpg.de/#/tools/alnviz>) from the Max Planck Institute website. Label indicate the position and number of the peptide sequences. The small logo (figure) that is present on top of the 'label' indicate the number of times the amino acids have appeared in that specific position. The larger the size of the amino acid the higher the times the amino acid have appeared in that specific position of the peptide sequences. For example, in the library lot 1 image, the amino acid V (valine) was the most frequently observed residue (14 times), followed by S (serine, 12 times) as second, Q (glutamine, 8 times) and so on in the first position of all the 77 silica binders. Thus, V (valine) has appeared larger in the first column followed by second bigger S (serine) and so on.....161

**Figure 4.9. Comparison of observed frequency of amino acid residues across all 124 peptide isolates identified from two separate lots of same library.** A) 77 peptide isolates from Lot 1, B) 47 peptide isolates from Lot 2 and C) 124 peptide isolates (by mixing 77 and 47 separate peptide isolates) identified from both lots 1 and 2 library. The X and Y-axis indicate the amino acid residues and the number of occurrences of each amino acid residue in the peptide isolates. All the amino acids residues are categorised and separated into 5 parts showing non-polar (black), polar uncharged (green), basic (blue), acidic (red) and special (magenta) amino acids in different colours.....163

**Figure 5.1. Primary structure of silica binding peptides a) YSLKQYQ b) HYIDFRW depicting the modified C-terminal group end.** Peptide primary structure generated using the online tool PepDraw (<http://pepdraw.com/>). Highlighted in red coloured ring showing the C-terminal group (Gln, Q) acid (COOH) modified with amide (CONH<sub>2</sub>).....174

**Figure 5.2. Primary structure of silica binding peptide ADIRHIK depicting the modified C-terminal group end.** Peptide structures generated using the online tool PepDraw (<http://pepdraw.com/>). Highlighted in red coloured ring showing the C-terminal group (Lys, K) acid (COOH) modified with amide (CONH<sub>2</sub>).....175

**Figure 5.3: Adsorption behaviour of selected phage displayed peptides on the surface of 82 nm sized silica nanoparticles at pH-7.5 (PBS buffer).** The y-axis represents the amount of peptide adsorbed to silica in mM, while the x-axis shows the initial peptide concentration or peptide added in mM. The theoretical 100% peptide adsorption is shown in black dotted line. The error bars represent the standard deviation error calculated as a result of the assay being repeated in triplicate. Based on the above data, the binding order of the peptides was ranked as HYIDFRW> ADIRHIK> YSLKQYQ> GASESYL.....177

**Figure 5.4. Analysis of the above peptides displayed in Figure 5.3.** The graph showing the peptides and their binding (%) amounts to silica at six different peptide

concentrations. The y-axis represents the percentage of peptide adsorbed to silica, while the x-axis shows the peptide added in mM. ....178

**Figure 5.5: Adsorption isotherms of peptides synthesized with either acid (COOH) or amide (CONH<sub>2</sub>) at C-terminal group of selected phage displayed peptides and their binding behaviour on the surface of hydrophilic silica nanoparticles at pH-7.5.** The y-axis represents the amount of peptide adsorbed to silica in mM, while the x-axis shows the initial peptide concentration or peptide added in mM. The error bars represent the standard deviation error calculated as a result of the assay being repeated in triplicate. The difference in ratio of peptides (CONH<sub>2</sub>/COO<sup>-</sup>) binding to silica at different concentrations (mM) are shown in the table on the right-hand side of the graphical plot. ....181

**Figure 5.6. Effect of C-terminal group as a function of pH v/s charge (z).** The x-axis and y-axis signifies the pH (0 to14) and charge (+7 to -7) range considered for plotting this graph. The change in the charge of the peptides at varied pH (either with acid or amide at C-terminal end group) was calculated from Bachem (<http://www.bachem.com/service-support/peptide-calculator/>) peptide property calculator. ....182

**Figure 5.7. TEM images of silica nanoparticles (82 nm) without EM stain 336 (a,b) and with EM stain 336 (c,d).** ....185

**Figure 5.8. TEM images of M13 Ph.D.7 phage library stained with EM stain 336.** The likely phage structures are indicated by white arrows. Alongside, some unusual shapes (irregular black bodies) are noticed which appear to be clump-like structures forming aggregates with the phage. ....185

**Figure 5.9. TEM images of YSLKQYQ phage attached to silica NPs.** Phage structures thought to bind to silica are shown by white arrows. ....186

**Figure 5.10. TEM images of ADIRHIK phage attached to silica NPs.** Phage structures thought to bound to silica are indicated by white arrows. ....187

**Figure 5.11. TEM images of HYIDFRW phage attached to silica NPs.** Phage structures thought to bound to silica are pointed by white arrows. ....187

**Figure 5.12. Microscopy images showing specific binding affinity between M13 phage displayed peptides and organic<sup>306</sup> or inorganic surfaces<sup>322</sup>.** TEM and Field emission-scanning electron microscopy images of phage ASTLPKA bound to organic TMX crystal surfaces (a, b). The AFM images of the phage displaying the peptide LGFREKE on pIII showing their ends are attached to (c) amorphous and (d) crystalline nickel boride nanoparticles at the tip of pIII, which were shown by white arrows. ....188

**Figure 6.1. Schematic representation of proposed adsorption and desorption mechanisms of phage clones upon interaction with silica at varied pH and the effectiveness of the three-step chemical elution approach (optimised biopanning) to that of traditional biopanning process.** ....193

**Figure 6.2. Schematic representation of proposed adsorption and desorption mechanisms of phage /peptides upon interaction with silica at varied pH.** ....195

## List of Tables

<b>Table 1.1:</b> Types of genes and their functions in filamentous bacteriophage <sup>76</sup> . .....	33
<b>Table 1.2. M13 phage coat proteins, composition and their display fusions.</b> .....	34
<b>Table 1.3. Classification of vectors and display fusions most commonly employed in phage display</b> <sup>76</sup> .....	36
<b>Table 1.4:</b> Types of M13 phage peptide libraries and their advantages. ....	37
<b>Table 2.1. Experimental conditions used to elute silica binding peptides via traditional and optimised biopanning methods.</b> Two different biopanning methods are presented in this table: traditional or standard (used in Chapter 3) and optimised (used in Chapter 4) methods. Both were performed at different times using two separate batches of same library (#E8100S). For the standard biopanning process, three different elution buffers were used but only one specific elution for entire respective biopanning experiment and rounds. In contrast, the optimised elution biopanning process presents 2 approaches (each differ from the former): Approach 1 differs from the standard biopanning method as each mentioned buffers were used successively at every single biopanning round of elution step, as apposed to one specific buffer being used for all rounds in individual traditional panning experiments; Approach 2 only used the Glycine-HCl elution buffer but at varying pH's. ....	67
<b>Table 2.2. Experimental conditions used for initial and repanning experiments via traditional biopanning process.</b> The experimental conditions include the washing of weakly bound phages with TBST detergent (0.1-0.5% Tween 20 [v/v] in TBS); the removal of strongly bound binders from silica surface that isolated the silica binders using three different elution buffers; the dates and the order of experiments performed for normal biopanning were shown in the below table. ....	70
<b>Table 2.3. List of polystyrene or plastic binding peptides identified by phage display process</b> .....	79
<b>Table 2.4. Experimental conditions (washing and elution) used for optimised biopanning process.</b> The experimental conditions include the number of times and washings performed with different concentrations of TBST detergent (0.1%-05% Tween 20 in TBS, v/v) to remove weakly bound or nonspecific phage binders from target silica surface; the elution of strongly bound phage clones from the silica surface that isolated the silica binders using alternative elution methods via three different elution buffers and conditions; the number of biopanning rounds and the way successive elution's carried out during each elution step were shown in the below table. ....	82
<b>Table 2.5. Schematic representation of experimental conditions used for repanning experiments.</b> The amplified phages obtained from different biopanning experiments where a small number of sequences screened were mixed together to verify the reproducibility of previously identified peptide sequences.....	83
<b>Table 2.6. Structural properties of silica nanoparticles including surface chemistry.</b> <sup>a</sup> Specific surface area was determined using the Brunauer-Emmett-Teller (BET) method in the range of $0.05 < P/P_0 < 0.35$ . <sup>b</sup> Barrett-Joyner-Halenda (BJH) desorption pore volume and size were calculated	

between 2 and 300 nm. <sup>c</sup> Determined from TGA measurements. The table was reprinted from ACS<sup>4,107</sup> ..... 86

**Table 2.7. List of silica binding peptides synthesized and their characterisation measurements using HPLC and Mass spectrometry.**..... 86

**Table 3.1. List of silica binding peptides reported in literature that were identified by phage display technique.**.....103

**Table 3.2. Schematic representation of experimental conditions (washing and elution) used for routine biopanning that isolated the silica binders from third panning round using three different elution buffers.** Experimental conditions include the order of experiments performed and their dates (month/ year); washing detergent TBST (TBS with 0.5 % (v/v) Tween 20) concentrations for removing non-specific binders from silica surface; elution buffers and conditions (low pH, high salt and high pH) to elute tightly bound phage clones from silica nanoparticles; selected rounds at which sequences were screened and the most frequently identified silica binders. Identical sequences repeated in one or more panning experiments are presented in a unique colour for clarity.....108

**Table 3.3. Results of repanning experiments showing both silica binders that were found previously identified and further new silica binders.** The silica binders found previously in the initial biopanning procedure and reproduced in this repanning method can be found under the sub-heading 'previous binders'. The new binders appearing only in the repanning experimental process are shown as 'entirely new'. Sequences repeated during different experiments as different round only in this series of repanning experiments are highlighted colour.....112

**Table 3.4. Physico-chemical properties of selected silica binding peptides displayed from routine biopanning process and repanning method.** <sup>a</sup>Physico-chemical properties of all the sequences were obtained from Innovagen and Bachem peptide property calculator<sup>211,212</sup>. Highlighted in bold are the sequences that appeared as the most frequently occurring silica binders repeated in one or more panning experiments (both initial and repanning). An asterisk (\*) indicates the peptides sequences that exhibited higher binding capability to silica in relative binding affinity assay. The amino acids that contain amine side chain (N, Q, P, W) and hydroxyl side chain (S, T, Y) containing groups in a peptide, which can help in forming hydrogen bonding between silica-peptide or among themselves are shown. ....117

**Table 3.5. Identification of amino acid motif (LP) by comparing the silica binders of this study with the peptide sequences published in literature.** An asterisk (\*) indicates the sequence displayed as one of the most abundant silica binders in bioopanning experiments or *in silico* designed and was shown to exhibit strong binding to substrate in binding studies. All the silica binders isolated from three sets of biopanning experiments (77 dissimilar sequences) are checked and the sequences having motif (LP) were shown in the first row of the table. While, the other sequences were displayed only once in different panning experiments in this study. The amino acid motif (LP) was shown highlighted in bold and underlined.....120

**Table 3.6. MimoDB search/ scan/ Blast analysis results of phage displayed silica binders found to have affinity for other materials indicating that they might be promiscuous binders.** Peptide sequences highlighted in bold are the

phage clones that appeared as highly abundant or tight binders to silica in initial biopanning and/ or repanning methods.....122

**Table 3.7. Physico-chemical properties and adsorption of silica binding peptides:** <sup>a</sup>Physico-chemical properties of all the sequences were obtained from Innovagen (<https://pepcalc.com/>) and Bachem (<http://www.bachem.com/>) peptide property calculator. Type of interactions likely be responsible for peptide-silica binding and their effect on increasing pH and particle size were shown. The asterisk (\*) represents the probable effect of increasing pH and particle size on binding to silica was estimated and predicted by comparing the peptide sequences of this findings with previous studies, where peptides of similar properties (eg. peptide length, net charge of peptide at pH-7 and same batch of silica nanoparticles) were investigated and assessed based on adsorption studies<sup>4,44,107</sup> .....130

**Table 4.1. Silica binding peptides identified from optimised biopanning process.** A total of two screening rounds were performed, the phage clones eluted separately after each elution step in a three-step elution process using three different elution buffers for each panning round were shown. To improve the screening stringency, the Tween 20 detergent (0.1-0.5% Tween 20 [v/v] mixed in TBS) concentration and wash times gradually increased as shown. NIL are the phage clones which were excluded from results due to the insertless or absence of any sequence, as the inherent rate of insertless phages in the NEB Ph.D.-7 library was about 5%. Frequently occurring sequences within the biopanning rounds are presented in a unique colour for clarity.....145

**Table 4.2: Silica binders identified in Table 4.1 and their elution, pI and charge based appearance.** The pI and net charge values for all the sequences were obtained from Innovagen and Bachem peptide property calculator (INNOVAGEN, 2014; Bachem, 2017). Blue colour indicates high pI and positive charge values of peptides at pH-7; no colour directs neutral charge and pI values and red colour indicates low pI and negative charge values.....149

**Table 4.3: Physico-chemical properties of selected silica binding peptides displayed in Tables 4.1 and 4.2.** <sup>a</sup>Physico-chemical properties of the sequences were obtained from Innovagen and Bachem peptide property calculator (INNOVAGEN, 2014; Bachem, 2017). Highlighted in bold are the sequences that appeared as the most frequently occurring silica binders repeated in first and second panning rounds. The amino acids that contain amine (N, Q, P, W) and hydroxyl side chain (S, T, Y) containing groups in a peptide that may help in forming hydrogen bonding between silica-peptide or among themselves are shown. ....150

**Table 4.4: Repanning experimental results to check the optimised biopanning approach and reproducibility.** Selected tight silica binders were shown here and full list of sequences can be found in appendix 4.2 and 4.3. Note: Black coloured sequences are found in both initial and repanning methods (Chapter 3). While, the red coloured sequences are the ones appeared in this repanning experiment. 'All 3 mix' are the phage clone samples that are mixed together from all 3 elution steps and pH within elution strategy 1 and 2.....153

**Table 4.5: Physico-chemical properties of selected silica binding peptides of identified in Table 4.4.** <sup>a</sup>Physico-chemical properties of all the sequences were

obtained from Innovagen and Bachem peptide property calculator <sup>211,212</sup>. Highlighted in bold are the sequences observed as most frequently repeated peptides. An asterisk (\*) represents the sequences that were present previously from initial and repanning experiments using lot 1 library (Chapter 3) and reappeared here. The amino acids that contain amine side chain (N, Q, P, W) and hydroxyl side chain (S, T, Y) containing groups in a peptide, which can help in forming hydrogen bonding between silica-peptide or among themselves are shown. ....153

**Table 4.6: Mimo search/ scan/ Blast analysis results of silica binders identified from both lots of same phage library and the differences in lot to lot behaviour.** The phage displayed silica binders that showed hits for other materials indicating that they might be promiscuous binders. Peptide sequences highlighted in bold are the phage clones that appeared as most abundant binders (within the small population sequenced) to silica in initial biopanning and/ or repanning methods (Chapter 3).....157

**Table 4.7. Physico-chemical properties of two consensus silica binding sequences identified in Figure 4.8.** <sup>a</sup>Physico-chemical properties of the sequences were obtained from Innovagen and Bachem peptide property calculator (INNOVAGEN, 2014; Bachem, 2017). The amino acids that contain hydroxyl side chain (OH) containing groups (S, T, Y) which may help in forming hydrogen bonding between silica-peptide or among themselves are shown.....162

**Table 5.1. Selection of peptides based on experimental phage display results (1-4), physico-chemical properties (5-9) and bioinformatics analysis (10-11).** Experimental phage display results (1-3) taken into consideration include the type of library lot used and biopanning approach through which they were identified, alongside their appearance (i.e most frequently repeated sequences within the small number of sequences analysed) at different phage display experiments and rounds. Physico-chemical properties (5-9) of the peptides taken into consideration anticipating their binding behaviour to silica include the pI, hydrophilicity and net charge of peptide at pH7; Bioinformatics analysis (10-11) MimoDB analysis results to check the authenticity of their binding to target. According to probability prediction analysis, any peptide value that is less than 0.5 should be considered a true target binder not a target unrelated peptide (described in section 4.3.4). MimoDB search results refers to the sequences that were reported to bind to other materials (based on published data) other than to silica (in this study).....173

**Table 5.2. Physico-chemical properties of selected phage displayed silica binding peptides.** <sup>a</sup>Physico-chemical properties of all the sequences were obtained from Innovagen (<https://pepcalc.com/>) and Bachem (<http://www.bachem.com/service-support/peptide-calculator/>) peptide property calculator. The side chain amino acid groups (R-CO-N) or (R-OH) that are likely responsible for hydrogen bonding are shown separately as hydroxyl (Ser, Thr and Tyr) and amine side chain (Asn, Gln) containing groups.....176

**Table 5.3. Likely type of interactions that might be responsible for adsorption of peptides and the likely effect of increasing pH and particle size on binding to silica particles in PBS solution.** The asterisk (\*) represents the likely effect of increasing pH and particle size on binding to silica was estimated based on the previous studies where peptides of similar properties (eg. peptide length, net

charge of peptide at pH-7 and same batch of silica nanoparticles) were investigated and assessed based on adsorption studies<sup>4,44,107</sup>. It has to be noted that the pH range and nanoparticle sizes considered for these studies include pH-3 to pH-8.5 and 28 nm, 82 nm and 210 nm.....179

**Table 5.4. Effect of C-terminal group on increasing the overall peptide net charge and/ or pI at pH-7.** <sup>a</sup>The change in the net charge or pI values of the peptides (either with acid or amide at C-terminal end group) were obtained from Bachem (<http://www.bachem.com/service-support/peptide-calculator/>) peptide property calculator.....181



## Chapter 1: Introduction

Over the past two decades, the popularity of using combinatorial phage display techniques for selecting and recognising material-binding peptides with a unique attraction for any target, and specifically inorganic materials has achieved considerable interest in the development of advanced bio- or nano-materials. However, the accuracy of molecular recognition for inorganic materials is still challenging due to the limitations of phage display libraries and biopanning process. It is still unclear whether (i) we are eluting all of the strong binders from the available phage library, (ii) what the limits of detergent and elution conditions are, (iii) the issue of binding to non-specific targets or fast growers<sup>1,2</sup>, (iv) under-representation of the desired sequences and their properties due to having bias towards peptide position, composition, and expression<sup>3</sup>, (v) pH and interaction specific intrinsic bias<sup>4</sup> and (vi) are their differences between aliquot to aliquot behaviour of same library. Additionally, another important factor to consider is the limited fundamental understanding of peptide- inorganic material interactions which is a major bottle neck for generating peptide based inorganic nanomaterials with improved biocompatibility, solubility, functionality and increased physico-chemical properties<sup>4-12</sup>. This thesis presents the isolation and identification of silica binding peptides using the standard and optimised phage display approaches by exploring the elution strategies. Although, the optimised elution approach developed is specifically from silica, it could be applied to other inorganic material surfaces. Experimental and bioinformatics methods are used to check the reproducibility and authenticate the target binders. Further, selected peptides identified by phage display were chosen to study the effect of overall or individual charge, pH, C-terminal groups (acid or amine) of peptides and changes occurring at peptide-silica interface *in vitro* in solution.

Chapter 1 introduces the literature review and discuss the status of combinatorial phage display techniques with inorganic materials, specifically silica, and their applications including patents relevant to this study. It also includes statements as to the importance, motivation, and objectives of this research project.

## 1.1 Overview of Combinatorial Phage Display Technologies

In the last century, a combinatorial approach originally adapted by the microbiology community has attracted considerable interest and brought an innovative dimension in synthesising and engineering new advanced materials by mimicking the naturally occurring biomolecules that direct biomineralization process. Molecular recognition is the central phenomenon of all biological systems and recognises molecules with high specificity and diversity. Using this molecular recognition principle, several systems have been studied to examine the binding events happening at the molecular level. Some of the well-studied systems include antigen-antibody, peptide-protein, protein-DNA, and more recently biomolecule-inorganic surfaces<sup>13,14</sup>.

Various techniques have been established for acquiring peptide sequences with specific affinity to inorganic material. The theoretical molecular approach is one of these techniques used to design inorganic-binding peptides. This approach is similar to that used in the pharmaceutical industry for target drugs<sup>15</sup>. However, this technique is currently both time consuming and expensive, thus making it not a suitable option. The other technique is to extract biomineralizing proteins; this is done by isolation, purification, and cloning of protein from hard tissue<sup>16-18</sup>. Proteins extracted *via* this method have previously been used as nucleators, growth modifiers, or for enzymes in the synthesis of specific inorganics. The key limitation of this technique is the complexity of extracting the required proteins, given that hard tissue contains several types of proteins that are differentially active in biomineralization and spatially distributed<sup>19,20</sup>. Proteins that are tissue-extracted are limited to be used in the regeneration of inorganics of their original association. Thus, an alternative route to the techniques mentioned would be combinatorial display techniques<sup>21-24</sup>.

Currently existing combinatorial display technologies include phage display<sup>25-30</sup>, cell surface display<sup>31-34</sup>, ribosome and mRNA display<sup>35-41</sup> and rational design<sup>42-44</sup> technologies. Ever since the establishment of *in vitro* combinational biology protocols, such as phage display (PD)<sup>25,45</sup> and cell-surface display (CSD)<sup>46</sup>, they have been used for the identification of biological ligands and for the mapping of epitopes of antibodies. Libraries have also been screened for different biological activities: catalyst properties, altered affinity and specificity to target molecules. This has applications in the designing of drugs, enzymes, antibodies, DNA-binding, proteins and diagnostic agents<sup>47-49</sup>. Combinatorial display technology has advantages as it does not require the prior knowledge of the required amino acid sequence; sequences can randomly be selected and enriched. In comparison to an *in vivo* system<sup>50</sup>,

which has a developed library size of  $10^{7-10}$ , *in vitro* methods have a much larger developed library size of  $10^{15}$ .

Cell surface display and phage display are approaches which are based on their link between the genotype and phenotype of different organisms. On one hand, phage display utilises bacteriophages as a vector, whereas cell surface display uses bacteria or yeast<sup>51</sup>. Through the genetic engineering of bacteriophage genomes or bacterial plasmids, randomised segments of a gene can be produced to gain a library<sup>52</sup>. This random library sequence is then expressed on the surface of a phage coat protein or a bacterial flagella protein. In the case of other *in vitro* selection techniques, such as Ribosome display and mRNA display, both commence with the transcription of the DNA library to generate the mRNA and do not require a transformation or cell growth step. Both methods are considered to be promising display technologies for antibodies as they consist of larger libraries ( $10^{15}$ ), cell-free system with fewer expression bias<sup>53</sup>. The key difference between these two approaches is that mRNA display involves DNA spacer linkers with puromycin which is responsible for forming covalent bonds between RNA and polypeptide<sup>54</sup>. The ribosome within Ribosome display contains a random peptide fold with is produced by fusing the DNA library to a C-terminal region absent of a stop codon. The absence of the stop codon helps in creating a protein-ribosome-mRNA complex. The mRNA dissociates as the complex binds with the immobilized target, thus allowing the determination of the peptide sequence through reverse transcription<sup>53</sup>.

### 1.1.1 Phage display and biopanning process

Phage display/Biopanning is an affinity selection technique commonly used for identifying novel peptides bound to a specific target through a repetitive process. This includes binding of phage displayed peptides to target material, removal of weakly bound phages through detergent washing; removal of strongly bound phages through elution and multiplying the eluted phage in a host bacterium *E. coli* ER2738 strain. Phage display library is created by fusing DNA fragments into the genome of the phage or phagemid and displaying the random peptides on the surface of the phage coat proteins<sup>4</sup>.

G.P Smith, for the first time used the phage display technology as a powerful tool to identify ligands for numerous targets in 1985<sup>25</sup>. The phage display approach was originally employed to recognise and particularly to study protein-protein, peptide-protein or antigen-antibody

interactions<sup>1,4,10,25,47,55</sup>. In the recent years, the phage display technique has extended its applications to engineering antibodies, targeting organs, studying networks and sites of protein-peptide interactions, studying their use in vaccines, therapeutics, diagnostics and drug discovery<sup>28,56-63</sup>. More recently, phage or cell surface displayed libraries have become ubiquitous in selecting and screening peptides having strong affinity towards a range of inorganic material surfaces<sup>64</sup>. Due to these advances, it is now possible to produce novel materials using biological linkers on more than one type of material to create hybrids with unique mechanical, electronic, photonic or magnetic properties<sup>24,65</sup>.

The techniques applied in combinatorial biology protocols are often also used in the field of molecular biomimetics, for the selection of peptide sequences with specific physical properties, that selectively bind to surfaces of inorganic compound in nano- and biotechnology<sup>22,24</sup>. The libraries are constructed by incorporating randomised oligonucleotides with a specific gene encoded on phage genomes or bacterial plasmids<sup>21,22</sup> (see step 1 of Figure 1.1). This then leads to the combining of a random peptide sequence with a protein existing on the surface of the organism (as shown in step 2). This leads to each phage or cell displaying a dissimilar and random peptide sequence (step 3). This step is followed with the heterogeneous mixture of cells or phages encountering the inorganic substrate (step 4). Any unbound or weakly bound phages, or cells are eliminated with several washing cycles, whereas the bound phage or cell are separately eluted from the surface (step 5 to 6). With phage display protocol, the strong binding eluted phage are intensified by infecting the host again (step 7), and as for cell surface display, the cell is permitted to grow (step 7 to 8). This step represents one complete round of biopanning. It is common practice to repeat at least three to five complete biopanning cycles to ensure enrichment of binders. The final step (step 9) involves sequencing the individual clones to attain the amino acid sequence of the peptide binders to the target substrate material<sup>66</sup>.

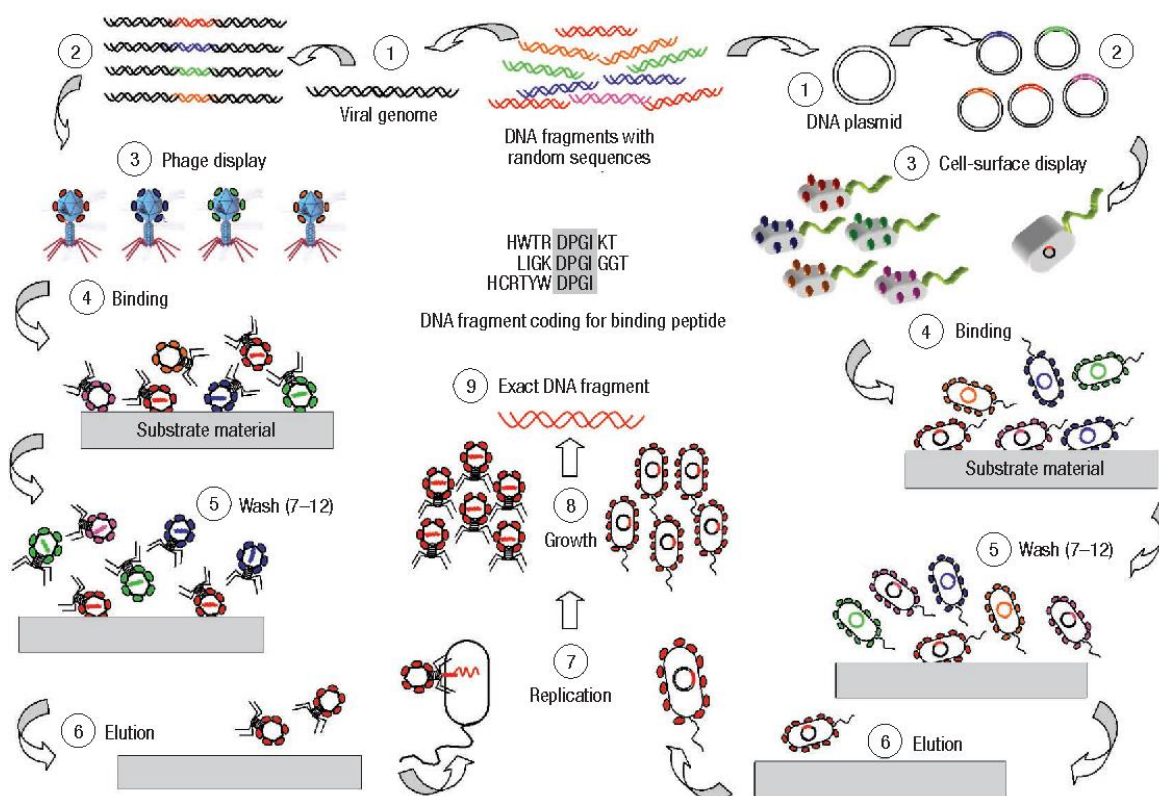


**Figure 1.1. Typical phage/ cell surface display and biopanning process used for selecting polypeptide sequences that have binding affinity to given inorganic substrates. Image reprinted<sup>66</sup>.**

An important advantage of phage display compared to other commercial technologies is the possibility of screening many clones. When compared to other standard screening methods of cDNA libraries, they are restricted to the number of plaques or colonies that can be screened by hybridization ( $\sim 10^4$ )<sup>67</sup>. Peptides from libraries which are synthetically manufactured are generally screened on grids or pins, with the binding peptides being identified by sequencing a tag associated to the selected bead in suspension. The disadvantage of the technology is the limiting number of random peptide sequences which can be screened, which is between  $10^3$ - $10^4$ . Synthetic peptides that are screened for libraries in solution may have up to  $10^{15}$  different sequences, but the requirement of low stringency during binding results in a selection of peptides with highly differing affinities. Phage display allows for the easy screening of more than  $10^9$  different sequences, and the amplification of the selected phage by propagating them in *E. coli* over multiple rounds of screening to ensure the selection of the most strongly binding peptide sequences.

Other advantages of using a phage display technique for selecting binding peptides includes 1) Large number of amino acid sequences can be screened easily. 2) Allows for a direct connection between the peptide and DNA sequence. This creates a physical link between the protein that is displayed and the DNA encoding, allowing for a vast number of proteins to be screened by an *in vitro* selection procedure known as "biopanning". 3) Phage displayed peptides or proteins can easily be exposed to solvents; hence the peptide/protein can hold its functions and affinities during the phage display process. 4) If the target is a biomolecule, the molecular recognition is highly specific and the results are mostly reproducible and reliable unlike inorganic material targets where molecular recognition is not highly specific and results appear to be dependent on a variety of physical (e.g. morphology, size, crystal phase, orientation) and chemical (hydrogen bonding, polarity and charge effects) properties<sup>25,68</sup>.

### 1.1.2 M13 Phage structure and life cycle

The filamentous bacteriophage are a group of viruses that belong to a genus known as Inovirus. The virus contains a circular DNA genome which is encased in a long protein capsid cylinder and the genome may consist of ssDNA, dsDNA, ssRNA or dsRNA<sup>69,70</sup>. The bacteriophage is known to mainly infect Gram-negative bacteria by binding to the pili and infecting the bacteria, while not killing the host bacteria<sup>71-73</sup>. The filamentous phage is separated into three classes which are closely related, both genetically and phenotypically: M13, fl and fd. M13 phage is one of the most commonly studied filamentous phage for phage display technology as their small genome makes them easy to manipulate. Assembly of a longer phage particles is possible by inserting DNA into non-essential parts of the phage. These phages have the possibility to be produced in higher amounts and are stable in hard environments<sup>74,75</sup>. In general, filamentous phage are not lytic and so strains of phage-infected *E. coli* can release new phage particles without bacterial lysis. Other types of virus-like systems used in phage display are the phagemid, which are plasmids containing an f1 origin of replication from a phage to enable their single-stranded replication and packaging into phage particles, as well as an origin of replication (ori) for double-stranded replication. Phagemids can be considered as cloning vectors but need helper phage for completing their infection process by providing the structural and functional proteins necessary for packaging phagemid into virion particles. The biofilm life cycle and virulence of *Pseudomonas aeruginosa* are dependent on a filamentous prophage<sup>76</sup>.

The M13 phage has roughly a diameter of 10 nm and a length of ~1  $\mu\text{m}$ , consisting of a single-stranded DNA genome of 6407 nucleotides. The genome is made up of 11 genes (as shown in Figure 1.2) which are grouped according to their individual function (Table 1.1): (i) Different types of capsid coat proteins present in the M13 bacteriophage includes, pIII, pVI, pVII, pVIII and pIX, (ii) All DNA replication proteins consist of pII, pV and pX, and (iii) the assembly proteins pI, pIV and pXI. pIII functions in cell recognition, stability and infection<sup>73,77-82</sup>. The phage is surrounded by a coat protein which is composed of two fusion proteins: one is pIII (minor coat protein), and the second is pVIII (major coat protein). pVIII contain ~2,700 proteins and covers the length of the particle, while at one end are pIII and pVI and at the other end are pVII and pIX, each containing roughly five proteins. The phage pIII has two main domains know as N-terminal (N1 and N2) and C-terminal domain. The N1 domain is responsible for the translocation of the viral DNA into *E. coli*. The domain N2 is responsible for increasing the recognition of the host cell by binding to the F pilus on the bacterium, while the C-terminal domain integrates the pIII into phage coat<sup>76,82,83</sup>.

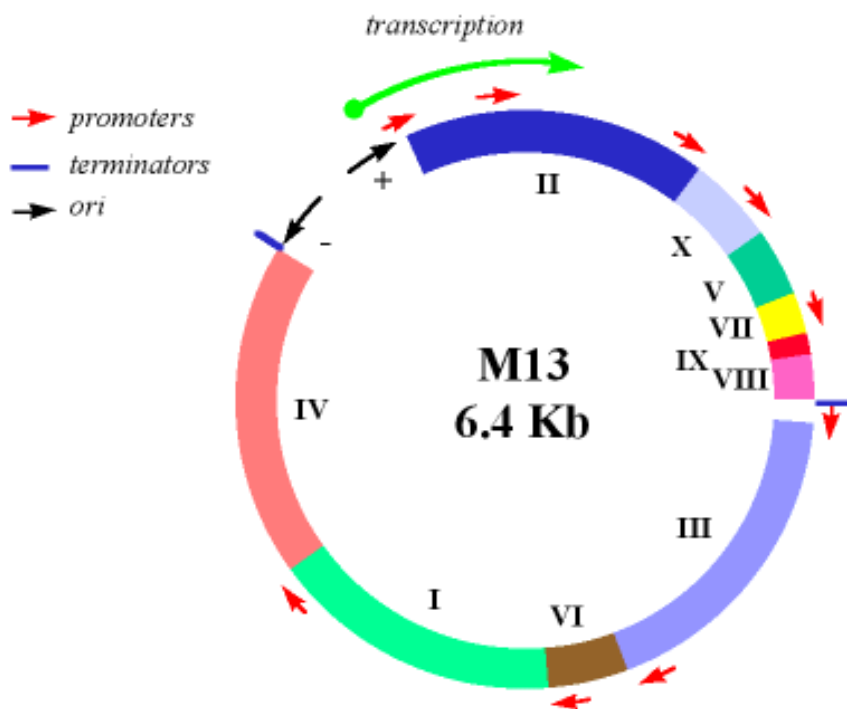


**Figure 1.2: Diagrammatic representation of M13 bacteriophage genome and the location of genes. Image adapted from ref<sup>84</sup>.**

The infection process starts when the code protein III N-terminus attaches to the tip of F-pilus on the bacterium. This binding leads to the injection of ss-DNA (+) strand of the phage into the bacterial cell. This is followed by the creation of a double stranded (or known as a replicative) form of phage, which forms when the host polymerase uses the (+) strand as a template to generate a complementary (-) strand. The (-) strand of RF DNA are responsible for generating the mRNA, which are used in the synthesis of phage proteins. To produce new phage, the genome needs to replicate by using newly generated pII to cut the RF DNA to begin the replication of the (+) strand, which results in a collection of RF DNA molecules to be produced by the host enzyme<sup>78-82</sup>. pII is also responsible for forming the ss-DNA by ligating the molecular ends of the newly synthesised (+) strand. The newly formed ss-DNA binds to the pV dimer to avoid the conversion back to RF DNA. The ratio of RF to (+) strand DNA synthesis is dependent on the amount of pV present. The pX is mostly involved in replication but is also believed to participate in the inhibition of pII function and regulate RF/ (+) strand synthesis. pI, pXI and pIV are all involved in assembly, which occurs in the inner membrane. The C-termini of pI and pXI interacts with pIV to create a channel to aid the secretion of phage. The pVII and pIX also required as it interacts with the pV-ss-DNA complex for the secretion step. During the extrusion step, the pV which is bound to ss-DNA is substituted with pVIII followed with the addition of pVI and pII near the central end of the releasing particle. During this first-generation post infection, which is then followed by bacterial cells, roughly 100-200 phages are produced per generation<sup>73,77-82</sup>.



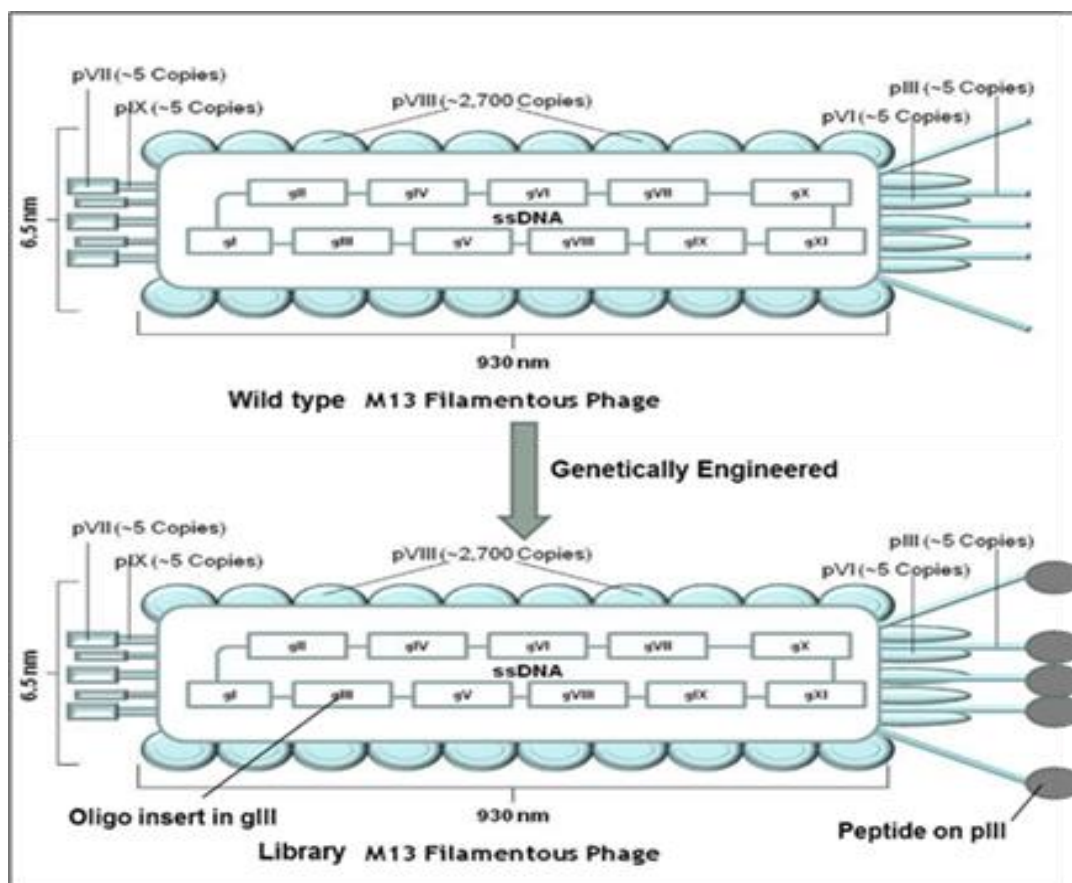


**Figure 1.3:** Schematic representation of the structure of filamentous phage (wild versus engineered) and their coat proteins (right). Image adapted<sup>84</sup>.

**Table 1.1:** Types of genes and their functions in filamentous bacteriophage<sup>76</sup>.

Genes	Function	Number of amino acids	Molecular weight (Da/mol)
pI	Assembly	348	39,502
pII	DNA replication	410	46,137
pIII	Minor capsid protein	406	45,522
pIV	Assembly	405	43,476
pV	Binding ssDNA	87	9682
pVI	Coat protein (minor)	112	12,342
pVII	Coat protein (minor)	33	3599
pVIII	Coat protein (major)	50	5235
pIX	Coat protein (minor)	32	3650
pX	DNA Replication	111	12,672
pXI	Assembly	108	12,424

The principal difference between the wild type and genetically engineered phage is that the addition of an oligo inserts at gene III and protein at pIII as shown in Figure 1.3. In the phage display process, the phage particle utilizes the copies of coat protein. The selection of coat proteins in the phage library depends on the type of display being looked for. For example, pIII phage capsid protein allows for monovalent display (binds to one target) making the selection of high affinity bodies. However, the polyvalent is also an option. While pVIII allows for polyvalent display (binds to many targets) displaying multiple copies allowing avid binding making the selection lower affinity. As shown in Table 1.2, filamentous phage display system is mostly constructed on the fusion of N-terminal to the coat protein. There are 5 copies of pIII present per virion which all can be fused to short peptides without interfering with phage infectivity. The main pVIII copies are present ~2700 per virion, with ~10% reliably being fused to peptide or protein. Thus, peptides expressed as pIII fusions exist at low valency (1-5 copies per virion) compared to pVIII fusions which are present at high valency (~200 copies per virion). The low valency of pIII display limits selection to higher affinity ligands, whereas the increased avidity and high valency of pVIII display allows selection of very low affinity ligands<sup>73,77,78,80-82</sup>.

**Table 1.2. M13 phage coat proteins, composition and their display fusions.**

Protein	Number of amino acids	Molecular weight (Da)	Copies per phage	Type of display
pIII	406	45,522	5	N or C
pVI	112	12,342	5	C
pVII	33	3599	5	N
pVIII	50	5235	2700	N or C
pIX	32	3650	5	N

All the Ph.D. libraries are pIII fusions (5 copies of the peptide per virion). Monovalent display on pIII has been enabled through the development of so-called phagemid systems, which have become the most commonly used type of phage display system<sup>73,77,79,82</sup>. Normally, the foreign sequence gets fused with the amino terminus of pIII (5 copies) or pVIII (2700 copies) coat proteins<sup>85,86</sup>. Coat protein III contains three domains D1, D2 and

D3. These domains are connected by glycine rich linkers. The D1 domain consists of 6  $\beta$  strands and 1 N-terminal  $\alpha$  helix<sup>87,88</sup>. In phage display technology, the peptides are displayed on the N-terminal  $\alpha$  helix on domain D1 by fusion as shown below<sup>73,76,78,80-82</sup>.

Displayed peptide	Tag	$\alpha$ helix	
XXXXXXXXXXXX	GGGS	AETVSCLAKSHTENS	.....

Vectors are used in phage display and are classified according to three parameters: 1) Type of coat protein used for display (pIII or pVIII). 2) Whether the displayed peptide or protein has fused to all clones of pIII or pVIII or just a portion of them. 3) Whether the insert is encoded by phage genome or other genomes (e.g. phagemid)<sup>47</sup>. The classification of vectors commonly used for phage display are shown in Table 1.3<sup>76</sup>. As an example, type 3 vector insert is encoded by pIII gene, which leads to the display of foreign protein or peptide in all pIII copied. As for type 33, the phage genome allows two types of pIII molecule; first is a recombinant while the other is wild type. This outcome only allows some of the expressed pIII protein to be fused with the foreign protein or peptide. One must be aware that type 33 is different from type 3+3, in that two copies of the pIII gene do exist in both but are on different systems: one is a wild type which is on a helper phage, while the recombinant form is found on the phagemid genome. Like the relation between 33 and 3+3, type 88 and 8+8 are the same respectively, except with pVIII being using for display<sup>76,82,83,85</sup>.

**Table 1.3. Classification of vectors and display fusions most commonly employed in phage display<sup>76</sup>.**

Type of display	Displayed coat protein	Display on all or few copies of coat proteins	Number of coat protein genes involved in fusion	Fusion type (phage or phagemid genome)	Example Vectors
3	pIII	All	1	Phage	M13KE
8	pVIII	All	1	Phage	M13KE
33	pIII	Few	2	Phage	M13KE
88	pVIII	Few	2	Phage	F88-4
3+3	pIII	Few	2	Phagemid	pComb 3
8+8	pVIII	Few	2	Phagemid	pComb 3

Compared to other phage used in phage display technology, M13 and filamentous bacteriophages fd and fl are more useful due to their non-lytic nature<sup>89</sup>. This allows for the simplification of the intermediate phage purification steps during the panning rounds<sup>70</sup>. Other phage that use in phage display research preciously (T4, T7 and lambda) are all lytic, thus requires more slow purification steps between panning round to avoid amplifying phage in presence on cellular protein or protease which may degrade the target during panning rounds<sup>72,82</sup>.

### 1.1.3 Phage display libraries

The most frequently used and commercially available phage display libraries are the filamentous phage M13 such as Ph.D. 7, Ph. 12, Ph.D. C7C (New England Biolabs) and spherical T7 phage (T7 select, Merck)<sup>55</sup>. Among the Ph.D libraries available in the market (Table 1.4), Ph.D. 7 is the best characterised and most reliable. Though Ph.D. 12 library is not sufficient enough to cover the entire sequence space but the library was the one mostly used in the recent literature<sup>11,90</sup>. Ph.D. C7C library is not a particular choice for phage display experiments due to conformational constraint.

**Table 1.4: Types of M13 phage peptide libraries and their advantages.**

<i>Ph.D. library type</i>	<i>Number of clones</i>	<i>Likely sequences</i>	<i>Comments</i>
Ph.D. 7	$2.8 \times 10^9$	$20^7 = 1.28 \times 10^9$	Best characterized
Ph.D. 12	$1.9 \times 10^9$	$20^{12} = 4.1 \times 10^{15}$	Insufficient to cover the whole sequence space
Ph.D. C7C	$3.7 \times 10^9$	$20^7 = 1.28 \times 10^9$	Conformational constraint

PhD.-7 library contains randomised 7-mer peptides, which is fused to a coated protein pIII of M13 via flexible linker, Gly-Gly-Gly-Ser. The PhD.-7 library consists of  $2.8 \times 10^9$  independent clones. This library is useful for targets requiring binding elements concentrated in a short stretch of amino acids. This is the best characterised library so far<sup>57</sup>. The PhD.-12 library contains randomised 12-mer peptides. Like PhD.-7 library, PhD.-12 are also fused to pIII via Gly-Gly-Gly-Ser. PhD.-12 library contain  $1.9 \times 10^9$  independent clones, or only a small fraction of the  $20^{12} = 4.1 \times 10^{15}$  possible sequences. This library is useful for targets requiring 7 or fewer defined residues for binding, but this which is not contained within the 7-residues of the PhD.7 library. For example, the motif ADTXXAPXY has only six defined positions, but cannot be present in the PhD.-7 library. In addition, 12-mer is long enough to fold into short structural elements, which may be useful when panning against targets requiring structured ligands. The limitation of this library is that the increased length of randomised segment may allow for the selection of sequences with multiple weak binding interactions, instead of a few strong interactions.

In contrast to the above two mentioned libraries, PhD.C7C library consists of randomised 7-mer peptides; each of these peptides are flanked by a pair of cysteine residues. Cysteine residues can spontaneously form disulphide bonds, in absence of a reducing agent. Similar to the other two libraries, this library is fused to pIII via the Gly-Gly-Gly-Ser spacer and contains  $3.7 \times 10^9$  independent clones. This library is useful for targets whose native ligands are in a surface loop (e.g. antibodies with structural epitopes). A major disadvantage of the PhD.C7C library is that the disulfide constraint may “freeze out” a conformation required for target binding. This results in outcomes that are impossible to predict in advance so one cannot predict which library is suitable for a given target. Thus, it is the recommendation of

research labs (e.g. New England Biolabs) for Ph.D.7 library to be tried first regardless of target. An alternative to this would be for all the libraries to be tried simultaneously, due to the ease of carrying out panning experiments in parallel using multiwell plates.

Phage display and cell surface display are both *in vivo* techniques which rely of the genetic modification of the vector to produce a library. The process by which phages or cells uptake DNA is at a disadvantage as the resulting library only contains up to  $10^{13}$  varieties<sup>46,49</sup>. An additional disadvantage of phage display and cell surface display are that it is more sensitive to biases. For example, during the amplification step the phages are required to infect the host bacteria, however this introduces the possibility of poor infectivity or loss of clones, regardless of them being strong target binders. Additionally, some phages are inclined to produce a larger progeny compared to other phages, leading to certain clones to repeatedly be identified. Despite these disadvantages to *in vivo* display technology, the technique is relatively simple and does not require high level of expertise compared to ribosome display and mRNA display. For these reasons, phage display and cell surface display have commercialized kits are most commonly used in display technologies<sup>91</sup>. For the purpose of screening inorganic materials, the structure of the of the target material must be taken into consideration to select a suitable display technique. As an example, during biopanning on materials which are in powder form, a prior centrifugation step will be required to separate the eluted phage from the powder. With this particular example, phage display would be a more suitable technique as flagella might be sheared off from the cell by centrifugal force<sup>92,93</sup>.

## 1.2 Overview of Silica (SiO<sub>2</sub>)

In nature, silica also known as silicon dioxide (SiO<sub>2</sub>) is the most commonly available and abundant mineral present in the earth's crust<sup>94</sup>. Naturally, it exists mainly in amorphous or in crystalline states that include quartz, cristobalite and tridymite forms<sup>94</sup>. The crystalline silica, also known as  $\alpha$ -quartz is the major and primary constituent present in sand, soil and even rocks. While, the amorphous silica is commonly precipitated or deposited in bacteria, diatoms, sponges, plants and animals<sup>95</sup>. The process by which silica forms in living organisms with the help of biomolecules involving complex polymerisation reactions is termed as biosilicification. These organic molecules such as proteins, polyamines and proteoglycans are reported to be the key biomolecules that are responsible for controlling the structure of silica during the biomineralization process<sup>10,96-98</sup>. To date, silica has been one of the most widely studied and used minerals with applications ranging from biocatalysis through to nanotechnology and biomedical fields due to its low toxicity and biocompatible properties<sup>99,100</sup>.

### 1.2.1 Silica synthesis and chemistry

Naturally, silica synthesis occurs through a process of biosilicification<sup>96</sup> with the help of biomolecules that are present within the organisms. A lot of studies have been reported showing the formation of silica *in vivo* with the help of proteins including silicatein in sponges<sup>101,102</sup> and silaffins in diatoms<sup>96,97,103-106</sup>. Inspired by nature's way of synthesising biosilica, research groups have started understanding the role of biomimetic peptides in synthesising silica particles in the laboratory or *in vitro* under controlled conditions<sup>4,10,59,107</sup>. Silica is mainly synthesised from orthosilicic acid, Si(OH)<sub>4</sub> under the influence of aqueous solution by sol-gel process. The sol-gel process refers to the solid dispersion of nanoparticles in liquid (sol) which later agglomerate to form a continuous three-dimensional network throughout the liquid (gel). The method involves initial hydrolysis of silicon alkoxide (e.g. tetraethoxysilane, TEOS or tetramethoxysilane, TMOS) to form an orthosilicic acid, Si(OH)<sub>4</sub>. This is then followed by subsequent condensation as shown in the following equation, specifically for the formation of TEOS which contain silanol groups<sup>108</sup>:

1. Hydrolysis;  $\text{Si}(\text{OC}_2\text{H}_5)_4 + \text{H}_2\text{O} \rightarrow \text{Si}(\text{OC}_2\text{H}_5)_3\text{OH} + \text{C}_2\text{H}_5\text{OH}$
2. Water condensation;  $\equiv\text{Si}-\text{O}-\text{H} + \text{H}-\text{O}-\text{Si}\equiv \rightarrow \equiv\text{Si}-\text{O}-\text{Si}\equiv + \text{H}_2\text{O}$
3. Alcohol Condensation;  $\equiv\text{Si}-\text{OC}_2\text{H}_5 + \text{H}-\text{O}-\text{Si}\equiv \rightarrow \text{Si}-\text{O}-\text{Si} + \text{C}_2\text{H}_5\text{OH}$

Polymerisation between adjacent silanol groups or ethoxyl groups leads to siloxane bridges Si-O-Si, thus forming the silica structure (example shown in Figure 1.4)<sup>94,108</sup>. The size of the silica particle is largely dependent on the rate of nucleation of hydrolysis and the rate of growth of condensation process<sup>109</sup>. The addition of acid (i.e. HCl) or base (i.e. NH<sub>3</sub>) is known to increase the rate of hydrolysis, either due to the increase of hydronium or hydroxide group in the system. The synthesis of silica particles in basic conditions with a size ranging 10 nm to 2 μm, is shown to be possible by changing the concentration of the reactants<sup>110</sup>. Studies carried out on the growth of silica microparticles in low pH (i.e. acetic acid<sup>111</sup>, tartaric acid<sup>112</sup> or nitric acid<sup>113</sup>) have in general shown low porosity and thus are more dense particles compared to silica synthesised in alkali condition. However a more recent method for making silica nanoparticles is through microwave-assisted acid catalysis using HCl<sup>114</sup>.

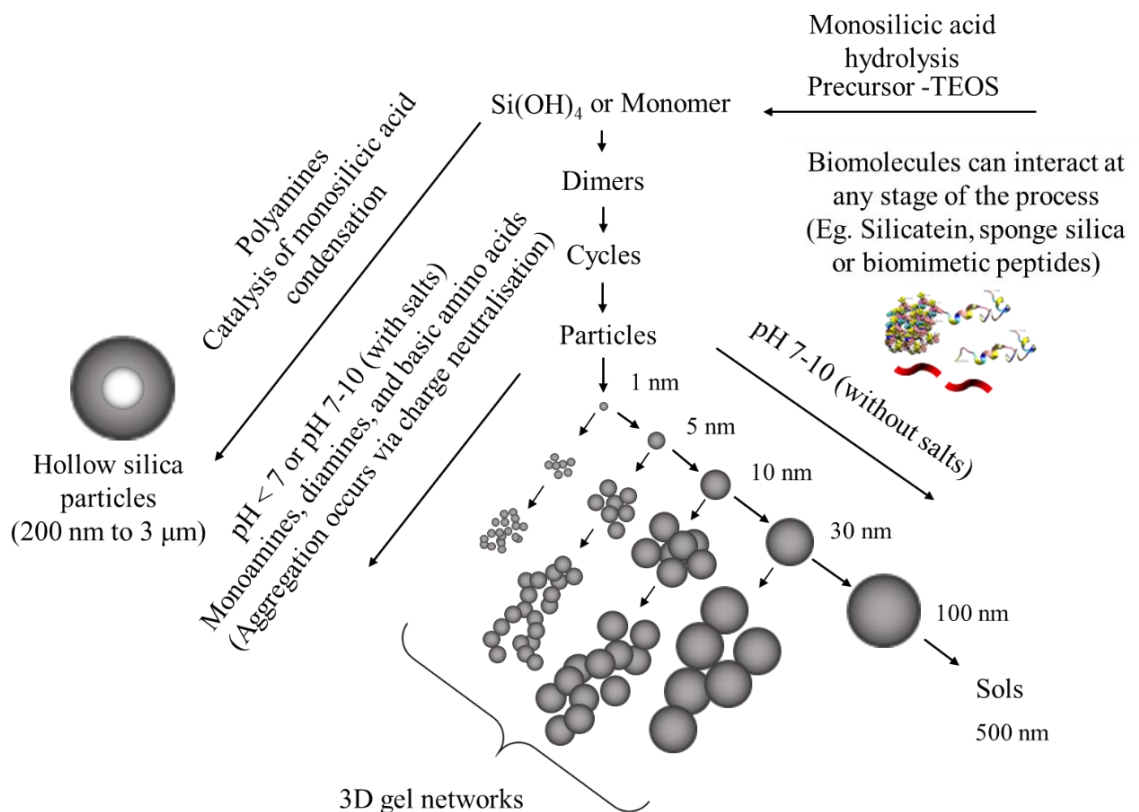
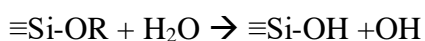


**Figure 1.4. Schematic representation of silica formation pathways from  $\text{Si(OH)}_4$  or orthosilicic acid through to dimers, oligomers, particles and sols.** Also, biomolecules are shown to act at any stage of the silica formation. Image adapted<sup>94</sup>.



At concentrations higher than the solubility of amorphous silica (~100 ppm), orthosilicic acid undergoes autopolymerisation between two orthosilicic acid molecules, forming a cyclic species with optimum number of Si-O-Si bonds. These cyclic structures later form the three-dimensional structure which makes the particle. This form of the oligomers aids the nucleation for stable particles to aggregate and forms a network or gel (Figure 1.4)<sup>115</sup>. Particles can continue to grow in circumneutral pH until the amount of soluble silica reaches the solubility of amorphous silica particle. In the presence of salt of other charged species, the repulsion between individual silica particle is reduced (or cancels out), leading to particle aggregation, forming a three-dimensional network. As the amount of orthosilicic acid decreases, smaller and more soluble particles of silica (< 5 nm) dissolve releasing silicic acid which gets deposited on bigger spheres by the process of 'Ostwald ripening'<sup>94,116</sup>. The process via which silica is synthesised in aqueous systems is dependent on the pH, the presence of salts, temperature and pressure in the system. In a natural environment silica formation occurs in the presence of various ions, and biomolecules, polyamines and proteins associating with silica from sponges which all will affect the condensation process for of silica<sup>94</sup>.

The structure of silica consists of a combination of oxygen and silicon forming silicates. The properties of a silica particle, regardless of its size, is largely dependent the chemistry of the silica surface. Silica is known to be sensitive to undergo hydrolysis in the presence of water. The process of hydrolysis converts siloxane bonds (Si-O-Si) of silica to silanol groups (Si-OH). The general mechanism via which silica gets hydrolysed with water is:



Literature studies have shown that organic molecules with polar bonds and water molecules are adsorbed onto silica surface via hydrogen bonding at silanol sites. These sites have the ability to both donate and accept a proton, resulting in a negative or positive charge respectively. These silanol groups can give silica either hydrophilic (silanol) or hydrophobic (siloxane) character by either accepting proton or by donating proton under the influence of aqueous solution. The pH plays an important role in deciding the type of groups present on the surface of silica<sup>117</sup>. For example, with increase in pH the silanol groups undergoes deprotonation giving more negative charge to the silanol groups<sup>117</sup>. The isoelectric point of pH was determined to be present at pH-2-3. Different forms of silanol groups found on the

silica surface include internal (Si-OH), isolated ( $\equiv\text{SiOH}$ ), geminal ( $=\text{Si}(\text{OH})_2$ ) and vicinal or bridged forms which can be seen in the Figure 1.5<sup>118</sup>.

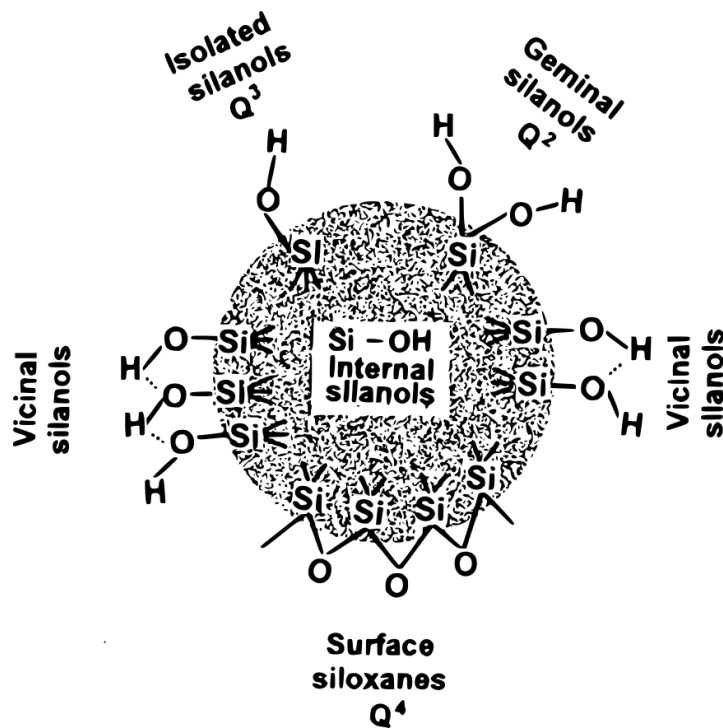


**Figure 1.5. Silica surface consisting of different types of silanol groups and their chemistry. Image reprinted<sup>119</sup>.**

Also, depending on the type of chemical solutions used during the Stöber silica process, the surface functionalisation of silica can be changed to either hydrophilic or hydrophobic surface. The hydrophobic silica surface consisting of methyl or phenyl groups can be achieved by using MTES (methyltriethoxysilane) and PTES (phenyltriethoxysilane). In the same way, by using TEOS (tetraethyl orthosilicate) and APTES ((3-Aminopropyl) triethoxysilane) the silica surface can be functionalised with pristine (amine) and amino propyl groups respectively. Therefore, these functionalised silica surfaces have been used to study the formation of cancer by monitoring the cell aggregation or disaggregation<sup>120–122</sup>. An example of this is the production of silica upon tissue culture polystyrene (TCP) and its application for further functionalization using fluorinated alkoxy silane. This has been shown to produce a material derived from cell culture media, which has differential adoption profile of serum, thence allowing for the better control of *in vitro* cancer cell aggregation-

disaggregation events<sup>122</sup>. Studies have also shown that with the right silica surface chemistry (i.e. hydrophilic or superhydrophobic film) may aid the adhesion and proliferation of cell<sup>120</sup>.

### 1.2.2 Silica biomolecule interactions and their applications

The growing applications of silica with chemically attached peptides or biomolecules in nanomedicine has driven researchers to focus on increasing their understanding of how peptides or biomolecules bind to silica, the type of interactions and the mechanisms involved<sup>4,10,122,123</sup>. In Figure 1.6 are shown a range of proposed interaction mechanisms involved at the silica-biomolecule interface. For example, Zhou *et al.*, (1999) proposed a mechanism by which silicatein- $\alpha$  (70% of the silicatein filament obtained from sponges) catalyses the hydrolysis of alkoxysilanes at neutral pH via an acid/base reaction through the activity of the serine and histidine side chains, specifically, between the hydroxyl group of serine-26 and the imidazole side group of histidine-165 (Figure 1.6, A)<sup>123</sup>. Because of high structural homology of silicatein- $\alpha$  to the hydrolytic enzyme, cathepsin L; this reaction was based on the mechanism of peptide bond hydrolysis by the analogous well known protease Cathepsin-L<sup>123</sup>. Nicklin and co-workers studied the absorption of serum proteins to specific surfaces<sup>122</sup>. In this study, it was demonstrated that fluorinated silica surfaces (FS) provide the necessary environment to selectively adsorb serum proteins from the medium, which, were able to disrupt cellular adhesion and promote cellular aggregation (Figure 1.6, B). Moreover, the capacity of the FS surface to support cellular adherence was seen to increase with culture time. The properties of the functionalised surface facilitate the study of cancer cell aggregation and disaggregation as a single dynamic process *in vitro*, as the cells biological response towards the material changes in tandem with the surface properties.

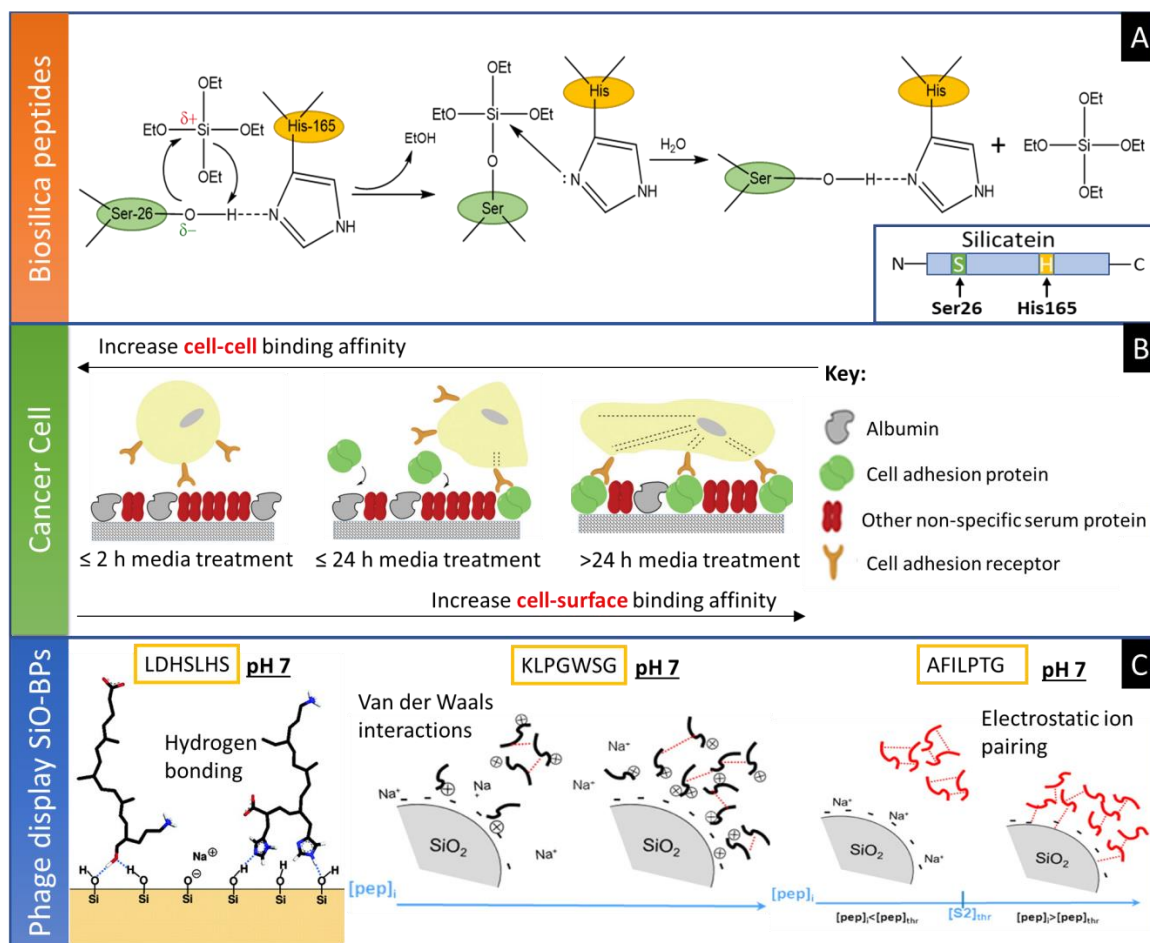


**Figure 1.6. Proposed interaction mechanisms involved at the silica-biomolecule interface** A) Mechanism proposed for alkoxy silane catalytic hydrolysis by silicatein active sites (serine and histidine) reprinted with permission<sup>123</sup>. B) competitive protein exchange occurring upon the fluoro-silica during cell culture in serum supplemented medium reprinted with permission<sup>122</sup>. C) type of interactions occurring at the silica-peptide interface of phage displayed peptides reprinted with permission<sup>4,10</sup>.

In an alternative approach, phage displayed peptides of different charge at neutral pH have also been studied at the aqueous silica interface (Figure 1.6, C)<sup>4,10</sup>. These peptides: KLPGWSG (positively charged), AFILPTG (neutral) and LDHSLHS (negatively charged); showed the role of electrostatic/hydrophobic interactions and hydrogen bonding at the aqueous silica interface. The study was also able to show that at low concentrations of peptide, peptide self-assembly is more likely favoured than silica-peptide interactions, thus, aggregates stay in solution until a certain concentration is reached<sup>4,10</sup>. Our research group have shown and given examples concerning silica-biomolecule adsorption mechanisms. A few examples include, study of the particular properties of the material itself (e.g. silica<sup>4,10,124</sup> and ZnO<sup>125–127</sup>), we have shown that the size of particles<sup>4,10,44</sup> and charge/ functionality on

particles<sup>4,107</sup> have clear effects on the binding of small peptides to minerals; and the route by which a material is formed<sup>125–127</sup> by moderating peptide mineral interaction.

As yet, many other studies regarding silica-biomolecule adsorption mechanisms have been reported, and have been summarized in highly recommended reviews such as peptide binding mechanisms on nanoparticle surfaces<sup>9</sup>, molecular biomimetics using genetically engineered peptides<sup>60</sup>, proteins and peptides-directed inorganic material synthesis<sup>5</sup>, amino acid adsorption on mineral surface<sup>128</sup>, computational modelling of silica-biomolecule interactions<sup>129</sup>, simulations studies and recognition mechanisms of biomolecules<sup>130</sup> and fundamental theoretical and experimental approaches to understand biomolecule-biomaterial interactions<sup>131</sup>.

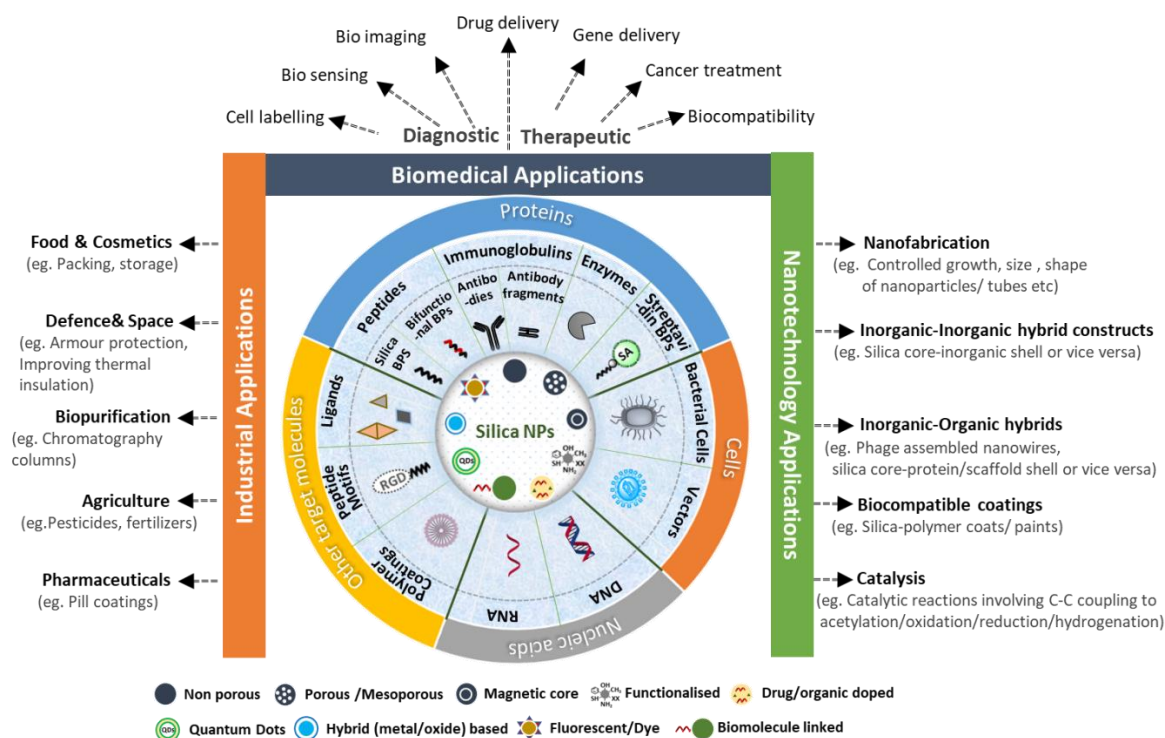


**Figure 1.7: Schematic representation of Silica-biomolecule interactions and their applications. Figure adapted from<sup>132</sup>.**

Continued research efforts by researchers has led to silica being a key material in the design of novel bio-nanostructures, further broadening its application from nanotechnology to biomedical and further industrial fields as shown schematically in Figure 1.7. Further, a review published by Thota and Perry<sup>12</sup> showed the recent advancements of solid material binding peptides including their applications and patents that have been reported.

Four examples specific to the applications of silica-biomolecule attachment are shown in Figures 1.8 and 1.9. The therapeutic use of mesoporous SiNPs as a potential drug delivering agent involving a variety of pharmaceutical drugs including ibuprofen, doxorubicin, docetaxel, therapeutic genes (plasmid DNA, antisense oligonucleotides, and siRNA), and therapeutic protein cytochrome C (Figure 1.8, A)<sup>133</sup>. A controlled silica biomineralization process involves selective exposure of lysine amino groups on genetically engineered tobacco mosaic virus templates, chemically conjugating the synthetic peptides and the subsequent final coating with silica (Figure 1.8, B).

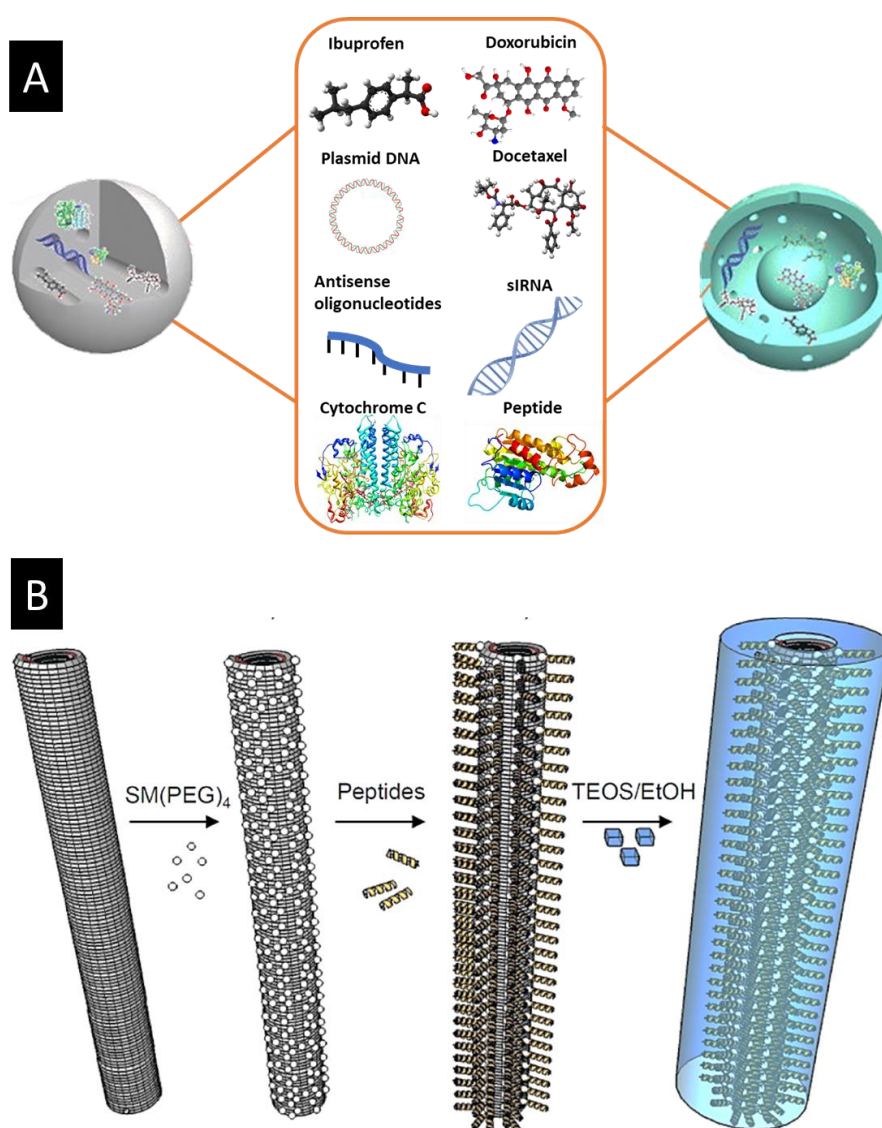


**Figure 1.8: Specific applications of silica-biomolecule attachment reported:** (A) mesoporous silica nanoparticles acting as delivery vehicles carrying potential drugs, peptides and proteins reprinted with permission from<sup>133</sup>. (B) controlled silica biomineralization process using peptide equipped TMV (tobacco mosaic virus) as templates reprinted with permission from<sup>134</sup>.

Altintoprak *et al.*, (2015). Jin and co-workers (Figure 1.9, A) synthesized a DNA-silica complex able to (i) condense DNA through the positively charged quaternary ammonium group of N-trimethoxysilylpropyl-N,N,N-trimethylammonium chloride (TMAPS) and (ii) stabilize silica mineralization by co-condensing with the silica source, in this case TEOS. Further, the formation of various DNA liquid crystals was achieved by varying DNA concentration and the TMAPS/DNA molar ratio, which allowed control of the DNA interaxial separation<sup>135</sup>.

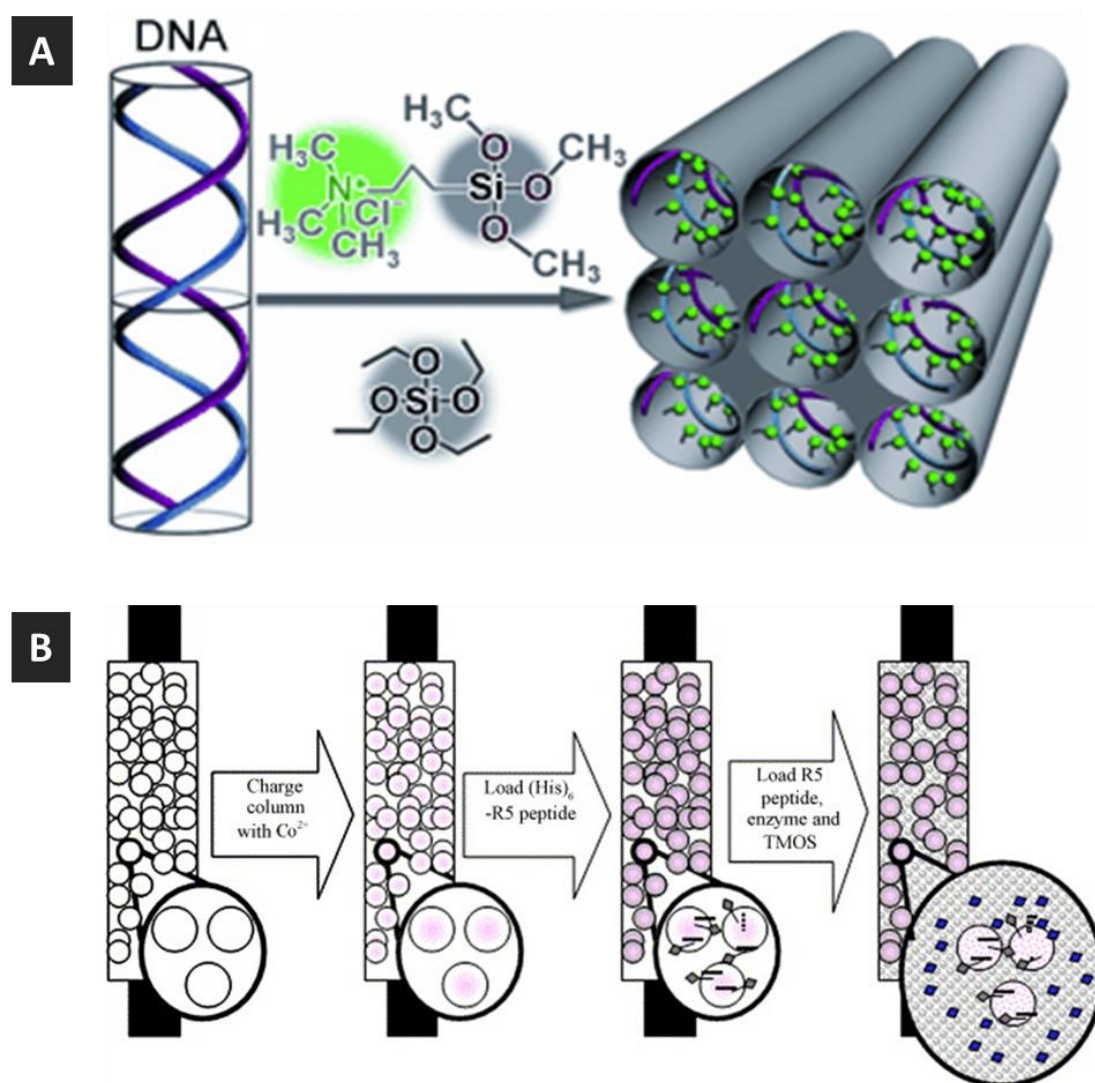


**Figure 1.9: Specific applications of silica-biomolecule attachment reported:** (A) Silica mineralisation induced by DNA liquid crystals reprinted with permission from <sup>135</sup> and (B) enzyme immobilization in silica nanospheres via attaching to cobalt coated resin by affinity binding where agarose beads (○),  $\text{Co}^{2+}$  coated agarose beads (○), his-tagged peptide (—), enzyme (■) and silica nanospheres (■) reprinted with permission from<sup>136</sup>.

Luckarift and co-workers (Figure 1.9, B) reported a method for preparation of a solid support for immobilization of the enzyme butyrylcholinesterase. For this, a pre-packed column with agarose beads was charged with cobalt (II) ions for the attachment of the His-tag R5 peptide. Afterwards, the tetramethyl orthosilicate (TMOS) solution together with the enzyme were added to the system and silica nanospheres precipitated onto the peptide bound to the column, subsequently, immobilising the enzyme. These silica-immobilised enzyme reactor columns were used as a model liquid chromatography system to effectively screen cholinesterase inhibitors<sup>136</sup>.

### 1.3 Combinatorial Display Process on Nanomaterial Surfaces

The connection between inorganic materials and biomolecules is not new in nature and exists naturally through the process of biomineralization. Through this, complex inorganic nanostructures including metal oxides and minerals are synthesized by certain species like magnetite, an iron oxide (Mms Proteins) in bacteria<sup>137-139</sup>, silica (silaffins) in diatoms<sup>96,97,103-106</sup>, silica (silicatein) in sponges<sup>101,102</sup>, aragonite and calcite (chitin, proteins and polysaccharides) in mollusks<sup>140</sup>. Though artificial processes have been used to reproduce the biominerals or materials, their quality is challenging. In order to meet the quality and demand, several research groups started a quest for better alternate routes to produce more efficient, reliable and bulk bionanomaterials using inspiration from nature.

This led to the discovery of novel biomimetic approaches where peptides having affinity towards any target inorganic material can be isolated and practically reproduced using a range of combinatorial display techniques (Figure 1.10) such as phage display<sup>25-30</sup>, bacterial/yeast display<sup>31-34</sup>, ribosome, mRNA or cDNA display<sup>35-41,141</sup> and rational design<sup>42-44</sup>.



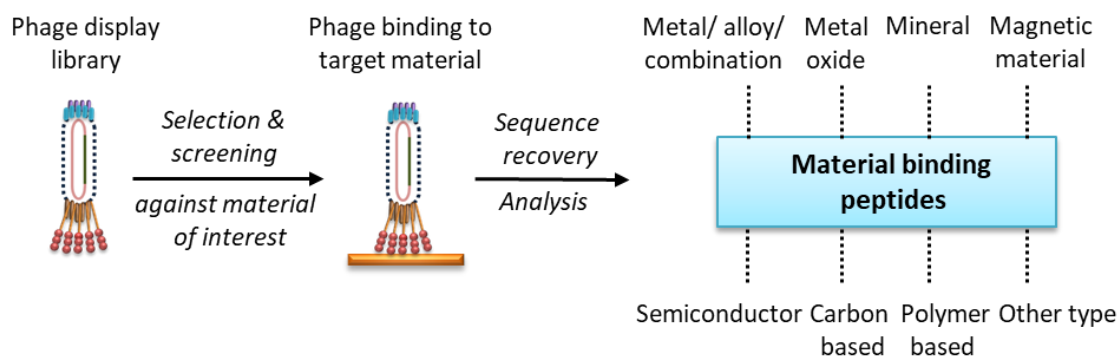


**Figure 1.10: Schematic representation of different types of combinatorial display approaches such as phage display, bacterial surface display, yeast surface display, ribosome display, mRNA or cDNA display and rational design used for selecting and screening of inorganic material<sup>12</sup>.**

So far, a range of biomimetic peptides showing specific affinity and molecular recognition for metals ( $\text{Ag}^{142-144}$ ,  $\text{Au}^{7,19}$ ,  $\text{Pt}^{66}$ ,  $\text{Pd}^{142}$ ), metal oxides ( $\text{SiO}_2^{4,10,24,65,145}$ ,  $\text{ZnO}^{146,147}$ ,  $\text{TiO}_2^{8,59,148}$ ,  $\text{Fe}_2\text{O}_3^{149,150}$ ,  $\text{IrO}_2^{151}$ ,  $\text{Al}_2\text{O}_3^{10,152}$ ,  $\text{Cu}_2\text{O}^{146}$ ), minerals (calcite, hydroxyapatite, graphite, mica, sapphire)<sup>153-155</sup>, semiconductors ( $\text{CdS}$ ,  $\text{GaN}$ ,  $\text{GaAs}$  and  $\text{ZnS}$ )<sup>23,86,156</sup>, carbon materials (graphene, carbon nanotubes)<sup>157,158</sup> and polymer materials<sup>159,160</sup> have been isolated as shown in Figure 1.10.

#### 1.4 Applications of Inorganic Material Binding Peptides

Material binding peptides have attracted considerable interest in the development of innovative nanostructured materials in particular because of their promising and growing applications in nanobiotechnology. These material binding peptides are also called inorganic binding peptides (IOBPs) or substrate binding peptides (SUBPs) or solid binding peptides (SBPs) or genetically engineered peptides for inorganics (GEPs). Material binding peptides are short amino acid peptide sequences that are genetically constructed and show specific affinity to a target material using combinatorial display approach. Although nanomaterials have been designed and produced decades ago, their utilization in nano- or bio-technology is limited due to poor solubility, stability and biocompatibility issues. The surface properties of nanomaterials including solubility, structure, charge and stability are all factors that determine its ability to interact safely in a system<sup>161</sup>. However, several strategies have been developed to overcome the toxicity concerns and eventually, material binding peptides came

into existence by managing greater control over the nanomaterials without compromising their physical, chemical and functional properties. These material binding peptides act as molecular linkers (Figure 1.11) by mediating immobilization between inorganic materials and biomolecules thereby replacing traditional chemical conjugation methods (e.g. coupling reactions) which required harsh chemical reagents and high temperatures, leading to the reduced stability and biocompatibility of the biomolecule to the nanomaterial surface.

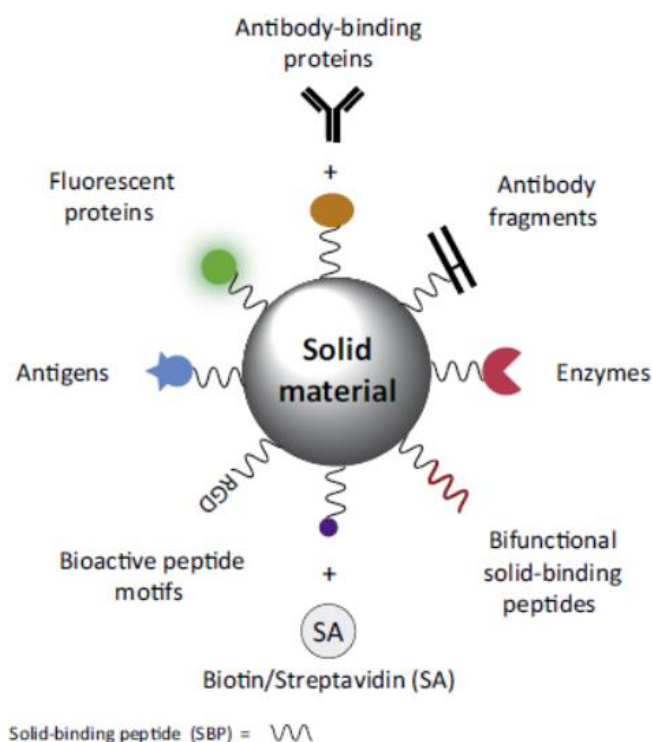


**Figure 1.11. Schematic representation of solid binding peptides as molecular linkers to link solid materials like nanoparticles and to a wide range of biomolecules such as antigens, antibodies, peptides, proteins, enzymes and functional peptide motifs. Image reproduced<sup>11</sup>.**

Inorganic material binding peptides have been shown to have many applications, including nanomaterial synthesis, self-assembly, coatings, biomolecule immobilization as shown in Figure 1.12. Specific examples of these applications are discussed in the following section. The material binding peptides have been used to produce a biocompatible coating which bind to the nanomaterial in highly-specific manner, which under biological condition are usually unable to initiate a cytotoxic or immunogenic response. An example of this is the lanthanide oxide binding short peptide sequence, known as RE-1, which was

found to form a coating on the surface on the nanocrystal. The stable immobilization of RE-1 on the lanthanide oxide nanocrystal eliminated the cytotoxicity by preventing sedimentation and reducing non-specific interaction with cell *in vivo* (mice) and *in vitro* (HeLa cells)<sup>162,163</sup>. The immobilization of biomolecules onto nanomaterial is believed to occur via weak interactions (such as hydrogen, electrostatic and hydrophobic bonding), direct coupling or coupling reaction on self-assembled monolayers (SAMs). However, under these conditions the biomolecule can attach to surfaces with changing positions and orientation, thus causing a loss in functional property<sup>164–166</sup>.

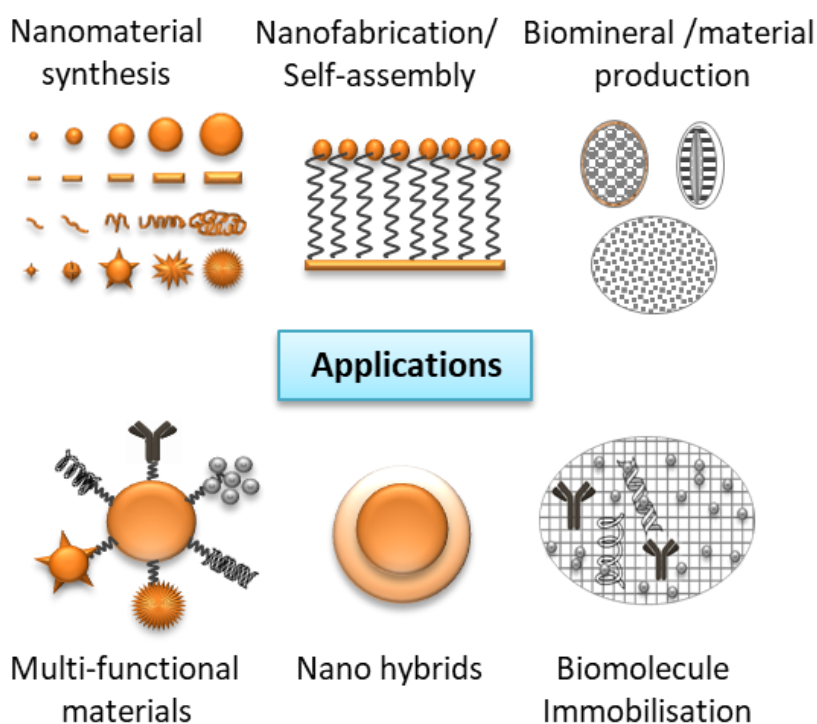


**Figure 1.12: Schematic representation of inorganic material binding peptides and applications.**

Discrimination of different materials in proximity is a critical requirement in nanofabrication technologies (e.g. lab-on-chip, microfluidics and microarray). Material binding peptides is ideal for this type of technology as it binds to nano- and macro- materials with high selectivity. Such example of material binding peptide ability has been demonstrated for the highly selective simultaneous co-assembly of varying fluorescein material on gold/silica

surface<sup>167,168</sup>. In contrast, SAMs lack the capacity to differentiate materials with similar surface such as gold and silver<sup>169</sup>.

The functionalization of nanomaterial with biomolecules such as enzymes and antibodies has been of interest for diagnostics and therapeutic technologies to improve enzyme activity, loading and stability as well as sensing, imaging and targeting<sup>170</sup>. The application of enzyme coupled nanomaterials is of specific interest for industrial processes such as bioremediation and biofuel production<sup>171</sup>. Earlier immobilization methods developed (adsorption, entrapment and covalent attachment) are not ideal as it can involve the use of functional groups that alter the active site of the enzyme, thus changing its catalytic properties<sup>172</sup>. Material binding peptides are useful for this purpose as it doesn't change catalytic functions during the immobilization of enzyme onto nanomaterials. An example of this is the use of gold-binding peptide (GBP1) for the self-assembly of organophosphorus hydrolase (OPH) onto gold nanoparticle-coated sensor<sup>173</sup>. Results showed that the coupled GBP1-OPH had retained its native conformation post immobilization and showed comparatively faster and more sensitive detection of organophosphorus pesticide than unmodified enzyme. Such reaction can also be economically friendly through the attachment of enzymes to magnetic nonmaterial, allowing easy recovery and reusability<sup>171</sup>. Some material binding peptides can bind to their respective materials even under extreme industrial conditions (pH and temperature). In specific, a silica-binding peptide (GGGGS) has shown aid the immobilization of thermostable enzymes on silica containing material at varied pH range (5-9 pH) and high temperature (80°C)<sup>174</sup>.

For immobilization of antibodies with nanomaterial, a novel method has been established to tackle the low immunogenicity of antibodies to produce material-binding antibodies using material binding peptides; conventional methods also often lead to unpredictable changes in the orientation on the antibody which decreased the density and availability of antigen-binding sites. For this new method, genetically engineered antibodies are grafted onto material binding peptides to form a fused protein, which then undergoes phage display and selection. Recent study have use to facilitate antibodies for the self-assembly of hybrid nanomaterial<sup>175</sup>. However, the use of antibodies as scaffolds for material binding peptides is complex and lacks versatility as it requires the initial modification of the antibodies. Using antibody-binding proteins (ABPs) that binds easily to the Fc region of an antibody can ensure the right orientation, thus avoids the prior modification of the antibody for increased versatility while retaining their biological activity<sup>176,177</sup>. Recent study has also shown the

ability of specific material binding peptides (zinc oxide-binding peptide, ZBP) to be used for the delivery of tumour-specific antigens into dendritic cells (DCs). The ZBP enables the assembly carcinoembryonic antigen (CEA) on Fe<sub>3</sub>O<sub>4</sub>-ZnO nanoparticle. Results from the study on mice immunized with modified DCs showed rapid recognition of the ZBP-CEA functionalized particle by the DCs, leading to suppressed tumour growth and prolonged survival when compared to the control mice<sup>11,178</sup>.

An alternative to using antibodies is bioactive peptide motifs, which are short amino acid sequences that can serve as biorecognition elements. Compared to antibodies, bioactive peptide motifs can easily be engineered and are stable in a range of conditions but unfortunately, contain several reactive sites which encourage non-specific coupling and orientation during bioconjugation process. The orientation of bioactive sensors during immobilization can be controlled using material binding peptides by forming bifunctional peptides. Synthesis of these peptides generally involves glycine-rich spacers between both functional regions which provided flexibility and prevents spatial constrains. However, it cannot be certain if a bifunctional peptide will retain the properties of both the bioactive peptide and the material binding peptides, thus further changes will be necessary for specific functionality<sup>179-181</sup>.

Studies by Brown (1992), pioneered the utilization and isolation of material binding peptides, initially exploring iron oxide binding peptides from cell surface libraries<sup>149</sup>, to later isolating gold binding peptides from bacterial cell surface display library<sup>19</sup>. The gold binding peptides isolated has had significant application in various human studies from becoming material synthesisers<sup>22</sup>, peptidic linkers for immobilization of nanomaterials<sup>180</sup>, protein fusion partners for oriented protein immobilization<sup>182</sup>. Whaley *et al.*, (2000), reported the first instance of positively charged gold binding peptides selected with phage display using gold powder as target material<sup>23</sup>. The same group of researchers, also isolated gold binding peptides carried out in thin gold film. In this study, the peptide was displayed on the pVIII phage coat protein = and was used to assemble gold nanoparticles while additional peptides expressed on the same coat protein were used to create 2D optical assemblies with CdSe nanocrystals<sup>183</sup>. Naik *et al.*, (2002), also reported the isolation of another gold binding peptide (AG3), which originally was targeted for silver surfaces but can also be used for the synthesis of gold nanoparticles<sup>184,185</sup>. Recent study by Kim *et al.*, (2008) has used PD approach and gold powder as target material for the isolation of gold binding peptides; one peptide called Midas-2 was specifically used for the synthesis of gold nanoparticle, which

yielded poly-disperse nanoparticles. Various mutation-based analysis was also carried out by replacing amino acid groups with glycine, to investigate the relationship between primary structure of the binding peptide and the shape-size of the nanoparticle synthesized. Midas-11 (a mutant of Midas-2) exhibited to produce large gold platelets with a width of 24  $\mu\text{m}$  and thickness of 30-150 nm, in both hexagonal and trigonal planar<sup>186</sup>. The work presented by Kim *et al.* and Brown *et al.* are both good examples of specific material binding peptide properties used in controlling size and shape of nanostructures.

Similar to gold, silver binding peptides were also screened and selected for binding with acid etched nanosized silver particles. The isolated 12-mer peptides, AG3 and AG4, were identified using localized surface plasmon resonance band, according to the ability to bind to silver and the capability to form silver nanoparticles<sup>186</sup>. Immobilized AG4 has also demonstrated the ability to grow a range of silver nanoparticles in a microfluidic system made of elastomers. The silver binding particles in solution were studied using nuclear magnetic resonance (NMR), and the data showed that residues Leu5, Phe6 and Arg7 were suggested to be the point of contact for the multiple AG4 peptides bound during the synthesis of the silver nanoparticle<sup>186</sup>.

Titanium is also a bionanomaterial that has widely studied and used due to its good biocompatibility and its application for implant material. For this reason, Liu *et al.*, (2010), screened peptides from 12-mer and 7-mer PD libraries for a commercially used titanium material (cp-Ti). The researchers were able to detect surface bound clones, and characterize the binding of the phages on cp-Ti using confocal microscopy<sup>187</sup>. The metal oxides form of titanium is titanium oxide, also known as titania ( $\text{TiO}_2$ ), and has also been used in various applications for biomedical systems and optoelectronic devices. Material binding peptides have also been used in conjunction with titania for the fabrication of conductive nanostructure (e.g., nanofibers and nanowires), for their application in nanoelectronics (i.e. power cells, computer processor and optical fibres). The purpose of the material binding peptide in this case is to mediate the synthesis of an inorganic-inorganic nanocomposite (see Figure 1.12). In a paper by Inoue *et al.*, (2014), a genetically modified self-assembling case-shaped protein (CDT1) was used to co-display a 12 single-walled carbon-nanotubes (SWNT)-binding and  $\text{TiO}_2$ -mineralising peptide. This bifunctional protein was used to mediate the formation of thin layers of titania on SWNTs. After further processing to eliminate protein using high temperature, a highly-conductive nanocomposite was produced for its application in dye-sensitised solar cell (DSSC) photoelectrodes<sup>188</sup>.

Silica is another metal oxide material which has similar applications to titania. Silica binding peptides was first isolated from a phage library by Naik *et al.*, which contained high amounts of arginine and histidine amino acid groups and displayed the ability to precipitate silica from silicic acid<sup>24</sup>. Another group of researchers were able to identify silica binding peptides, which is high in proline amino acid groups, that has affinity towards single crystalline quartz surface. The analysis of these strongly binding peptides was carried out using a surface plasmon resonance spectroscopy (SPR)<sup>189</sup>.

Another metal oxide that has application in optoelectronic application is Zinc oxide (ZnO)<sup>190</sup>. Certain zinc oxide binding 12-mer peptides have already been identified using micrometre sized ZnO particles as the target material; the identified peptides were also able to distinguish between ZnO and ZnS<sup>147</sup>. Another study has proposed a novel method to synthesize fluorescent ZnO particle with unique morphology, not previously achieved with low temperature approach which required complex chemicals<sup>191</sup>. Though the research on using phage display technology to discover material binding peptides for the metal oxides mentioned here (titanium oxide, silica, zinc oxide) is vast, there is still more to be explored for the remaining oxide materials. A possible reason for this may be because other metal oxides are not as widely used and/or that peptides may not be suitable for functionalization of other metal oxide surfaces under their specific processing.

## 1.5 Motivation of Project and Objectives

Nature is always an inspiration and mystery when it either comes to synthesizing materials either on its own or by using biomolecules thereby providing greater control of physical, chemical and biological parameters<sup>60,94,183,185</sup>. One way to find solutions is to mimic nature. However, to mimic nature's method of synthesizing materials needs the identification of functionally active biomolecules as well as the capacity to direct the synthesis in *in vitro* conditions. Molecular recognition is the central principle of all biological systems. Using this molecular binding feature, several systems have been well studied including peptide-protein, antigen-antibody, enzyme-protein and nucleic acid-protein interactions. With increasing use of biopanning to display material specific peptides and then use those identified peptides to reproduce same materials *in vitro* or *in vivo* under controlled conditions that have potential applications in biomedical and bio-nanotechnology have grown rapidly, it is very important to elute, identify and verify the authenticity of genuine target binders without falling into the net of non-specific binders. Though, significant progress has been made in selecting and screening of biomolecule binding peptides, but when the target is a mineral/ inorganic material surface it is challenging due to their complex surface chemistry. It is still unclear whether we are eluting and recovering all of the strong binders from the available phage library and whether there are differences between library batch to batch behaviour. Amorphous silica nanoparticles have been selected as a target material because of its importance as 20<sup>th</sup> century materials and for their growing potential applications due to low toxicity and biocompatible properties. The M13 Ph.D.-7 library system was selected because this is one of the best-characterised and most reliable recommended libraries. Compared to 12-mer peptides, shorter 7-mer peptides are easier to work with as they can be easily exposed to solvent environments during the process of phage display, unlike 12-mer peptides which are known to degrade, are harder to purify and are unstable in harsh conditions (at high temperature and changes in pH). In addition, the increased length of the sequence in 12-mer peptide library may result in identifying sequences with multiple weak interactions, rather than selecting few strong interactions. However, the 7-mer peptide sequences are useful targets that require binding elements concentrated in a short stretch of aminoacids. Furthermore, not many studies on heptapeptides which have affinity toward silica have been reported using the Ph.D.- 7 library. Thus, keeping in mind the limitations of using 12-mer peptides, 7-mer peptides were chosen to be studied as they easy to work with and



have various applications in nanomaterial synthesis<sup>24,65,192</sup> and for understanding mechanism via which silica-biomolecules interact<sup>4,59,107,124,132</sup>.

The main goal of the project was to develop alternate approaches to elute and identify material binding peptides using phage display technique. Then, to explore and understand the influence of electrostatic/non- electrostatic interactions on the molecular scale in governing biomolecule selection.

Specific objectives of the project were:

- Isolate and identify silica binding peptides (7mers) through biopanning against hydrophilic silica by exploring different elution strategies.
- Investigate and predict the behaviour of biomolecules (sequence diversity, functionality and promiscuity) such as the identified peptides by looking at their physicochemical properties and related bioinformatics.
- Study and understand *in vitro* interactions between selected peptides isolated by phage display and silica surfaces in solution.
- Explore conditions such as pH, detergent, washing and elution buffers needed to bind or detach the peptide from silica surfaces via electrostatic/ non-electrostatic interactions in solution.

## **Chapter 2: Instrumentation and Experimental Section**

In brief, this chapter introduces the instrumental principles and experimental methods including the materials that have been used to identify mineral binding peptides with reference to silica, to synthesize and characterize peptides and/ or silica nanoparticles and to study their interactions. The phage display of biopanning technique has been used to select NEB Ph.D.-7 mer library against silica nanoparticles which were amplified in bacteria by a repetitive process. The amplified phages from the biopanning round of interest were isolated and phage clones collected by carrying out a blue-white screening process. Using polyethylene glycol (PEG) solution, single-stranded phage DNA has been precipitated and the purity of the DNA analysed using a NanoDrop spectrophotometer. Further, these DNA samples have been sequenced with a modified Sanger sequencing method by Eurofins Genomics UK and the authenticity of sequences determined using bioinformatics tools such as in-silico sequence convertor; multiple sequence alignment programs (Clustal W2 and Clustal Omega), npeptide property calculators (Innovagen and Bachem) and peptide database search engine (MimoDB tools) respectively. Selected peptides identified by the phage display process have been synthesized using solid phase peptide synthesis (SPPS) protocol while the quality and purity of these synthesized peptides have been analysed by matrix-assisted laser desorption ionization time-of-flight (MALDI-TOF) mass spectrometry and high-performance liquid chromatography (HPLC) respectively. The silica nanoparticles used for phage display and binding studies were already available in the Perry laboratory and had been synthesized by the Stöber process and characterized using dynamic light scattering (DLS), zeta potential and transmission electron microscopy (TEM). A range of quantitative and qualitative techniques including fluorescamine assay, Raman spectroscopy and transmission electron microscopy has been used to study the binding of peptides onto the surface of silica nanoparticles.

## 2.1 Materials and Methods

### 2.1.1 Materials

#### 2.1.1.1 Heptapeptide phage display peptide library (Ph.D.<sup>TM</sup>-7)

In this study, Ph.D.-7 phage display peptide library kit (#E8100S) purchased from New England Biolabs (NEB) has been used for panning against already characterized amorphous silica nanoparticles of size  $82 \pm 4$  nm. This library is based on M13 phage vector engineered for pentavalent display of peptides on pIII minor coat protein. The Ph.D.-7 phage display peptide library kit was supplied with 100  $\mu$ l of Ph.D.-7 library (enough for 10 biopanning experiments) containing  $1 \times 10^{13}$  pfu/ml ( $2.8 \times 10^9$  independent clones supplied in TBS with 50% glycerol). Also, this library contains roughly  $10^9$  electroporated sequences amplified once to give approximately 100 copies of each sequence in 10  $\mu$ l of the provided phage peptide library.

For the entire phage display work, two separate aliquots of NEB Ph.D.-7 phage library kits (Lot: 0211212 and Lot: 0221501) were used at different times of this project. The first library (Lot: 0211212) batch was used for initial biopanning and repanning experiments via following traditional biopanning process as described in chapter 3. As, the first batch of library was finished for more panning experiments, a second batch (Lot: 0221501) was ordered and used to test the optimised biopanning approach (alternative three step elution process) as defined in Chapter 4.

#### 2.1.1.2 *E. coli* host strain (K12 ER2738)

F' *proA+B+ lacIq  $\Delta$ (lacZ)M15 zzz::Tn10(TetR)/fhuA2 glnV  $\Delta$ (lac-proAB) thi-1  $\Delta$ (hsdS-mcrB)5*. The *E. coli* host strain ER2738 was supplied with 50% glycerol and included within the NEB Ph.D.-7 phage display peptide library kit (#E8100S). This *E. coli* F<sup>+</sup> strain has been used for the entire phage display work for propagating and screening the M13 phage clones.

#### 2.1.1.3 Silica nanoparticles

The same batch of amorphous hydrophilic silica nanoparticles of size  $82 \pm 4$  nm was used as target for biopanning and subsequent binding studies that were already available in the Perry laboratory and had been synthesized by the Stöber process and characterized using varied techniques<sup>4,107</sup>. More information about the properties and measurements of silica particles is described in Table 2.6 under the section 2.1.2.6 in this chapter.

#### 2.1.1.4 Phage display reagents

All the phage display work was performed under aseptic conditions using a Bunsen burner, disinfectants and by sterilizing the chemicals and materials used in the process for 15 minutes under 1.5 atm at 121 °C in an autoclave. All other chemicals and reagents used for phage display or biopanning were purchased from Sigma Aldrich and Fisher scientific. These include LB broth and LB agar from Fisher scientific; and the remaining chemicals including isopropyl  $\beta$ -D-1 thiogalactopyranoside (IPTG), 5-bromo-4-chloro-3-indolyl  $\beta$  D galactopyranoside (X-gal), tris-HCl, sodium chloride (NaCl), polyethylene glycol (PEG-8000), TBS tablets, Tween 20 detergent, sodium iodide (NaI), sodium azide ( $\text{NaN}_3$ ), ethylenediamine tetra acetic acid (EDTA), tetracycline, glycine-HCl, magnesium chloride ( $\text{MgCl}_2$ ) and triethylamine (TEA) were brought from Sigma Aldrich.

The following stock solutions were prepared prior to starting the biopanning procedure and kept for use as required.

##### 2.1.1.4.1 Washing buffers

- **TBS buffer stock solution**

One tablet (purchased from Sigma Aldrich) dissolved in 15 ml of deionized water yields 50 mM Tris and 150 mM sodium chloride, pH 7.5, at room temperature (25 °C). Thirty TBS tablets were dissolved in 300 ml of deionized distilled water and the solution was sterilized by autoclaving for 15 minutes under 1.5 atm at 121 °C. After autoclaving for 15 minutes the pH was adjusted to 7.5 using 1 M HCl concentration and stored at room temperature.

- **TBST buffer solution (TBS with 0.1%-0.9% [v/v] Tween 20)**

An appropriate amount of Tween 20 detergent (volume fraction) (Sigma Aldrich) was added to the sterilized TBS solution of pH 7.5 to reach the desired detergent concentrations as below.

20  $\mu$ l of Tween 20 was added to 20 ml TBS to get 0.1% TBST (TBS +0.1% [v/v] Tween 20)

60  $\mu$ l of Tween 20 was added to 20 ml TBS to get 0.3% TBST (TBS +0.3% [v/v] Tween 20)

100  $\mu$ l of Tween 20 added to 20 ml TBS to get 0.5% TBST (TBS +0.5% [v/v] Tween 20)

140  $\mu$ l of Tween 20 added to 20 ml TBS to get 0.7% TBST (TBS +0.7% [v/v] Tween 20)

180  $\mu$ l of Tween 20 added to 20 ml TBS to get 0.9% TBST (TBS +0.9% [v/v] Tween 20)

#### 2.1.1.4.2 Elution buffers

- 0.2 M Glycine-HCl, pH-2.2, pKa = 2.35  
446.12 mg of Glycine-HCl was dissolved with 50 ml of autoclaved nuclease free water and pH was adjusted to 2.2 by adding drop by drop of 0.2 M HCl. Stored at 4 °C.
- 4 M MgCl<sub>2</sub>, pH-6.1  
40 g of magnesium chloride hexahydrate was dissolved with 50 ml of distilled water and pH was noted as 6.1. Stored at 4 °C.
- 100 mM Triethylamine, pH-11  
1.75 ml of concentrated triethylamine solution was dissolved in water and made up to the final volume to 50 ml with distilled water. The pH was noted as 11. Stored at 4 °C.
- 0.2 M Glycine-HCl, pH-7  
446.12 mg of Glycine-HCl was dissolved with 50 ml of autoclaved nuclease free water and pH was adjusted to 7 by adding drop by drop of 1 M NaOH. Stored at 4 °C.
- 0.2 M Glycine-HCl, pH-11 pKa = 9.78  
446.12 mg of Glycine-HCl was dissolved with 50 ml of autoclaved nuclease free water and pH was adjusted to 11 by adding drop by drop of 1 M NaOH. Stored at 4 °C.

#### 2.1.1.4.3 Culture media

The culture media and reagents used for culturing the phage or bacteria were purchased from Sigma Aldrich and Fisher scientific. The LB broth and LB agar media were obtained from Fisher scientific; while the chemicals tetracycline isopropyl β-D-1 thiogalactopyranoside (IPTG) and 5-bromo-4-chloro-3-indolyl β D galactopyranoside (X-gal) were bought from Sigma Aldrich.

- **Luria-Bertani (LB) agar medium**

17.5 g of LB agar Lennox powder (tryptone: yeast extract: sodium chloride: select agar) was dissolved in 500 ml of distilled water and was sterilized by autoclaving for 15 minutes under 1.5 atm at 121 °C. In order not to solidify, the agar media was stored at 45 °C to 55 °C until the media was used for preparing LB agar and X-Gal/ IPTG plates.

- **Luria-Bertani (LB) broth medium**

2g of LB broth Lennox powder (tryptone: yeast extract: sodium chloride) was dissolved in 100 ml of distilled water. Stored at room temperature after autoclaving at 121 °C for 15 min.

- **Tetracycline stock solution**

200 mg of tetracycline (20 mg/ ml) was taken and made to the final volume of 10 ml by adding 70% ethanol. To protect the light sensitive tetracycline stock, the tube was wrapped with aluminium foil and stored in the dark at -20 °C.

- **X-Gal/ IPTG stock solution**

0.31 g of IPTG and 0.25 g of X-Gal were dissolved and made up to a volume of 6.25 ml with dimethyl formide (DMF). To protect the light sensitive X-Gal/ IPTG stock solution, the tube was wrapped with aluminium foil and stored in dark at -20 °C.

#### 2.1.1.4.4 Other stock solutions

All other chemicals and reagents used for preparing stock solutions including sodium chloride (NaCl), polyethylene glycol (PEG-8000), sodium iodide (NaI), sodium azide (NaN<sub>3</sub>), ethylenediamine tetra aceticacid (EDTA), Tris base, Tris-HCl and 1M HCl were brought from Sigma Aldrich.

- **PEG/ NaCl stock solution** (20% (w/v) PEG 8000 and 2.5 M NaCl)

4 g of PEG 8000 and 2.92 g of NaCl were taken and total volume was made up to 20 ml with sterilized nuclease free water. Stored at room temperature after autoclaving for 15 minutes under 1.5 atm at 121 °C.

- **Sodium Iodide (NaI) buffer stock solution** (10 mM Tris-HCl of pH-8.0, 1 mM EDTA, 4 M NaI)

24.2 mg of Tris-HCl, 5.8 mg of EDTA and 11.99 g of NaI were taken and the volume was made up to 50 ml with autoclaved nuclease free water. To protect the light sensitive iodide buffer stock, the tube was wrapped with aluminium foil and stored in the dark at room temperature.

- **Sodium azide (NaN<sub>3</sub>)-TBS stock solution**

1 mg of NaN<sub>3</sub> was taken and dissolved in 50 ml of TBS solution to get 0.02% (w/v).

- **Tris HCl solution**

6 g of ultrapure Tris base was dissolved with 50 ml of autoclaved nuclease free water to get 1M concentration and pH was adjusted to 9.1 by adding 1M HCl. Stored at 4 °C.

#### 2.1.1.4.5 Peptide synthesis reagents

Selected silica binding peptides identified by phage display were synthesised by using the following reagents in an automated single channel microwave assisted solid phase peptide

synthesizer (CEM Corporation Liberty1) by following the standard peptide synthesis procedure via Fmoc chemistry as described in the following chapter under the section 2.1.2.6.1. These reagents include piperazine, trifluoroacetic acid (TFA), DODT (3,6-dioxo-1,8-octanedithiol), DIEA (N, N-diisopropylethylamine) and thianisole (TIS) were purchased from Sigma Aldrich. Other chemicals like N, N-dimethylformamide (DMF), dichloromethane (DCM), N-methyl-2-pyrrolidone (NMP) and diethyl ether were bought from Fisher Scientific. All Fmoc protected amino acids and resins used for peptide synthesis were purchased from Novabiochem®. The resins used for synthesising C-terminal with acid and amide groups include C1-TCP Pro Tide and Fmoc-Rink Amide ProTide Resins respectively. Further details about the synthesis process, reagents used, and the peptides synthesized is described in the following chapter under the section 2.1.2.6.1.

#### 2.1.1.4.6 Peptide characterization reagents

The high purity solvents including HPLC graded acetonitrile ( $\geq 99.93\%$ ), water and TFA ( $\geq 98.0\%$ ) used for preparing samples for HPLC and mass spectrometry were purchased from Sigma Aldrich.

#### 2.1.1.4.7 Reagents used for binding studies

The chemicals used for binding studies including phosphate buffered saline (PBS) tablets, fluorescamine dye were purchased from Sigma Aldrich. The EM Stain 336 (Uranyl Acetate Alternative) used for staining phage samples on TEM grids of QUANTIFOIL 100 Holey carbon films +2 nm (Cu 300 mesh) were obtained from Agar Scientific.

- **Phosphate buffered saline (PBS) stock solution**

One tablet (Sigma Aldrich) dissolved in 200 ml of deionized water yields 137 mM NaCl, 2.7 mM KCl and 10 mM phosphate buffer solution of approximately pH 7.4 at room temperature (25 °C). Five PBS tablets were dissolved in 1 litre of deionized distilled water and the solution was sterilized by autoclaving for 15 minutes under 1.5 atm at 121 °C. After autoclaving for 15 minutes the pH was adjusted to 7.5 using 1 M HCl concentration and stored at 4 °C.

- **Peptides stock solutions**

Peptide stock solutions ranging 2 -5 mM of selected peptides were prepared by dissolving calculated amount of peptide with desired autoclaved PBS buffer solution.

- **Fluorescamine dye stock solution**

5 mg of fluorescamine dye with purity  $\geq 98\%$  (TLC) was dissolved with 1 ml of HPLC graded acetonitrile. To protect the light sensitive fluorescamine stock solution, the tube was wrapped with aluminium foil and stored in the dark at room temperature.

- **EM Stain 336 (Uranyl Acetate Alternative) solution**

EM Stain 336 (Uranyl Acetate Alternative) used for staining phage samples on TEM grids was brought from Agar Scientific. This stain is a mixture of lanthanum salts, samarium triacetate ( $\text{Sm}(\text{CH}_3\text{COO})_3$ ) and gadolinium triacetate  $\text{Gd}(\text{CH}_3\text{COO})_3$ . The supplied EM stain 336 was dissolved 4x times with distilled water and stored at 4 °C.

- **TEM Grids**

TEM grids of QUANTIFOIL 100 Holey carbon films +2 nm (Cu 300 mesh) were purchased from Agar Scientific.

## 2.1.2 Methods

### 2.1.2.1 Phage Display Process

Chapter 1 provides a general introduction to the phage display process and more details including step by step protocol followed to isolate silica binders is described in the subsequent sub sections under this “Phage Display Process”.

#### 2.1.2.1.1 Biopanning technique and protocol

Biopanning, is a powerful affinity-based technique used to screen genetically engineered phage library with a proposed target through a series of repetitive processes *in vitro* or *in vivo*. The typical biopanning process (Figure 2.1) involving continuous repetitive steps include binding of peptide library with target material, incubation, washing with detergents to remove unbound phages; eluting strong target binders by elution buffers, amplification in bacteria, extraction and purification of single stranded phage DNA; selection of genetically inserted target binders by blue-white screening process and analysis of phage DNA<sup>57</sup>. Due to its growing importance in basic to applied sciences for identifying peptides or antibodies having specific molecular affinity for protein (e.g. cell or organic specific, antigens, receptors etc.)<sup>193</sup> and non-protein targets (e.g. nanoparticles)<sup>66</sup>; it has been widely employed for epitope mapping, monoclonal antibody production and in the development of advanced vaccines, diagnostics and therapeutics<sup>194–199</sup>.



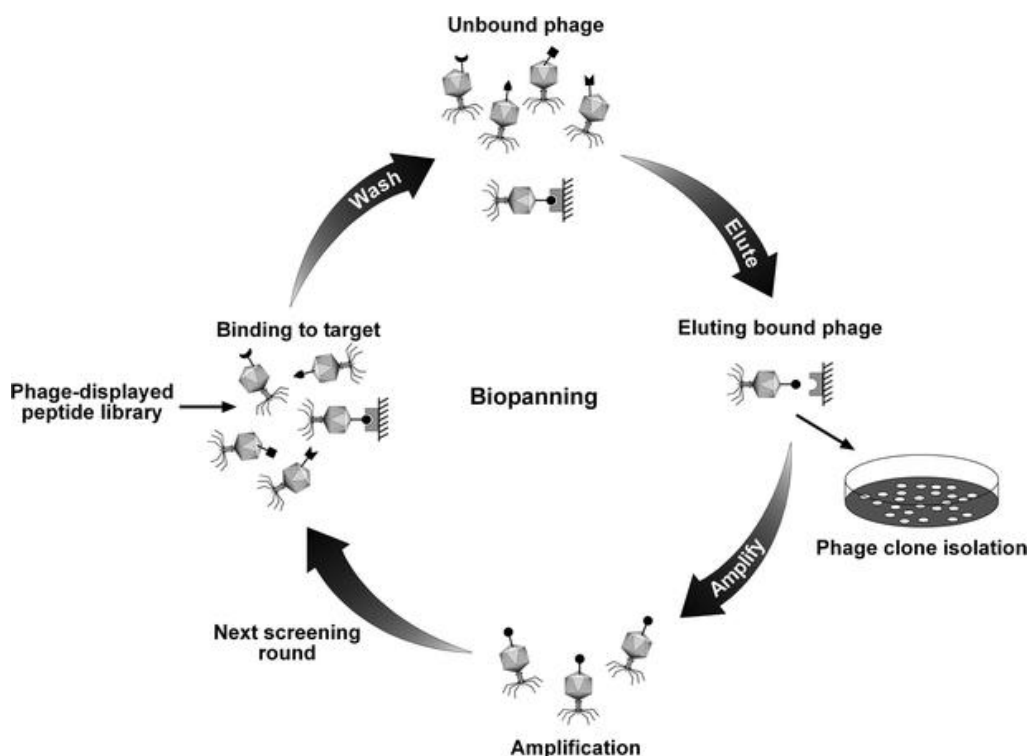


**Figure 2.1. Typical working principle of biopanning affinity process, selection and screening of material binding peptides using peptide phage libraries.** Image reproduced with permission from Springer 2006<sup>57</sup>.

Also, antibody phage display technique permits *in vitro* selection or in *E.coli* to produce monoclonal antibody fragments with specificity to a given target<sup>27</sup>. This technology is a suitable source for reagents as it overcomes some of the limitations associated with conventional animal-produced antibodies, such as variations for batch-to-batch production<sup>200</sup>. Antigen binding fragments (Fab) are one of the fragments most commonly used in research. Using the phage display vectors (eg. pComb3X) the antibody fragments are fused to the coat protein pIII of bacteriophage in *E.coli* to generate library of phages<sup>201</sup>. More details about the phage display technique has been discussed in section 1.1, Chapter 1.

### Experimental protocol:

For this phage display study, the typical protocol applied for the initial (traditional) and optimised biopanning methods are clearly discussed in the following sub steps. While, the details of phage display experiments and elution conditions used to elute silica binding peptides via traditional and optimized elution biopanning methods were shown in the Table 2.1.

### **Target cleaning step**

To remove any impurities, present in the target silica nanoparticles, 1 mg of target silica was weighed in a 1.5 ml micro centrifuge tube, washed with 1 ml 0.1% TBST concentration (0.1% Tween 20 [v/v] in 1ml of TBS), vortex rotated for 3 min and centrifuged (Eppendorf MiniSpin® GL010) at 10,000 x g for 4 min. The pellet was collected by removing the supernatant. The same process was repeated 3 times to make sure all the contaminants were washed off from silica surface.

### **Binding step**

In this target binding step, 10 µl of Ph.D.-7 (Lot: 0211212) library containing  $1 \times 10^{13}$  pfu/ml was exposed to 1 mg/ ml of silica nanoparticles in TBS buffer. This phage library-silica precipitate was incubated for 1 hour by gently rotating with Eppendorf disk rotator (Eins-Sci E-RDM-A) giving enough time for phage-silica interaction.

### **Washing step**

After 60 min incubation step, washing and spinning cycles were repeated 10 times for each biopanning round with desired TBST concentration in order to remove weakly bound or non-specific phages from silica surface. The concentration of the detergent Tween 20 mixed with TBS (TBST) was increased in the additional panning rounds to improve the washing condition stringency. For example, the washing buffer (TBST) concentrations used for rounds 1-5 panning were 0.1%, 0.3%, 0.5%, 0.7% and 0.9% (Tween 20, volume fraction) respectively. After each washing cycle, the phage-silica suspension was vortexed for 3 min followed by centrifugation at 10,000 x g for 4 min. After each spinning cycle, the supernatant was transferred to a fresh 1.5 ml Eppendorf microcentrifuge tube and the remaining pellet consisting of phage-silica precipitate washed with fresh TBST buffer solution for each wash.

### **Elution step**

After the washing and spinning steps, the strongly bound phages were recovered from the silica surface by disrupting the strongest possible interactions present between phage and silica through elution. To the final phage-silica precipitate from the last washing step, added 1 ml of elution buffer of interest (0.2 M Glycine-HCl of pH-2.2, 4 M MgCl<sub>2</sub>, pH-6.1 and 100 mM Triethylamine, pH-11) to remove the strongly bound phages from mineral silica. This solution containing phage-silica precipitate in elution buffer was then vortex rotated for 5 min and centrifuged at 10,000 x g for 4 min. Here, the supernatant eluted containing tightly bound silica phage was recovered and transferred to a fresh micro centrifuge tube.

**Table 2.1. Experimental conditions used to elute silica binding peptides via traditional and optimised biopanning methods.** Two different biopanning methods are presented in this table: traditional or standard (used in Chapter 3) and optimised (used in Chapter 4) methods. Both were performed at different times using two separate batches of same library (#E8100S). For the standard biopanning process, three different elution buffers were used but only one specific elution for entire respective biopanning experiment and rounds. In contrast, the optimised elution biopanning process presents 2 approaches (each differ from the former): Approach 1 differs from the standard biopanning method as each mentioned buffers were used successively at every single biopanning round of elution step, as apposed to one specific buffer being used for all rounds in individual traditional panning experiments; Approach 2 only used the Glycine-HCl elution buffer but at varying pH's.

Experimental method type	Library lots used	Elution buffers used	Molarity	pH	Times eluate (target bound phage) obtained separately at each elution step	Total screened panning rounds		
<b>Traditional biopanning</b>	Lot 1 (0211212)	Glycine-HCl	0.2 M	2.2	1	1→5		
		MgCl <sub>2</sub>	4 M	6.1	1			
		Triethylamine	100 mM	11	1			
Approach 1								
<b>Optimized biopanning</b>	Lot 2 (0221501)	Glycine-HCl	0.2 M	2.2	3 (1 <sup>st</sup> , 2 <sup>nd</sup> and 3 <sup>rd</sup> )	1→2		
		MgCl <sub>2</sub>	4 M	6.1				
		Triethylamine	100 mM	11				
		Approach 2						
						2.2	3 (1 <sup>st</sup> , 2 <sup>nd</sup> and 3 <sup>rd</sup> )	1→2
		Glycine-HCl	0.2 M	7				
				11				

### Neutralization step

During this neutralization step, the supernatant recovered from the last low pH (i.e. 0.2 M Glycine-HCl of pH-2.2) elution step was immediately neutralized with 150 µl of 1 M Tris HCl of pH-9.1 by nullifying the final solution pH to approximately 7 and stored at 4° C. This is called B1E (Biopanning round one unamplified eluent) as shown in Figure 2.2. While the neutralization step in case of elution buffers 4 M MgCl<sub>2</sub>, pH-6.1 and 100 mM Triethylamine was carried out by adding 50 µl of 1 M Tris HCl of pH-9.1 and 150 µl of 1 M Tris HCl of pH-5 respectively.

**Phage amplification step**

900 µl of the unamplified eluate (i.e. B1E, see Figure 2.2) obtained after the neutralization step was added to 20 ml of LB broth inoculated in a 250 ml autoclaved conical flask with 200 µl of 1:100 overnight grown *E.coli* ER2738 strain and incubation carried out by vigorous shaking at 37 °C, preferably 250 x g speed for 4-5 hours until the optical density at 600 nm reached between 0.4 and 0.6 using a UV visible spectrophotometer. After reaching the desired optical density at 600 nm, the entire culture was transferred to an autoclaved 30 ml capacity NALGENE™ Oak Ridge centrifuge tube and centrifuged at 10,000 x g for 4 min at 4 °C. The supernatant was transferred to a fresh autoclaved centrifuge tube and respun at 10,000 x g for 4 min at 4 °C. Now, the upper 80% of the supernatant was transferred to a fresh autoclaved centrifuge tube and 1/6 volume (i.e. 3.3 ml) of 20% PEG/ 2.5 M NaCl stock solution was added. This PEG solution was allowed to precipitate the phage by leaving the tube overnight at 4 °C.

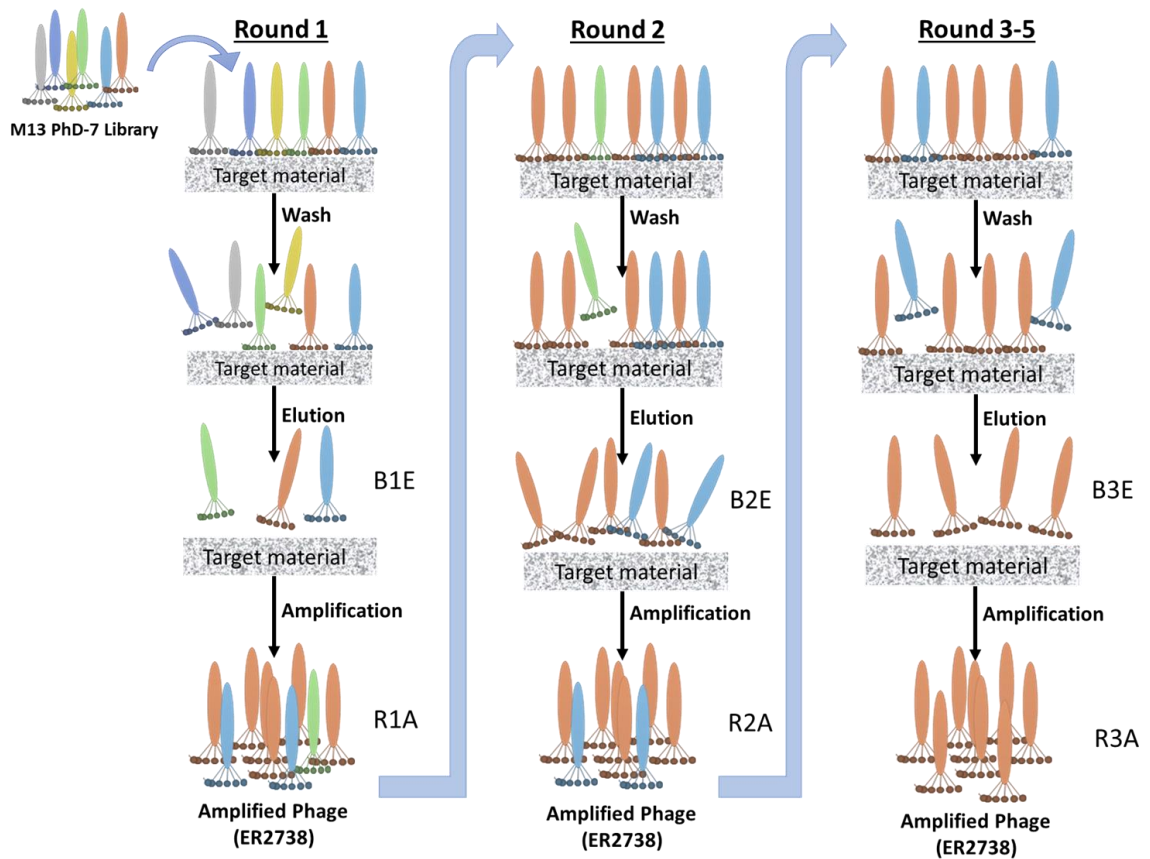


**Figure 2.2. Diagrammatic representation of biopanning process and steps involved.**

The next day, the PEG containing precipitate was centrifuged at 10,000 x g for 15 min at 4 °C. The supernatant was transferred to fresh 15 ml centrifuge tubes without disturbing the pellet. Centrifugation was performed for the pellet containing centrifuge tube and the supernatant containing centrifuge tubes to remove any residual supernatant present leaving only the pellet. The pellet present in the centrifuge tubes was suspended carefully with 1 ml of TBS buffer (pH-7.5) and all the material moved to a single autoclaved 1.5 ml micro centrifuge tube. The suspension was quickly centrifuged at 12,000 x g for 5 min at 4 °C to pellet any remaining residual cells. The supernatant was transferred to a fresh autoclaved centrifuge tube and 1/6 volume (i.e. 160 µl) of 20% PEG/ 2.5 M NaCl stock solution was added and then incubated on ice for 1 hour. After incubation, the suspension was again centrifuged at 12,000 x g for 10 min at 4 °C and the supernatant discarded. At this stage, the pellet was not clearly visible but none the less the centrifuge tube was respun to remove any remaining supernatant cells. The pellet which was then slightly visible when under normal tube light was resuspended carefully in 200 µl of 0.02% NaN<sub>3</sub>-TBS stock buffer (pH-7.5). To remove any insoluble material, it was then spun at 11330 x g for 1 min, transferred to a fresh autoclaved microcentrifuge tube and stored at 4 °C. This suspension is called the biopanning round one amplified eluate (R1A, see Figure 2.2) product and would be used for phage titering.

The whole biopanning process described above is termed biopanning round 1 and the amplified phage product obtained here called the amplified eluate (R1A, see Figure 2.2). From here on, the above biopanning process was repeated up to 3-5 biopanning rounds by taking R1A to get R2A, R2A to get R3A and so on until getting to a maximum of R5A (Figure 2.2) but by changing the washing buffer conditions. With increasing the number of biopanning rounds the washing detergent (Tween 20) concentration was also increased. For example, the washing buffer TBST (0.1% Tween 20 in TBS) concentrations used for 1-5 panning rounds were 0.1, 0.3%, 0.5%, 0.7% and 0.9% (Tween 20, volume fraction) respectively. A clear picture of biopanning experimental conditions used for initial biopanning experiments is detailed in Table 2.2. Also, to start the second round of panning, 150 µl of round 1 amplified eluate (i.e amplified phage library obtained from round 1) was added to a fresh 1mg of silica followed by series of steps involving incubation, washing, elution followed by amplification (as described above) to get to round 2 amplified eluate R2A. The same process (i.e adding 150 µl of round 2 amplified eluate (R2A) to a fresh 1mg

of silica to get R3A and so on) was repeated until reaching the biopanning rounds 3-5 for every biopanning experiment.

**Table 2.2. Experimental conditions used for initial and repanning experiments via traditional biopanning process.** The experimental conditions include the washing of weakly bound phages with TBST detergent (0.1-0.5% Tween 20 [v/v] in TBS); the removal of strongly bound binders from silica surface that isolated the silica binders using three different elution buffers; the dates and the order of experiments performed for normal biopanning were shown in the below table.

Exp. Order	Dates (month/year) of experiments performed	Wash times (cycles) and Tween 20 detergent concentration (v/v) in TBS.	Elution buffer and Conditions	Biopanning round screened
<b>Initial biopanning experiments</b>				
1	07/13	0.5%, 10 washes	Glycine-HCl 0.2 M, pH-2.2	3
	07/13			
3	09/13			
4	02/14			
5	07/13		MgCl <sub>2</sub> , 4 M, pH-6.1	
6	08/13		Triethylamine 100 mM, pH-11	
<b>Repanning experiments</b>				
7	07/15	0.5-0.9% (10 washes with each detergent concentration in successive rounds)	Glycine-HCl 0.2 M, pH-2.2	3-5
8	11/15	0.7%, 10 washes	Triethylamine 100 mM, pH-11	4

The amplified phage obtained from the biopanning round of interest (3-5) further underwent phage titring, plaque amplification, DNA extraction, purification and sequencing followed by the interpretation and identification of target binding peptides as detailed in the following sections. Overall three different elution buffers (0.2 M Glycine-HCl, pH-2.2; MgCl<sub>2</sub>, pH-6.1; TEA, pH-11) with varied pH conditions (low or high pH and neutral pH) have been used

separately and the biopanning process was performed for each experiment to identify silica binding peptides.

#### 2.1.2.1.2 Phage titering and blue-white screening

The blue-white screening method is fast, efficient and the most commonly followed protocol in molecular biology to detect bacteria carrying recombinant vectors<sup>202–204</sup>. The simple procedure includes ligation, transformation and screening. The principle is based on  $\alpha$ -complementation of the lacZ gene that carries information of  $\beta$ -galactosidase enzyme. This technique entirely depends on the activity of the  $\beta$ -galactosidase enzyme that is present in *E.coli* thereby cleaving lactose into the products of glucose and galactose.

When the plasmid vector carrying the lac Z gene is plated on specific antibiotic resistant agar medium containing *E.coli* (carrying lac Z deletion sequence) in the presence of X-gal (chromogenic substrate) and IPTG (an inducer of lac Z expression), an  $\alpha$ -complementation process occurs resulting in the formation of  $\beta$ -galactosidase enzyme, thus hydrolysing X-gal and producing blue coloured colonies. However, if the foreign DNA is taken up by the plasmid vector, then the  $\alpha$ -complementation process does not occur resulting in no formation of the  $\beta$ -galactosidase enzyme producing white coloured plaques.

M13 phage libraries which are made using a plasmid vector carrying the lac Z gene will display blue plaques, when interacting with  $\alpha$ -complementing K12 ER2783 bacterial strain resistant to tetracycline, in a LB-Xgal/IPTG plate. However, the host strain in M13 PhD. -7 phage library, *E. coli* ER2738, lacks the lacZ gene in its DNA and thus will not be able to produce  $\beta$ -galactosidase, resulting in a phage clones that look like blue plaques on LB-Xgal/IPTG plate. The mechanism of blue-white screen is connected to the lac operon in *E. coil* (host cell) with a complementing subunit vector of the phage. It is possible for the  $\beta$ -galactosidase to be secreted when it is present when the recombinant *E, coil* DNA with the target vector keeps the lacZ gene. If not, the  $\beta$ -galactosidase secretion will get blocked if lacZ gene is disturbed due to foreign DNA, or repressors interact with operator.

The intercellular enzyme  $\beta$ -galactosidase is responsible for cleaving the disaccharide lactose into galactose and glucose. For the detection of  $\beta$ -galactosidase, the indicator Xgal (modified galactose) is generally used. The solution changes from a colourless to blue as the Xgal catalyses the  $\beta$ -galactosidase, forming the product 5-bromo-4-chloroindole. Simultaneously,

the molecule  $\beta$ -D-1-thiogalactopyranoside (IPTG) also interacts with receptors to prevent the  $\beta$ -galactosidase secretion. The blue colour of plaques is due to the library cloning vector (M13KE), which is prepared from the cloning vector M13mp19 consisting of the lacZ  $\alpha$  gene and become easier to observe when using a strain (such as ER2738) alongside Xgal/ IPTG plates. Additionally, the bacterial strain for the planting in the Xgal/ IPTG plates, must be capable of  $\alpha$ -complementation (lacZDM15 or equivalent), such as the strain ER2738 supplied for the blue-white screening to work well.

This experiment is done to estimate the number of phage titers at the completion of each biopanning round. There are three steps associates to the blue-white screen experiment: first is preparation of Xgal/IPTG plates, next is the serial dilution of eluted phage samples, and final step involving the estimation of phage titers for each biopanning round.

**Preparation of LB-Xgal/IPTG plates:** 1 ml of Xgal/ IPTG stock solution was added to the 1 litre of freshly autoclaved liquid warm LB agar bottle and mixed gently by slowly moving the bottle up and down until all the added Xgal/ IPTG solution dissolved. Then, the solution of LB agar- Xgal/ IPTG mixture was poured onto a 60 nm sterile plastic petri dish plates and allowed to solidify at room temperature. These plates were with parafilm and aluminum foil and stored at 4°C in the dark for a maximum of 1 month.

**Serial dilution of phage samples:** 10 ml of LB broth was inoculated in a 250 ml autoclaved conical flask with 200  $\mu$ l (1:100 dilutions) of overnight grown *E.coli* ER2738 strain and incubation was carried out by vigorous shaking at 37 °C, preferably 250 x g speed for 4-5 hours until the optical density at 600 nm observed between 0.4 and 0.6. The shaking speed was turned down from 250 to 100 in the last 10 minutes after reaching the desired O.D to make sure that none of the F-pili was lost. Now, ten 1.5 ml autoclaved microcentrifuge tubes were taken with 1 ml LB broth in each of the tubes and 10  $\mu$ l of amplified phage eluate from biopanning round of interest was added to the first tube ( $10^{-2}$  dilution) followed by successive serial dilutions by transferring 100  $\mu$ l from each dilution until the last microcentrifuge tube ( $10^{-10}$  dilution). While the bacteria were growing, ten 15 ml autoclaved red top tubes were taken with 3 ml of LB broth and LB agar (2:1 dilution) and were stored at 45 °C -55 °C. To increase the binding between phage clones and the *E.coli* cultures, ten 1.5 ml fresh autoclaved microcentrifuge tubes were taken with 10  $\mu$ l of the above phage dilutions and 200  $\mu$ l of mid-log phased *E.coli* culture ( $OD_{600} \sim 0.5$ ) ; this was then allowed to incubate at



37 °C for 5 min. Then, the bound *E.coli* phage dilution was transferred to the red top tubes which were stored, vortexed for at least 10 seconds before pouring onto the freshly prepared X-gal/IPTG plates. These plates were kept upside down and incubated overnight preferably for 12-14 hours at 37 °C.

**Calculation of Phage Titters:** The next day, the plates with few colonies preferably last dilution plates containing 25~50 plaques from each eluted page solution were chosen to calculate the amount of phage with the equation as follow: For instance, 10 µl of diluted phage (from 9<sup>th</sup> dilution) was introduces to a 3 ml top agar and vortexed. The solution was then transferred onto LB-Xgal/IPTG plate and was kept under incubation overnight. As 10 phage plaques were accounted for on the LB-Xgal/IPTG plate, there calculation for phage amount is as follows:

$$\begin{aligned} \text{The total amount of phage} &= \frac{10 \text{ (phage plaques)}}{0.01 \text{ mL (diluted volume)}} \times 10^9 \text{ (dilution factor)} \\ &= 1.00 \times 10^{12} \text{ pfu/mL} \end{aligned}$$

pfu: plaque forming unit

In accordance with the phage titers for each round, the phage amount is calculated to create a phage pool for the following experiments.

#### 2.1.2.1.3 **Plaque amplification**

Plaque amplification is a very crucial step to obtain proper single stranded phage DNA sequences. Selecting improper or pooled plaques will lead to the overlapping of phage DNA sequences. It is always good to pick an isolated blue plaque from the last two plaque plates. By using 1.5 ml blue centrifuge tube tips, each single plaque was picked carefully and inoculated with 2 ml of LB broth containing 20 µl (1:100 dilution) of overnight grown *E.coli* culture and incubation was carried out by vigorous shaking at 37 °C, preferably 250 x g speed for 4-5 hours until the optical density at 600 nm observed between 0.4 and 0.6 reached. It is important to turn down the shaking speed from 250 to 100 for the last 10 minutes after reaching the desired wavelength to make sure that none of the F-pili was lost. After reaching the desired optical density at 600 nm, the entire culture was transferred to 2 ml autoclaved centrifuge tubes and centrifuged at 12,000 x g for 30 sec. The supernatant was transferred to

a fresh autoclaved centrifuge tube and the spinning process repeated. Then, the upper 80% of the supernatant was transferred to a fresh autoclaved centrifuge tube. This is called the amplified phage stock and can be stored for several weeks (for long term storage the sample was mixed with an equal volume of glycerol and kept at -20 °C to -40 °C) at 4 °C.

#### **2.1.2.1.4 Phage DNA purification (Modified procedure)**

The purity of the DNA samples to be sent for sequencing largely depends on how well the purification step is carried out. Autoclaved nuclease free water was used for preparing all the solutions for this purification step. 1000 µl of each amplified phage stock solution was transferred to a fresh autoclaved centrifuge tube and 400 µl of 20% PEG/ 2.5 M NaCl stock solution stored at 4 °C was added to each centrifuge tube and allowed to stand for 15 min at room temperature. This suspension was then centrifuged at 12,000 x g for 10 min at 4 °C. After discarding the supernatant, the remaining material in the microcentrifuge tubes were respun at 12,000 x g for 10 min at 4 °C. Then, the phage precipitate was collected by carefully removing (slowly without disturbing the pellet) any remaining supernatant. At this stage, the pellet was not clearly visible, but the phage precipitate was first suspended with 100 µl of iodide buffer stock by vigorously tapping the tube and then with 250 µl of 70% ethanol. It was then allowed to incubate at room temperature for 15 min. This incubation step was to preferentially precipitate phage ssDNA leaving all the phage protein in solution. Then the suspension was centrifuged at 12,000 x g for exactly 10 min at 4 °C. Longer incubation times or centrifugation of precipitate resulted in co-precipitation of phage proteins and salt. The precipitate collected was washed with 0.5 ml of 70% ice cold ethanol and respun at 12,000 x g for exactly 10 min at 4 °C. The precipitate which contained pure phage ssDNA was resuspended with 17 µl of Tris buffer of pH-8.

#### **2.1.2.1.5 Purity testing of phage DNA using a NanoDrop spectrophotometer**

A Nano Drop™ ND-8000 8-sample spectrometer was used for testing the purity of all the phage DNA samples. The principle behind the NanoDrop spectrophotometer is that nucleic acids especially nitrogenous bases absorb UV light maximally at a wavelength of 260 nm while proteins absorb UV light maximally at a wavelength of 280 nm<sup>205,206</sup>. After the sample loading surface was cleaned with nuclease free water and double distilled water, a drop containing 1.5 µl of phage DNA was loaded and measured. The minimum concentration needed for the phage DNA sample was 15ng/ µl. The purity of the DNA samples was

evaluated by calculating the A260/A280 ratio. Ideal DNA samples have an A260/A280 ratio of 1.8, but samples having a value between 0.6 and 2.0 were sent for phage DNA sequencing.

#### 2.1.2.1.6 DNA sequencing and analysis

The DNA sequencing method applied to sequence all the phage DNA samples in this work used a modified cycle sequencing technology on Applied Biosystems™ 3730XL sequencing apparatus<sup>207,208</sup>. The cycle sequencing is a modified Sanger's dideoxy chain termination method which contains an additional thermo stable DNA polymerase and fluorescently tagged dideoxy nucleotide triphosphates (ddNTPs) unlike the traditional Sanger sequencing method<sup>209</sup>.

Dideoxy nucleotides are similar to regular deoxy nucleotides, but with one key difference: they lack a hydroxyl group on the 3' carbon of the sugar ring (Figure 2.3, a). In a regular nucleotide, the 3' hydroxyl group acts as a "hook," allowing a new nucleotide to be added to an existing chain. Once a dideoxy nucleotide has been added to the chain, there is no hydroxyl available and no further nucleotides can be added resulting the chain to terminate the growing DNA strand (Figure 2.3, b). The chain ends with the dideoxy nucleotide, which is marked with a particular color of dye depending on the base (A, T, C or G) that it carries.

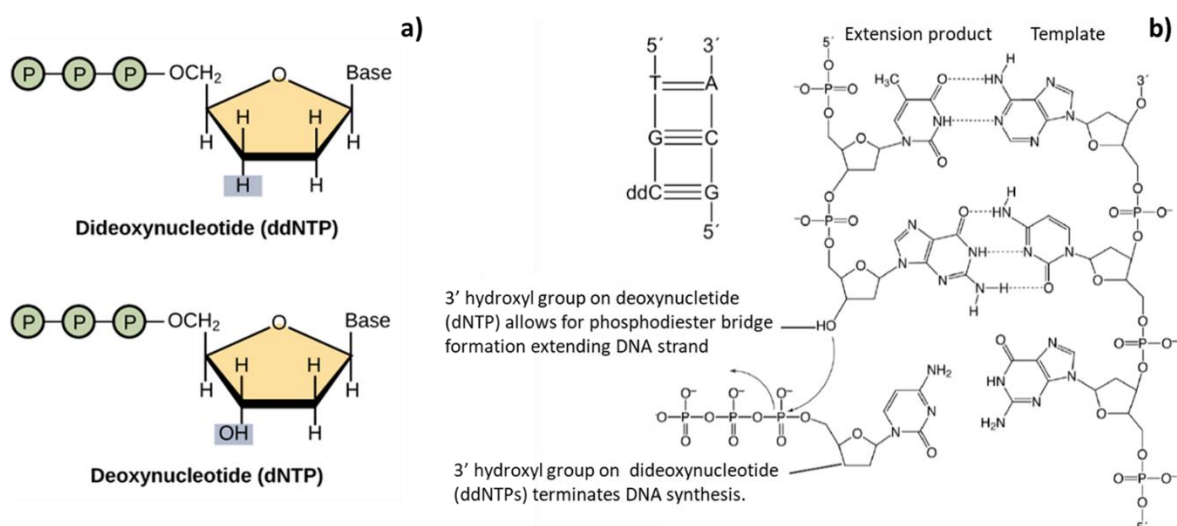


**Figure 2.3. Illustration depicting the normal dNTPs and fluorescently tagged ddNTPs and their mechanism in DNA synthesis.** Panel A shows the structures of normal deoxy nucleotide with hydroxyl (OH) group and dideoxy nucleotide without hydroxyl group (H) at 3' carbon sugar ring. Panel B show how the extension of DNA strand synthesis happens upon addition of deoxy nucleotides (dATP, dCTP, dGTP, and dTTP) while the growing chain terminates with the attachment of dideoxy nucleotides (ddATP, ddCTP, ddGTP, and ddTTP) to the 3' end. Image adapted from Applied Biosystems manual<sup>210</sup>.

This method involves the random incorporation of ddNTPs in the place of dNTPs (deoxy nucleotide triphosphate) causing the growing chain to terminate during the process of DNA synthesis, thereby separating all the fragments by size on capillary electrophoresis which can then be visualised on a chromatogram. The cycle of events that occur during the sequencing process include denaturation, annealing, extension and separation by capillary electrophoresis (Figure 2.4). The cycle sequencing process starts with the addition of a reaction mixture consisting of thermostable DNA polymerase, sequencing primers, dNTPs, ddNTPs and buffer comprising of  $Mg^{++}$  and  $K^+$  to the original template thereby activating the annealing process. During the DNA synthesis process, the fluorescently labelled ddNTPs (ddATP, ddTTP, ddGTP, ddCTP) terminates the reaction.

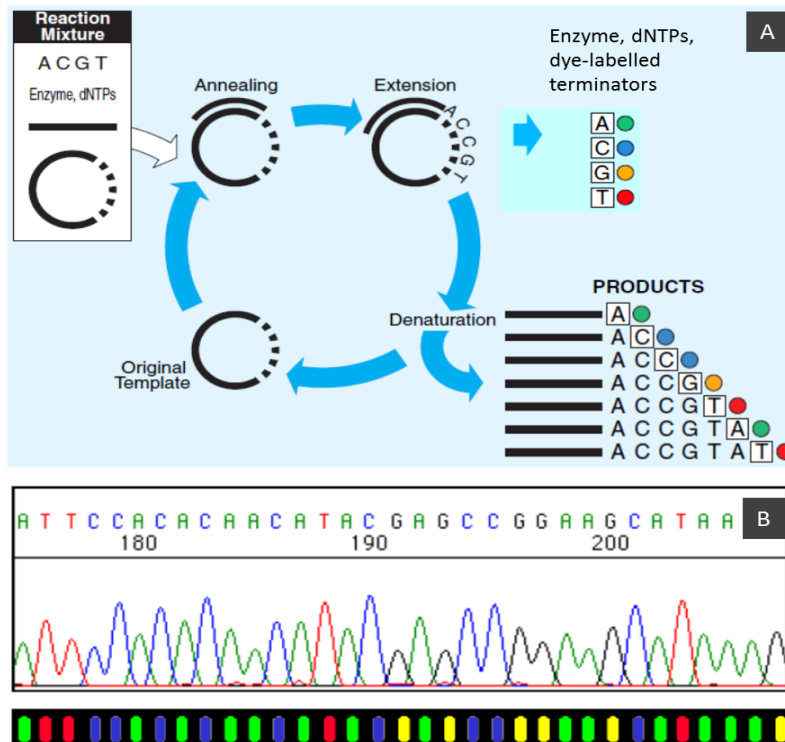


**Figure 2.4. Schematic representation of cycle of events that occur in cycle sequencing technology.** A) Process of denaturation, annealing, extension and termination forming DNA fragments in thermal cycler B) Electrophoresis separation of fluorescently tagged DNA fragments based on molecular weight. Image adapted from Applied Biosystems manual <sup>210</sup>.

In this work, all the phage DNA samples were sent to Eurofins Genomics, UK for sequencing. They used a modified cycle sequencing technology and sequenced DNA samples via their Applied Biosystems™ 3730XL sequencing apparatus as described above. After obtaining the sequenced data from Eurofins, further analysis was carried out to identify the target binding peptides.

### 2.1.2.2 Bioinformatics

A range of bioinformatics tools have been used to identify and analyse the authenticity of sequences. These include in-silico sequence convertor, peptide property calculators such as Innovagen and Bachem<sup>211,212</sup> and peptide database search engine HLAB BDB (Biopanning data bank) or formerly called as MimoDB. Moreover, to find any sequence similarities in the identified silica binders, the sequence alignment was performed using MSA Viewer<sup>213</sup>.

#### Interpretation of phage DNA sequence:

The interpretation of sequenced data obtained from Eurofins has been done by primarily checking and selecting the good quality chromatogram peaks using Finch TV software (<http://www.geospiza.com/Products/finchtv.shtml>). Then, a series of steps that includes interpreting the sequenced data by identifying the anticodon, building the complementary strand and translating those codons to amino acid codes was done to recognize the peptide that bound to target material as shown below. An example of data processing and analysis performed to identify the peptide TVNFKLY was shown as an example in the Figure 2.5.

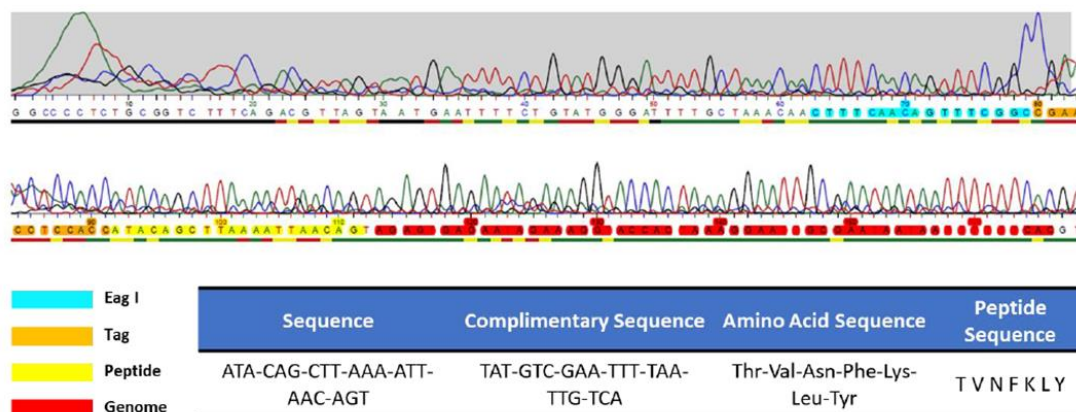


**Figure 2.5. An example of the sequencing data obtained from Eurofins (top) and how the peptide TVNFKLY has been interpreted (bottom) and identified.**

The in-silico sequence converter<sup>214</sup> has been used to build complementary strand for identified DNA sequence and translate to amino acids. Innovagen and Bachem peptide calculators have been used to investigate the selected peptide physico-chemical properties such as charge, pI, amino acid groups, hydrophobicity etc<sup>211,212</sup>.

#### Peptide database search engines:



Biopanning data bank (BDB) or formerly called as MimoDB, an online available database having a collection of 29,333 peptide sequences that were shown to have an affinity to

compounds ranging from small substances to the whole organisms isolated using phage and surface display methods<sup>215</sup>. Besides the peptide sequences, supplementary information that relates to the peptide sequences including the target material, template and type of libraries collected from public sources including Uniport, GenBank, published works and from PDBsum can be found free of cost (<http://immunet.cn/bdb/index.php>). All the phage displayed mineral binding peptides in this project have been checked against MimoDB<sup>216,217</sup> and BLAST<sup>218</sup> to find the whole or exact part of phage display or surface display peptide sequences that were identical or similar to identified binders. As an example, a screenshot of MimoDB Search, Blast, Scan and TUPredict results were shown in Figure 2.6.

#### MimoSearch

Your Query Sequence	BiopanningDataSet ID	Target Name
GQSEKHL	<a href="#">3152</a>	<a href="#">Sera of peanut-tolerant subject 2</a>
	<a href="#">3153</a>	
	<a href="#">2987</a>	<a href="#">Fe3O4 nanoparticles</a>
	<a href="#">2988</a>	

#### MimoBlast

Your Query Peptide	Similar Peptide in BDB	Blast Report 
GQSEKHL	<a href="#">GQSEKHL in BiopanningDataSet: 3153</a>	<a href="#">Report 1</a> 
	<a href="#">GQSEKHL in BiopanningDataSet: 3152</a>	
	<a href="#">GQSEKHL in BiopanningDataSet: 2988</a>	
	<a href="#">GQSEKHL in BiopanningDataSet: 2987</a>	

#### MimoScan

Your Query	Matched Peptide	BiopanningDataSet ID
GQSEKHL	GQSEKHL	<a href="#">2987</a>
	GQSEKHL	<a href="#">2988</a>
	GQSEKHL	<a href="#">3152</a>
	GQSEKHL	<a href="#">3153</a>

#### TUPredict - PhD7Faster

Number 	Query Sequence 	Length 	Voting 	Probability 	Yes/No
1	GQSEKHL	7	3	0.42	No

**Figure 2.6. A screen shot showing the result obtained for peptide GQSEKHL using MimoDB search, Blast, Scan and TUPredict tools.**

Another example includes, the phage displayed peptide sequence TVNFKLY identified as a silica binder in this project was found to have affinity for Fe<sub>3</sub>O<sub>4</sub> nanoparticles indicating that this peptide might be having promiscuous binding nature to multi-materials. MimoDB database consists of few tools which include Mimo Search, Mimo Scan, Mimo Blast and Target un-related peptides (TUPs). The default search parameters were used by entering or pasting the sequence (either in FASTA format or raw sequence) in the query to obtain the data. The MimoSearch will search to find the similar sequence gained by other groups with for various targets. While the MimoScan and MimoBlast tools will check for any matched patters or similar query sequences. In addition to BDB search or Blast, the acceptability of

the silica binding peptides from this project were checked with TUPrdecit tool from BDB databank. This tool was developed using machine learning algorithms and currently three predictors are available including PhD7Faster, SABinder and PSBinder<sup>215</sup>. For example, the PhD7Faster tool can be used to predict if phages bearing randomly displayed peptides from the Ph.D.-7 library might grow faster due to propagation advantage<sup>217,219</sup>. The predictor was built using Support Vector Machine, trained with peptides from the unselected Ph.D.-7 library after one round of amplification<sup>219</sup>. Moreover, the list of peptides reported to bind to polystyrene-based components (i.e. TUPs) such as well plates, beads, petri dishes and films during biopanning the process is shown in Table 2.3.

**Table 2.3. List of polystyrene or plastic binding peptides identified by phage display process**

No	Peptide Sequence	Target Name	Phage library	Reference
1	PWWVSWVDAG- GGSLALPTQPSD	Polystyrene and polyvinyl chloride	TSAR-12 phage display	220
2	VDWVGWASW	Polystyrene/ polyurethane (magnetic beads)	fUSE5-based X10 phage display library	221
3	SAWVRWGRVW			
4	PWNAWGRTWV			
5	WHRWPWLVS	Polystyrene (petri dish)	X10 phage display library	222
6	WHWYALDR			
7	FHENWPS	Polystyrene (96-well plate)	Ph.D.-7	223
8	FHWTWYW			
9	CRAKSKVAC	Dysplastic skin	CX7C T7	224
10	KGLRGWREMISL	Polystyrene (96-well plate)	FliTrx bacterial display library	225
11	APFYYSWFPSYM- AEGLPSPSPLDPV- QDNLY	Polystyrene (96-well plate)	Not known	226
12	FFPSSWYSHLGLV	Polystyrene (96-well plate)	X6PX6 and X6YX6	227
13	FFSFFFPASAWGS			
14	RAFIASRRIKRP	Polystyrene (petri dish)	FliTrx bacterial display library	228
15	AGLRLKKAIIHR			
16	GETRAPL	Syndiotactic polystyrene film	Ph.D.-7	229
17	FPGRPSP			
18	FKFWLYEHVIRG	Polystyrene (96-well plate)	Ph.D.-12	230
19	HWGMWSY	Polystyrene	Ph.D.-7	231
20	WHWRLPS			
21	TLHPAAD	Polystyrene 6 well plate	Ph.D.-7	232
22	VHWDFRQWWQPS	Polystyrene 96-well microtiter plate	Ph.D.-12	233

### 2.1.2.3 Optimised Biopanning Method and Elution Strategies

In the optimised biopanning method, a separate batch of M13 Ph.D.-7 phage display library (#E8100S, Lot: 0221501) has been used for panning against same batch of already characterized amorphous silica nanoparticles. Two alternative elution-based approaches (Figure 2.7) were tested. In the first approach, three different elution buffers consecutively one after other (Gly-HCl, pH-2.2; MgCl<sub>2</sub>, pH-6.1; TEA, pH-11) were used during each elution step of panning round; while, in the second approach, we used single elution buffer (for example, Gly-HCl) but by varying the pH one after other (pH-2.2, pH-7, pH-11) to eluate all the phages including the ones that might have been left attached to the silica during the traditional biopanning and repanning experiments. The typical protocol used for the optimised biopanning methods are discussed in the following sub steps. While, the details of phage display experiments and elution conditions used to elute silica binding peptides via traditional and optimized elution biopanning methods were shown in the Table 2.4.

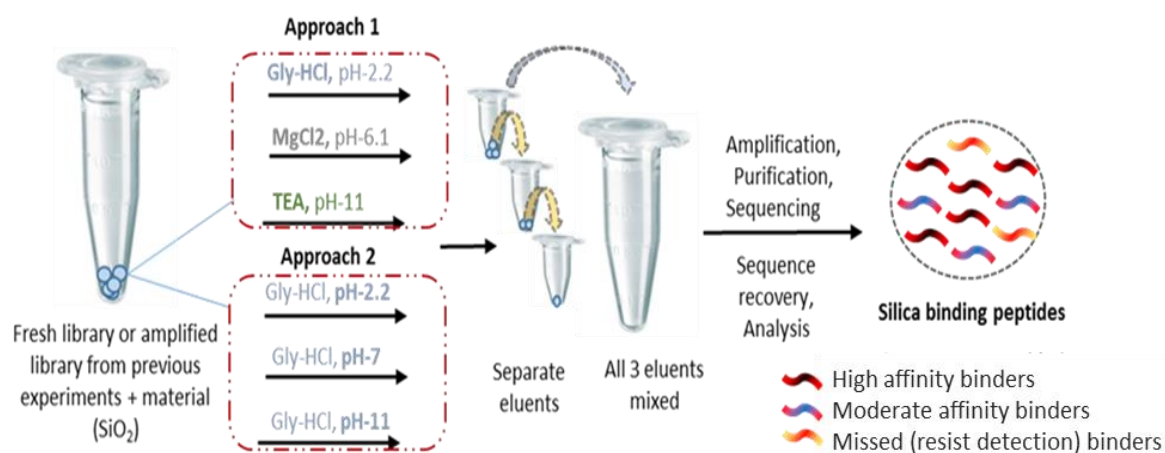


**Figure 2.7. Diagrammatic representation of optimised biopanning method by exploring elution strategies.** A separate second batch (Lot: 0221501) of M13 Ph.D.-7 phage display library (#E8100S) has been used for performing the optimised biopanning method. The optimised biopanning process presents 2 elution approaches (each differ from the traditional biopanning method of Chapter 3) used for Chapter 4: Approach 1 differs from the traditional biopanning method as each mentioned buffers (Gly-HCl, pH-2.2; MgCl<sub>2</sub>, pH-6.1; TEA, pH-11) are used consecutively one after other for each screening (biopanning) round, as appose to one specific buffer being used for all rounds in traditional biopanning and repanning experiments (chapter 3); Approach 2 only used the same Glycine-HCl elution buffer but at varying pH's (i.e. Gly-HCl of pH-2.2; pH-7; pH-11). However, for verifying this optimised elution based biopanning experiments, further panning was done by taking the mixture of amplified library attained by mixing together the already amplified phage libraries that were obtained from the biopanning round 1 of previous separate experiments (Table 2.2) via using Lot 1(Lot: 0211212) of Ph.D.-7 phage display library.



### **Target cleaning step**

1 mg of target silica was washed with 1 ml 0.3% TBST concentration (0.1% 0.3% Tween 20 in 1ml of TBS, v/v), vortex rotated for 3 min and centrifuged (Eppendorf MiniSpin® GL010) at 10,000 x g for 4 min. The pellet was collected by removing the supernatant. The same process was repeated 3 times to make remove the contaminants from silica surface.

### **Binding step**

10 µl of Ph.D.-7 library (Lot: 0221501) containing  $1 \times 10^{13}$  pfu/ml was exposed to 1 mg/ ml of silica nanoparticles in TBS buffer at pH-7.5. This phage library-silica precipitate was incubated for 1 hour by gently rotating with Eppendorf disk rotator (Eins-Sci E-RDM-A) giving sufficient time for phage-silica interaction.

### **Washing step**

After 60 min incubation step, washing and spinning cycles were repeated 10 times for each biopanning round with 0.1%-0.5% TBST (v/v) concentration used for rounds 1-2 panning rounds respectively. After each washing cycle, the phage-silica suspension was vortexed for 3 min followed by centrifugation at 10,000 x g for 4 min. After each spinning cycle, the supernatant was transferred to a fresh 1.5 ml Eppendorf tube and the remaining pellet consisting of phage-silica precipitate washed with fresh TBST buffer solution for each wash.

### **Elution step**

Here, instead of using single elution buffer throughout out biopanning experiment as in traditional biopanning, all the same three elution buffers were used consecutively one after other in a single panning round (three step elution), to elute and recover the strongly bound silica binders. In the first elution step, 1ml of 0.2 M Glycine-HCl, pH-2.2 was added to the final phage-silica precipitate from the last washing step to elute, followed by second and third elution steps with 1ml of 4 M MgCl<sub>2</sub>, pH-6.1 and 100 mM Triethylamine, pH-11 respectively to remove the strongly bound phages from mineral silica. The solution containing phage-silica precipitate in elution buffer was vortexed for 5 min, centrifuged at 10,000 x g for 4 min and transferred to a fresh micro centrifuge tube.

### **Neutralization step**

The supernatant recovered from the last low pH (i.e. 0.2 M Glycine-HCl of pH-2.2) elution step was immediately neutralized with 150 µl of 1 M Tris HCl of pH-9.1 by nullifying the final solution pH to approximately 7 and stored at 4° C. While the neutralization step in case of elution buffers 4 M MgCl<sub>2</sub>, pH-6.1 and 100 mM Triethylamine was carried out by adding 50 µl of 1 M Tris HCl of pH-9.1 and 150 µl of 1 M Tris HCl of pH-5 respectively.

The above steps were repeated by adding 150 µl of round 1 amplified eluate (i.e amplified phage library obtained from each elution step separately) to a fresh 1mg of silica followed by doing a series of steps involving washing, elution followed by amplification to get to round 2 amplified eluate R2A and then silica binders from round 1 and 2 underwent titration, plaque amplification, purification and sequence analysis as described in section 2.1.2.1.

**Table 2.4. Experimental conditions (washing and elution) used for optimised biopanning process.** The experimental conditions include the number of times and washings performed with different concentrations of TBST detergent (0.1%-05% Tween 20 in TBS, v/v) to remove weakly bound or nonspecific phage binders from target silica surface; the elution of strongly bound phage clones from the silica surface that isolated the silica binders using alternative elution methods via three different elution buffers and conditions; the number of biopanning rounds and the way successive elution's carried out during each elution step were shown in the below table.

Biopanning round	Wash times and TBST detergent concentration (v/v)	Elution step and conditions		
		Elution buffer	pH	Eluent
1	0.1-0.3% 5 each Total 10 washes	0.2 M Glycine-HCl	2.2	1 <sup>st</sup>
		4 M MgCl <sub>2</sub>	6.1	2 <sup>nd</sup>
		100 mM TEA	11	3 <sup>rd</sup>
2	0.3-0.5% 5 each Total 10 washes	0.2 M Glycine-HCl	2.2	1 <sup>st</sup>
		4 M MgCl <sub>2</sub>	6.1	2 <sup>nd</sup>
		100 mM TEA	11	3 <sup>rd</sup>

In this optimised biopanning process, only two biopanning rounds were carried. The biopanning rounds were reduced to two to check the effectiveness of the optimised biopanning approach. The amplified phages from the biopanning rounds 1 and 2 underwent phage titring, plaque amplification, DNA extraction, purification and sequencing as described briefly under phage display process section 2.1.2.1. In order to verify the optimised elution process, further panning experiments were carried out by exposing fresh silica to 10 µl of the mix of amplified phage which is prepared by mixing the amplified elute (i.e phage populations obtained from initial biopanning tests via using Lot 1 library) stored from each biopanning round 1 of traditional biopanning experiments (Table 2.2).

## 2.1.2.4 Repanning Experiments

To cross check the reproducibility of the above phage displayed sequences, further repanning experiments (Table 2.5) were performed by mixing the amplified phage pool obtained from the panning round of interest and by taking from each different biopanning experiments. In this process, 50  $\mu$ l from each round 2 amplified eluate (R2A) obtained from separate normal biopanning experiments (Exp1, 2, 4, 5 and 6) varying different elution buffers (Table 2.2) were mixed together in a clean 1.5 ml microcentrifuge tube and stored at -20 °C. This mixture was named as ‘mix of amplified phage’. The whole biopanning process is then again performed starting with incubation step by exposing 50  $\mu$ l of mix of amplified phages with fresh silica followed by repeated multiple steps involving washings (with detergent TSBT of 0.5%, 0.7% and 0.9% concentrations for rounds 3, 4 and 5), elution, phage amplification, phage titering, plaque amplification, DNA extraction/ purification and sequencing as described in section 2.1.2.1.

**Table 2.5. Schematic representation of experimental conditions used for repanning experiments.** The amplified phages obtained from different biopanning experiments where a small number of sequences screened were mixed together to verify the reproducibility of previously identified peptide sequences.

Experiments checked by repanning	Amplified phage stocks taken and mixed together from			Re-panned till what round	Experimental numbers performed order	Elution buffers used	pH condition
	Library lot number	Experiment numbers	Round				
<b>Repanning experiments to check traditional biopanning method</b>							
Initial biopanning (Chapter 3)	Lot 1 0211212	1,2,4,5 and 6	2	3-5	7	Glycine-HCl	Low pH, 2.2
					8	Triethyl amine	High pH, 11
<b>Repanning experiments to check optimised biopanning method (Chapter 4) and as comparator for traditional biopanning method (Chapter 3)</b>							
Optimised biopanning (Chapter 4)	Lot 1 0211212	1,2,4,5 and 6	2	3	n/a	Glycine-HCl	Low pH, 2.2
						MgCl <sub>2</sub>	High salt pH-6.1
						Triethyl amine	High pH, 11

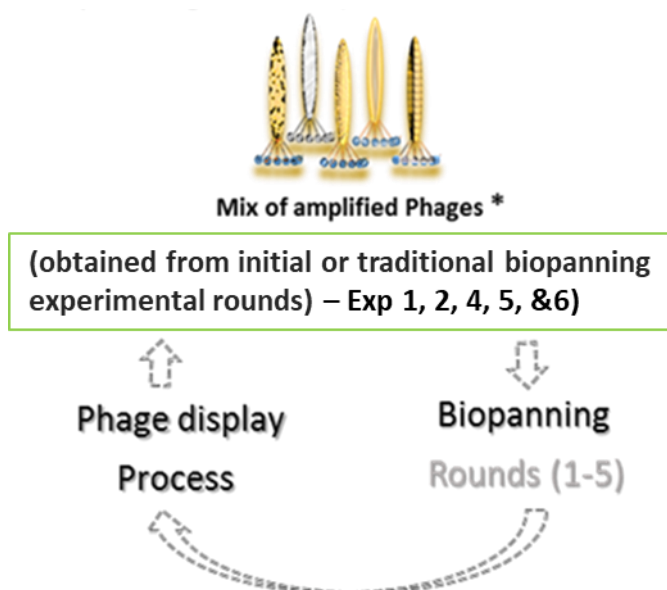


**Figure 2.8. Schematic representation of repanning method.** The amplified phages obtained from different biopanning experiments where a small number of sequences screened were mixed together to verify the reproducibility of previously identified peptide sequences.

In this study, 2 different repanning experiments were carried out with each experiment using one of the elution buffers (0.2M Glycine-HCl, pH-2.2 or 100 mM Triethylamine, pH-11). The detailed step by step phage display process was explained in section 2.1.2.1. Encouraged by the optimised elution biopanning approach results, we tried both elution strategies on M13 Ph.D.-7 phage display library (#E8100S, Lot: 0211212) by taking the previously stored amplified stocks from round 1 of different experiments (experiment 1, 2, 4, 5 and 6 as described in Figure 2.8) to check the reproducibility and to verify the optimised elution biopanning process.

#### 2.1.2.5 Selection of Single Phage Clones for Binding Studies

The individual phage clones displaying peptide of interest have been selected from the above phage titring (blue-white screening method) and plaque amplification steps. As mentioned in section 2.1.2.1.3, under plaque amplification step, each single plaque from the last titring plates were carefully picked using 1.5 ml blue centrifuge tube tips and inoculated to an individual 10 ml red top tubes with 2 ml of LB broth containing 20  $\mu$ l (1:100 dilution) of overnight grown *E.coli* ER2738 culture. Incubation was then carried out by vigorous shaking at 37 °C, preferably 250 x g speed for 4-5 hours until the optical density at wavelength 600 nm observed was between 0.4 and 0.6. After reaching the desired optical density at

wavelength 600 nm, the entire culture was transferred to 2 ml autoclaved Eppendorf tubes and centrifuged at 12,000 x g for 30 sec. The supernatant was transferred to a fresh autoclaved Eppendorf tubes and the spinning process repeated. Later, the upper 80% of the supernatant was transferred to a fresh individual autoclaved Eppendorf tube. This is called the amplified phage stock and was stored few weeks at 4 °C. The amplified phage stock samples containing individual clones were divided into two lots. One lot was initially stored for few weeks at 40C to perform titering experiments and later moved to -20 °C. While the other lot were mixed with equivalent amounts (1:1 ratio) of sterile glycerol and stored at -40 °C. However, the amplified phage stock solutions can be stored for several years (long term) by mixing the samples with an equal volume of glycerol and by storing at -40 °C to -80 °C. At this step, we have sent 1 ml for sequencing and the remaining 1 ml was marked and stored at 4 °C. This amplified phage stock solution containing 1 ml of same type of single phage plaque underwent phage amplification, DNA extraction and sequencing as defined in sections 2.1.2.1.1, 2.1.2.1.4 and 2.1.2.1.6. Each single plaque will have single silica binding phage DNA sequence which was identified after performing the DNA extraction and purification (refer section 2.1.2.1.4) and sequence analysis. After identifying the peptide from the sequence analysis results, the selected phage clone samples of known sequences were further amplified in *E.coli* followed by purification step as mentioned earlier. The known peptide sequence displaying individual phage clones were further used for relative binding experiments and for TEM studies.

#### 2.1.2.6 Synthesis and Characterization of Silica Binding Peptides and Nanoparticles

To avoid any inconsistent results, the same batch of amorphous silica nanoparticles of size  $82 \pm 4$  has been used for phage display and binding studies that were already available in the Perry laboratory and had been synthesized by the Stöber process and characterized using varied techniques<sup>4,107,234</sup>. The physical properties including surface chemistry of silica nanoparticles (Table 2.6) had been reported in our previous papers<sup>4,107</sup>.

**Table 2.6. Structural properties of silica nanoparticles including surface chemistry.** <sup>a</sup> Specific surface area was determined using the Brunauer–Emmett–Teller (BET) method in the range of  $0.05 < P/P_0 < 0.35$ . <sup>b</sup> Barrett–Joyner–Halenda (BJH) desorption pore volume and size were calculated between 2 and 300 nm. <sup>c</sup> Determined from TGA measurements. The table was reprinted from ACS<sup>4,107</sup>.

sample	size (nm)	SSA (m <sup>2</sup> /g) <sup>a</sup>	pore volume (cm <sup>3</sup> /g) <sup>b</sup>	pore size (nm) <sup>b</sup>	#OH/nm <sup>2</sup> <sup>c</sup>	ζ, pH 7.4 (mV)	pzc
SiO <sub>2</sub> -82	82 ± 4	65.0 ± 0.3	0.334	32	4.5	-38 ± 5	2.4

Selected peptides (LPVRLDW, NDLMNRA, GQSEKHL, GASESYL, KIAVIST, YSLKQYQ-OH, YSLKQYQ-NH<sub>2</sub>, ADIRHIK-OH, ADIRHIK-NH<sub>2</sub>, HYIDFRW-OH and HYIDFRW-NH<sub>2</sub>) identified by phage display were synthesized and chemically modified using automated single channel microwave assisted solid phase peptide synthesizer (CEM Corporation Liberty1) by following the standard peptide synthesis procedure via Fmoc chemistry as stated in section 2.1.2.6.1. These synthesized peptides were characterized by HPLC and mass spectrometry. The list of peptides synthesised including their molecular weights, the number of times peptides were synthesised, HPLC and Mass spectrometry measurements and the type of binding study they were used for can be seen from the Table 2.7.

**Table 2.7. List of silica binding peptides synthesized and their characterisation measurements using HPLC and Mass spectrometry.**

Peptide Sequence	Mol. Wt of pep (g/mol)	MALDI-TOF mass analysis (g/mol)		HPLC of pep purity (%)		Times peptide synthesized	Type of binding studies peptides used for
KIAVIST	730.89	731.41		93.8		1	Verification (Fluorescamine assay and Raman spectroscopy)
LPVRLDW	898.07	898.3	898.5	92	94	2	
NDLMNRA	832.94	833.3	833.3	72	80	2	
GQSEKHL	797.87	798.3	798.4	92	95	2	
GASESYL	725.75	726.06	726.2	93	94	2	
YSLKQYQ-Acid	929.03	N/A		94		1	Verification (Fluorescamine assay and TEM)
YSLKQYQ-Amide	928.04	N/A		93		1	
ADIRHIK-Acid	852	N/A		94		1	
ADIRHIK-Amide	851.01	N/A		98		1	
HYIDFRW-Acid	1036.14	N/A		78		1	
HYIDFRW-Amide	1035.16	N/A		73		1	

#### 2.1.2.6.1 Solid phase peptide synthesis (SPPS)

Solid phase peptide synthesis (SPPS) has become an essential day to day laboratory tool for constructing synthetic peptides under controlled chemical conditions due to their vast usage in academia and industry. In 1963, Merrifield revolutionised peptide science by synthesizing a tetra peptide using a cross linked polystyrene solid support that allowed the anchoring of  $N\alpha$ -amino acids resulting C to N terminus peptide formation<sup>235</sup>. The principle (Figure 2.9) of SPPS is based on the acid liable attachment of C-terminal amino acid to an insoluble polymeric solid support (resin) and subsequently extending the length of the peptide chain by a series of repeated chemical steps including deprotection, activation and coupling<sup>236,237</sup>. Once the desired peptide synthesis is completed, the unwanted resin and side chain protecting groups are removed by simultaneous deprotection and cleavage steps. Further, these cleaved and deprotected free peptides are filtered and washed before freeze drying. To cleave the  $N\alpha$ -protecting groups, either mild or harsh chemicals are used. Usually, free peptides are precipitated and washed in chilled suitable organic solvents (eg. diethyl ether).

This SPPS method is suitable to synthesize small proteins and in particular peptides due to convenience of using excess reagents, easy removal of any unreacted products or by products and no need of purification and characterization steps each time after the addition of new amino acid and most importantly minimal loss of peptide due to peptide being anchored to solid support during the entire synthesis process<sup>238-240</sup>. The most commonly used chemistries to protect  $N\alpha$ -amino acid (AA) side chain groups include 9-fluorenylmethoxycarbonyl (Fmoc)<sup>241</sup> and t-butyloxycarbonyl (Boc)<sup>242</sup>. Here, N-terminus Fmoc amino acid groups are acid stable but base liable while the temporary side chain protecting groups are acid liable and base stable.

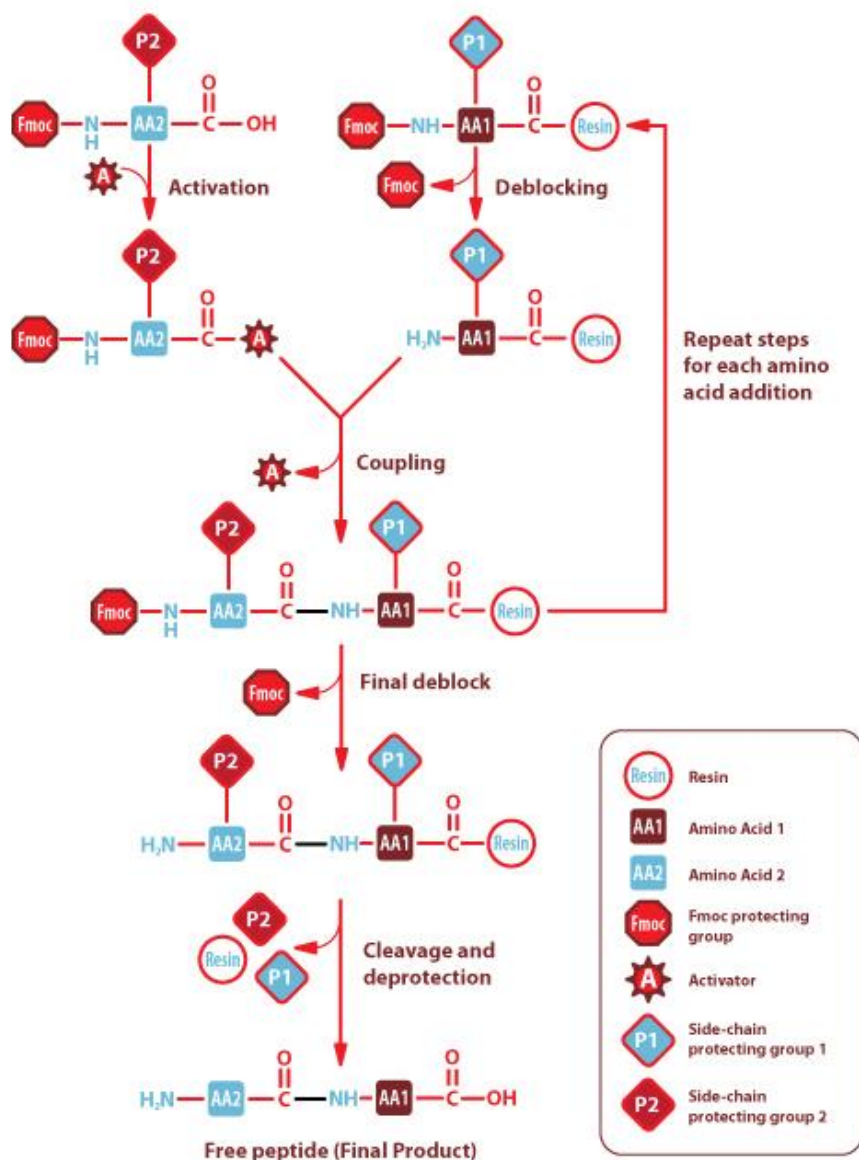


**Figure 2.9. General principle and scheme of solid phase peptide synthesis via Fmoc chemistry.** First, the  $N\alpha$ -protected C-terminal amino acid is anchored to the insoluble solid supported resin with the help of linker. Subsequently, the desired peptide will be assembled by elongating the length of the peptide chain by a cycle of repetitive chemical steps involving 1) deblocking of the temporary Fmoc protecting amino acid group 2) activation of carboxy group of new incoming amino acid 3) coupling. Once the chosen peptide length is achieved, the unwanted resin and side chain protecting groups will be removed by performing final deprotection and cleavage steps. Later, these cleaved and deprotected free peptides will be washed and purified. Image reproduced from Sigma Aldrich website.

However, the success of SPPS depends upon the choice of selecting the right resins, linkers, and protected groups and using suitable chemical reagents at appropriate times either to activate or remove specific side chain amino acids during the activation, deprotection, coupling, cleavage and purification steps<sup>236,243</sup>. Harsh acids like trifluoroacetic acid (TFA)



and hydrofluoric (HF) are used to release Boc-protected groups and completed peptide from the solid support<sup>242</sup>. While, Fmoc protected groups can easily be removed under mild conditions using a combination of piperidine and N, N-dimethylformamide (DMF)<sup>241</sup>. Solvents such as DMF, N-methyl-2-pyrrolidone (NMP), are used for coupling and removing Fmoc protected groups under microwave energy<sup>244</sup>. While N,N-dicyclohexyl-carbodiimide (DCC) or diisopropylcarbodiimide (DIC), N,N-diisopropyl-ethylamine (DIEA) along with a combination of DMF, HBTU or Hydroxybenzotriazole (HOBt) helps in swelling resins and activating incoming acid by reacting with carboxylic acid group thereby improving coupling reaction<sup>240</sup>.

### **Protocol:**

In this study, selected peptides identified by phage display have been synthesized using an automated single channel microwave assisted solid phase peptide synthesizer (CEM Corporation Liberty1) by following the standard peptide synthesis procedure via Fmoc chemistry as described above. These peptides have been programmed in such a way that C-terminal end group ended up with either acid (OH) or amide (NH<sub>2</sub>) groups. Preloaded Wang resins protected with Fmoc chemistry have been used as a solid support and for initiating the peptide synthesis reaction in a vessel. For example, 7-mer peptide ADIRHIK was preloaded with Fmoc protected lysine (K) Wang resin as a starting point to initiate peptide synthesis reaction and ended up recovering final peptide as ADIRHIK-OH or ADIRHIK-NH<sub>2</sub>. The other chemicals that were used in this process include DMF for swelling resin and as a system solvent for rinsing, piperazine mixed with DMF for removing N-terminal protected groups, HBTU mixed with DMF for coupling reactions, DIEA mixed with DMF for activating the new incoming amino acid, TFA mixed with thianisole (TIS), 3,6-Dioxa-1,8-octanedithiol (DODT) and ddH<sub>2</sub>O for cleaving and removing unwanted protected side groups of final peptide and diethyl ether for precipitating and filtering pure peptide.

The first list of peptides synthesised was selected mainly based on experimental phage display results that include LPVRLDW, NDLMNRA, GQSEKHL, GASESYL and KIAVIST. The second list of peptides such as YSLKQYQ, ADIRHIK, HYIDFRW were selected by taking various parameters into consideration including phage experimental results, physico-chemical properties and bioinformatics analysis. Additionally, these peptides were synthesized by chemically modifying the C-terminal end groups with amide (i.e YSLKQYQ-NH<sub>2</sub>, ADIRHIK-NH<sub>2</sub>, HYIDFRW-NH<sub>2</sub>).

### 2.1.2.6.2 High performance liquid chromatography (HPLC)

Chromatography is the process of separating or isolating a compound from a mixture. This is a powerful and versatile single-step process for modern analysts. There are many forms of chromatography depending on the phase of the sample (gas, liquid or solid) and the type of analyte (enantiomer, ionic and etc.) required for isolation<sup>245</sup>. The Russian botanist M.S. Tswett was among the first scientist to recognise the separation method, as he used a rudimentary form of liquid-solid chromatography to separate the plant pigments<sup>246,247</sup>. Also, this seems to be the origin for the prefix ‘chroma’ in the word chromatography; although color has little to do with separation, the word has persisted<sup>246,247</sup>. High-performance liquid chromatography (HPLC) is a leading technique for chemical analysis to separate, analyse and/or purify almost any sample. HPLC begins by placing the sample in a tray for automatic injection into a packed column (usually silica). A solvent is pumped constantly into the column resulting in compounds to separate according to their affinity to the packing (Figure 2.10). The separated compounds are then sensed by the detector as they leave the column. The coupling of HPLC with MS allows for the further separation and detection as the fragmented analytes are detected according to their  $m/z$  ratio<sup>248–250</sup>. A significant development has been made in the types HPLC, yet reverse-phase chromatography (RPC) is the most widely used for the sample preparation or separation. This techniques has a significant impact of proteomics where enriched, trapped, pre-fractionated or desalted peptides can be eluted and separated on column<sup>251</sup>.

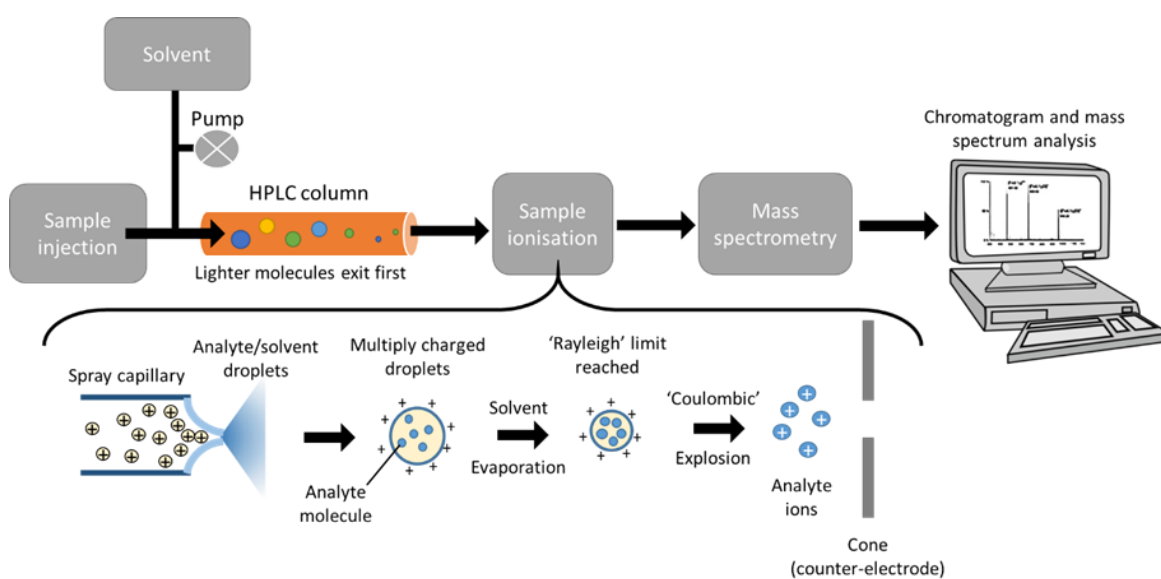


**Figure 2.10. Illustration depicting the instrumentation principle and working mechanism of HPLC.**

**Protocol:**

In this peptide study, RP-HPLC (Dionex) equipped with a UV detector fixed at 214 nm and Phenomenex made reverse phase porous column (Jupiter® 4 µm Proteo 90 Å C12) has been used to detect the purity of lyophilized (VirTis® 110 freeze dryer) peptides. The stationary phase in the column is tightly packed with porous silica particles that are functionalized with hydrophobic groups which can help in binding to an analyte. While, for eluting the analyte, a mixture of solvents has been used to construct two different mobile phase gradients comprising of HPLC graded acetonitrile and water. First mobile phase (highly polar) consists of a mixture of 95% acetonitrile, 5% water and 0.01% TFA, whereas for second mobile phase, the nature of polarity decreased by changing the acetonitrile and water percentages to 5% and 95% respectively. Priming and degassing was performed for both mobile phase solvent mixtures to adjust the column by clearing the impurities present earlier. The Peptide sequence along with a multitude of other factors will influence the retention time of the analyte on the column, this may result in a higher/ lower affinity for a non-silica binding sequence but then this is silica with C12 groups and capped silanols on the surface so no significant amounts of free SiO<sub>2</sub> groups are present for binding to silica binding sequences. Also, the electrostatic interactions with the silica surface is reduced by running in TFA (0.01% TFA pH ~ 1.8 – 2.0) which would provide slightly protonated silica by allowing only hydrogen bonding and van der waals interactions with the peptides. In addition to this, the column used has been end capped with TMS (trimethyl silane) which effectively blocks access to the silica surface to the peptides by replacing any residual Si-OH with Si-methyl groups. As a result, the silica binding peptides were eluted out without binding to the column that is packed with silica.

For comparison, a blank sample consisting of 50% HPLC graded water, acetonitrile and 0.01% TFA was run before and after each peptide sample run. Furthermore, Chromeleon® software has been used for processing the data peaks thereby analyzing the purity of the peptide samples. The purity of first list of peptides LPVRLDW, NDLMNRA, GQSEKHL, GASESYL and KIAVIST was measured as 94%, 80%, 94%, 95% and 94% respectively (Appendix 2.1). On the other side, the purity of second list of synthesized peptides YSLKQYQ-OH, YSLKQYQ-NH<sub>2</sub>, ADIRHIK-OH, ADIRHIK-NH<sub>2</sub>, HYIDFRW-OH and HYIDFRW-NH<sub>2</sub> was measured as 93.8%, 92.9%, 94.1%, 97.7%, 77.3% and 72.9% respectively (Appendix 2.2).

### 2.1.2.6.3 Matrix-assisted laser desorption ionization time-of-flight (MALDI-TOF) mass spectrometry

Mass spectrometry (MS) is an analytical technique for studying masses of atoms, molecules or fragment of molecules such as proteins and peptides. The instrument (Figure 2.11) consists of an ion source to produce ions from the sample, a mass analyser for the separation of the various ions according to their  $m/z$  ratio and the detector. Mass spectrum is obtained when gas-phase ions of compounds are produced by ionising the condensed phase. The molecular ions undergo fragmentation<sup>252</sup>. The ions are accelerated by an electric field, then through a magnetic field where ions are separated according to their mass-to-charge ratio,  $m/z$ . The area of peak in each mass spectrum is proportional to the abundance of each isotope. The magnet within the mass spectrometer, deflects the ions towards the detector; where the trajectory of each ion varies with their respective mass and magnetic field strength<sup>253–255</sup>. Mass spectrometry has been used to classify amino acid sequences in proteins, nucleic acids in DNA and structure of complex carbohydrates<sup>256,257</sup>. MALDI requires less sample preparation and is popular for the analysis of biomolecules such as oligonucleotides, proteins and glycoproteins<sup>258–261</sup>.

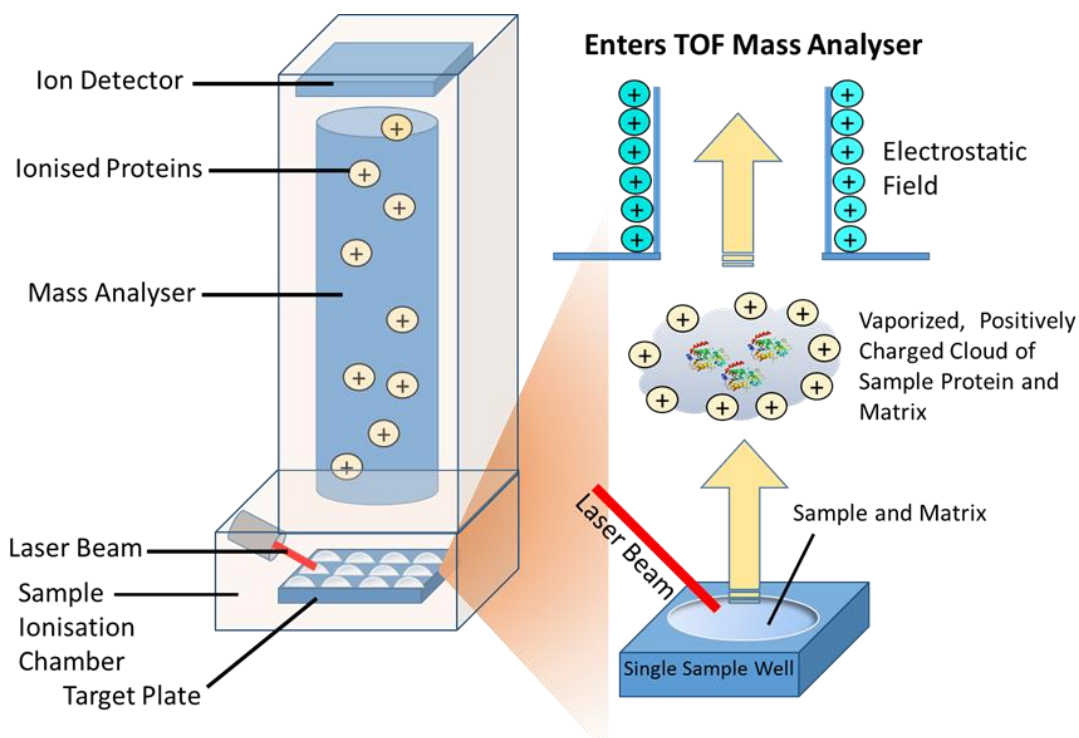


**Figure 2.11. Illustration describing the principle and mechanism of MALDI-TOF mass spectrometry.**

The technique 'Matrix-Assisted Laser Desorption' was first mentioned in the paper by Karas *et al.* 1985<sup>262</sup>. MALDI-MS samples are prepared by embedding the analyte in a matrix (crystalline structure of small organic compounds) and deposited on a conductive sample support. This forms a co-crystal which is then irradiated with a high energy (commonly UV) laser pulse with a wavenumber of 266 or 337 nm. The bombardment of the laser causes a structural decomposition of the cocrystal and generates a plume of particles from which ions are extracted travelling by the electric field. The mechanism (Figure 2.11) for the process of desorption is best described as the conversion of the laser energy into vibrational oscillation of the crystal molecules. After acceleration of the ions through the electric field, the ion drifts through a field-free path and reaches the detector<sup>263,264</sup>. The pulse generation of ions in the MALDI technique lent itself to be used in combination with time-of-flight (TOF) mass analysers<sup>265</sup>.

**Protocol:**

For this peptide study, an automated matrix-assisted laser desorption ionization time-of-flight (Bruker Ultrflex III TOF/TOF) mass spectrometer has been used to characterize the quality of lyophilized (VirTis® 110 freeze dryer) peptides based on the molecular mass of the peptides. The fragments separated based on mass to charge ratio ( $m/z$ ) with MALDI-TOF/TOF and MS/MS spectrums have been considered for identifying the peptides. The data for these peptides was performed and collected at Van Geest Cancer Research Centre, NTU by Dr. Graham Hickman (postdoc within the Perry group) with a resolution mass in between 700 and 6000 Da as well as using Bruker Daltonicflex analysis software. A mixture of mass spectrometry and HPLC graded solvents comprising of a mixture of 50% acetonitrile, 50% water and 0.1% formic acid has been used to run peptide samples (1mg/ml). A blank sample consisting of the same mixture (prepared for peptides) was run before running each peptide sample. The Bruker Ultraflex MS system is calibrated with ProteoMass™ Peptide Calibration Kit (Sigma) which includes a series of calibration standards across the range of 756.3997 to 3,494.6513 Da. The molecular weight of the peptides LPVRLDW, NDLMNRA, GQSEKHL, GASESYL and KIAVIST was measured as 898.5 g/mol, 833.3 g/mol, 798.4 g/mol, 726.2 g/mol and 731.41 g/mol respectively (Appendix 2.3).

## 2.1.2.7 Silica-Peptide Binding studies

## 2.1.2.7.1 Fluorescence spectroscopy

Fluorescence spectroscopy is a special type of electromagnetic spectrofluorometry commonly used to measure the emitted fluorescence from a sample<sup>266</sup>. The principle of fluorescence can easily be explained using Jablonski diagram (Figure 2.12, a). When a light hits the molecule, the electrons get excited by reaching a higher energy level. An excited state of any molecule is short-lived, the electrons from higher energy state can undergo non-radiative transition or vibration relaxation. Furthermore, the electrons from excited vibrational level state slowly reaches to the lower vibration state and making it possible for the electron to return to the ground state. This flow of emission is termed as fluorescence. On the other hand, fluorescamine, a non-fluorescent dye reacts rapidly with primary amine groups of proteins or peptides that are found attached to terminal amino acids or positively charged  $\epsilon$ -amino group of lysine, thereby forming a fluorescent compound that can be measured using fluorescence spectroscopy (Figure 2.12, b).

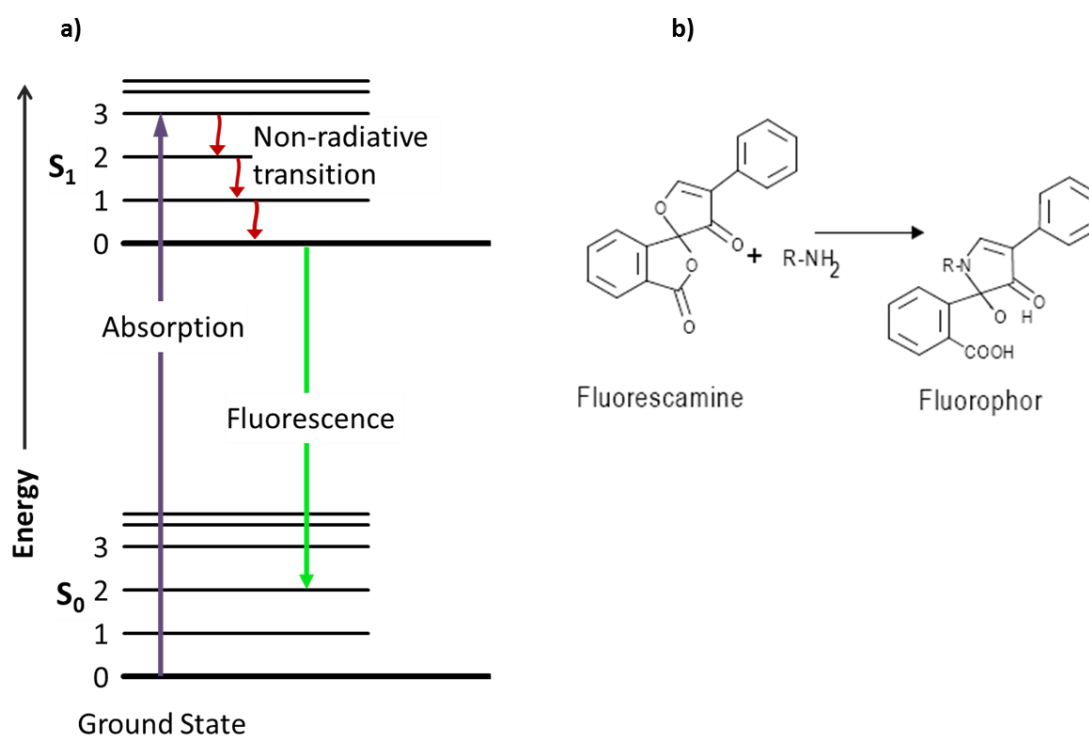


**Figure 2.12. Illustration depicting the working principle of absorption and fluorescence spectroscopies and fluorescamine binding mechanism to proteins.**

a) Jablonski diagram depicting the mechanism of absorption and fluorescence emissions including their electronic and vibrational transitions of a molecule and the transition between them <sup>267</sup>. b) Reaction mechanism of fluorescamine and primary amine groups of terminal amino acids <sup>268</sup>.

Several assays based on fluorescence have been established for quantifying the proteins or peptides in an effort to improve the absorbance-based assays such as Bradford and Lowry<sup>269</sup>. Fluorescamine is a non-fluorescent compound upon interaction with peptides rapidly reacts with primary amines that are present attached to the terminal end of biomolecule or with  $\epsilon$ -amino side chain residue of lysine, hence forming a fluorescent product which can be measured by Fluorescence Spectroscopy<sup>270</sup>. This assay measures the fluorescence intensity of total protein content present in the samples using fluorescamine assay protocol. Thus, provided that calibration data is available for the particular protein/ peptide and can be used in our peptide-silica binding studies. Note, the amount of peptide remaining in solution at specific time points is measured and the amount of peptide adsorbed to silica surface calculated by difference to the amount present at the start of the reaction.

The limitations or issues with method include i) The reagent is unstable (i.e) non-fluorescent compound fluorescamine reacts readily with the primary amino groups in milliseconds, thereby forming a fluorescent compound. However, the unreacted compound gets hydrolysed in seconds and removing the fluorescamine from the reaction. Hence, the measurements were taken immediately after adding fluorescamine to samples. ii) The assay is not well-suited with amine-containing buffers. Hence, phosphate buffer saline was used not TBS which can interfere with the experiment. iii) Sensitivity depends on the number of amines present and is limited to solution-based studies.

#### **Protocol:**

For studying the peptide-silica binding, samples prepared on 96-well plate (Corning® black polystyrene) using fluorometric quantification assay method<sup>271,272</sup> were stained with fluorescamine dye which effectively binds to primary amine groups of peptides<sup>273</sup>. This non-fluorescent upon interaction with peptides rapidly becomes fluorescent in nature by forming fluorophore<sup>270</sup>. The procedure used for preparing sample was schematically shown in Figure 2.13. A calibration line was initially plotted by preparing a series of dilutions of the peptide of interest with the known concentrations of peptide ranging from 0.2-1.6 mM in phosphate-buffered saline buffer of pH-7.5.

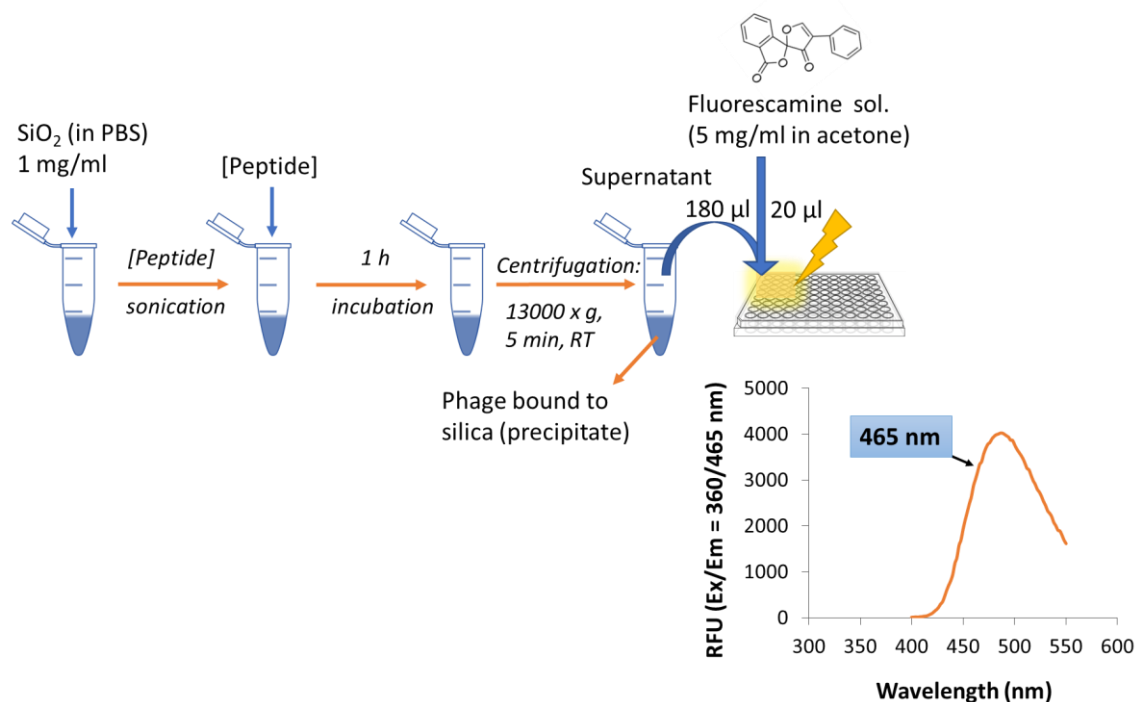


**Figure 2.13. Schematic representation of fluorescamine assay protocol used for preparing samples.**

On the other hand, a series of samples were prepared in individual 2 ml Eppendorf tubes by adding suspension of silica nanoparticles (1 mg/ml) in phosphate-buffered saline buffer and sonicated for 1 hour to uniformly disperse the particles. To the sonicated suspension, suitable amounts of peptide (concentration ranging from 0.2-1.6 mM) was added to all the Eppendorf tubes containing PBS dispersed silica nanoparticles to achieve the desired initial peptide concentration. These mixtures were then shaken vigorously and left them for incubation for 1 hour at room temperature. At this point centrifugation was performed at  $11330 \times g$  for 5 min. Then the supernatant was transferred to a new clean Eppendorf tube followed by quantifying the amount of peptide left in the solution. Thereafter, 180  $\mu\text{l}$  of the supernatant solution along with 20  $\mu\text{l}$  of fluorescamine (5 mg/ml) in acetonitrile was added to a 96-wellplate (Corning® black polystyrene) and the fluorescent intensity of the samples was then measured using fluorescence multiplate reader (TECAN Infinite® M200 PRO) by setting excitation and emission wavelengths at 360 nm and 465 nm respectively<sup>4,107</sup>. The concentration of each peptide was measured using a peptide calibration curve, and the amount of peptide adsorbed was calculated by the difference from the initial peptide concentration. To attain the best signal-noise ratio, the gain was set at 60 a.u. All assays were repeated for 2-3 times to get reliable and best fitting data.



## 2.1.2.7.2 Raman spectroscopy

Raman spectroscopy is a scattering technique, commonly used to detect vibrational, rotational and low frequency movement of molecules in the system. Over the past decades, it has become a versatile research or analytical tool for applications ranging from biomedical to pharmaceutical and even for analysing nanomaterials<sup>274–277</sup>. The principle is based on inelastic scattering of light (Figure 2.14). When a monochromatic incident light hits the molecule or crystal, the photons of light get scattered in all directions. Most of the scattered light has a frequency (wavelength) equal to that of the incident light and is called Rayleigh scattering. A tiny fraction of the scattered light has a frequency different from that of the incident laser light and is called Raman Scattering. The difference in the energy frequency of the incident and the scattered light represents the characteristics of the molecule vibrations or bonds and is used to construct a Raman spectrum. If the scattered light has a frequency lower or higher than the incident light, Anti-Stokes and Stokes Raman appear respectively.

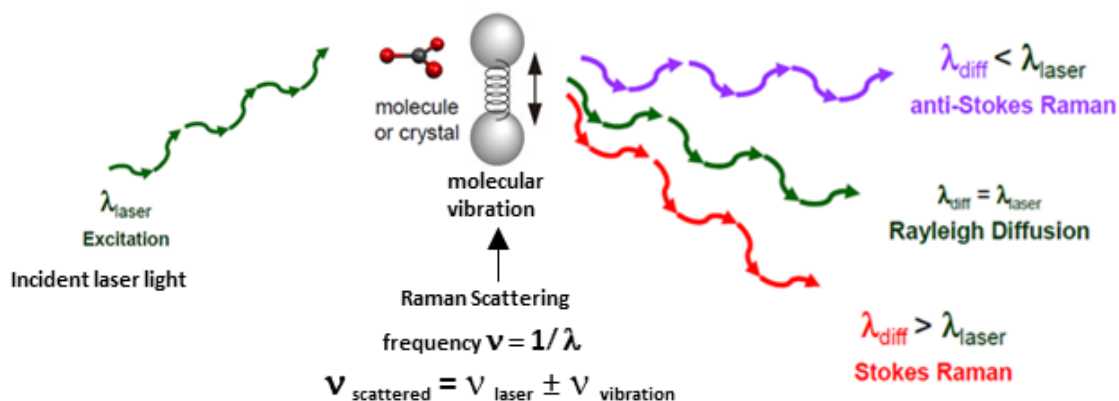


**Figure 2.14. Working principle of Raman spectroscopy.** Raman scattering is based on the frequency of incident and scattered radiations upon laser hitting the sample forcing the sample to vibrate forming Rayleigh, anti-stokes and stokes Raman spectrum. Image adapted from HORIBA Scientific webinar<sup>278</sup>.

Raman spectroscopy is well suited for solid and liquids due to its advantages. i) Minimum sample preparation is needed, for example 1mg for solids and 50-100  $\mu$ l for liquids. ii) suitable for both solids and liquids iii) has much weaker signal for water than any other materials, hence the analysis of solids or particles becomes easy with no interference of water. iv) non-destructive and quick. However, using an intense laser power can destroy the samples and is not suitable for studying of metals or metal composites<sup>275</sup>.

**Protocol:**

In this work, Raman spectroscopy has been used for the identification of peptide LPVRLDW and to probe its interaction with silica particularly to see the changes in the amino acid residues. For analysing the sample, the Nicolet iS50 spectrometer equipped with a 785 nm near infrared laser with power 2.5 Watt has been used. While, Thermo Scientific OMNIC™ software was used for fitting the mixture spectra. The samples prepared for Raman analysis include solid samples of silica alone (1 mg), peptide LPVRLDW alone (1 mg), and the mixture of peptide LPVRLDW-silica samples including liquid air-dried (1mg of peptide-silica suspension in 1ml in water w/v), solid powdered (1 mg of peptide with 1 mg of silica w/w) and the samples from fluorescamine assay (1mg of peptide-silica suspension in 1ml in PBS w/v). The precipitated peptide samples (adsorbed to silica nanoparticles) obtained from the fluorescamine assay (after the centrifugation step) were washed twice with water, air-dried and investigated using Raman spectroscopy to see if change in the peptide structure on binding could be identified.

**2.1.2.7.3 Transmission electron microscopy (TEM)**

Transmission electron microscope (TEM) is one type of electron microscope. It operates in the same manner as a light microscope but uses electron as opposed to light. The electron within the TEM is generated by the source. The source contains an anode and a cathode, which when heated, emits electrons which are then accelerated toward the specimen (Figure 2.15, a). Electrons at the rim of the beam will plunge onto the anode while the others will pass through the centre small hole of the anode. Electrons become scattered as the beam of electrons pass through the thin section of the specimen. A series of electromagnetic lenses focus the scattered electrons into an image or diffraction pattern (Figure 2.15, b), or a nano-analytical spectrum, depending on the operating mode. TEM has application in various diagnostic fields such as cancer research, virology, pathology and material science and pollution<sup>279–281</sup>.

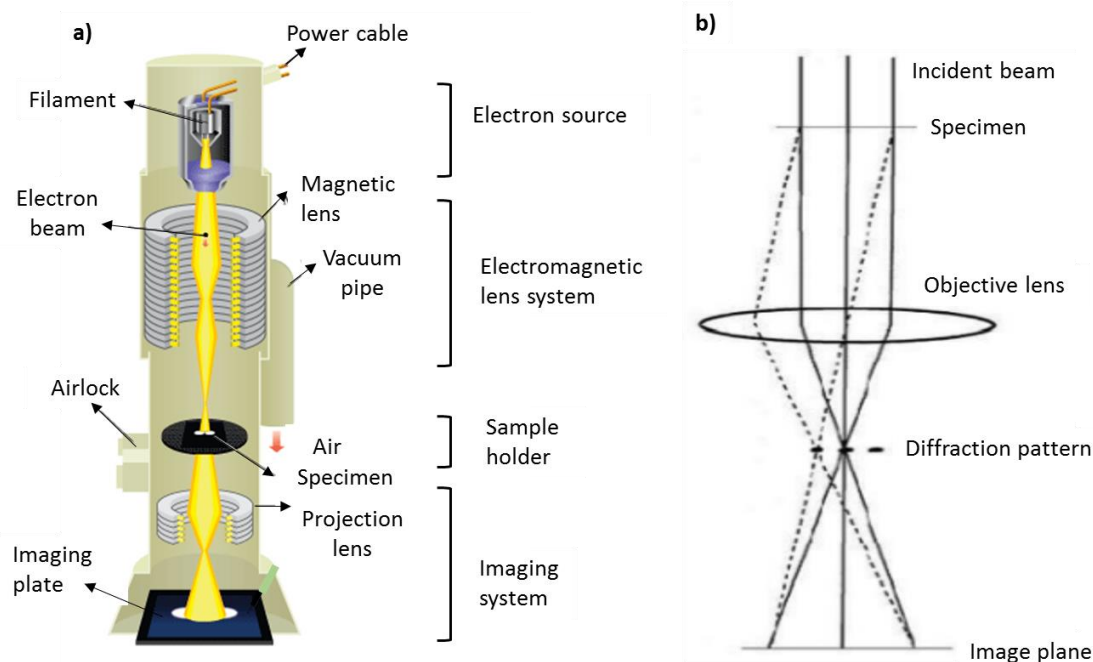


**Figure 2.15. Diagrammatic representation of TEM working principle and mechanism** a) The schematic outline of a TEM b) A ray diagram from the diffraction mechanism in TEM. Image adapted from <sup>279,282</sup>.

For studying the peptide-silica interactions, TEM (JEOL JEM-2010) equipped with LaB<sub>6</sub> emitter (filament) and with 80-200 kV operating voltage range was used. TEM grids used for sample analysis were coated with Poly-L-lysine and/ or paraformaldehyde. A non-radioactive dye EM Stain 336 (Uranyl Acetate Alternative) purchased from agar scientific, diluted 4x times in double distilled water (ddH<sub>2</sub>O) was used to stain the peptide-silica complex affixed on TEM grid. The uranyl type acetate ions present in the dye binds to peptides which can be visualized under TEM. Furthermore, the stained samples were washed with ddH<sub>2</sub>O and air dried at room temperature before analyzing with TEM. For comparison, silica alone, silica with dye and Ph.D.<sup>TM</sup>-7 phage display peptide library (New England Biolabs) with dye was observed under TEM.

**Protocol:**

The JEOL 2010 TEM has been used to examine the phage bound to silica and observe the surface morphology of the silica particles. The amplified phage clones displaying the selected peptides YSLKQYQ, ADIRHIK and HYIDFRW were mixed with silica nanoparticles (1mg/ ml) and incubated on either Poly-L-lysine and/ or paraformaldehyde coated TEM grids. The TEM grid containing silica-phage suspension was washed thrice with distilled

water to remove weakly bound phages followed by adding a drop (roughly 5  $\mu$ l) of EM stain 336 diluted in water (purchased from Agar Scientific) and left for 30 min at room temperature for the dye to stain phage peptides. Then the grids were air dried before washing three times with distilled water by adding drop by drop leaving 10 sec intervals between each drop (roughly 5  $\mu$ l). These air-dried samples were visualised under TEM by setting the voltage as 2000 volts and using LaB6 filament to confirm the phage-silica binding. The known peptide sequence displaying YSLKQYQ, ADIRHIK and HYIDFRW single phage clones were selected for probing phage-silica binding studies using TEM. The process by which these phage clones were prepared has already been described in section 2.1.2.5.

## Chapter 3: Selection and Screening of Silica Binding Peptides by Phage Display Process

### 3.1 Introduction

Over the last two decades, silica has attracted considerable interest because of its developing use in bio- and nano-technology. Silica is commonly found in nature as quartz, which is in crystalline form but with metal impurities thereby limiting its usage in scientific and industrial applications<sup>283</sup>. Thus, to meet the rising demand of pure silica nanoparticles with controlled size and shape, synthetic routes are being used to synthesize silica nanoparticles with improved physical, chemical and functional properties<sup>106,133,284</sup>.

In recent years, amorphous silica nanoparticles have gained tremendous attention for their growing applications in biomedical<sup>285</sup> and nanomedical applications<sup>286</sup>, mainly due to its distorted structure, comparatively higher surface area, decent permeability with cell or plasma membranes, very low to no toxicity compared with crystalline silica nanoparticles. The unique characteristics of amorphous SiNPs including biocompatibility and biodegradation with biological or cellular systems combined with functionalisation makes them unique candidates for nanomedical applications<sup>286</sup>. The toxicity of amorphous SiNPs in biological systems is directly dependant on various physical, chemical and environmental factors such as the particle size, shape, crystallinity, surface functionalisation, chemical composition, dosage, time and type of organism or cell lines exposed *in vitro* or *in vivo* conditions<sup>64,287-291</sup>. For instance, studies have shown that with decrease in the size or surface area of the SiNPs (< 20 nm) the toxicity was increased causing cytotoxic damage to cells thereby affecting the cellular uptake process<sup>292-294</sup>.

To date, a wide range of synthetic SiNPs have been generated by tuning their chemical and functional properties either by directing silica nanoparticles themselves or by modifying them with inorganic or organic molecules. For example, the abundant number of hydroxylic groups on the silica surface allows them to be used for further functionalization, including moieties such as carboxyl<sup>295</sup>, amine<sup>296,297</sup>, methyl<sup>296,297</sup> phenyl<sup>298</sup> or thiol<sup>299</sup> groups leading to functionalized silicas. Furthermore, SiNPs have also been functionalized with dye molecules to generate fluorescent silica NPs in order to study biological processes and conduct cell imaging assays<sup>300,301</sup>. A study carried out by Ha et al. showed that fluorescent

SiNPs can increase thermal, photochemical, and pH stabilities as well as its biocompatibility for in vivo assays<sup>302</sup>.

The organic molecules reported to bind to silica NPs include proteins (silica binding peptides, antibodies or antibody fragments, enzymes and streptavidin or avidin BPs<sup>4,12,303–306</sup>, cells (bacterial or viral)<sup>134,307,308</sup>, nucleic acids (DNA or RNA)<sup>135,309</sup> and other targeting molecules (ligands and peptide motifs)<sup>310,311</sup>. Although nanomaterials have been designed and produced decades ago, their utilization in nano- or bio-technology is limited due to poor solubility, stability and biocompatibility issues. Several strategies have been developed to overcome the potential safety concerns including poor solubility, stability and biocompatibility issues; and eventually, phage display technology was able to provide greater control over the nanomaterials.

Phage display technique, initially developed for screening biological targets (as mentioned in section 1.1.1, Chapter 1) has now become ubiquitous in selecting and screening peptides having high affinity towards a range of inorganic material surfaces. Until now, a range of biomimetic peptides displaying specific affinity and molecular recognition for metals (Ag<sup>142–144</sup>, Au<sup>7,19</sup>, Pt<sup>66</sup>, Pd<sup>142</sup>), metal oxides (SiO<sub>2</sub><sup>4,10,24,65,145</sup>, ZnO<sup>146,147</sup>, TiO<sub>2</sub><sup>8,59,148</sup>, Fe<sub>2</sub>O<sub>3</sub><sup>149,150</sup>, IrO<sub>2</sub><sup>151</sup>, Al<sub>2</sub>O<sub>3</sub><sup>10,152</sup>, Cu<sub>2</sub>O<sup>146</sup>), minerals (calcite, hydroxyapatite, graphite, mica, sapphire)<sup>153–155</sup>, semiconductors (CdS, GaN, GaAs and ZnS)<sup>23,86,156</sup>, carbon materials (graphene, carbon nanotubes)<sup>157,158</sup> and polymer materials<sup>159,160</sup> have been isolated.

Further, these material specific peptides have been used as creators and builders for synthesizing simple to complex bio- or nano-materials, mediating the controlled biomineralization process<sup>147,312,313</sup>, directing self-assembly and nanofabrication of ordered structures<sup>93,125,153,186,189,314–316</sup>, facilitating the immobilization of functional biomolecules and for constructing inorganic-inorganic or organic-inorganic nano hybrids<sup>6,8,151,181,317</sup>. More details of inorganic material binding peptides and their applications were discussed in section 1.4.

In the recent years, several groups have identified silica binding peptides using Ph.D.-7 and Ph.D.-12 random peptide display libraries as shown in Table 3.1. Further, these peptides were utilised in various applications including nanomaterial synthesis<sup>24,65,192</sup> and to understand the mechanisms involved at silica-biomolecule interface<sup>4,59,107,124,132</sup>. Further

details of silica-biomolecule interactions and their applications have been discussed in section 1.2.2.

**Table 3.1. List of silica binding peptides reported in literature that were identified by phage display technique.**

No	Peptide Sequence	Target info	Biopanning round screened	Phage peptide library type	Reference
1	APPGHHWHIHH MSASSYASFWS KPSHHHHTGAN	Silica	3	Ph.D.-12	24
2	MSPHPHPRHHHT MSPHHMHSHGH LPHHHLHTKLP APHHHPHHLR RGRRRRLSCRL	Silica	4	Ph.D.-12	
3	HPPMNASHPHMH HTKHSHTSPPL	SiO <sub>2</sub> films (100 nm)	3	Ph.D.-12	65
4	CHKKPSKSC	SiC1	6	Ph.D.-7	145
5	CTSPHTRAC CSYHRMATC	Ge-on-Si	3	Ph.D.-C7C	318
6	RLNPPSQMDPPF QWPPPLWFSTS	Quartz-binder	3-5	Ph.D.-12	319
7	YITPYAHLRGGN	Silica (15 nm)	5	Ph.D.-12	10
	KSLSRHDHIIHH	(82 nm)	5	Ph.D.-12	
	LDHSLHS		5	Ph.D.-7	
	MHRSDLMSAAVR	(450 nm)	5	Ph.D.-12	
8	KLPGWSG AFILPTG	(82 nm)	3-5	Ph.D.-7	4
9	LSNNNLR	SiO <sub>2</sub>		Ph.D.-7	320
10	AAPSEHRHSRQ ALAHNPKTTHHR ERPLHIHYHKGQ TTHSKHHFPSSA	Siliceous spicules	3	Ph.D.-12	321

However, very few studies were reported identifying heptapeptides displaying affinity to silica using Ph.D.-7 library. As mentioned in chapter 1, the Ph.D.-12 library contain  $1.9 \times 10^9$  independent clones, or only a small fraction of the  $20^{12} = 4.1 \times 10^{15}$  possible sequences and useful for targets requiring 7 or fewer defined residues for binding but cannot be present in the Ph.D.7 library. Although, 12-mer is long enough to fold into short structural elements,

which may be useful when panning against targets requiring structured ligands. The limitation of this library is that the increased length of randomised segment may allow for the selection of sequences with multiple weak binding interactions, instead of a few strong interactions. However, the PhD.-7 library which contain  $2.8 \times 10^9$  independent clones, enough to encode most of the  $20^7 = 1.28 \times 10^9$  possible 7-residue sequences are useful for targets requiring binding elements concentrated in a short stretch of amino acids. Also, these short heptapeptides peptides are easy to work with and can simply be exposed to solvents during the phage display process unlike larger peptides which are easily degradable, problematic to purify and are unstable at higher temperature and pH changes.

In this study, we used a traditional biopanning process using three different chemical elution buffers (low pH, high pH and high salt) with specific elution conditions that removed unique heptapeptide binding phages from amorphous silica nanoparticles via disrupting the electrostatic and non-electrostatic interactions. Moreover, a repanning method to biopanning reported here has reproduced more or less the same silica binders alongside identifying/recovering additional sequences that may have missed in the previous biopanning experiments. Furthermore, selected silica binding peptides isolated from both biopanning and repanning processes have been artificially synthesized and their binding to silica verified using fluorometric quantitative assay and Raman spectroscopy.



## **3.2 Materials and Methods**

### **3.2.1 Materials**

Chapter 2, section 2.1.1 provides details of materials used for adsorption studies.

### **3.2.2 Methods**

#### **3.2.2.1 Phage display protocol**

For this phage display study, the typical protocol applied for the initial (traditional) and repanning biopanning experiments are discussed in methods sections 2.1.2.1 and 2.1.2.4. While, the details of phage display experiments and elution conditions used to elute silica binding peptides via initial and repanning methods can found in the Tables 2.1, 2.2 and 2.5.

#### **3.2.2.2 Relative binding affinity method**

To assess the binding of phage clones to silica, the individual phage clones were amplified and selected as described in methods section 2.1.2.5. A total of 15 different individual phage clones identified from both initial and repanning experiments were chosen. The silica nanoparticles (1mg) were washed 10 times with TBST (0.3% Tween 20 [v/v] in 1ml of TBS) at pH-7.5, incubated with equivalent selected phages ( $2.5 \times 10^{10}$  pfu/ml) separately and then washed 10 times with TBST. Bound phages were eluted by three step elution process, neutralised (section 2.1.2.3), mixed together and determined by phage titer assay and blue/white screening methods (section 2.1.2.1.2). Out of the 15 individual phage clones selected, six individual clones which were identified less frequently (QQTNWSL, QLAVAPS and VGSYLG I) or only once (GTGSQAS, ETALIAA and SQTFTSD) in either of the initial and repanning experiments were randomly picked as controls along with M13KE (wild type). The M13KE phage with no random peptides displayed on pIII coat protein was chosen as a main control. By calculating the ratio of bound or output to input amounts of phage clones the binding ratio for phage clones were estimated. The phage titer calculations including the number of input to output phages and the binding ratios from two separate experiments (repeats) can be seen in Appendix 3.1.

#### **3.2.2.3 Bioinformatics searching**

Chapter 2, section 2.1.2.2 provides details of materials used for bioinformatics analysis.

#### **3.2.2.4 Silica-peptide interaction studies**

Two techniques, including fluorescamine assay and Raman spectroscopy has been used to verify silica-peptide binding. Five peptide sequences LPVRLDW, NDLMNRA, GQSEKHL,

GASESYL and KIAVIST synthesized (section 2.1.2.6.1) and characterized (sections 2.1.2.6.2 and 2.1.2.6.3) were selected for fluorometric fluorescamine based quantification assay. The protocol and materials used for this assay are described in chapter 2, section 2.1.2.7.1. While for Raman spectroscopy analysis the peptide LPVRLDW was chosen. The protocol and materials used for this assay are described in chapter 2 under section 2.1.2.7.2.

### **3.3 Results and Discussion**

For the entire phage display study, the same batch of amorphous silica nanoparticles of size 82 nm prepared in the Perry laboratory and previously characterised<sup>4,107,234</sup> has been used as a target to avoid any inconsistencies that might occur due to differences in the surface properties of inorganic material. More information about the properties and measurements of silica particles is described in Table 2.6 under the section 2.1.2.6. Similarly, the results presented in this chapter, used the same batch of M13 Ph.D.-7 phage display peptide library kit (#E8100S, Lot: 0211212) for all phage display experimentations including initial biopanning and repanning methods, as described in Chapter 2 under materials section 2.1.1.1). Three different elution buffers (0.2 M Glycine-HCl, pH-2.2; MgCl<sub>2</sub>, pH-6.1; TEA, pH-11) with varying pH 2-11 were randomly chosen for this chapter, to elute and collect the phages that bound to the target material. The list of phage display experimental conditions including experimental numbers, three different elution buffers and conditions (i.e pH and number of times elution and screening rounds performed) used in the initial biopanning and repanning experiments are shown in Tables 2.1, 2.2 and 2.5. More details including step by step biopanning protocol used to isolate silica binders was described in chapter 2, under methods section 2.1.2.1.

#### **3.3.1 Silica binders identified from initial (traditional) biopanning**

Here, a total of six separate biopanning experiments, and for each biopanning experiment, three panning rounds were performed. In each panning round, phage binding, washing, elution and amplification steps were carried out. At the end of third round, blue/white screening method was used to select phage plaques. A total of 79 individual phage plaques were selected randomly from third round of different panning experiments (Table 3.2, 1-6) and analysed by DNA sequencing. Out of 79 individual phage plaques picked for sequence analysis, 52 plaques (eluted via Glycine-HCl, pH-2.2) were selected from four separate

panning experiments (Table 3.2, 1-4). While, 14 and 13 phage plaques (eluted via MgCl<sub>2</sub>, pH-6.1 and TEA, pH-11) were picked from panning experiments 5 and 6 respectively (Table 3.2, 5-6).

In the very initial biopanning tests (Table 3.2, 1-2), a small number of individual phage plaques (i.e 3 and 4 plaques for the panning experiments performed in the years 2013 and 2014; three being the lowest number) obtained from third round of biopanning were selected for sequencing, which resulted in variable peptide sequences showing no or single similar binder SAAWNKS (two out of three from experiment 2, Table 3.2) being repeated. Research groups differ in their selection of phage plaques for identifying inorganic material binding peptides<sup>10,24,69,322,323</sup>. It was reported in the literature that 15-20 phage plaques selected from biopanning rounds 3-5, displayed peptide sequences with high affinity for silver<sup>24</sup>, silica<sup>4,10</sup> and metallic boride<sup>322</sup> nanoparticles. According to NEB manual, 10-20 clones selected from third round are recommended to detect a consensus binding sequence. However, Donatan and co-workers, at the end of each panning rounds 1-4, five individual phage plaques were chosen out of a large amplified pool of binders and were able to isolate mica binding peptide sequences<sup>69</sup>. This variation in selection of clones in terms of numbers can be due to the limitations of experimental process (blue/white screening) used for selecting plaques (i.e only a few clearly visible individual plaques can be picked at a time from plaque plates for sequencing) and the expense of sequencing<sup>66</sup>. Although it is not clear how many clones are needed to isolate the high affinity target binders; from previous studies<sup>4,10,185</sup>, it is appreciated that the larger the number of phage clones selected, the better the results in terms of identifying reliable target binders. To further improve the selection process, we gradually increased the number of phage plaque selection to 13 (experiment 6, 2013), 14 (experiment 5, 2013), 20 (experiment 4, 2014) and 30 (for all other panning experiments including repanning and three step elution biopanning methods) in the subsequent phage display tests.

In the biopanning experiments, after performing three rounds of selection, the phage clones obtained from third round displayed a range of silica binding peptide sequences (Table 3.2) due to the progressive enrichment of phage clone population. Biopanning rounds should not be repeated more than five times because too many rounds of selection tends to collect phage that elute or amplify better than the strong target binders<sup>24,146</sup>. A summary of peptide sequences (repeated, identical and dissimilar) identified from third round of biopanning to amorphous silica using three different elution buffers is shown in Table 3.2. Overall, 21

peptide sequences were isolated coding for 7 identical repeats and 14 different silica binding sequences.

**Table 3.2. Schematic representation of experimental conditions (washing and elution) used for routine biopanning that isolated the silica binders from third panning round using three different elution buffers.** Experimental conditions include the order of experiments performed and their dates (month/ year); washing detergent TBST (TBS with 0.5 % (v/v) Tween 20) concentrations for removing non-specific binders from silica surface; elution buffers and conditions (low pH, high salt and high pH) to elute tightly bound phage clones from silica nanoparticles; selected rounds at which sequences were screened and the most frequently identified silica binders. Identical sequences repeated in one or more panning experiments are presented in a unique colour for clarity.

Exp. order	Date	Wash TBST	Elution buffer and condition	Round screened	Displayed sequence and frequency of appearance	Frequently observed peptides
1	07/13	0.5%	Glycine HCl, 0.2 M, pH-2.2	3	SSFRLDW 1/4 WSLSELH 1/4 SSNQFHQ 1/4 ETTLITA 1/4	<b>LPVRLDW</b> <b>GQSEKHL</b> GASESYL <b>NDLMNRA</b> <b>VSRDTPQ</b>
2	07/13				<b>VGSYLG</b> 1/3 SAAWNKS 2/3	
3	09/13				<b>LPVRLDW 25/25</b>	
4	02/14				GASESYL <b>6/20</b> <b>QLAVAPS</b> 1/20	
					<b>VSRDTPQ</b> <b>3/20</b> ETALIAA 1/20	
					<b>QQTNWSL</b> 2/20 GTGSQAS 1/20	
		WQWPARV 2/20 ALQPQKH 1/20				
					<b>NDLMNRA</b> 1/20 VASHSKP 1/20	
					<b>GQSEKHL</b> 1/20	
5	07/13	0.5%	MgCl <sub>2</sub> , 4 M, pH-6.1	3	<b>LPVRLDW</b> 5/14 <b>QQTNWSL</b> 1/14 <b>NDLMNRA</b> 4/14 <b>VGSYLG</b> 1/14 <b>GQSEKHL</b> 2/14 <b>QLAVAPS</b> 1/14	
6	08/13	0.5%	Triethylamine, 100 mM, pH-11	3	<b>GQSEKHL</b> 7/13 <b>VSRDTPQ</b> 1/13	
					ELTPLPL 2/13 KIAVIST 1/13	
					<b>NDLMNRA</b> 1/13 QHMPQPR 1/13	

From the above findings, it was found that five phage clones displaying peptide sequences LPVRLDW (25/25, 100%), GQSEKHL (10/47, 21%), GASESYL (6/20, 30%), NDLMNRA (6/47, 13%) and VSRDTPQ (4/33, 12%) appeared as the most frequently occurring silica binders (i.e more abundantly observed sequences from a randomly selected few phage clones after third panning round) within the small sequenced population from separate panning experiments (Table 3.2, 1-6). While, some sequences were displayed more than once (highlighted in a unique color) in separate experiments within the biopanning process. The list of repeated silica binders identified from three different elution buffers (0.2 M Glycine-

HCl, pH-2.2; MgCl<sub>2</sub>, pH-6.1; TEA, pH-11) include LPVRLDW, GQSEKHL, NDLMNRA, VSRDTPQ, QQTNWSL, QLAVAPS and VGSYLG I. The peptide sequences GQSEKHL (1/20, 2/14 and 7/13) and NDLMNRA (1/20, 4/14 and 1/13) were displayed in all the three elution buffers used; whereas the LPVRLDW (25/25, 5/14 and 0/13), QQTNWSL (2/20, 1/14 and 0/13), QLAVAPS (1/20, 1/14 and 0/13) and VGSYLG I (1/3, 1/14 and 0/13) peptides were identified from two elution buffers (Glycine-HCl, pH-2.2 and MgCl<sub>2</sub>, pH-6.1). In contrast, the peptide VSRDTPQ (3/20, 0/14/ and 1/13) was eluted from low and high pH buffers (Glycine-HCl, pH-2.2 and TEA, pH-11) respectively. It must be noted that, all the above-mentioned peptide sequences were found at least once in the Glycine-HCl buffered biopanning experiments (Table 3.2, 2-4). However, no apparent sequence similarity peptides were observed from the very initial biopanning experiment 1, using elution buffer 1 (0.2 M Glycine-HCl, pH-2.2). Note that, the term 'tightly bound' silica binders as stated in this thesis refers to the sequences that appeared most frequently from the small number of phage clones that were randomly selected for sequencing out of a large amplified population obtained during multiple rounds of phage display experiments.

The most frequently observed individual silica binding peptide sequences LPVRLDW, GQSEKHL, GASESYL, NDLMNRA and VSRDTPQ shows the total number of functional amino acid groups involved in binding to silica and the percentage of eluted amino acid residue distribution. The peptide LPVRLDW which appeared as the main silica binders in the experiments 3 (25/25), and 4 (5/14) consists of 72% hydrophobic (LPVLW), 14% each acidic (D) and basic (R) amino acid composition. Whereas, the GQSEKHL and NDLMNRA peptide sequences identified in experiments 4 (1/20), 5 (2/14, 4/14) and 6 (7/13, 1/13) distributed 33% and 43% hydrophobic and 57% each hydrophilic amino acid residues. However, the peptides GASESYL (found only in experiment 4, 6/20) and VSDRTPQ (found in experiments 4 (3/20) and 6 (1/13)) displayed 57% and 43% hydrophilic residues.

The distribution of the total number of amino acid groups present in the isolated silica binders from all 6 panning experiments and eluted by three different elution buffers were shown in the Figure 3.1. The low pH elution buffer (0.2 M Glycine- HCl, pH-2.2) from experiments 1-4 eluted clones consisting of 42% hydrophobic and 41% polar uncharged groups in addition to the acidic (8%) and basic (9%) residues. Thus, indicating the low pH

elution buffer might have eluted phages bound to silica mostly by interactions involving electrostatic alongside hydrophobic forces.

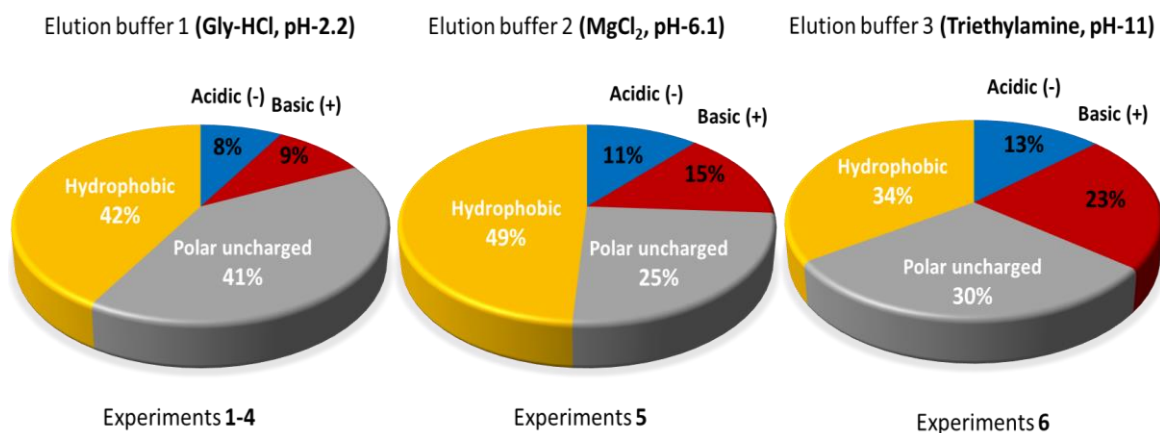


**Figure 3.1. Comparison of functional amino acid groups distributed specific to elution buffer.** All the phage clones identified from panning experiments 1-4 (Glycine-HCl, pH-2.2), 5 (MgCl<sub>2</sub>, pH-6.1) and 6 (Triethylamine, pH-11) are considered while plotting the pie diagrams.

Interestingly, the high salt magnesium chloride elution buffer (4 M MgCl<sub>2</sub>, pH-6.1) from experiment 5 eluted the phage clones displaying peptide sequences containing 49% of hydrophobic amino acids, in contrast to 34% and 42% using high pH triethylamine (100nM Triethylamine, pH-11) and low pH (0.2 M Glycine- HCl, pH-2.2) respectively. However, the total number of functional amino acid groups present in the isolated peptide sequences eluted by high pH triethylamine showed both hydrophobic (34%) and polar (30%) side chained groups alongside removing more acidic (13%) and basic (23%) residue composition than the other two elution buffers. Also, an increase in the acidic and basic charged amino acid residue composition was noticed with increase in the pH of the elution buffers. For instance, the phage clones eluted from elution buffer 1 (low pH) exhibited 8% acidic and 9% basic amino acid groups. While, the same acidic and basic charged residue composition gradually increased to 11% and 15% for the clones identified from elution buffer 2 (high salt, near neutral pH) and 13% and 23% with elution buffer 3 (high pH) respectively.

### **3.3.2 Repanning to check the reproducibility of silica binders identified in 3.3.1**

Repanning experiments were carried out to check the reproducibility of the identified sequences, as described in Chapter 2 under methods section 2.1.2.4 by exposing the mixture of amplified phage pool from the initial tests with fresh silica. This amplified phage mixture was prepared by mixing the round 2 amplified phage samples stored from initial biopanning experiments 1, 2, 4, 5 and 6. Experiment 3 is not taken into account (or excluded) for repanning, as it was thought that the sequence may represent a fast grower (due to panning advantage), as the same peptide sequence was identified repeatedly in rounds 2 (4/4) and 3 (25/25). However, the experiment 5 is included for repanning exercise, where the same peptide was also observed as one of the main silica binders (5/14). More detailed description about the fast growers and their ability to get selected in the further biopanning rounds due to bias in the amplification process was explained in the following discussion. The experimental conditions used for repanning experiments including which amplified phage stocks were taken and then how far carried forward in subsequent biopanning rounds can be found in Table 2.5.

The results of the repanning experiment reproduced similar silica binders (Table 3.3) as were identified previously in the above initial biopanning experiments (Table 3.2) along with few new peptide sequences. Out of 120 phage clones sequenced from two separate repanning experiments (7 and 8) and rounds (3-5), 102 phage clones were reproduced indicating 85% reproducibility. However, 18 new phage clones (15%) were also isolated. The silica binders reproduced which were also isolated previously include LPVRLDW, KIAVIST, GQSEKHL, NDLMNRA, VSRDTPQ, ELTPLPL, QLAVAPS, QQTNWSL, ETALIAA, WSLSELH and GTGSQAS. Also, four peptide sequences that had displayed as tight silica binders (LPVRLDW, GQSEKHL, NDLMNRA, VSRDTPQ) in the initial biopanning experiments (Table 3.2) are reproduced and repeated with in two separate experiments that are eluted by two different elution buffers (Table 3.3, 7-8). While, the peptide sequence GASESYL that had identified only in experiment 4 (six times out of twenty sequenced clones), has not appeared in the repanning method. However, the same sequence KIAVIST that had found only once in previous routine biopanning experiment 6, re-appeared as the main abundant silica binder in both repanning experiments 7 and 8 in all the rounds sequenced (i.e 3-5). Therefore, this repanning process may be used as an obvious way to check the

reproducibility of target binders as well as to recover or identify new binders; and thus, representing a larger fraction of the population.

**Table 3.3. Results of repanning experiments showing both silica binders that were found previously identified and further new silica binders.** The silica binders found previously in the initial biopanning procedure and reproduced in this repanning method can be found under the sub-heading ‘previous binders’. The new binders appearing only in the repanning experimental process are shown as ‘entirely new’. Sequences repeated during different experiments as different round only in this series of repanning experiments are highlighted colour.

Exp. order	Date	Wash TBST	Elution condition	Round	Displayed peptide sequence and frequency			
					Previous binders		Entirely new	
7	07/15	0.5%	Glycine-HCl 0.2 M, pH-2.2	3	<b>KIAVIST</b> 7/30	<b>VSRDTPQ</b> 1/30	<b>HYIDFRW</b> 2/30	
					QLAVAPS 3/30	<b>LPVRLDW</b> 1/30	<b>HVPRAMA</b> 1/30	
					ETALIAA 2/30	ELTPLPL 1/30		
				<b>GQSEKHL</b> 2/30				
	07/15	0.7%		4	<b>KIAVIST</b> 10/30	ELTPLPL 1/30	<b>HVPRAMA</b> 4/30	
					<b>VSRDTPQ</b> 7/30	<b>QQTNWSL</b> 1/30	<b>HYIDFRW</b> 1/30	
					<b>LPVRLDW</b> 2/30	WSLSELH 1/30	SQTFTSD 1/30	
					<b>GQSEKHL</b> 1/30	GTGSQAS 1/30		
	07/15	0.9%		5	<b>KIAVIST</b> 22/30		<b>HYIDFRW</b> 1/30	
					<b>NDLMNRA</b> 8/30			
8	11/15	0.7%	Triethyl amine 100 mM, pH-11	4	<b>KIAVIST</b> 12/30	<b>VSRDTPQ</b> 1/30	<b>HYIDFRW</b> 3/30	
					<b>GQSEKHL</b> 4/30	<b>NDLMNRA</b> 1/30	SFPLSKY 3/30	
					ELTPLPL 3/30	<b>QQTNWSL</b> 1/30	TVNFKLY 1/30	
						HGGVRLY 1/30		

Interestingly, a few sequences HYIDFRW, HVPRAMA, SQTFTSD, SFPLSKY, TVNFKLY and HGGVRLY appeared only in this repanning process. The isolation of new peptide sequences only in this repanning process could perhaps be due to two possible reasons. As they were not identified before in the initial biopanning experiments suggests that these entirely new peptide sequences are the ones that might have been missed probably due to too few phage clones being picked randomly from the large pool for sequencing. In the repanning experiments representing a larger proportion of the initial population was recovered. In other terms, only a subset of sequences within the small proportion of clones sequenced were identified via the initial biopanning process. In performing repanning experiments, some clones have been further selected due to the conditions used. The other possible reason might be that these phage clones are the ones that perhaps have selected in the repanning experiments due to their amplification advantage (encouraged by propagation



preferences of phage in bacteria) or binding to other components of the screening process including the blocking agents, contaminants and other reagents<sup>1,2,324</sup>.

However, the recurrence of the phage clone displaying the peptide LPVRLDW in this series of repanning experiments, also proves the sequences that appeared as tight silica binders have not undergone any propagation advantage in the biopanning rounds which is a common problem in phage display<sup>1,233</sup>. For instance, the reappearance of LPVRLDW peptide sequence in the repanning experiments suggests this phage clone does not have any propagation advantage which implies this peptide sequence is not a fast grower but a genuine target binder. The sequences holding proliferation advantage have the capacity to select as main target binders even after the first round of biopanning during the amplification step which can be very notorious and ruin the entire phage display work by hiding the actual binders, thus giving false results<sup>325</sup>. Several databases have been designed to identify fast growers and/or target unrelated peptide binders (TUPs). The PepBank and MimoDB was designed based on published experimental results and as well as theoretical predications knowing that the 7-mer phage library having  $2 \times 10^{11}$  phages should theoretically contain  $2 \times 10^9$  peptide sequences<sup>55,216,217,326</sup>. Other web-based tools like SAROTUP have been built to aid in the identification of peptides that bind to unrelated target materials that were used during the biopanning process<sup>327</sup>. For example, a list of phage displayed peptide sequences identified to have affinity for plastic or polystyrene based components such as well plates, beads, petri dishes and films during biopanning process are shown in Table 2.3, section 2.1.2.2, Chapter 2. Although, the results of these databases are mainly constructed based on already published sequences and theoretical predictions, the repanning method may experimentally verify your own target binding results giving information about any possible non-specific binding due to panning limitation or amplification bias and thereby checking the direction of the ongoing phage display work. Thus, the repanning method reported for the first time for silica binders appeared to be a straight forward approach to verify all phage display experimental results simply by mixing phage clones from different biopanning experiments and rounds.

### **3.3.3 Relative binding affinity experiment to evaluate phage binding to silica**

The phage clones that appeared and were identified as main silica binders in all phage display experiments (i.e. initial and repanning tests) were further analysed by performing the relative binding affinity assay<sup>306,322,323</sup>. It is important to note that the phage clones isolated as main binders (i.e. most abundantly occurred) in the bioapanning experimental rounds do not necessarily have to be a strong binder to the target material. It could also be due to propagation advantage or binding to other components of the screening system<sup>1,2,324</sup>. Although the repanning method was carried to check the reproducibility of the phage clones, this method is limited to testing the overall experimental process, thereby examining the direction of the ongoing phage display work. Thus, the relative binding affinity assay was used to assess the binding capability of each of the 15 different phage clones to silica nanoparticles by phage titer assays at pH-7.5 (Figure 3.2). In addition to the nine phage clones selected as main silica binders (highlighted in asterisk), six individual clones which were identified less frequently (QQTNWSL, QLAVAPS and VGSYLG I) or only once (GTGSQAS, ETALIAA and SQTFTSD) in either of the initial and repanning experiments were randomly picked as controls along with M13KE (wild type). The M13KE phage with no random peptides displayed on pIII coat protein was chosen as a main control. Calculating the ratio of bound or output to input amounts of phage clones has been known as a comparatively simple and quick method to evaluate the target binding ability of the displayed sequence. Consequently, a higher binding ratio signifies the higher binding ability of phage or recovery rate of phage to substrate silica nanoparticles.

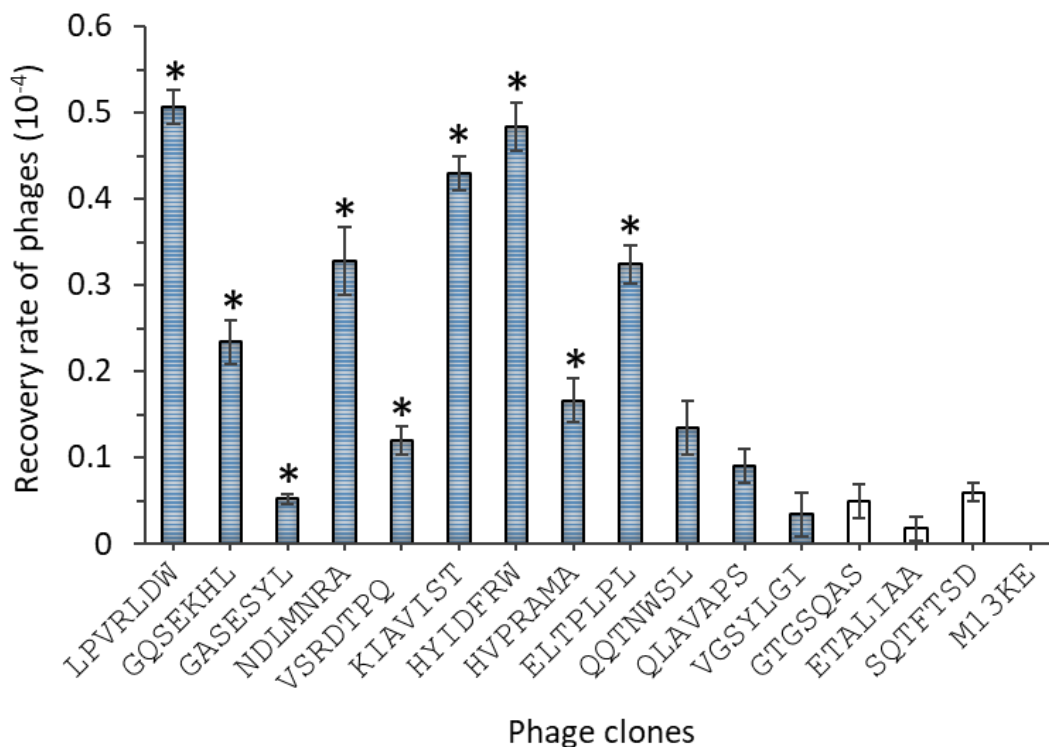


**Figure 3.2. Binding ratio (bound/input) of each of the 15 different phage clones to silica nanoparticles.** The relative binding affinity of the phage clones isolated from both initial and repanning experiments was determined by titer assay at pH-7.5. The asterisk (\*) indicates the phage clones displayed most frequently (abundantly observed) and repeated in the screening rounds 3-5. The sequences QQTNWSL, QLAVAPS and VGSYLG I were identified in more than one experiment but not repeated so often. The M13KE (wild type) phage with no random peptides displayed on pIII coat protein was chosen as a main control. In addition, the phage clones GTGSQAS, ETALIAA and SQTFTSD were randomly picked as they found only once in either of the initial and repanning experiments. The assay was repeated twice for each phage clone and the explained phage amounts were arithmetically averaged. The errors bars indicate the standard error obtained from the two separate experimental repeats.

As presented in the Figure 3.2, all the 15 phage clones showed higher binding than the control M13KE, which did not show any plaques at  $10^{-4}$  dilution but observed binding ratio at  $10^{-3}$  dilution as 0.0072 (see Appendix 3.1). Thus, verifying the binding of the phage clones displaying the peptides to the silica was a result of the randomly displayed peptide sequence and not due to non-specific coat proteins interactions. While, the nine phage clones picked as tight silica binders (highlighted in asterisk) from initial and repanning results showed dissimilar binding to silica but greater binding than the other six phage clones that were selected randomly as secondary controls except for GASESYL and VSRDTPQ. The phage clones GQSEKHL, VSRDTPQ and GASESYL that had appeared more frequently in the biopanning experiments (initial and repanning) displayed less binding to silica in relative binding studies. However, the phage clones displaying peptides LPVRLDW, HYIDFRW and

KIAVIST have emerged as the top three strong binders for amorphous silica nanoparticles followed by NDLMNRA and ELTPLPL out of the nine phage clones that had displayed most frequently and repeatedly observed in the screening rounds 3-5 from initial and repanning results. Interestingly, the ELTPLPL sequence that was isolated a few times in both initial (2/79) and repanning (5/120) experiments 6, 7 and 8 has exhibited a higher binding ability to silica nanoparticles.

#### **3.3.4 Prediction and bioinformatics analysis of silica binders: Comparison studies**

It has been an accepted way to predict the likely type of interactions through which the peptides bind to silica nanoparticles by analysing the physico-chemical properties such as the charge, pI and functional amino acid groups of the isolated peptides from phage display<sup>124,328</sup>. These interactions include electrostatic (ion pairing and hydrogen bonding), hydrophobic and other weak binding forces. The selected silica binding peptides that displayed binding to silica nanoparticles in biopanning (initial and repanning) and relative binding experiments exhibit a range of physicochemical properties (Table 3.4).

The peptide KIAVIST which appeared as the main silica binder in all biopanning rounds of repanning and relative binding affinity experiments exhibited high pI (10.1) with net positive charge 1. At the same time, the peptides GQSEKHL, LPVRLDW, NDLMNRA, VSRDTPQ, QLAVAPS and QQTNWSL showed a close range of neutral pI (6-7) values with overall neutral charge, while the GASESYL and ELTPLPL showed acidic pI-3-4 with net negative charge 1. However, the GQSEKHL, VSRDTPQ and GASESYL that appeared more frequently in the biopanning experiments (initial and repanning) displayed less binding to silica in relative binding studies.

**Table 3.4. Physico-chemical properties of selected silica binding peptides displayed from routine biopanning process and repanning method.** <sup>a</sup>Physico-chemical properties of all the sequences were obtained from Innovagen and Bachem peptide property calculator<sup>211,212</sup>. Highlighted in bold are the sequences that appeared as the most frequently occurring silica binders repeated in one or more panning experiments (both initial and repanning). An asterisk (\*) indicates the peptides sequences that exhibited higher binding capability to silica in relative binding affinity assay. The amino acids that contain amine side chain (N, Q, P, W) and hydroxyl side chain (S, T, Y) containing groups in a peptide, which can help in forming hydrogen bonding between silica-peptide or among themselves are shown.

Peptide sequence	pI <sup>a</sup>	Net charge @pH 7 <sup>a</sup>	Functional amino acid residue composition <sup>a</sup>					
			Polar (-ve, +ve and uncharged)			Hydrop-hobic	Amine side chain (N,Q,P,W)	Hydroxyl side chain (S,T,Y)
			Acidic	Basic	Uncharged			
<b>KIAVIST*</b>	10.1	1	0	1	2	4	0	2
<b>GQSEKHL</b>	7.82	0.1	1	2	2	1	1	1
<b>HYIDFRW*</b>	7.8	0.1	1	2	1	3	1	1
<b>LPVRLDW*</b>	6.78	0	1	1	0	5	2	0
<b>NDLMNRA*</b>	6.78	0	1	1	2	3	2	0
<b>VSRDTPQ</b>	6.78	0	1	1	3	2	2	2
QLAVAPS	6.01	0	0	0	2	5	2	1
QQTNWSL	6.01	0	0	0	5	2	3	2
<b>ELTPLPL*</b>	3.3	-1	1	0	1	5	2	1
<b>GASESYL</b>	3.3	-1	1	0	3	3	0	3

From the results, the physico-chemical properties (i.e charge, pI and functional groups) of the isolated silica binders suggest that the three different elution buffers (0.2 M Glycine-HCl, pH-2.2, 100 mM Triethylamine, pH-11 and 4 M MgCl<sub>2</sub>, pH-6.1) used have extracted phage clones displaying peptides of both electrostatic and non-electrostatic interactions. It is not surprising that the isolated silica binders differ in their charge (i.e positive, neutral and negatively charged) and amino acid composition (Table 3.4). From the previous studies, it was evidenced that the groups have isolated peptide sequences with dissimilar physico-chemical properties including both positive, neutral and negatively charged sequences by panning against same inorganic nanoparticles such as silver<sup>24</sup> and metallic boride nanoparticles<sup>322</sup>. In particular, a range of peptide sequences varying in charge and functional amino acid groups have been identified by phage display against silica nanoparticles<sup>24</sup> of same size<sup>10</sup> and same batch<sup>4,44</sup>. In a recent contribution, Patwardhan and colleagues, have

shown that synthetically synthesized (Stöber process) amorphous silica nanoparticles with even comparable size reported minimal binding to highly dissimilar peptide sequences, mainly due to changes in the degree of surface ionization on nanoparticles of slightly different sizes<sup>10</sup>. Thus, this variation in peptide selection to the same inorganic nanoparticles is thought to be due to the complex amorphous structures, degree of surface ionization and minor differences in size of the nanoparticles synthesized by Stöber process<sup>4,10,44,107</sup>.

Moreover, to find any sequence similarities in the identified silica binders, the multiple sequence alignment was performed using MSA Viewer<sup>213</sup>. A total of 77 different silica binding peptide sequences were taken for this sequence alignment. All these silica binders were isolated from three different sets of biopanning experiments but using the same aliquot of NEB Ph.D.-7 phage library (Lot: 0211212). The three-separate series of biopanning tests include the initial or traditional biopanning (section 3.3.1), repanning experiments performed to check the reproducibility of traditional biopanning (section 3.3.2) and the optimised biopanning methods (section 4.2.2, discussed in Chapter 4). From the multiple sequence analysis (Figure 3.3), it was found that the sequence (VSTPLLA) has been emerged as a consensus silica binder.

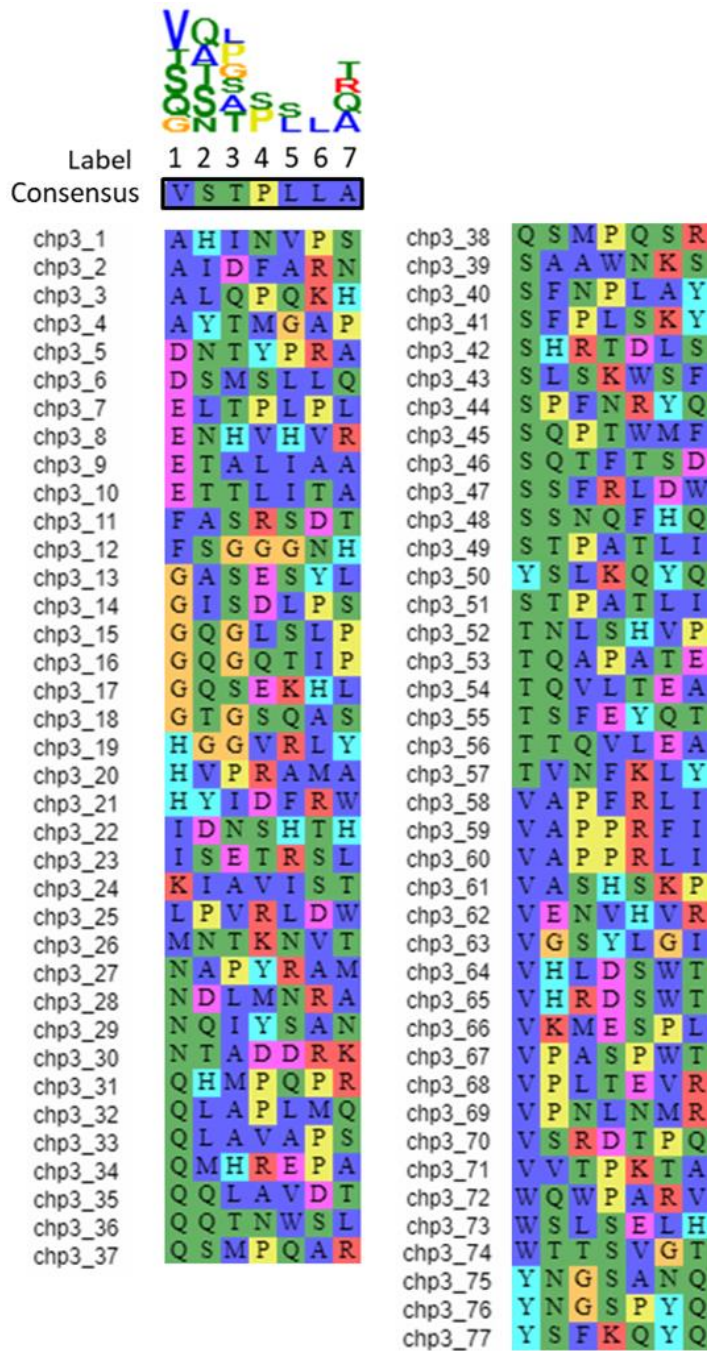


**Figure 3.3. Multiple sequence alignment of silica binders.** All the silica binding peptides used for generating this figure were isolated from three sets of biopanning experiments. A total of 77 dissimilar sequences were chosen and analysed. An identified consensus peptide sequence (VSTPLLA) from the multiple sequence alignment was also highlighted and shown. The sequence alignment was generated by using the freely available MSA viewer (<https://toolkit.tuebingen.mpg.de/#/tools/alnviz>) from the Max Planck Institute website. Label indicate the position and number of the peptide sequences. The small logo (figure) that is present on top of the 'label' indicate the number of times the amino acids have appeared in that specific position. The larger the size of the amino acid the higher the times the amino acid have appeared in that specific position of the peptide sequences. For example, the amino acid V (valine) was the most frequently observed residue (14 times), followed by S (serine, 12 times) as second, Q (glutamine, 8 times) and so on in the first position of all the 77 silica binders. Thus, V (valine) has appeared larger in the first column followed by second bigger S (serine) and so on.

This consensus sequence was then compared with all the silica binders identified in this and previous studies to find any similarities. Interestingly, the motif LP was commonly found in most of the peptide sequences that were reported to be the strong silica binders. Also, these peptides were identified in biopanning experiments against silica and reported in the literature (Table 3.5).

**Table 3.5. Identification of amino acid motif (LP) by comparing the silica binders of this study with the peptide sequences published in literature.** An asterisk (\*) indicates the sequence displayed as one of the most abundant silica binders in biopanning experiments or *in silico* designed and was shown to exhibit strong binding to substrate in binding studies. All the silica binders isolated from three sets of biopanning experiments (77 dissimilar sequences) are checked and the sequences having motif (LP) were shown in the first row of the table. While, the other sequences were displayed only once in different panning experiments in this study. The amino acid motif (LP) was shown highlighted in bold and underlined.

Peptide sequence	Target binder	Library type	Panning round	Reference
<u>LP</u> VRLDW* ELT <u>PLPL</u> * GISD <u>LPS</u> QLA <u>PLMQ</u> SFN <u>PLAY</u> SFN <u>PLAY</u> SF <u>PLSKY</u> VKMES <u>PL</u> V <u>PLTEVR</u>	Silica nanoparticles (82 nm)	Ph.D.-7	3-5	Identified in this study
<u>KLP</u> GWSG* AFI <u>LPTG</u> *	Silica nanoparticles (82 nm)	Ph.D.-7	3-5	4,44
<u>LP</u> HHHHLHTK <u>LP</u> *	Silica	Ph.D.-12	4	24
HTKHSHTSPP <u>PL</u> *	SiO <sub>2</sub> films (100 nm)		3	65
QTWPP <u>PL</u> WFSTS* VPHPPFP <u>HLPPH</u> *	Quartz only Quartz and Hydroxyapatite		3-5	319
<u>LP</u> PP <u>PLPLQPLP</u> * PPPW <u>LYMPPWS</u> * SPPRL <u>LPWLRMP</u> * <u>LP</u> DWWPPQLYH*	Quartz (100)	<i>in silico</i> designed	n/a	42,43

In a recent contribution, Oren et al. reported a bioinformatics approach and generated quartz binding peptides with a predictable binding affinity for silica using the experimental results of combinatorial selection and characterization studies of quartz binding peptides<sup>42</sup>. To



achieve this, the total similarity scores were calculated using BLOSUM 62, PAM 250 and QUARTZ I scoring matrices and generated 1000000 peptides having the highest similarity scores from PhD-7 and 12 libraries<sup>42,43</sup>. The sequences with the highest similarity scores representing the strongest four quartz silica binders were identified and reported (Table 3.6). The amino acid proline (P) has been reported as a major constituent responsible for specific binding of peptide to silica<sup>167</sup>. Proline (P) followed by hydrophobic amino acid residues like Leucine (L) and Tryptophan (W) were shown to have the strongest affinity to quartz silica<sup>43</sup>. Using this knowledge, an amino acid motif (LP) that may be responsible for higher binding to silica has been identified.

Furthermore, all peptides displayed against SiO<sub>2</sub> were initially checked against MIMOdb and BLAST database to find the whole or exact part of phage display or surface display peptide sequences that are similar to the identified silica binders. The analysis of MIMOdb and BLAST results showed no hits for all the silica binders with the exception to the peptides shown in Table 3.6. The sequences that appeared as tight binders to silica such as QLAVAPS, GQSEKHL HYIDFRW, VSRDTPQ and GASESYL were found to have affinity for one or more than one different targets (Table 3.6) including Fe<sub>3</sub>O<sub>4</sub> nanoparticles, Human prostate cancer cell line PC3, Sera of peanut-tolerant subject 2, Sera of peanut allergic patient 1, 3, 4, Plasma of peanut allergic patient 4 and Anti-TIM polyclonal antibody<sup>323,329-331</sup>, while other peptide sequences appeared to have some affinity for silica in one of the biopanning rounds were found to have attraction for other targets (Table 3.6). This suggests that peptides isolated mostly were target-related sequences and rather true silica binders without any human or pathogen or sample contamination, whereas the peptide sequences that were found to have exact or part of motif similarity for other targets indicate the possibility of promiscuous binding behaviour to multitude of materials.

From the previous studies, it is important to note that certain sequences having affinity to more than one material have been identified and explored for their ability to bind to different inorganic molecules. For example, the sequence KLSLRHDHIHHH has been identified against FePt nanoparticles<sup>332</sup>, titania<sup>333</sup> and 82nm silica nanoparticles<sup>10</sup>. In addition, the same sequence searched against MIMOdb database appeared to bind to organic molecules such as lipopolysaccharide<sup>334</sup> and Anti-PRRSV monoclonal antibody<sup>335</sup> and would appear to be 'target unrelated peptide'.

**Table 3.6. MIMOdb search/ scan/ Blast analysis results of phage displayed silica binders found to have affinity for other materials indicating that they might be promiscuous binders.** Peptide sequences highlighted in bold are the phage clones that appeared as highly abundant or tight binders to silica in initial biopanning and/ or repanning methods.

Peptide	Target Found	Matched Sequence	Library type	Biopanning round	Reference
<b>QLAVAPS</b> TVNFKLY	Fe <sub>3</sub> O <sub>4</sub> Nanoparticles	Full sequence	Ph.D.-7	4, 5	323
<b>HYIDFRW</b>	Fe <sub>3</sub> O <sub>4</sub> Nanoparticles, Plasma of peanut allergic patient 4 and Human prostate cancer cell line PC3	“	Ph.D.-7	2-5	323,329,330
<b>GQSEKHL</b>	Fe <sub>3</sub> O <sub>4</sub> Nanoparticles, Sera of peanut-tolerant subject 2	“	Ph.D.-7	2-5	323,330
HGGVRLY	Agrobacterium vitis polygalacturonase, Plasma of peanut allergic patient 4	“	Ph.D.-7	2, 3	330,336
<b>VSRDTPQ</b>	Sera of peanut allergic patient 1-4, and tolerant subject 2	“	Ph.D.-7	1-3	330
ETALIAA	Plasma of peanut-tolerant subject 3	“	Ph.D.-7	2, 3	330
WSLSELH SSNQFHQ SAAWNKS GTGSQAS	Sera of peanut allergic patient 1, 3, 4	“	Ph.D.-7	1-3	330
<b>GASESYL</b>	Sera of peanut allergic patient 1, Anti-TIM polyclonal antibody	“	Ph.D.-7	2, 3	330,331
IDNSHTH	Agrobacterium vitis polygalacturonase,	“	Ph.D.-7	3	336
SWTALGP	E3 ubiquitin-protein ligase Mdm	<u>TWLDNIWT</u> <u>TLGP</u>	Ph.D.-12	3	337
TTQVLEA	Mouse brain microvasculature	<u>CTGRMTXQ</u> <u>XXXXA</u>	CX10C	5	338

However, the same sequence has been well studied both experimentally and *in silico* and have shown to be a better binder to the above mentioned inorganic molecules<sup>10,332,334,335,339</sup>.

Some more examples include the peptide sequences DRPWMFPPHWSV (gold, quartz and hydroxyapatite) and VPHPPFPHLPPH (Quartz and Hydroxyapatite) identified from biopanning against one of the above mentioned inorganic materials but displayed binding towards multitude of materials<sup>60,189,340</sup>.

Also, the binding of short peptides to different targets depends on the number of defined binding sites available on substrate surface for binding, thus providing information about the diversity being eluted<sup>324</sup>. For instance, If the target molecule has a single well-defined binding site for binding (eg. monoclonal antibodies) then one can expect low number of sequences. Whereas the targets holding multiple binding sites (polyclonal antibodies) or less defined sites (proteins with greater binding interfaces or inorganic particles) to thousands of sites (organs or cells) available for binding will result in identifying relatively higher number of sequences<sup>324</sup>.

Recently, the artificial binding proteins have become popular due their ability to bind specifically to different target molecules like peptides, proteins or small molecules, leading to different applications by engineering or modifying these small molecules<sup>341-344</sup>. In a recent contribution, a small protein (Adhiron) displaying variable binding loops was developed and designed Adhiron library<sup>345</sup>. Using this this adhiron technology, few groups have designed Adhiron library and identified binders to more than 100 target molecules including a receptor (CD31), 12 mer peptide, yeast SUMO proteins, fibroblast growth factor (FGF1), platelet molecule (PECAM-1) and the SH2 domain Grb2<sup>346-348</sup>.

The most commonly reported problems for identifying the peptide sequences that show affinity to other targets (unrelated targets) likely arise due to amplification bias such as the binding of phage to *E.coli* pili, rare mutations in the regulatory region of phage genes and interference with infection<sup>2,325,349</sup>. However, these effects are generally lesser for the pIII or smaller display systems compared with the pVIII systems. It is more common to observe a loss in the sequence diversity for the peptide libraries displayed on pVIII than pIII coat proteins<sup>350,351</sup>. To minimise this unspecific binding, few solutions have been reported. These include i) use of buffers with detergents and by increasing the washing stringency and number of wash cycles. This process will suppress the nonspecific binding. ii) competitive elution to remove the wanted (target) or unwanted (unrelated) binders using binder specific

proteins (eg. Biotin can act as specific binder to streptavidin) or by excess target concentration. iii) to eliminate the amplification step to reduce the nonspecific binding.

Even after minimising the nonspecific binding, there is chance that few peptides might show binding to other materials due to close structural or chemical characteristic similarities between different inorganic material surfaces<sup>318,323,352</sup>. Also, it is possible that short peptides specifically 7 mers could show binding to different molecules exact or part of the similar sequences could be matched towards different molecules due to the absence of defined tertiary structure<sup>353</sup>. However, the working of each method can differ depending on the target substrate. So, there is a need to design washing or elution buffers and conditions that specifically suite the target materials.

Nonetheless, the target unrelated peptides can be identified by performing relative and competitive binding experiments, thus showing that these TUPs do not have true affinity for the target substrate. In addition, many databases are available to check the authenticity of the target binders. Nevertheless, the BLAST search alignment results might end up finding random hits due to the short length of the peptide sequences that are being searched with the typical large proteins and the entire genome of the organisms<sup>218</sup>. Therefore, using both experimental binding results along with bioinformatics checking will help to identify a true binder from nonspecific binders.

Therefore, to confirm that most of the sequences identified for silica are not target unrelated peptides, a number of steps were followed. These include increasing the washing stringency and number of wash cycles; repanning and relative binding experiments complemented by bioinformatics verification.

### 3.3.5 Assessment of silica-peptide interactions

#### 3.3.5.1 Fluorometric quantification of peptide adsorbed to silica

A fluorometric method, based on the use of fluorescamine<sup>4,10,271,272,354</sup> was carried out to check and test the ability of the peptide sequences obtained from the experimental phage display processes to bind to silica. This quantitative assay was performed in PBS buffer by maintaining the similar environment (i.e. media condition at pH-7.5 and same batch of silica nanoparticles) employed previously during the biopanning process. The approach used enabled quantitation of the amount of peptide adsorbed on the surface of the silica as a function of peptide concentration by measuring the amount of peptide left unattached to silica in the supernatant<sup>4</sup>. The procedure including the materials used for this assay was already described in Chapter 2, section 2.1.2.7.1.

The molecular mechanism between peptide-protein or peptide-solid surface has been shown to be a complex process and is highly dependent on electrostatic, hydrogen bonding, hydrophobic and other weak interaction like van der Waal forces<sup>4,129,234,355-357</sup>. Five peptides were selected for experimental binding studies to study their binding behaviour with silica nanoparticles under *in vitro* conditions. At the solid-peptide interface, the complex adsorption chemistry is not only dependent on the nature of inorganic material surface but also on other factors like the binding environment (eg. pH, buffer and temperature)<sup>107,333,356</sup>; peptide sequence and conformations (eg. size, structure and orientation)<sup>9,10,129,234</sup>; peptide kinetics (eg. atomic level movement involving binding forces and energies)<sup>7,13,44,355,357</sup> together with their physico-chemical properties<sup>4,132</sup> and motifs<sup>43</sup>. Thus, all the peptides selected were derived using result of the biopanning approach, binding assay, pI values and net charge at pH 7 (Figure 3.4). For this binding study, five peptides were chosen. Four out of five peptides such as KIAVIST (high pI value and net positive charge), LPVRLDW, NDLMNRA and GQSEKHL (neutral pI and charge) selected were identified (most frequently observed) in both initial (traditional) biopanning and repanning experiments; while peptide GASESYL (low pI and net negative charge) was only found in one experiment (4) of initial routine biopanning process. However, in relative binding studies, the LPVRLDW, KIAVIST and NDLMNRA exhibited higher binding, while, the GQSEKHL and GASESYL displayed medium to low binding to amorphous silica nanoparticles (Figure 3.4).

As it is very difficult to find a peptide that truly does not bind to silica, the peptide GASESYL was chosen as a control peptide for the binding studies described in this thesis. Also, from

our previous studies, it was evident that the peptide LDHSLHS with nearly similar properties in terms of charge and composition to GASESYL showed less binding to silica nanoparticles at pH-7.5 compared with other peptide sequences<sup>4,107</sup>. In addition, the same peptide GASESYL displayed less binding to silica in relative binding studies.

Firstly, all the five peptides selected for this adsorption studies showed distinctive binding to silica nanoparticles as shown in Figure 3.4. Secondly, the KIAVIST peptide which has been identified as a silica binder (only once out of thirteen peptides sequenced) in experiment 6 of routine biopanning but displayed in all the panning rounds of repanning experiments (i.e 3-5 screened rounds in experiments 7 and 8) appeared as the best binder to silica nanoparticles at higher peptide concentrations (1.2 and 1.6 mM) compared with the other four peptides used in this study. Thus, confirming the repanning process may be used for recovering the target binders that might have been missed (due to selecting a small number of clones for sequencing) in the routine biopanning process and by representing a larger population now. Also, with increasing the pI and net charge of peptides, the binding behaviour towards silica increased at pH 7.5 (Figure 3.4 and 3.5). For example, the peptide KIAVIST with high pI (10.1) and net positive charge (+1) showed high binding to silica, while the peptides LPVRLDW and NDLMNRA having neutral pI values (6.8) and net charge (0) showed low binding than KIAVIST peptide. However, the peptide LPVRLDW displayed better binding than that of KIAVIST at lower concentrations (i.e up to 1mM). In contrast, the peptide GQSEKHL with nearly similar pI (7.8) and net neutral charge (0.1) values to that of the peptides LPVRLDW and NDLMNRA, exhibited lower binding to silica nanoparticles. The peptide GASESYL with low pI (3.3) and net negative charge (-1), which was selected as a control for this adsorption investigations showed least binding to silica nanoparticles. Note, the isoelectric point of silica pH was determined to be present at pH-2-3 and with increasing the pH of the solution, the silica attains more negative charge due to the rapid deprotonation of silanol (Si-OH) groups<sup>4,10,107</sup>. Therefore, the silica was negatively charged during these binding events at pH-7.5.

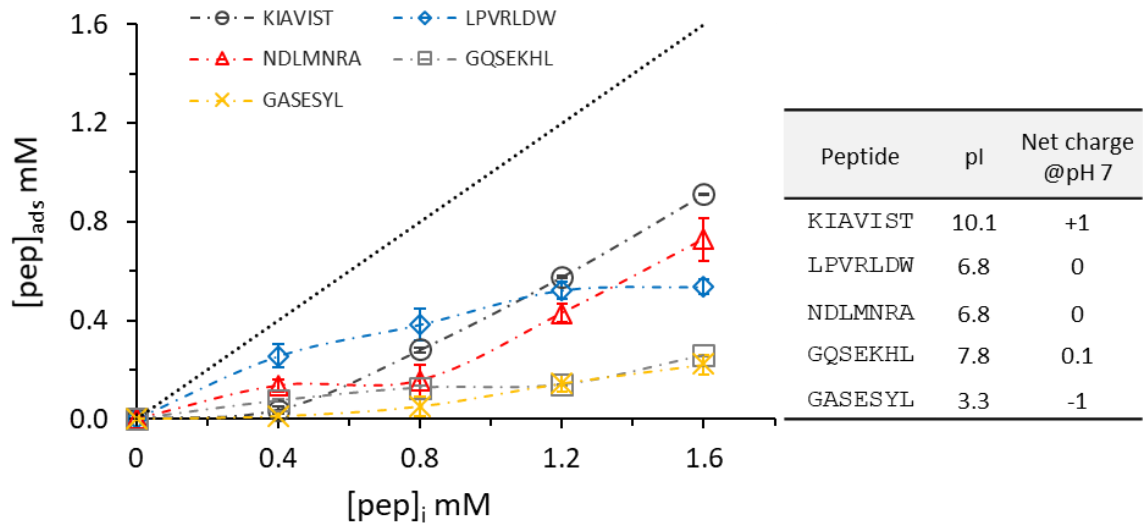


**Figure 3.4. Adsorption behaviour of peptides on the surface of hydrophilic silica nanoparticles at pH-7.5.** The y-axis represents the amount of peptide adsorbed to silica in mM, while the x-axis shows the initial peptide concentration or peptide added in mM. The theoretical 100% peptide adsorption is shown in black dotted line. The error bars represent the standard deviation error calculated as a result of the assay being repeated in triplicate. Based on the above data, the binding order of the peptides was ranked as KIAVIST > LPVRLDW > NDLMNRA > GQSEKHL and GASESYL.

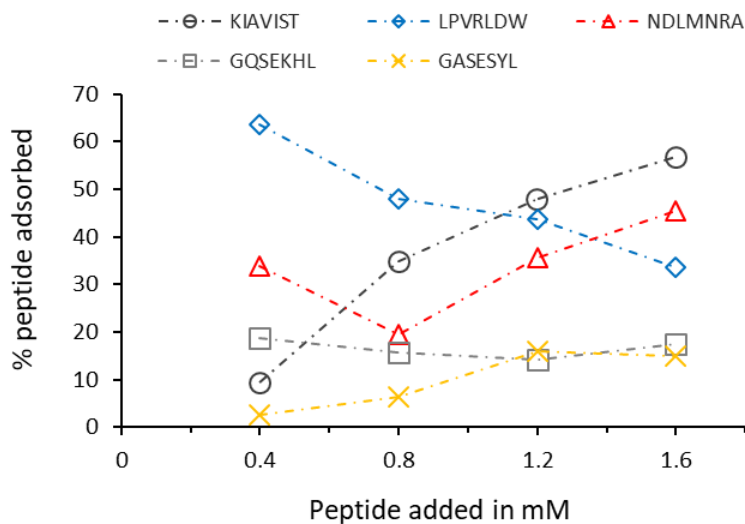


**Figure 3.5. Analysis of the above peptides displayed in Figure 3.4.** The graph showing the peptides and their binding (%) amounts to silica at four different peptide concentrations. The x and y-axis represent the peptide added and percentage of peptide adsorbed to silica in mM.

The isolation and high binding of peptide KIAVIST to silica surface is not surprising due to the fact that biomolecules including peptides or proteins or even individual amino acids

comprising of positively charged groups have been found to display high binding behaviour to negatively charged silica surfaces at neutral or high pH; mainly due to the likely involvement of ion pairing mechanism complemented by hydrophobic interactions<sup>10</sup>. The likely electrostatic mechanism that directed the peptide to bind to deprotonated silanol sites on the silica surface might have come primarily from the positively charged sites of lysine (i.e due to the presence of positively charged lysine (K) at both N terminus and the side chain comprising a basic amino group with pKa=10.4); thus giving the peptide KIAVIST a constant net positive charge (+1), resulting in the strongest possible ionic interactions. This is supported by the results from our previous studies<sup>4,107</sup>, where it was evident that the peptide KLPGWSG with similar properties (i.e same pI-10.1, +1 net charge at pH-7, position of lysine and composition) to KIAVIST showed identical binding to the same batch of silica nanoparticles<sup>4,107</sup>. This study also described that with increase in the pH of the system, the peptides possessing positive charge tend to increase the strength of their interaction to negatively charged silica surface due to an increase in the overall charge of the system; thereby confirming the role of electrostatic interactions in solution<sup>4</sup>.

The peptide LPVRLDW, which appeared as the second-best binder from the above adsorption studies, showed high binding until 1.2 mM concentration and saturation remained constant thereafter (Figure 3.5). In this case, a non-electrostatic interaction mechanism is likely to happen. This type of binding behaviour of LPVRLDW peptide may perhaps be due to the presence of five non-polar residues (Leu, Pro, Val and Trp) in the sequence resulting in an increase in the hydrophobic character, leading to hydrophobic interactions at the peptide-silica surface<sup>4</sup>. Although, hydrophobic interactions are the key forces likely to be responsible for LPVRLDW peptide adsorption<sup>9,43</sup>; it might be also be due to the presence of a high binding motif LP (Leucine followed by Proline)<sup>42,43,167</sup>. Note, although, quartz silica is pure SiO<sub>2</sub>, amorphous silica nanoparticles synthesised by Stöber process display dissimilar chemistries. For instance, a significant increase in the surface acidity and in the area density of ionic groups due to little differences in the size of the silica nanoparticles was reported<sup>10</sup>.

The peptide NDLMNRA showed reasonable binding at lower concentrations (0.4 and 0.8 mM) but with drastic increase in binding at higher concentrations from 1.2 to 1.6 mM with no sign of saturation. This sort of binding behaviour of peptide NDLMNRA to silica surface is likely to be due to the presence of polar and non-polar amino acids. The polar uncharged amino



acids Asn (N) present at the N-terminus and at 5<sup>th</sup> position along with other charged polar residues including Asp (D) and Arg (R) are likely responsible for initiating hydrogen bonding due to increased binding at a higher peptide concentration with no sign of saturation resulting in multilayers connected by hydrogen bonds<sup>4</sup>. Also, the possibility of hydrophobic interactions cannot be ruled out due to the presence of hydrophobic groups at 3<sup>rd</sup> position (Leucine) and at the carboxyl end (Alanine). In contrast, the GQSEKHL peptide with nearly neutral pI (7.8) and neutral charge (0.1) similar to the pI and charge of peptides LPVRLDW and NDLMNRA, exhibited low binding to silica nanoparticles. This might be due to the presence of weaker interactions such as hydrogen bonding and van der Waals forces. Nonetheless, the peptide GASESYL with low pI (3.3) and net negative charge (-1), which was selected as a control for this adsorption studies showed least binding to silica nanoparticles. The possible reason that prevented binding of peptide GASESYL to silica might be due to the involvement of electrostatic repulsions between the negatively charged peptide and silica under these pH conditions<sup>4</sup>. As a result, the minimum binding to silica occurred only due to the participation of weaker hydrogen bonding (serine and tyrosine) and hydrophobic interactions.

Based on the above peptide-silica adsorption findings, the likely type of interactions that aided in binding of specific peptides to silica nanoparticles at pH-7.5 are shown in Table 3.7. Additionally, the probable effect of increasing pH and particle size on binding to silica was predicted by comparing the peptide sequences of this adsorption study with previous studies<sup>4,44,107</sup>, where peptides of similar properties (eg. peptide length, net charge of peptide at pH-7 and same batch of silica nanoparticles) were investigated and assessed based on adsorption studies<sup>4,44,107</sup>. It must be noted that the pH range and nanoparticles size considered for these studies include pH-3 to pH-8.5 and 28 nm, 82 nm and 210 nm respectively<sup>4,44,107</sup>.

**Table 3.7. Physico-chemical properties and adsorption of silica binding peptides:**

<sup>a</sup>Physico-chemical properties of all the sequences were obtained from Innovagen (<https://pepcalc.com/>) and Bachem (<http://www.bachem.com/>) peptide property calculator. Type of interactions likely be responsible for peptide-silica binding and their effect on increasing pH and particle size were shown. The asterisk (\*) represents the probable effect of increasing pH and particle size on binding to silica was estimated and predicted by comparing the peptide sequences of this findings with previous studies, where peptides of similar properties (eg. peptide length, net charge of peptide at pH-7 and same batch of silica nanoparticles) were investigated and assessed based on adsorption studies<sup>4,44,107</sup>.

Peptide sequence	pI <sup>a</sup>	Net charge @pH 7	Functional groups and composition of peptide sequence <sup>a</sup>					Likely key type of interactions liable for binding to silica	Expected effect of increasing pH and particle size on binding*
			Acidic (-ve)	Basic (+ve)	Hydrophobic	Polar Uncharged	Average Hydrophilicity		
KIAVIST	10.1	+1	0	1	4	2	-0.4	Electrostatic/ Hydrophobic	↑
LPVRLDW	6.8	0	1	1	5	0	-0.4	Hydrophobic	=
NDLMNRA	6.8	0	1	1	3	2	0.4	H-bonding/ Hydrophobic/ van der Waals	=
GQSEKHL	7.8	0.1	1	2	2	2	0.6	H-bonding/ van der Waals	=
GASESYL	3.3	-1	1	0	3	3	-0.1	Electrostatic repulsion/ H-bonding	↓

Therefore, these results indicate that peptide adsorption to silica surfaces may exhibit more than one type of interaction and can be influenced by the experimental conditions such as pH, subject to the peptide charge and pI in solution-based assays.

### 3.3.5.2 Raman spectroscopy for probing peptide-silica interactions

In this study, Raman spectroscopy has been used for the identification of peptide structure and to probe their interaction with silica particularly to see small conformational changes (due to their sensitivity to microenvironment) in some amino acid residues in aqueous and solid states<sup>274–277</sup>. These minor shifts has been used as a marker to assess the microenvironment (i.e hydrophobicity or hydrophilicity)<sup>274,275,278</sup>. The sequence LPVRLDW was chosen for this Raman study due to the peptide composition (i.e the variation in functional amino acid residues) representing hydrophobic (Leu at N terminus and at 5<sup>th</sup>

position), polar basic (Arg), polar acidic (Asp) aromatic (Trp) and motifs (LP) that are crucial to identify the likely type of binding to silica. In addition, the sequence contains special amino acid (pro) at 2<sup>nd</sup> position of the peptide sequence. The peptide samples in different formats including solid, liquid air-dried, solid powdered samples were used. In addition, the residual pellet (peptide adsorbed to silica) collected from the fluorescamine assay were washed twice with water, air-dried and investigated using Raman spectroscopy to see if change in the peptide structure on binding could be identified. The crowded Raman shift region also known as finger print region (500-1600  $\text{cm}^{-1}$ ) was taken to uniquely identify specific amino acids or any other structural conformations of the peptide<sup>274</sup>. For all these peptides, the Raman spectra was collected from 100  $\text{cm}^{-1}$  to 3600  $\text{cm}^{-1}$  but only the finger print region from 500  $\text{cm}^{-1}$  to 1600  $\text{cm}^{-1}$  was used for this analysis, as this area is of focal interest for both peptide and silica.

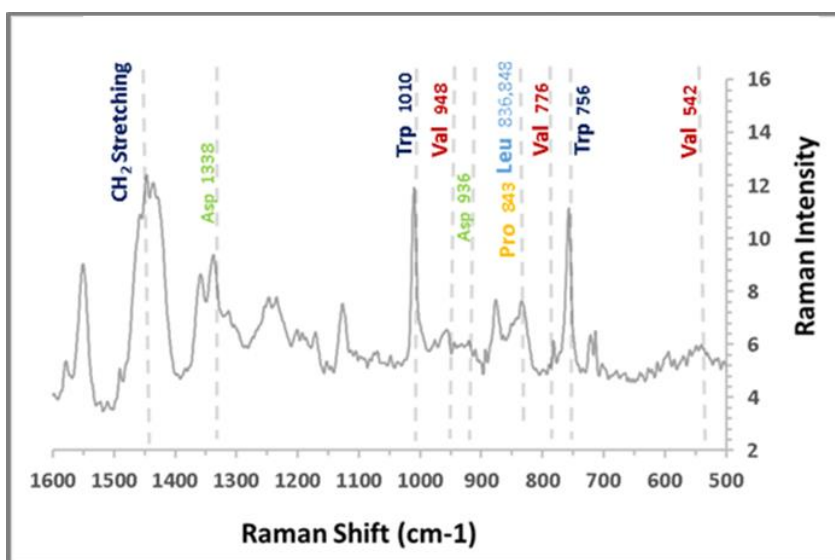


**Figure 3.5. Raman spectrum of amino acids identified in LPVRLDW peptide.** A strong signal has been noticed for Tryptophan (W) at 756  $\text{cm}^{-1}$  and 1010  $\text{cm}^{-1}$ .

A few amino acids present in LPVRLDW peptide such as Trp (W), Leu (L), Pro (P) and Asp (D) gave strong to medium signals while the Val (V) gave medium range signals and for the remaining amino acid Arg (R) did not give any sign of peak or band signals (Figure 3.5).

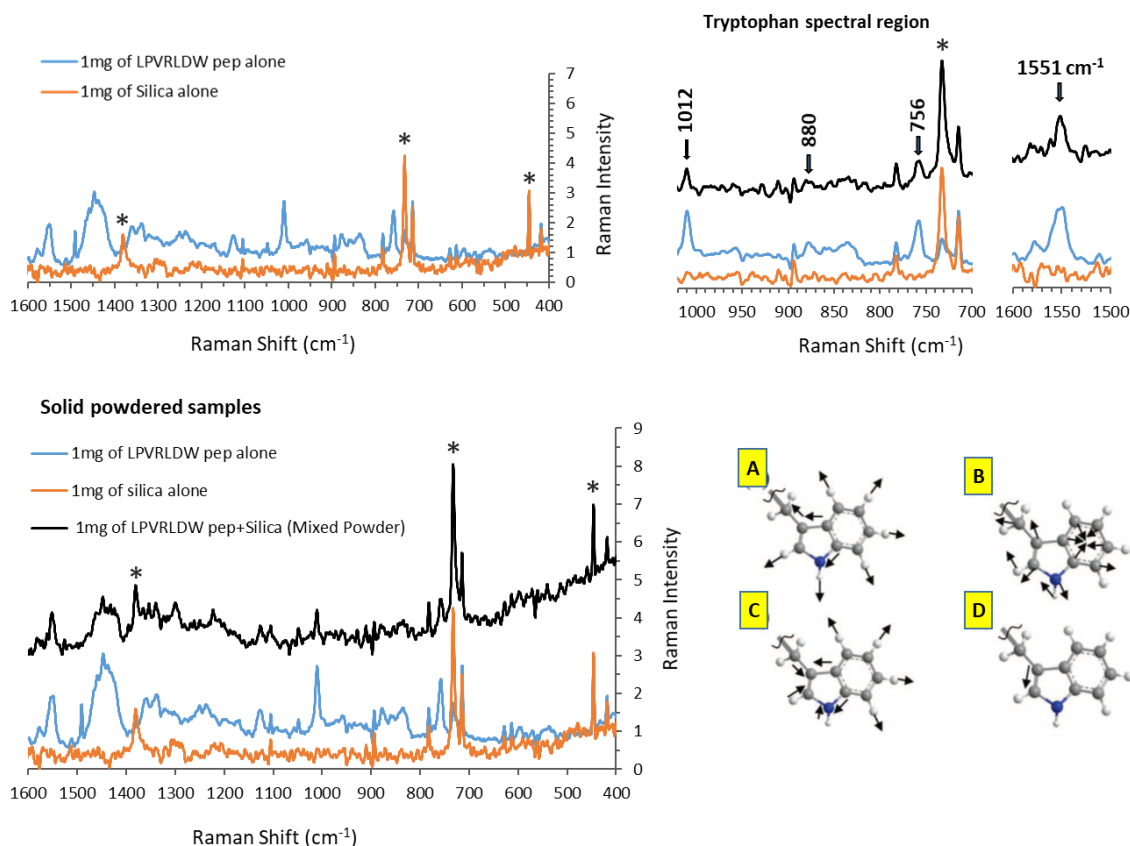


**Figure 3.6. Raman spectrum showing the LPVRLDW peptide alone, silica alone and when peptide adsorbed to silica particularly for the aromatic amino acid tryptophan.** Asterick \* represents the silica bands found at around 440, 732 and 1390  $\text{cm}^{-1}$ . A) Symmetric benzene/pyrrole in-phase breathing mode of Trp at 756  $\text{cm}^{-1}$  B) Indole ring vibration with NH bending mode of Trp 880  $\text{cm}^{-1}$  C) Symmetric benzene/pyrrole out-of-phase breathing mode of Trp at 1012  $\text{cm}^{-1}$  D) Pyrrole C2-C3 stretching mode of Trp found at 1551  $\text{cm}^{-1}$ .

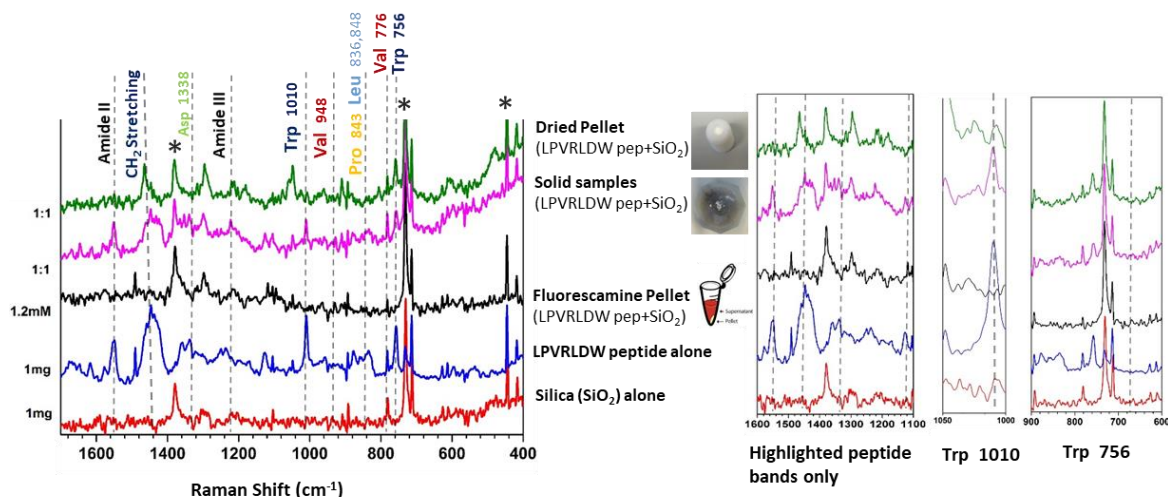


**Figure 3.7. Raman spectra obtained from different samples of peptide (LPVRLDW) and silica.** Five different samples such as peptide alone, silica alone, peptide adsorbed to silica (solid powdered and dried pellet from solution) and the dried peptide-silica pellet obtained from the fluorescamine assay showing the variation and shifts in the Raman spectra. Asterick \* represents the silica bands found at around 440, 732 and 1390  $\text{cm}^{-1}$ .

In silica alone samples, the Raman bands were found at around 440, 732 and 1390  $\text{cm}^{-1}$  respectively<sup>129</sup>, while strong bands of Trp (W) were observed in LPVRLDW peptide alone samples at 756  $\text{cm}^{-1}$  and 1010  $\text{cm}^{-1}$ <sup>274,277</sup> (Figure 3.6). These strong signals are due to the symmetric benzene in and out phase breathing mode of Tryptophan<sup>358</sup>. The LPVRLDW peptide adsorbed silica samples (mixed solid and dried pellet) showed signals at 440  $\text{cm}^{-1}$ , 732  $\text{cm}^{-1}$ , 1390  $\text{cm}^{-1}$ , 756  $\text{cm}^{-1}$  and 1010  $\text{cm}^{-1}$  respectively but slightly lower signals (Figure 3.7). This clearly indicates that changes in vibrational shifts or signals for particularly aromatics occur in solids (strong) and solutions (weak) but showing some signals for peptide backbone. However, only silica bands were found in case of dried peptide-silica pellet after fluorescamine assay by masking the peptide bands with silica (Figure 3.7). The possible reasons for masking of peptide signals with silica may be due to not enough peptide required for obtaining Raman signals because of fluorescamine experimental sample limitation. Thus, verifying the peptide LPVRLDW binding to silica by Raman spectroscopy revealing the differences in the spectrum may be due sensitivity of microenvironment at peptide-silica interface in solids and solutions. The binding signal observed was mainly from aromatic Trp (W) amino acid; indicating this technique has potential to be used for identifying the peptides or specific amino acids and use them as markers to assess the local environment in silica-peptide composites.

### 3.4 Conclusion

In summary, heptapeptides having affinity for amorphous silica nanoparticles (hydrophilic, 82 nm) have been identified. To achieve this, elution buffer conditions (low pH, high pH and high salt) and the elution buffer itself were changed to remove peptide binding phages from silica surface during the phage display process. The experimental results gave information about the tight peptide silica binders eluted and the functional amino acid groups may be responsible for electrostatic and non-electrostatic interactions. Also, complementary bioinformatics results prove that most of the sequences checked do not exist in MimoDB database and are not identified as contaminants. This demonstrates that peptides isolated were not target-unrelated sequences but rather genuine target binders without any human, pathogen or sample contamination.

A repanning method has been reported to recheck the phage display process and verify silica binders by checking the reproducibility of the process. The repanning method may experimentally verify your own target binding results giving information about any possible non-specific binding due to panning limitation (amplification bias), thereby checking the direction of the ongoing phage display work. Thus, the repanning method reported for silica, appeared to be a straight forward approach to verify phage display experimental results by mixing phage clones from different biopanning experiments and rounds. The results of the repanning experiment reproduced mostly similar silica binders that were identified previously along with additional peptide sequences which were hidden in the previous biopanning experiments. The tightly bound silica binders reproduced which were also isolated previously include LPVRLDW, GQSEKHL, NDLMNRA, VSRDTPQ, ELTPLPL and QLAVAPS gave us indication of reproducibility of material binding peptides by verifying the experimental biopanning process. Additionally, this experiment also prove that no possible human, pathogen and sample contamination was present. While the sequences such as HYIDFRW, HVPRAMA, SQTFTSD, SFPLSKY, TVNEKLY and HGGVRLY appeared only in this process but were not identified before via traditional biopanning process suggest that these entirely new peptide sequences are the ones that might have been missed in the few phage clones that were selected from a large pool for sequencing. The KIAVIST peptide sequence in repanning process appeared as a main silica binder which has been identified in both elution experiments (0.2 M Glycine-HCl, pH-2.2 or 100 mM Triethylamine, pH-11) and has displayed in all rounds sequenced; while the same sequence was found only once in previous traditional biopanning experiments. Therefore, this verification process may be used to identify the tight silica binder (KIAVIST). The reappearance of LPVRLDW peptide sequence in repanning experiment prove that this phage clone does not have any propagation advantage, which means this peptide sequence is not a fast grower but a genuine target binder. The results and physico-chemical properties of isolated silica binders suggest that the three different elution buffers (low pH, high salt and high pH) used have isolated peptides of both electrostatic and non-electrostatic interactions.

The phage clones displaying peptides LPVRLDW, HYIDFRW and KIAVIST that occurred more frequently in the phage display experiments, showed higher binding to amorphous silica nanoparticles. However, the phage clones GQSEKHL, VSRDTPQ and GASESYL that had appeared frequently in the biopanning experiments (initial and repanning) displayed less

binding to silica in relative binding studies. While, the ELTPLPL sequence that was isolated a few times in both initial and repanning experiments has exhibited a higher binding ability to silica nanoparticles. In addition, the multiple sequence analysis was performed for all the silica binding peptide sequences and a sequence (VSTPLLA) has been emerged as a consensus silica binder. This consensus sequence was then compared with all the silica binders identified in this and previous studies and the motif LP was commonly found in most of the peptide sequences that were reported to be the strong silica binders.

Furthermore, selected silica binding peptides (LPVRLDW, NDLMNRA, GQSEKHL, GASESYL and KIAVIST) identified from experimental biopanning (traditional and repanning) and relative binding methods were chemically synthesized and characterized for studying the peptide-silica interactions using fluorescamine assay and Raman spectroscopy. All the five peptides selected for adsorption studies (fluorescamine based quantification assay) showed distinctive binding to silica nanoparticles. The peptide KIAVIST with high pI (10.1) and net positive charge (+1) showed high binding to silica, while the peptides LPVRLDW and NDLMNRA having neutral pI values (6.8) and net charge (0) showed lower binding than KIAVIST peptide. However, the peptide LPVRLDW displayed better binding than that of KIAVIST at lower concentrations (i.e up to 1mM). In contrast, the peptide GQSEKHL with nearly similar pI (7.8) and net neutral charge (0.1) values to that of the peptides LPVRLDW and NDLMNRA, exhibited lower binding to silica nanoparticles. The peptide GASESYL with low pI (3.3) and net negative charge (-1), which was selected as a control for this adsorption investigations showed least binding to silica nanoparticles. Also, these results indicated that peptide adsorption to silica surfaces may exhibit more than one type of interaction and can be influenced by the experimental conditions such as pH, subject to the peptide charge and pI in solution-based assays. Besides, complementary binding studies of LPVRLDW using Raman spectroscopy exposed that there are differences in the spectrum after binding of peptide with silica. The binding signal observed was mainly from aromatic Trp (W) amino acid; indicating this technique has potential to be used for identifying the peptides or specific amino acids and use them as markers to assess the local environment in silica-peptide composites.

## Chapter 4: Isolation of Silica Binders by Optimised Biopanning Method and Bioinformatics

### 4.1 Introduction

With increase in the demand of using biopanning to display material specific peptides and then to synthesize the biobased materials *in vitro* and *in vivo*, it is very important to efficiently elute and recover the strongly bound phage from the inorganic material surfaces without degenerating the material or the phage peptide. In general, to elute strong binders a single elution buffer is used and to isolate the best consensus binders, the number of biopanning rounds are increased<sup>24</sup>. During the successive controlled washing steps, mostly any binder unrelated to the target should have been removed, leaving only the target selective phage to remain<sup>68</sup>. Moreover, the non-specific binding of peptides to materials is an issue that can nurture the wrong results. The non-specific peptides may have affinity for the chemicals or substrates including plastic tubes or plates or films or petri dishes, washing or elution buffers and their components and blocking or coating agents that are used during the biopanning process. This type of non-specific binding behaviour can hide the actual binders thereby promoting the wrong or untargeted binders or fast growers. A full list of peptides reported to bind to polystyrene based components such as well plates, beads, petri dishes and films during biopanning process was shown in Table 2.3, Chapter 2. Considerable effort has been made to isolate material binding peptides by targeting washing and elution strategies. Elution for target-binding phage can be done using various methods, as shown in Figure 4.1.

Chemical based elution methods are more traditionally used, which can involve eluting the stronger binders using buffer conditions, such as extreme pH, salts (ionic strength) or reductants such as DTT<sup>69,359</sup>. During the biopanning procedure, the extreme low pH elution or high salt buffers tend to cause changes in the phage-target interface, or sometimes degrade or denature either the substrate or phage surface. As a result, they may become inactive or may change the original reaction between the inorganic surface and the phage peptide. Because of these modifications, strong binders may be removed incompetently; consequently, a large number of strongly bound phages can be left on the material surface<sup>4,153</sup>. Washing and elution steps in the phage display process are key to know whether



all the strong binders are eluted completely from the available phage library; alongside removing the loosely bound phage clones using appropriate detergents and elution buffers.

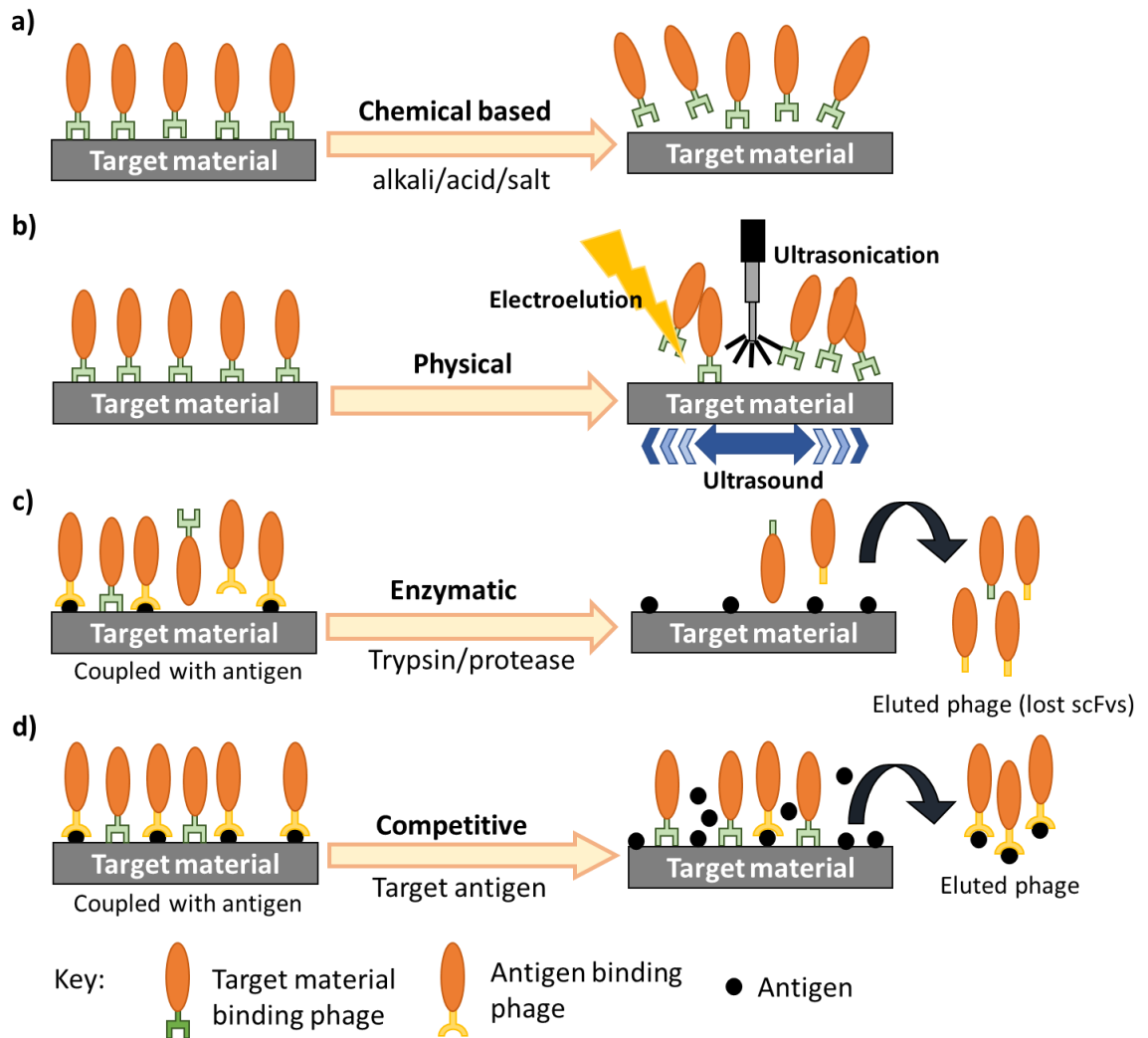


**Figure 4.1. Schematic representation of different types of elution methods.** a) Chemical elution: The non-specific or weakly bound phage are first washed away, and the remaining strongly bound phage are eluted by low or high pH or high salt buffer b) Physical elution: The strongly bound phage is eluted either by using sonication or ultrasound or with a combination a) and b). c) Enzymatic elution: enzymes (such as trypsin or protease) are used to cleave phage bodies at specific sites (capsid or scFv). Only the immobilized phage bound to the bait (target material or antigen) will be eluted. Any non-specific phages present will be marginalized during several panning rounds. d) Competitive elution: high concentration target antigen is introduced to elute bound phage, with the material binding phage still bound to surface.

The phages clones which are eluted using high or low pH solutions often display just low to medium affinity to the target<sup>360</sup>. Suggestions for the improvement of this procedure, for the selection of high affinity clones include: gradually decreasing in pH of the elution buffer

during the last biopanning round<sup>361</sup>, using target protein as the elution buffer<sup>362</sup> and eluting the bound phage with triethylamine over multiple time<sup>359,363</sup>.

In another article, the selection of high affinity binders was improved from a 7-mer peptide phage library, using a strategy known as an alternating elution procedure. In this elution procedure, solutions of low pH buffer (glycine buffer) and target protein (at higher concentration) were used in turns as eluting reagents for all the panning rounds, and by the third round were able to select high affinity clones for sequencing. Lysozyme was here used as model protein to evaluate the selection strategy. It was established that the using low pH buffer alone is not enough to remove the high affinity binders due to propagation effect of the atoms close to the affinity site. Using alternating elution from the initial round can prevent the loss of strong phage binders in the start of biopanning<sup>359</sup>. Similarly, another article has also commented on the problem with using conventional pH (acid and alkali) washing regimes which in previous studies has resulted in the loss of high affinity binder. With the intention to maximise recovery of binding sequence, Rawlings *et al.* at end of the selection rounds would use the eluted phage, and the remaining magnetic nanoparticle with any attached residual phage, to directly infect the *E. coli* cells<sup>364</sup>.

Cell bound phage in general are eluted using acidic buffers, but recent studies have suggested that low pH may not be enough as significant amount of phage remains bound with the cell pellet post centrifugation<sup>365-367</sup>. A possible alternative method for improving phage recovery maybe to use higher pH (alkali) solution or to infect the cell-bound phage directly with growing *E. coli* bacterium<sup>368,369</sup>. Certain studies have suggested that some phages may be internalized into the cell before binding to the cell surface antigen, thus using a combination of low pH solution, regardless the presence of a non-denaturing detergent (such as Tween 20 or NP-40), will enhance the phage recovery dramatically<sup>370,371</sup>

Recent research showed some advancement by using ultrasonication based physical elution combined with chemical elution and can be used as an alternative to the traditional chemical elution method<sup>69</sup>. In this biopanning approach, 100% of selected strong binders to solid materials have been recovered, by firstly eluting the peptides through chemical elution and followed by an additional step of 30 seconds physical elution by passing the ultra-sonic energy via ultrasonication<sup>69</sup>. Whereas, by using only single physical elution step, they

managed to recover 45% of the selected peptides from solution by ultra-sonication and also only a few numbers of clones were identified<sup>69</sup>. Likewise, in another study, inorganic binding peptides with electroactive properties were eluted by using a tiny electronic device in the biopanning media<sup>92,372,373</sup>. As a result of electric field application, the reversible electro activated peptides that have sensor applications were desorbed from the material surface after the chemical elution step<sup>92,372,373</sup>. However, the high power ultrasonication causes the production of cavitation bubbles which cause hydrodynamic sheering stress and helps in dissociating the phage<sup>68</sup>.

Enzymatic elution method involves using an enzyme such as trypsin or protease to cleave the link between the phage capsid and the library protein. Trypsin cleaves between the scFV and pIII phage (phage coat protein) thus, any scFV-attaching phage (surface binding and antigen binding) will be eluted, except for the phage-head-attaching phage which will still be bound to the surface. For the manipulation of the scFV phage, a helper protein is required. Engineered pIII has a helper phage known KM13 which also has a trypsin specific cleavage site, which post trypsin treatment is non-infective. However in the case of scFv-pIII fusion will lose the scFv protein post trypsin treatment, but still will remain infective<sup>374</sup>. Any non-specific binders in the eluted phage is reduced in phage display panning rounds with trypsin treatment compared to conventional elution methods (such as triethylamine elution)<sup>375,376</sup>. 3C protease has shown effective cleavage of phage proteins at 4°C, allowing the specific elution of phages bound to the bait (target material or antigen). The results showed that 3C protease treatment at 4°C elutes ~80 times more bound phage compares to traditional elution method with 1% SDS T7 phage<sup>349</sup>.

Within competitive binding elution methods, there are some strategies which use specific blockers and biological ligands to elute bound phages. As an example, Hageman *et al.* has used CCL22 and CCL17 (G-protein coupled chemokine receptor (CCR4)-specific chemokines) to determine anti-CCR4 mAbs that were able oppose receptor specific ligands<sup>377</sup>. Competitive elution methods are certainly useful for experiment that require the panning of native cell lines, as it is capable for expressing many antigens on the surface. A good example of this property would be the competitive elution of CK 8 and T4 cell line targeted phage binders, using anti-CK8 mAbs (RCK 102)<sup>378,379</sup>. However with this elution method, to achieve the desired outcome, optimisation of the incubation period and concentration of eluent agents is vital<sup>378</sup>. Competitive elution is an alternative elution method

which can be useful in experiments where the ligands of the certain target are known and accessible<sup>68</sup>.

Some literature suggests that scientists have tried to overcome the elution and recovery problems by two approaches. The bound phage recovery method<sup>93,319</sup> is one of the solutions, where the phage still remains bound to the surface of the material which is then amplified and sequence analysis is performed following PCR. A second approach is the PCR derived phage display<sup>153</sup>. In this method, the bound phages were eliminated, amplified and the phage DNA isolated through lysis buffer, followed by sequence analysis of the binders following PCR; however, under some harsh chemical conditions, the question concerning the materials stability remains unsolved and also there still remains the laborious labor-intensive nature of the process of biopanning. Taylor and co-workers achieved some success by introducing two new variations to the phage display technology<sup>380</sup>. Firstly, they introduced 10% wild-type phages and phage library into the panning mixture which enabled them to identify phage DNA for both non-specific and specific binding. Secondly, they used rolling circle amplification with polymerase phi29 where phage DNA bound to substrates after a series of washings for direct amplification<sup>380</sup>.

A study has also developed a phage display strategy for Affimer phage library that uses comparatively low amounts of target and non-target homologous antigen, thus making this a suitable method for proteins that are difficult to express or are expensive. The highly specific selected Affimer clones can distinguish between protein isoforms with similar structures. The method also allows for negative selection by which a small amount of homologous protein is premixed with the phage library from the round two of panning onward. Round two onward of panning involves the phage population to be initially incubated with homologous proteins to the target protein to eliminate any phage that binds to the closely related homologs, after which it is incubates with the planned target. This process may also be able to block or capture the cross-relative Affimer-displaying phage, thus allowing the enrichment and isolation of highly selective Affimers in the successive panning rounds. The method can potentially be suitable for any phage library for similar highly selectivity and for developing reagents to study signalling cascade by blocking of protein-protein interactions<sup>381</sup>.

Although various alternative elution strategies (eg. physical based such using as sonication, ultrasound etc.) are being tested to improve the elution step in biopanning process, the popularity of using chemical buffers (eg. low or high pH and salts) to elute the strongly bound target binders from material surfaces is still on rise and most preferred means.

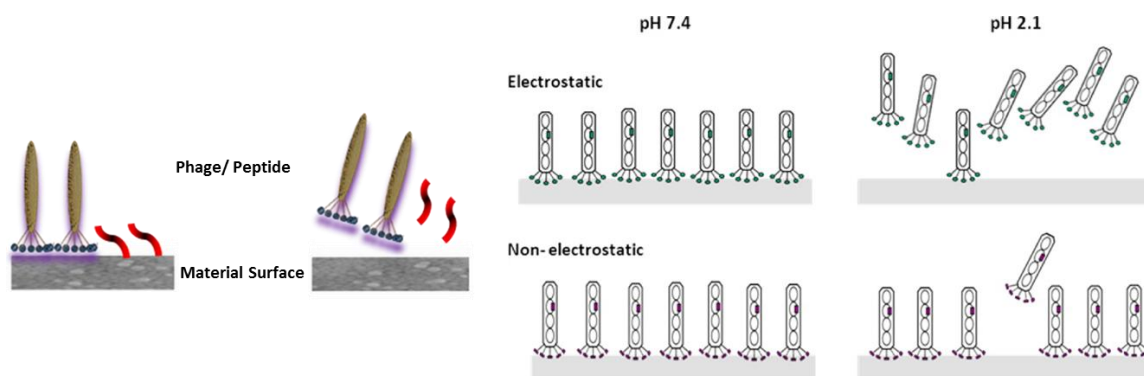


**Figure 4.2. Schematic representation of peptide/ phage adsorption or desorption onto silica nanoparticle surface and intrinsic bias during biopanning due to pH or charge. Image adapted<sup>4</sup>.**

From our previous biopanning studies<sup>4</sup>, it is evident that at pH 7.4, silica binding peptides identified by the phage display process, exhibit different binding patterns to the silica surface and are directly dependent on the sequence and charge specific interactions. However, when a low pH (2.1) elution buffer is used, the strong binders are eluted from the silica surface by disrupting the electrostatic interactions present at peptides-silica interface, thereby efficiently removing the electrostatically bound peptides from the silica surface and leaving the non-electrostatically (hydrogen or hydrophobic or van der Waals) bound consensus peptides on the material surface resisting detection as shown in Figure 4.2. Due to this behaviour of peptides during biopanning process, some silica binders that are bound by non-electrostatic interactions are being lost and the information about their diversity is unknown. This intrinsic bias of the biopanning process is due to the elution step. Also, the peptides adsorbed to silica nanoparticles in this study were pH dependent and found to be sequence dependent subject to the peptide charge. Therefore, any changes in washing and elution steps will affect the adsorption or desorption of peptide on silica surface.

Therefore, we have used an alternative elution strategy by using more than one elution buffers varying elution conditions to effectively elute and recover most phage clones from the available library. In this study, an optimised chemical elution to biopanning method reported here, has identified and recovered more silica binders from the phage pool in just 2 biopanning rounds. Although the approach is tested with silica, it could perhaps be applied other inorganic materials that resemble silica properties. Moreover, complementary experimental and bioinformatics methods are used to check and test the authenticity of true silica binders.

## **4.2 Materials and Methods**

### **4.2.1 Materials**

Chapter 2, section 2.1.1 provides details of materials used for adsorption studies.

### **4.2.2 Methods**

#### **4.2.2.1 Phage display protocol**

The typical protocol applied for optimised biopanning and repanning biopanning experiments are discussed in methods sections 2.1.2.3 and 2.1.2.4. The details of phage display experiments and elution conditions used to elute silica binding peptides via optimised and repanning methods can found in the Tables 2.1, 2.4 and 2.5.

#### **4.2.2.2 Relative binding affinity method**

For this chapter, 14 different individual phage clones isolated from optimised biopanning process were chosen for the relative binding assay. The protocol used for this assay are described in Chapter 3, section 3.2.2.2. The phage titer calculations including the number of input to output phages and the binding ratios from two separate experimental repeats was added in Appendix 4.1.

#### **4.2.2.3 Bioinformatics searching**

Chapter 2, section 2.1.2.2 provides details of materials used for bioinformatics analysis.

### **4.3 Results and Discussion**

In this chapter, the same batch of amorphous hydrophilic silica nanoparticles (as for chapter 3) of size 82 nm prepared in the Perry laboratory and previously characterised<sup>4,107,234</sup> has been used as a target. Further details about the properties and measurements of silica nanoparticles is described in Table 2.6 under the section 2.1.2.6. However, as the first batch of library (Lot: 0211212) was finished for more panning experiments, a second batch (Lot: 0221501) ordered and used for the optimised biopanning process (alternative three step chemical elution method). It is known that most of the phage clones eluted by either low or high pH buffers via traditional elution methods often displayed low to medium affinity for the target<sup>360,382</sup>. Few studies reported improved procedures by gradually decreasing the elution buffer pH<sup>361</sup> and constantly eluting the substrate bound phage with high pH triethylamine<sup>363</sup> in the successive biopanning rounds for selecting high affinity clones. Also, from the results of Chapter 3, the physico-chemical properties (i.e charge, pI and functional groups) of the isolated silica binders suggested that the three different elution buffers (0.2 M Glycine-HCl, pH-2.2, 100 mM Triethylamine, pH-11 and 4 M MgCl<sub>2</sub>, pH-6.1) used have extracted phage clones displaying peptides of both electrostatic and non-electrostatic interactions. Hence, by using the same three elution buffers consecutively one after other in a single panning round (described in methods section, Chapter 2), we expect to elute and recover elution and /or charge specific silica binders that are bound to silica by both electrostatic and non-electrostatic interactions; thereby improving the elution procedure previously used in Chapter 3. The optimised biopanning approach differs from the traditional biopanning method as each mentioned buffer (Gly-HCl, pH-2.2; MgCl<sub>2</sub>, pH-6.1; TEA, pH-11) are used consecutively one after other in a single screening (biopanning) round, as appose to one specific buffer being used for all panning rounds including elution steps in traditional biopanning and repanning experiments (Chapter 3).

Despite obtaining a new aliquot of library, we did not repeat traditional biopanning according to Chapter 3 as a comparator with the work described in Chapter 4 because of the similarity of elution buffers (Gly-HCl, pH-2.2; MgCl<sub>2</sub>, pH-6.1; TEA, pH-11) and pH conditions that were used for Chapters 4 (optimised panning method) and 3 (traditional panning method). Nevertheless, for testing the optimised biopanning method, repanning experiments were carried out by exposing the mixture of amplified phage pool (prepared by mixing together the round 1 amplified phage pool samples stored from initial panning

experiments as shown in Table 2.5) from the initial (traditional) biopanning tests with fresh silica. The reason for taking all the separate amplified phage stocks from round 1 is to i) test the optimised chemical elution method with the first aliquot of library (Lot: 0211212, Chapter 3) as a comparator with the work described in Chapter 4 (new library, Lot: 0221501). ii) use this repanning test as a repeat for the traditional biopanning method as described in Chapter 3, because of the similarity of elution buffers and pH conditions.

#### **4.3.1 Silica binders isolated from optimised biopanning method**

Details including step by step optimised biopanning procedure used to isolate silica binders is described in Chapter 2, under methods section 2.1.2.3. Similarly, the experimental conditions (washing and elution) used for optimised biopanning process are shown in Table 2.4. In the optimised biopanning experiment, a few phage clones selected from the early panning rounds (1-2) displayed a range of silica binding peptides including the most frequently repeated sequences in all three sequentially used elution buffers as shown in Table 4.1. Here, a single biopanning experiment involving two panning rounds were performed. In each panning round, phage binding, washing, three step elution and amplification steps were carried out. At the end of first and second rounds, phage titering and blue/white screening method was used to select individual phage plaques. A total of 180 phage clones were selected randomly from first and second rounds (30 clones each from the three elution buffers separately) and analysed by DNA sequencing.

The phage clones obtained from the first and second biopanning rounds displayed a range of silica binding peptide sequences as shown in Table 4.1. Overall, 47 peptide sequences were isolated coding for 15 identical repeats and 32 different sequences. The sequences identified from the second round of panning showed more repeating peptide sequences that appeared in first round. Also, some phage clones selected in first round were further selected in second panning round due to the progressive enrichment in the phage clones displaying the same peptide sequences. The possible reason for an increase in enrichment in the early panning rounds itself (second panning round) might be due to i) the stepwise increase in the detergent concentration (for every 5 washes, out of 10 wash cycles performed for a single panning round) in the washing step and ii) the additional elution steps (three step elution) covering a pH range 2-11 including high salt in a single panning round unlike single elution step in Chapter 3.



**Table 4.1. Silica binding peptides identified from optimised biopanning process.**

A total of two screening rounds were performed, the phage clones eluted separately after each elution step in a three-step elution process using three different elution buffers for each panning round were shown. To improve the screening stringency, the Tween 20 detergent (0.1-0.5% Tween 20 [v/v] mixed in TBS) concentration and wash times gradually increased as shown. NIL are the phage clones which were excluded from results due to the insertless or absence of any sequence, as the inherent rate of insertless phages in the NEB Ph.D.-7 library was about 5%. Frequently occurring sequences within the biopanning rounds are presented in a unique colour for clarity.

Biopanning (screened) round	Wash TBST	Elution conditions			Peptide sequence and frequency				Frequently observed peptides						
		Buffer	pH	Eluent											
1	0.1-0.3% 5 each Total 10 washes	Glycine- HCl, 0.2 M	2.2	1 <sup>st</sup>	MPRLPPA	3/30	ALVLSLSQ	1/30	MPRLPPA						
					ADIRHIK	2/30	SVDIWVTI	1/30	ADIRHIK						
					SILPVTR	2/30	AGHVVPR	1/30	SILPVTR						
					MQEMRQM	2/30	EVISAAS	1/30	MQEMRQM						
					LMPGYQL	1/30	LLALPYW	1/30							
					LTQQLHT	1/30	VDTSIFN	1/30							
					LETVVSS	1/30	YPWQSDN	1/30							
					TAVTYKS	1/30	TNLHINP	1/30							
					VITLDTY	1/30	ADARYKS	1/30							
					QMQTGKL	1/30	LLAPPYW	1/30							
					KSLWTYP	1/30	MHEAVLN	1/30							
					SLETMSN	1/30	NIL	2/30							
1	0.1-0.3% 5 each Total 10 washes	MgCl <sub>2</sub> 4 M	6.1	2 <sup>nd</sup>	ADARYKS	4/30	LETVVSS	1/30	ADARYKS						
					MPRLPPA	4/30	ASMNQGG	1/30	MPRLPPA						
					HDSPTAA	3/30	SFLVTRN	1/30	HDSPTAA						
					HWNTVVS	2/30	SPSTNPS	1/30	HWNTVVS						
					ANPTFFS	2/30	GPLIWFS	1/30	ANPTFFS						
					ADIRHIK	1/30	GSTSFSK	1/30							
					DNDLSLS	1/30	ASSHIHH	1/30							
					HDVMWQR	1/30	ANLPQLL	1/30							
							NIL	4/30							
					2	0.3-0.5% 5 each Total 10 washes	Glycine- HCl, 0.2 M	2.2	1 <sup>st</sup>	SILPVTR	18/30	ADARYKS	1/30	SILPVTR*	
										ADIRHIK	4/30	MVQSPRD	1/30	ADIRHIK*	
										ANPTFFS	4/30	NIL	2/30	ANPTFFS*	
MgCl <sub>2</sub> 4 M	6.1	2 <sup>nd</sup>	HWNTVVS	16/30						ANPTFFS	2/30	HWNTVVS*			
			SPLHSNY	3/30						SILPVTR	2/30	SPLHSNY			
			ADARYKS	2/30						NIL	3/30	ADARYKS*			
			ADIRHIK	2/30											
			TEA 100 mM	11						3 <sup>rd</sup>	ANEDTGT	22/30	SPLHSNY	2/30	ANEDTGT*
											EGWIQTF	5/30	FGGPTTR	1/30	EGWIQTF*

From the results, it was found that ten phage clones displaying peptide sequences ANEDTGT (22/30, 73%), SILPVTR (18/30, 60%), HWNTVVS (16/30, 53%), EGWIQTF (5/30, 17%), ADIRHIK (4/30, 13%), ADARYKS (4/30, 13%), MPRLPPA (4/30, 13%), ANPTFFS (4/20, 13%), FGGPTTR (3/20, 10%) and SPLHSNY (3/30, 10%) appeared as the most frequently occurring silica binders (i.e more abundantly observed sequences from a randomly selected few phage clones) eluted from the first and second panning rounds via three different elution buffers (Table 4.1). While, some identical sequences were displayed more than once but less frequently within the three different elution steps (highlighted in a unique colour). It is important to note that, no single peptide sequence was present in all the three different elution steps.

More importantly, the sequences isolated in this optimised biopanning process (using second batch of same library (Lot: 0221501) showed no identical sequences compared with sequences identified from first batch in Chapter 3 (traditional and repanning experiments via Lot:0211212). Although, this batch-to-batch variation has been frequently reported as a problem in the antibody production<sup>200,372,383</sup>, there is no evidence for lot-to-lot variation for M13 phage display, specifically for Ph.D-7 libraries. However, this could happen possibly depending on how the outgrowth and amplifications in a larger scale proceed in the bacteria in the initial preparation of phage library<sup>384,385</sup>. The other possible reasons might be due to performing extended amplifications or many rounds of selections during the biopanning resulting mutations in *E.coli* leading to insert less clones. However, according to NEB Manual, no mutations were reported for Ph.D-7 phage display library so far. Hence, limited information is known about the full diversity of the phage libraries, more experimental evidence would be needed to determine if this Ph.D.-7 library system leads to lot-to-lot sequence variability. Nevertheless, it must be noted that only two panning rounds were performed in the optimised biopanning process suggesting very low chance of amplification bias could have happened within the experiment. In addition, a similar trend in the distribution of amino acid residue occurrences for all the peptide isolates eluted and identified from two separate lots of library against silica was observed (Figure 4.9) after analysing all the sequences from both batches (described in the following section 4.3.4). Furthermore, the two consensus sequences identified from both lots of library showed similar trend towards silica surfaces (Figure 4.8). Thus suggesting, this dissimilarity in the

isolated sequences may be due to the selection of few clones from a large phage pool for sequencing.

The amino acid distribution of the isolated silica binders from optimised bioapnning process were shown in the Figure 4.3. A total of 47 peptide sequences identified from both first and second panning rounds displaying 15 identical repeats and 32 different sequences were analysed and separated specific to the elution step and/ or buffer.

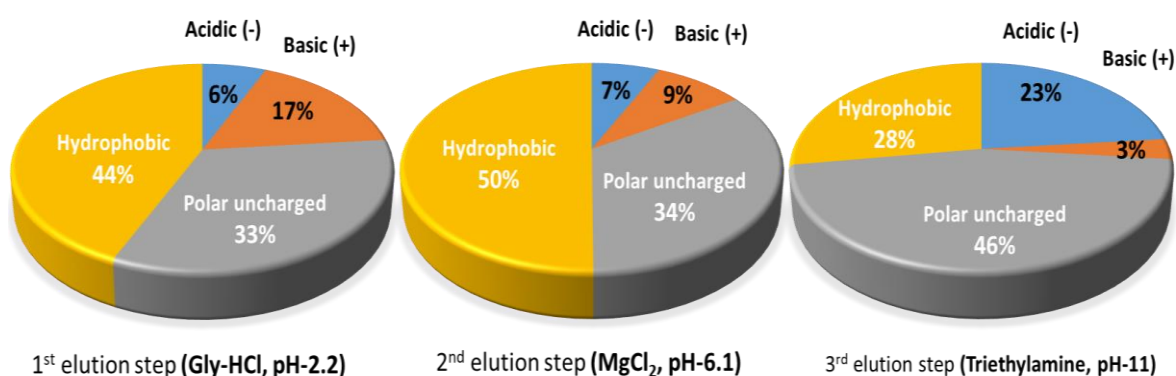


**Figure 4.3. Distribution of functional aminoacids of silica binders eluted from three step elution (optimised biopanning) process.** All the phage clones identified from first and second panning rounds (Table 4.1) using three different elution buffers for each panning round were considered while plotting the pie diagrams.

The high salt magnesium chloride elution buffer (4 M MgCl<sub>2</sub>, pH-6.1) eluted the phage clones displaying peptide sequences containing 50% of hydrophobic amino acids, in contrast to 44% and 28% using low pH (0.2 M Glycine- HCl, pH-2.2) and high pH triethylamine (100 mM Triethylamine, pH-11) respectively. It is noteworthy that the high salt elution buffer showed similar pattern for the phage clones eluted in the initial biopanning experiments (Chapter 3). Thus, indicating the high salt buffer may be used for eluting the phage clones mostly bound to silica by hydrophobic interactions. It has been reported that the peptide sequences removed from indium zinc oxide (IZO) surface eluted via high salt elution buffer (4 M MgCl<sub>2</sub>, pH-6.1) showed more blocks of hydrophobic amino acids than the low pH buffered solution<sup>92,373</sup>.

Besides, an increase in the acidic (-) and polar uncharged amino acid residue composition was noticed with step wise increase in the pH of the elution buffers. However, a reversed trend was observed for the for the groups with basic (+) charged. For example, the phage

clones eluted from elution buffer 1 (low pH) exhibited 6% acidic and 33% polar uncharged amino acid groups. While, the same acidic and polar uncharged residue composition gradually increased to 7% and 34% for the clones eluted from second elution step (4 M MgCl<sub>2</sub>, pH-6.1) and 23% and 43% with elution buffer 3 (high pH) respectively. Hence, indicating the single elution buffer used for eluting the phage clones (Chapter 3) may have resulted in incomplete removal of all strong binders and resist detection to substrate silica<sup>69</sup>. By using sequential three step elution process (optimised biopanning) varying elution buffers and pH condition in a single panning round, the phage clones that resist detection in single elution step may have eluted in the other successive elution steps. Also, the increase in the acidic amino acid composition for the phage clones eluted by high pH triethylamine (100 mM Triethylamine, pH-11) may be due the electrostatic repulsions resulting in the removal of strong silica binders.

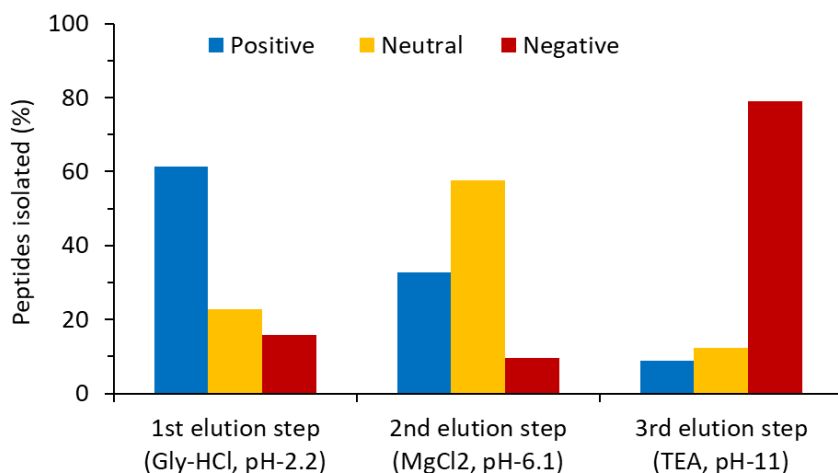
Moreover, Gly-HCl at low pH has eluted 63% of peptides with net positive charge, while 58% and 79% of peptides eluted in the second elution (4 M MgCl<sub>2</sub>, pH-6.1) and third elution (100 mM Triethylamine, pH-11) steps displayed net neutral and negative charged sequences respectively (Table 4.2 and Figure 4.3). The percentage of the peptide sequences eluted was calculated by counting and averaging the number of sequences and times identified in both first and second panning rounds. Also, it was noticed that as the pH condition of the elution buffers increase in the elution steps, the net charge of the sequences being eluted from silica surface change from positive to negative. For example, the sequences SILPVTR (20/60), MPRLPPA (3/60), ADIRHIK (6/60) and ADARYKS (2/60) having high pI (11.1 to 9.7) and net positive charge (+1) were eluted mostly in the first elution (high pH) step. While, the peptides HWNTVVS (18/60), SPLHSNY (3/60) and ANPTFFS (4/60) holding near neutral pI (7.8 to 6) and charge (0); as well as sequences ANEDTGT (35/60) and EGWIQTF (7/60) possessing low pI (3) and net negative charge (-1 to -2) were eluted mostly in the second (high salt) and third (high pH) elution steps (Table 4.2 and 4.3). However, a few sequences that were isolated in the first elution (MPRLPPA 4/60, ADIRHIK 3/60 and ADARYKS 6/60) also appeared in the second elution step. Similarly, the sequence SPLHSNY (3/60) that was eluted in the second elution step, reappeared in the third elution step, but fewer times. This may suggest that the residual sequences remaining from the previous elution steps were carried forward sequentially.

**Table 4.2: Silica binders identified in Table 4.1 and their elution, pI and charge based appearance.** The pI and net charge values for all the sequences were obtained from Innovagen and Bachem peptide property calculator (INNOVAGEN, 2014; Bachem, 2017). Blue colour indicates high pI and positive charge values of peptides at pH-7; no colour directs neutral charge and pI values and red colour indicates low pI and negative charge values.

1 <sup>st</sup> elution (Gly-HCL, pH-2.2)				2 <sup>nd</sup> elution (MgCl <sub>2</sub> , pH-6)				3 <sup>rd</sup> elution (TEA, pH-11)			
Round 1 (R1A)	pI	Net charge @7			pI	Net charge @7			pI	Net charge @7	
MPRLPPA	3/30	11.1	1	MPRLPPA	4/30	11.1	1	FGGPTTR	3/30	11.1	1
SILPVTR	2/30	11.1	1	SFLVTRN	1/30	11.1	1	LNGNWTR	1/30	11.1	1
ADIRHIK	2/30	10.18	1.1	ADIRHIK	1/30	10.1	1.1	VDGARTH	1/30	7.8	0.1
AGHVVPR	1/30	11.1	1.1	GSTSFASK	1/30	10.1	1	SPLHSNY	1/30	7.8	0.1
QMQTGKL	1/30	10.1	1	<b>ADARYKS</b>	<b>4/30</b>	<b>9.7</b>	<b>1</b>	TNLHINP	1/30	7.8	0.1
ADARYKS	1/30	9.7	1	ASSSHIH	1/30	8.1	0.3	SSTPANL	1/30	6	0
TAVTYKS	1/30	9.7	1	<b>HWNTVVS</b>	<b>2/30</b>	<b>7.8</b>	<b>0.1</b>	TCASQFP	1/30	5.3	0
KSLWTYP	1/30	9.7	1	HDVMWQR	1/30	7.8	0.1	<b>EGWIQTF</b>	<b>2/30</b>	<b>3.3</b>	<b>-1</b>
LTQQLHT	1/30	7.81	0.1	<b>ANPTFFS</b>	<b>2/30</b>	<b>6</b>	<b>0</b>	VWQPELQ	1/30	3.3	-1
TNLHINP	1/30	7.8	0.1	ANLPQLL	1/30	6	0	FVMSDPI	1/30	3.1	-1
<b>MQEMRQM</b>	<b>2/30</b>	<b>7</b>	<b>0</b>	ASMNQGG	1/30	6	0	VDTSIFN	1/30	3.1	-1
ALVLSLQ	1/30	6	0	SPSTNPS	1/30	6	0	<b>ANEDTGT</b>	<b>13/30</b>	<b>3</b>	<b>-2</b>
LMPGYQL	1/30	5.9	0	GPLIWFS	1/30	6	0				
LLAPPYW	1/30	5.9	0	<b>HDSPTAA</b>	<b>3/30</b>	<b>4.9</b>	<b>-0.9</b>				
LLALPYW	1/30	5.9	0	LETVVSS	1/30	3.3	-1				
MHEAVLN	1/30	5.1	-0.9	DNDLSLS	1/30	2.9	-2				
SLETMSN	1/30	3.3	-1								
LETVVSS	1/30	3.3	-1								
EVISAAW	1/30	3.3	-1								
VITLDTY	1/30	3.1	-1								
VDTSIFN	1/30	3.1	-1								
YPWQSDN	1/30	3.1	-1								
TLTEEYF	1/30	3.1	-2								
SVDIWTI	1/30	3.1	-1								

Round 2 (R2A)											
	pI	Net charge @7			pI	Net charge @7			pI	Net charge @7	
SILPVTR	18/30	11.1	1	ADIRHIK	2/30	10.1	1.1	FGGPTTR	1/30	11.1	1
ADIRHIK	4/30	10.1	1.1	SILPVTR	2/30	11.1	1	SPLHSNY	2/30	7.8	0.1
ADARYKS	1/30	9.7	1	<b>ADARYKS</b>	<b>2/30</b>	<b>9.7</b>	<b>1</b>	<b>ANEDTGT</b>	<b>22/30</b>	<b>3</b>	<b>-2</b>
MVQSPRD	1/30	6.4	0	<b>HWNTVVS</b>	<b>16/30</b>	<b>7.8</b>	<b>0.1</b>	<b>EGWIQTF</b>	<b>5/30</b>	<b>3.3</b>	<b>-1</b>
<b>ANPTFFS</b>	<b>4/30</b>	<b>6</b>	<b>0</b>	SPLHSNY	3/30	7.8	0.1				
				ANPTFFS	2/30	6	0				



**Figure 4.4. Charge based distribution of peptides eluted in Table 4.2.** The percentage of peptides eluted was calculated by taking the net charge (at pH-7) values for all the peptides (Table 4.2) eluted in three elution buffers separately. For example, A total of 56, 53 and 57 peptide sequences were identified from first (Gly-HCl, pH-2.2), second (MgCl<sub>2</sub>, pH-6.1) and third elution steps counting both panning rounds (R1A and R2A). Out of 56 sequences from first elution, 35, 13 and 8 sequences, showed net positive charge, neutral and net negative charge values. Then dividing the 35/56\*100 will give 63% of peptides eluted in the first elution step using Gly-HCl, pH-2.2, displayed net positive charge. The same calculation were repeated to get other values.

**Table 4.3: Physico-chemical properties of selected silica binding peptides displayed in Tables 4.1 and 4.2.** <sup>a</sup>Physico-chemical properties of the sequences were obtained from Innovagen and Bachem peptide property calculator (INNOVAGEN, 2014; Bachem, 2017). Highlighted in bold are the sequences that appeared as the most frequently occurring silica binders repeated in first and second panning rounds. The amino acids that contain amine (N, Q, P, W) and hydroxyl side chain (S, T, Y) containing groups in a peptide that may help in forming hydrogen bonding between silica-peptide or among themselves are shown.

Peptide sequence	pI <sup>a</sup>	Net charge @pH 7 <sup>a</sup>	Functional amino acid residues <sup>a</sup>					
			Polar (-ve, +ve and uncharged)			Hydrophobic	Amine side chain (N,Q,P,W)	Hydroxyl side chain (S,T,Y)
			Acidic	Basic	Uncharged			
<b>SILPVTR</b>	11.1	1	0	1	2	4	0	2
MPRLPPA	11.1	1	0	1	0	6	3	0
<b>ADIRHIK</b>	10.18	1.1	1	3	0	3	0	0
<b>ADARYKS</b>	9.7	1	1	2	2	2	0	2
SPLHSNY	7.8	0.1	0	1	4	2	2	3
HWNTVVS	7.8	0.1	0	1	3	3	1	2
ANPTFFS	6	0	0	0	3	4	2	2
ANEDTGT	3	-2	2	0	3	1	1	2
EGWIQTF	3	-1	1	0	2	2	2	1

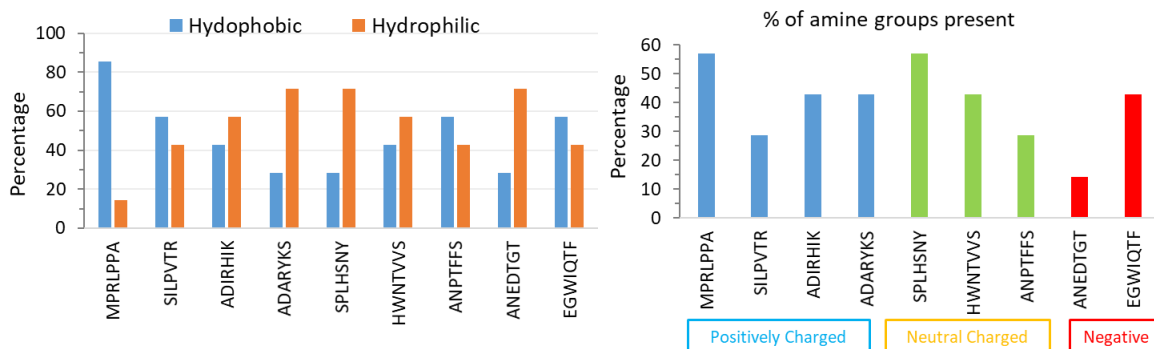


**Figure 4.5: Percentage of hydrophobic v/s hydrophilic and amine containing side groups present in selected silica binding peptides mentioned in Table 4.3.** The percentage of functional amine groups calculated by considering amino acids containing amine groups at side chain or N-terminus of the peptide.

The reappearance of MPRLPPA in the second elution step (high salt) may also be due to having six hydrophobic (MPLPPA, 86%) and four amine side chain (PRPP, 57%) containing groups representing the phage clone bound to silica by hydrophobic and hydrogen bonding were fully recovered by high salt buffer (Figure 4.5). Similarly, the recurrence of SPLHSNY in the third elution step (high pH) might be due to the presence of only polar uncharged (SHSNY, 71%) or amine side chain (PHSN, 57%) containing groups representing the phage clone bound to silica by hydrogen bonding were fully recovered by high pH buffer. While the high pH elution buffer eluted and recovered peptides ANEDTGT and EGWIQTF mostly with low pI (3) and net negative charge (-2 and -1) in final elution step, indicating the peptide bound to silica by electrostatics may have been removed as a result of electrostatic repulsions between negatively charged peptides and silica. Similarly, the high salt elution buffer eluted peptides with close neutral pI and charged peptides that could be responsible for hydrophobic/ hydrogen bonding or van der Waals forces.

Furthermore, the appearance of peptide sequences in second and third elution steps show that we are not eluting and recovering most of the silica binders by traditional elution process (i.e. only one elution buffer throughout panning experiment and rounds). By using sequential three step elution process (optimised biopanning) varying elution buffer pH condition in a single panning round, the phage clones that resist detection in one elution step may have eluted in the other successive elution steps. Hence, suggesting the efficiency of the method to elute and isolate most of the silica binders in the early rounds of biopanning, removing

the sequences that resist detection during traditional biopanning method; thereby by reducing the number of biopanning rounds, saving time, cost and effort. In addition, these three different elution buffers could be used to remove interaction or charge specific peptides subject to change in elution and pH condition.

#### **4.3.2 Experiment to check the optimised biopanning process 4.3.1**

Encouraged by the optimised elution approach results, we tried optimised elution (three step elution) process in two different strategies (as described in methods section 2.1.2.4). The first strategy differs from the traditional biopanning method as each mentioned buffers (Gly-HCl, pH-2.2; MgCl<sub>2</sub>, pH-6.1; TEA, pH-11) are used consecutively one after other in a single screening (biopanning) round, as appose to one specific buffer being used for all panning rounds including elution steps in traditional biopanning and repanning experiments (Chapter 3); Second strategy only used the same Glycine-HCl elution buffer but at varying pH's (i.e. Gly-HCl of pH-2.2; pH-7; pH-11).

The repanning experiment reproduced more or less the same silica binders (Table 4.4) as were identified previously in the above initial biopanning experiments (Tables 3.3 and 3.4, Chapter 3) along with few new peptide sequences. Some silica binders reproduced which were also isolated previously include VSRDTPQ, GQSEKHL, TVNFKLY, LPVRLDW, WSLSELH, NDLMNRA, QQTNWSL, KIAVIST, ELTPLPL and WSLSELH. All the main silica binders identified in Chapter 3 using three different elution buffers from separate biopanning experiments reappeared in this repanning experiment. Also, a few sequences YSLKQYQ, YSFKQYQ, YNGSANG, VENVHVR, and FASRSDT appeared in this repanning process.



**Table 4.4: Repanning experimental results to check the optimised biopanning approach and reproducibility.** Selected tight silica binders were shown here and full list of sequences can be found in appendix 4.2 and 4.3. Note: Black coloured sequences are found in both initial and repanning methods (Chapter 3). While, the red coloured sequences are the ones appeared in this repanning experiment. 'All 3 mix' are the phage clone samples that are mixed together from all 3 elution steps and pH within elution strategy 1 and 2.

Strategy 1 (Similar to optimised biopanning process)					Strategy 2 (Same elution buffer but varying pH)								
Gly-HCl pH-2.2	Freq	MgCl2 pH-6.1	Freq	TEA pH-11	Freq	Gly-HCl			All 3 mix				
pH-2.2	Freq	pH-6.1	Freq	pH-11	Freq	pH-2.2	Freq	pH-7	Freq	pH-11	Freq	All 3 mix	
Silica binders recovered					Silica binders recovered								
VSRDTPQ	3/30	VSRDTPQ	12/30	-	-	VSRDTPQ	5/30	VSRDTPQ	6/30	VSRDTPQ	6/30	VSRDTPQ	2/30
GQSEKHL	2/30	GQSEKHL	6/30	-	-	GQSEKHL	1/30	GQSEKHL	3/30	GQSEKHL	1/30	GQSEKHL	2/30
TVNFKLY	8/30	TVNFKLY	1/30	-	-	TVNFKLY	4/30	TVNFKLY	3/30	TVNFKLY	3/30	TVNFKLY	3/30
-	-	ELTPLPL	1/30	-	-	-	-	ELTPLPL	2/30	ELTPLPL	1/30	ELTPLPL	1/30
LPVRLDW	1/30	-	-	-	-	LPVRLDW	1/30	LPVRLDW	1/30	-	-	LPVRLDW	1/30
-	-	-	-	-	-	WLSSELH	1/30	-	-	WLSSELH	1/30	WLSSELH	1/30
-	-	-	-	-	-	-	-	NDLMNRA	1/30	-	-	-	-
-	-	-	-	-	-	QQTNWSL	2/30	QQTNWSL	1/30	-	-	-	-
-	-	-	-	-	-	KIAVIST	2/30	-	-	-	-	-	-
YSLKQYQ	2/30	-	-	YSLKQYQ	12/30	-	-	YSLKQYQ	3/30	YSLKQYQ	1/30	YSLKQYQ	3/30
-	-	-	-	YSEKQYQ	5/30	-	-	-	-	-	-	-	-
YNGSANG	2/30	-	-	YNGSANG	3/30	-	-	YNGSANG	1/30	-	-	YNGSANG	2/30
VENVHVR	2/30	-	-	VENVHVR	1/30	-	-	-	-	VENVHVR	1/30	VENVHVR	1/30
FASRSDT	2/30	-	-	-	-	FASRSDT	1/30	-	-	FASRSDT	1/30	-	-
For extra sequences (see appendix 4.2)					For extra sequences (see appendix 4.3)								
NIL	2/30	NIL	4/30	NIL	4/30	NIL	6/30	NIL	4/30	NIL	7/30	NIL	1/30

**Table 4.5: Physico-chemical properties of selected silica binding peptides of identified in Table 4.4.** <sup>a</sup>Physico-chemical properties of all the sequences were obtained from Innovagen and Bachem peptide property calculator <sup>211,212</sup>. Highlighted in bold are the sequences observed as most frequently repeated peptides. An asterisk (\*) represents the sequences that were present previously from initial and repanning experiments using lot 1 library (Chapter 3) and reappeared here. The amino acids that contain amine side chain (N, Q, P, W) and hydroxyl side chain (S, T, Y) containing groups in a peptide, which can help in forming hydrogen bonding between silica-peptide or among themselves are shown.

Peptide sequence	pI <sup>a</sup>	Net charge @pH 7 <sup>a</sup>	Functional distribution of amino acid residues <sup>a</sup>					
			Polar (-ve, +ve and uncharged)			Hydrophobic	Amine side chain (N,Q,P,W)	Hydroxyl side chain (S,T,Y)
			Acidic	Basic	Uncharged			
KIAVIST*	10.1	1	0	1	2	4	0	2
<b>TVNFKLY*</b>	9.7	1	0	1	2	3	1	2
<b>YSLKQYQ</b>	9.33	1	0	1	3	1	2	3
<b>YSEKQYQ</b>	9.33	1	0	1	3	1	2	3
<b>VSRDTPQ*</b>	6.78	0	1	1	3	2	1	2
<b>GQSEKHL*</b>	7.82	0.1	1	2	2	2	1	1
<b>LPVRLDW*</b>	6.8	0	1	1	0	5	0	0
NDLMNRA*	6.8	0	1	1	2	3	2	0
<b>ELTPLPL*</b>	3.3	-1	1	0	1	5	0	1

Additionally, the reappearance of these peptide sequences in the current approach prove that this phage clone does not have any propagation advantage during biopanning rounds which means this peptide sequence is not a fast grower but a genuine target binder. The physico-chemical properties of isolated silica binders suggest that the three different elution buffers (0.2 M Glycine-HCl, pH-2.2, 100 mM Triethylamine, pH-11 and 4 M MgCl<sub>2</sub>, pH-6.1) used have eluted peptides of both electrostatic and non-electrostatic interactions (Table 4.5).

A similar trend in terms of eluting the sequences in the first two sequential elution steps using low pH, high salt buffers that had eluted mostly positively and neutral charged in optimising biopanning process was observed in this repanning experiment (Table 4.4). For example, the frequently repeated sequences TVNFKLY (8/30, 4/30), KIAVIST (2/30) and YSLKQYQ (2/30) with high pI (10.1 to 9.3) and net positive charge (+1) were mostly eluted and recovered in the first elution step in both strategies. While, the neutral pI and charged sequences VSRDTPQ (12/30, 5/30), GQSEKHL (6/30, 3/30) occurred more frequently were recovered in the second elution step for two strategies. It must be noticed that the low pH and high salt elution buffers showed similar pattern for the phage clones eluted in the optimised biopanning process. However, the peptides YSLKQYQ (12/30, 1/230) and YSFKQYQ (5/30) displaying high pI (9.3) and net positive charge (+1) were identified and mostly recovered in the last elution step using high pH condition.

Thus, indicating these two positively charged phage clones may have bound strongly to negatively charged silica surface and were not able to elute and recover in the first and second successive elution steps resisting detection. Hence, in the third and final elution step (high pH elution buffer) the two phage clones were fully recovered, and this may be due the electrostatic repulsions between the negatively charged silica and positively charged phage clones at high pH resulting in the removal of strong silica binders. Thus, verifying the optimised biopanning process using the first aliquot of library (Lot: 0211212, Chapter 3) as a comparator with the work described in section 4.2.1; and further confirming the reproducibility of the repanning method, because of the similarity of elution buffers and pH conditions and importantly same aliquot of library.

### 4.3.3 Relative binding affinity assay to assess phage binding to silica

The relative binding affinity assay was carried out to evaluate the binding capability of each of the 14 different phage clones isolated by optimised biopanning process against silica nanoparticles. This phage-silica binding was determined by phage titer assay at pH-7.5<sup>306</sup>. Nine phage clones, that were isolated as main silica binders (highlighted in asterisk) and displayed repeatedly (abundantly observed) in the first and second screening rounds of optimised biopanning method (three step elution process) and two phage clones YSLKQYQ and YNGSANG displayed as new sequences in the repanning experiment of optimised biopanning process were chosen for binding assay. While, three individual clones were identified only once (LETVVSS, ASMNQGG and VDTSIFN) in the first or second screening round of the optimised biopanning method were randomly picked in addition to control M13KE.

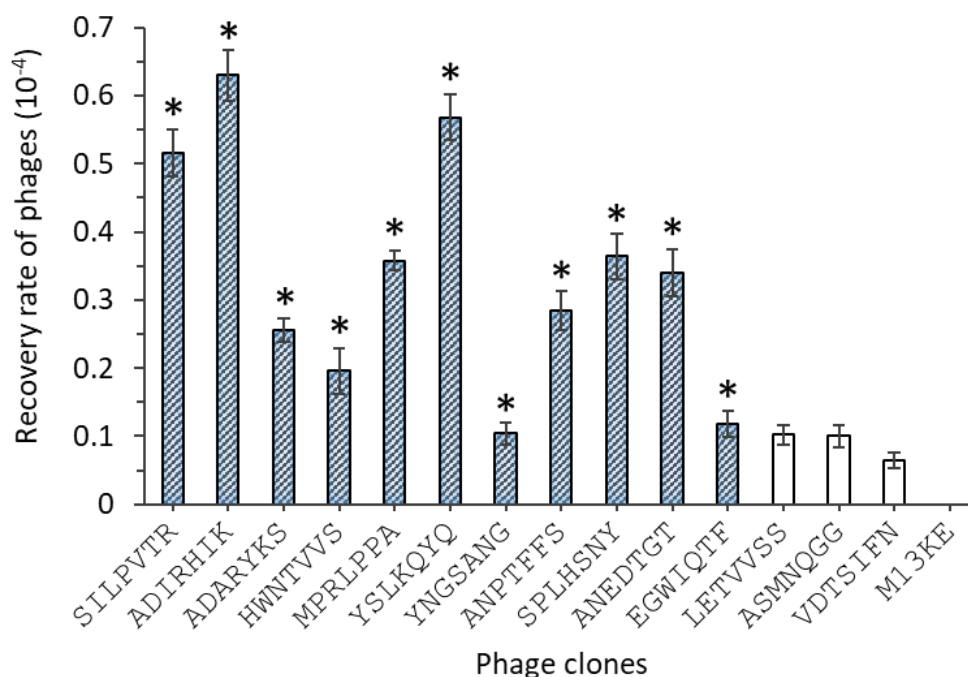


**Figure 4.6. Binding ratio (bound/input) of each of the 14 different phage clones to silica nanoparticles.** The relative binding affinity of the phage clones isolated from three step elution process (11 phage clones) and repanning experiment (2 phage clones) was determined by titer assay at pH-7.5. The asterisk (\*) indicates the phage clones displayed most frequently (abundantly observed) and repeated in the first and second screening rounds. The assay was repeated twice for each phage clone and the explained phage amounts were arithmetically averaged. The errors bars indicate the standard error from the two separate experimental repeats.

It can be seen from the Figure 4.6, that all the 14 phage clones selected for binding assay showed higher binding than the control M13KE. The same readings that were obtained for M13KE in Chapter 3 are considered while plotting the graph. Eleven phage clones picked as tight silica binders (highlighted in asterisk) from optimised biopanning findings showed higher binding than M13KE and the other three phage (LETVVSS, ASMNQGG and VDTSIFFN) clones that were selected randomly. Hence, checking the binding of the phage clones displaying the peptides to the silica is due to the randomly displayed peptide sequence and not due to non-specific coat proteins interactions. The phage clones displaying peptides SILPVTR, ADIRHIK and YSLKQYQ showed higher binding ratio to silica nanoparticles than the rest. Interestingly, the phage clones displaying MPRLPPA and SPLHSNY sequences that were isolated a few times in the first (7/60) and second round (5/60) of optimised biopanning showed better binding than the ANEDTGT (35/60) HWNTVVS (18/60), ADARYKS (6/60), ANPTFFS (6/60) sequences. This higher binding to silica might be due to the presence of motif (LP) in both the sequences. It must be noted that the motif LP was previously found in the identified consensus binder (VSTPLLA) to silica and in the literature (Table 3.5). To further confirm the phage clones are truly binding to silica and not to any other target unrelated materials, all the silica binders isolated from optimised biopanning (via Lot 2 library) were checked against MimoDB database alongside comparing with the sequences identified from traditional and repanning experiments (via Lot 1 library).

#### **4.3.4 Bioinformatics analysis to check authenticity of target binders**

MimoDB database, an online available bioinformatic tool has been used to identify and analyse the authenticity of silica binding sequences<sup>216,217</sup>. This mimotope peptide database search engine also called as HLAB BDB (Biopanning data bank) or formerly called as MimoDB. All peptides displayed against SiO<sub>2</sub> were checked against MimoDB to find the whole or exact part of phage display sequences that resemble the silica binders identified from both library lots. Interestingly, the MimoDB results did not show any no hits for all the silica binders that were identified from optimised biopanning approach (via using Lot 2 library) with the exception to the part of motif (GWXQT) being matched for the peptide EGWIQTF as shown below in Table 4.6.

**Table 4.6: Mimo search/ scan/ Blast analysis results of silica binders identified from both lots of same phage library and the differences in lot to lot behaviour.**

The phage displayed silica binders that showed hits for other materials indicating that they might be promiscuous binders. Peptide sequences highlighted in bold are the phage clones that appeared as most abundant binders (within the small population sequenced) to silica in initial biopanning and/ or repanning methods (Chapter 3).

Library lot used	Peptide	Target Found	Matched Sequence	Library type	Biopanning round	Reference
Lot 2 (0221501)	EGWIQTF	Anti-T7·Tag monoclonal antibody	NSLSMAP <u>QQGWVQ</u> <u>TG</u>			386
Lot 1 (0211212)	<b>QLAVAPS</b>	Fe3O4 Nanoparticles	Full sequence	Ph.D.-7	4, 5	323
	TVNFKLY	Fe3O4 Nanoparticles,	“	Ph.D.-7	2-5	323,329,330
	<b>HYIDFRW</b>	Fe3O4 Nanoparticles,	“	Ph.D.-7	2-5	323,330
	<b>GQSEKHL</b>	Fe3O4 Nanoparticles, Sera of peanut-tolerant subject 2	“	Ph.D.-7	2-5	323,330
	<b>VSRDTPQ</b>	Sera of peanut allergic patient 1-4, and tolerant subject 2	“	Ph.D.-7	2, 3	330
	ETALIAA	Plasma of peanut-tolerant subject 3	“	Ph.D.-7	1-3	“
	WSLSELH SSNQFHQ SAAWNKS GTGSQAS FASRSDT	Sera of peanut allergic patient 1, 3, 4	“	Ph.D.-7	2, 3	“
	<b>GASESYL</b>	Sera of peanut allergic patient 1, Anti-TIM polyclonal antibody	“	Ph.D.-7	1-3	330,331
	HGGVRLY	Agrobacterium vitis polygalacturonase , Plasma of peanut allergic patient 4	“	Ph.D.-7	2, 3	330,336
	IDNSHTH	Agrobacterium vitis polygalacturonase	“	Ph.D.-7	3	336
	SWTALGP	E3 ubiquitin-protein ligase Mdm	<u>TWLDNI</u> <u>WTTLGP</u>	Ph.D.-12	3	337
	TTQVLEA	Mouse brain microvasculature	<u>CTGRMT</u> <u>XQXXXA</u>	CX10C	5	338

As discussed in Chapter 3, the silica binders recovered from biopanning experiments (initial and repanning) via using Lot 1 library showed peptide sequences such as QLAVAPS, GQSEKHL, HYIDFRW, VSRDTPQ and GASESYL were found to have affinity for one or more than one different targets (Table 4.6) including binding to Fe<sub>3</sub>O<sub>4</sub> nanoparticles, Human prostate cancer cell line PC3, Sera of peanut-tolerant subject 2, Sera of peanut allergic patient 1, 3, 4, Plasma of peanut allergic patient 4 and Anti-TIM polyclonal antibody<sup>323,329-331</sup>. While other peptide sequences appeared to have some affinity for silica in one of the biopanning rounds were found to have some affinity for other targets. Details about the silica binders that showed hits for other targets was explained in Table 3.6, section 3.3.4, Chapter 3.

In addition to BDB search or Blast, the acceptability of the silica binding peptides from this project were checked with TUPredict tool from BDB databank. This tool was developed using machine learning algorithms and currently three predictors are available including PhD7Faster, SABinder and PSBinder<sup>215</sup>. For example, the PhD7Faster tool can be used to predict if phages bearing randomly displayed peptides from the Ph.D.-7 library might grow faster due to propagation advantage<sup>217,219</sup>. The predictor was built using Support Vector Machine, trained with peptides from the unselected Ph.D.-7 library after one round of amplification<sup>219</sup>. The silica binders identified in this study were checked by entering the sequence data either in FASTA or raw sequence data format. The threshold to distinguish between predicted positives and negatives (*tp*) was fixed ranging from 0 to 1. However, it was set to 0.5 by default. A peptide will be predicted to be a target unrelated peptide (TUPs) if the probability is 0.5 or higher.

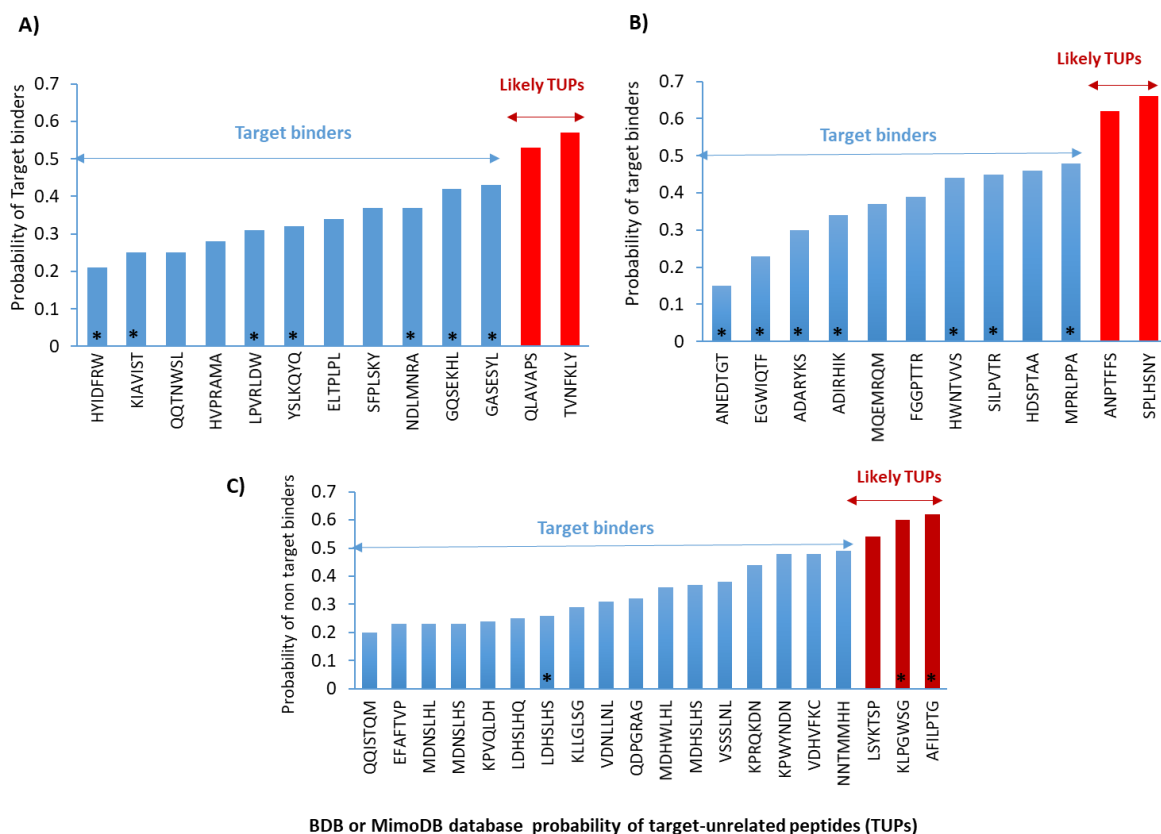


**Figure 4.7. Prediction of probability of target unrelated peptides or target binders.** The probability values for silica binders were generated using TUP predict tool (<http://immunet.cn/bdb/index.php/site/tools?type=TUPredict>) from BDB or MimosDB database and plotted. Silica binders identified from A) Lot 1 library (initial biopanning and repanning methods) and B) Lot 2 library (optimised biopanning process) were analysed to check the probability of silica binders to non-targets. In addition, the silica binders identified from C) previous studies were also checked for comparison <sup>4,10</sup>. An asterisk (\*) indicate the sequences appeared as tight binders to silica in experimental phage display. From the analysis, the sequences appeared to be likely silica binders and target unrelated peptides were highlighted in blue and red colours.

From the prediction results (Figure 4.7), most of the silica binders appeared to be the true sequences having affinity for silica and not target unrelated peptides. Some sequences QLAVAPS, TVNEFKLY, ANPTFFS and SPLHSNY that were observed less frequently in the phage display work found to be likely TUPs. However, the sequences ANPTFFS and SPLHSNY displayed to have some binding to silica in the relative binding assays (Figure 4.6) predicted to be likely fast growers or target unrelated peptides in this analysis. Even so, these sequences likely have some degree of ‘function’ against the screened material but also probably have some target-unrelated advantage over other library members<sup>219</sup>.

Interestingly, the silica binders KLPGWSG and AFTLPTG identified by our previous group members<sup>4</sup> via traditional biopanning approach and were shown to have high binding affinity for silica nanoparticles in both experimental and computational studies<sup>4,107,124</sup> appeared to be likely untargeted binders or fast growers. This clearly shows that both experimental phage results along with the theoretical databases should be used during the selection or validation of isolated peptides but should not rely solely on theoretical databases even though they give useful information about the possibility to predict fast growers. Thus, suggesting majority of the peptides isolated were target-related sequences and rather true silica binders without any human or pathogen or sample contamination, whereas the peptide sequences that were found to have exact or part of motif similarity for other targets indicate the possibility of promiscuous binding behaviour to multi-materials and more importantly the differences in selection of library to library.

Additionally, to find any sequence similarities in the identified silica binders, the multiple sequence alignment was performed using MSA Viewer<sup>213</sup>. A total of 77 and 47 different silica binding peptide sequences identified from two different aliquots of same NEB Ph.D.-7 phage library were taken for this sequence alignment. All the silica binders were isolated from four different sets of biopanning experiments using two different aliquots (Lot 1: 0211212 and Lot 2: 0221501). Using the Lot 1 library, three-separate series of biopanning tests include the initial or traditional biopanning (section 3.3.1), repanning experiments performed to check the reproducibility (section 3.3.2) and the optimised biopanning method (section 4.3.2, discussed in Chapter 4). While, the optimised biopanning process was carried out using second lot (section 4.3.1). From the multiple sequence analysis (Figure 4.8), two consensus sequences (ADLSVTS and VSTPLLA) were identified from the all the silica binders. Although, there is a huge difference in the aliquot to aliquot library in terms of isolating sequences, the two consensus sequences identified from both lots showed lot of similarities (Table 4.7).



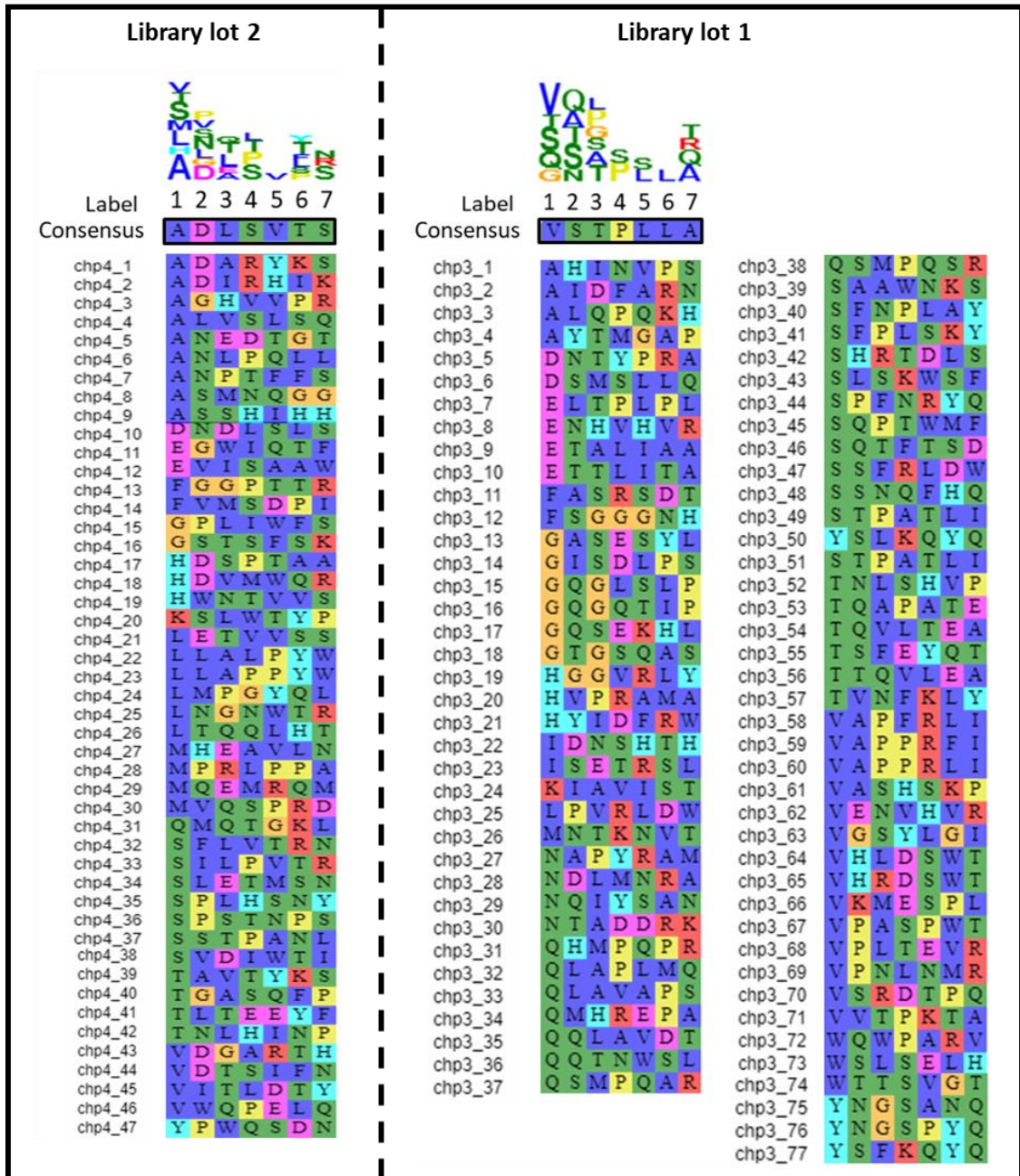


**Figure 4.8. Multiple sequence alignment of silica binders isolated from two different master lots (aliquots) of library.** The silica binding peptides used for generating these two figures were isolated from two different lots (Lot 1: 0211212 and Lot 2: 0221501) of same library. A total of 77 (Lot 1) and 47 (Lot 2) dissimilar sequences were chosen and analysed. The identified consensus peptide sequences (ADLSVTS and VSTPLLA) from the multiple sequence alignment was highlighted and shown. The sequence alignment was generated by using the freely available MSA viewer (<https://toolkit.tuebingen.mpg.de/#/tools/alnviz>) from the Max Planck Institute website. Label indicate the position and number of the peptide sequences. The small logo (figure) that is present on top of the 'label' indicate the number of times the amino acids have appeared in that specific position. The larger the size of the amino acid the higher the times the amino acid have appeared in that specific position of the peptide sequences. For example, in the library lot 1 image, the amino acid V (valine) was the most frequently observed residue (14 times), followed by S (serine, 12 times) as second, Q (glutamine, 8 times) and so on in the first position of all the 77 silica binders. Thus, V (valine) has appeared larger in the first column followed by second bigger S (serine) and so on.

**Table 4.7. Physico-chemical properties of two consensus silica binding sequences identified in Figure 4.8.** <sup>a</sup>Physico-chemical properties of the sequences were obtained from Innovagen and Bachem peptide property calculator (INNOVAGEN, 2014; Bachem, 2017). The amino acids that contain hydroxyl side chain (OH) containing groups (S, T, Y) which may help in forming hydrogen bonding between silica-peptide or among themselves are shown.

Consensus sequence	Mol.wt (g/mol)	Library Lots	pI <sup>a</sup>	Net charge @pH 7 <sup>a</sup>	Functional amino acid residues <sup>a</sup>				
					Polar (-ve, +ve and uncharged)			Hydrophobic	Hydroxyl side chain (S,T,Y)
					Acidic	Basic	Uncharged		
VSTPLLA	699	Lot 1	6	0	0	0	2	5	2
ADLSVTS	691	Lot 2	3.1	-1	1	0	3	3	3

More importantly, six out of seven (ALVST) amino acid groups are similar in both the sequences with either Leucine (L) or Serine (S) repeating twice in each peptide sequence. The functional amino acids present in both sequences have hydrophobic (ALV) and polar uncharged (ST) amino acids. Thus, indicating that all the three different elution buffers (0.2 M Glycine-HCl, pH-2.2; MgCl<sub>2</sub>, pH-6.1; TEA, pH-11) used for biopanning experiments including three step elution process (optimised biopanning) may have eluted phage clones that are bound to silica mainly by the hydrophobic and hydrogen bonding at pH-7.5. Besides this, a block of three (SVT), two (ST), (SV) amino acid groups were noticed present next to each other in both the sequences (ADLSVTS and VSTPLLA).

To further confirm the similarities, in terms of the functional amino acid groups and composition present in all the eluted silica binders from two different aliquots of library, three graphs (Figure 4.9) were plotted. The first (Figure 4.9. A) and second plots (Figure 4.9. B) were drawn by taking 77 and 47 peptide sequences that were identified from Lot 1 and Lot 2 of same library against same 82 nm sized amorphous silica nanoparticles. However, the third graph (Figure 4.9. C) was plotted by mixing both 77 and 47 silica binders altogether (total 124 sequences). A similar trend in the distribution of amino acid residue occurrences for all the peptide isolates eluted and identified from two separate lots of library was observed (Figure 4.9).

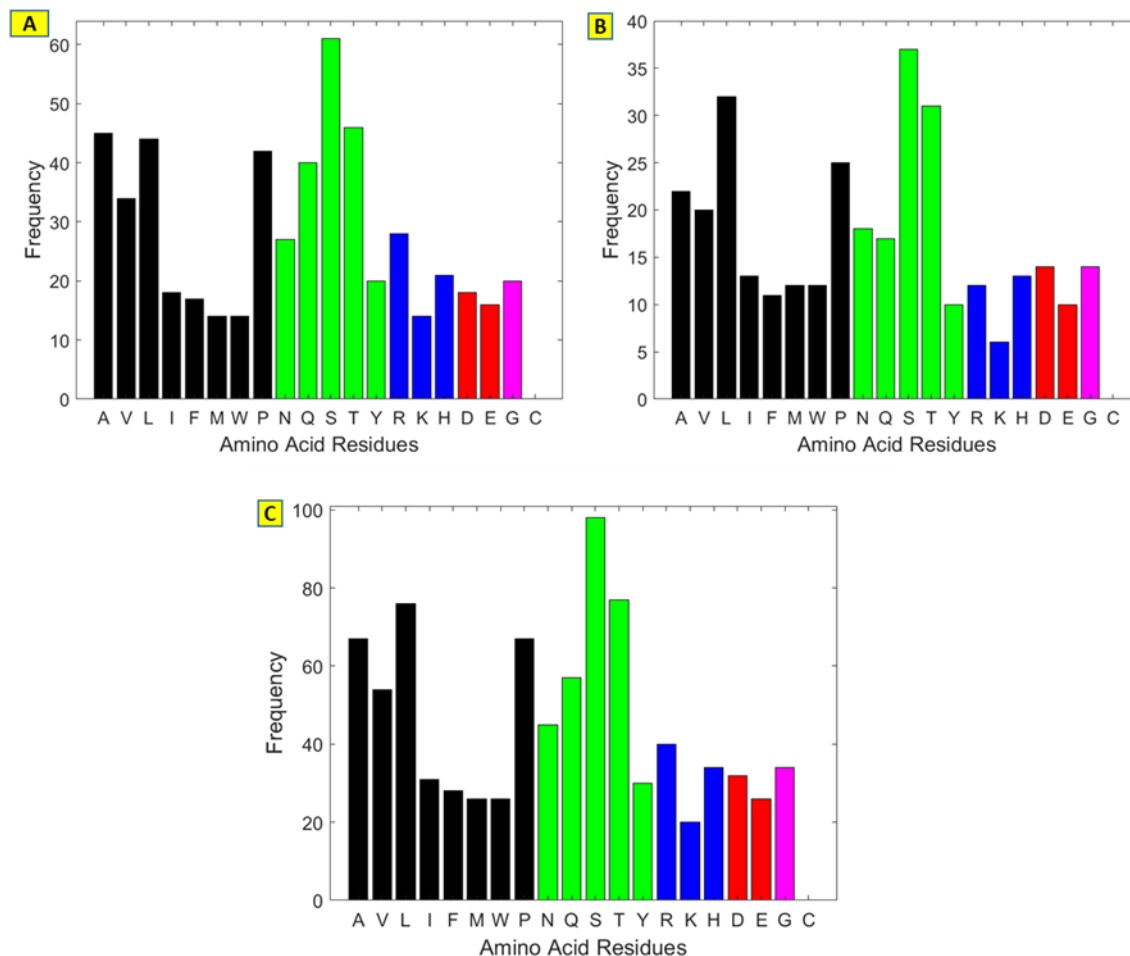


**Figure 4.9. Comparison of observed frequency of amino acid residues across all 124 peptide isolates identified from two separate lots of same library.** A) 77 peptide isolates from Lot 1, B) 47 peptide isolates from Lot 2 and C) 124 peptide isolates (by mixing 77 and 47 separate peptide isolates) identified from both lots 1 and 2 library. The X and Y-axis indicate the amino acid residues and the number of occurrences of each amino acid residue in the peptide isolates. All the amino acids residues are categorised and separated into 5 parts showing non-polar (black), polar uncharged (green), basic (blue), acidic (red) and special (magenta) amino acids in different colours.

The blocks of hydrophobic and polar uncharged groups were frequently distributed throughout in both lots of libraries. Primarily, the hydroxyl containing residues (S, T) occurred more frequently and distributed throughout all the silica binders than other residues. Similarly, the hydrophobic block (AVLP) displayed more frequently. While, the basic residues (R, H) elevated slightly higher than the basic residues (D, E). However, the amino acid Cysteine (C) was not found in any of the sequences identified from both lots of library. This might be due the interference of single amino acid Cysteine with the secretion of pIII protein and phage infectivity<sup>387</sup>. It must be noted that the peptide sequences isolated by optimised biopanning process (three step elution) using Lot 2 library showed no similar

sequences compared with the traditional biopanning and repanning experiments that used Lot 1 library. Although, there is a huge difference in the aliquot to aliquot library in terms of isolating sequences, the two consensus sequences and the amino acid occurrences identified from both lots showed similar trend towards silica surfaces. Thus, suggesting the optimised biopanning process (three step elution) using three elution buffers consecutively one after other in a single panning round may have eluted and recovered the phage clones that are bound to silica by hydrophobic, hydrogen bonding and electrostatic attractions or repulsions; as oppose to one specific buffer being used for all panning rounds including elution steps in traditional biopanning experiments. Hence, by using sequential three step elution process (optimised biopanning) varying elution buffers in a single panning round, the phage clones that resist detection to one elution step may be eluted in the other successive elution steps, thereby improving the elution procedure for silica surfaces.

#### **4.4 Conclusion**

To summarise, an optimised biopanning process (sequential three step elution) reported here, has eluted and identified most of the silica binders in the early panning rounds, using a sequential three step elution process varying elution buffers or pH condition in a single panning round. In addition, these three different elution buffers have eluted phage clones that may be interaction or charge specific subject to change in the elution buffer pH condition. Moreover, complementary experimental and bioinformatics methods have demonstrated that the isolated sequences are not target unrelated peptides but rather true binders to silica nanoparticles.

An alternative three step elution method developed have eluted and recovered the phage clones that are bound to silica by hydrophobic, hydrogen bonding and electrostatic attractions or repulsions; as oppose to one specific buffer being used for all panning rounds including elution steps in traditional biopanning experiments. Also, the phage clones that resist detection to one elution step have been eluted in the other successive elution steps, thereby recovering and improving the elution procedure for silica surfaces. The experimental results showed that the high salt magnesium chloride elution buffer have eluted the phage clones containing 50% of hydrophobic amino acids, in contrast to 44% and 28% using low pH glycine-HCl and high pH triethylamine respectively. Also, with increase in the pH of the elution buffers the acidic (-) and polar uncharged amino acid residue composition was increased in a step wise manner. However, a reversed trend was observed for the for the

groups with basic (+) charged. For example, the phage clones eluted from elution buffer 1 (low pH) exhibited 6% acidic and 33% polar uncharged amino acid groups. While, the same acidic and polar uncharged residue composition gradually increased to 7% and 34% for the clones eluted from second elution step (MgCl<sub>2</sub>, pH-6.1) and 23% and 43% with elution buffer 3 (high pH) respectively. Hence, indicating the single elution buffer used for eluting the phage clones (Chapter 3) may have resulted in incomplete removal of all strong binders and resist detection to substrate silica. Hence, by using sequential three step elution process (optimised biopanning) varying elution buffers and pH condition in a single panning round, the phage clones that resist detection in single elution step may have eluted in the other successive elution steps. Also, an increase in the acidic (-) amino acid composition for the phage clones eluted by high pH triethylamine was noticed and might have been due the electrostatic repulsions resulting in the removal of strong silica binders.

Additionally, the low pH buffer that was used in the first elution step had eluted 63% of peptides with net positive charge, while the high salt and high pH buffers have eluted 58% and 79% of peptides in the second and third elution steps displaying net neutral and negative charged sequences. Also, it was noticed that as the pH condition of the elution buffers increase in the elution steps, the net charge of the sequences being eluted from silica surface change from positive to negative. For example, the sequences SILPVTR, MPRLPPA, ADIRHIK and ADARYKS having high pI (11.1 to 9.7) and net positive charge (+1) were eluted mostly in the first elution (high pH) step. While, the peptides HWNTVVS, SPLHSNY and ANPTFFS holding near neutral pI (7.8 to 6) and charge (0); as well as sequences ANEDTGT and EGWIQTF possessing low pI (3) and net negative charge (-1 to -2) were eluted mostly in the second (high salt) and third (high pH) elution steps. However, a few sequences that were isolated in the first elution (MPRLPPA, ADIRHIK and ADARYKS) also appeared in the second elution step. Similarly, the sequence SPLHSNY that was eluted in the second elution step, reappeared in the third elution step, but fewer times. This may suggest that the residual sequences remaining from the previous elution steps were carried forward sequentially.

Moreover, the optimised biopanning process has been tested with a panning experiment using amplified library mixture obtained from Lot 1 library as a comparator to check the three-step elution as well as repanning processes. In this experiment, more or less the same silica binders that were identified previously in the Chapter 3 (initial and repanning)

experiments reproduced along with few new peptide sequences. A similar trend in terms of eluting the sequences in the first two sequential elution steps using low pH, high salt buffers that had eluted mostly positively and neutral charged in optimising biopanning process was observed in this experiment. However, high pI (9.3) and net positive charge (+1) peptides were identified and mostly recovered in the last high pH elution step. Thus, indicating the positively charged phage clones might have bound strongly to negatively charged silica surface and were not able to elute and recover in the first and second successive elution steps resisting detection. Hence, with high pH elution buffer in the third step, these phage clones were fully recovered might be due to the electrostatic repulsions. Thus, verifying the optimised biopanning process and confirming the reproducibility of the repanning method.

The results of the relative binding assay showed SILPVTR, ADIRHIK and YSLKQYQ as top binders to silica. In addition, the peptides (MPRLPPA and SPLHSNY) displaying the motif LP sequences showed better binding. Furthermore, the MimoDB Blast search results showed no hits for all the sequences identified from optimised biopanning process (via Lot 2 library). Similarly, the results obtained from TUPrdecit prediction tool showed (identified from separate aliquots of library) very few sequences as target unrelated and most of them as target binders theoretically. More importantly, the sequences isolated from phage display experiments via two different batches of same library showed no identical sequences. However, in the comparative analysis, the two consensus sequences (ADLSVTS and VSTPLLA) and the frequency distribution of the amino acids (identified from separate lots) showed near similarities towards silica surfaces, thereby indicating the batch to batch library diversity.

## **Chapter 5: Interaction studies of silica binding peptides / phages with silica nanoparticles**

### **5.1 Introduction**

This chapter explores an alternate way of selecting material binding peptides and the mechanisms by which the phage identified, or synthetically modified peptides bind to the surface of silica nanoparticles. Also, this section investigates the effect of C-terminal end group modification (acid or amide) and the difference in binding behaviour to silica in solution. Moreover, the phage clone displaying the peptide sequences YSLKQYQ, ADIRHIK and HYIDFRW have been used for checking phage-silica binding using Transmission electron microscopy.

To date, SiO<sub>2</sub>-biomolecule interactions have been investigated by a wide range of experimental and theoretical techniques. In this section, some of the most recent and innovative studies are discussed together with the techniques that have contributed to the understanding of molecular interactions. Even though the popularity of using combinatorial display techniques for recognising unique peptides having specific affinity for various inorganic target materials (discussed in chapter 1, section 1.4) including silica have grown rapidly, the precision of molecular recognition for inorganic materials is still challenging due to their binding to non-specific targets or limited understanding of the properties and changes occurring during silica-peptide interfacial studies. This gap in knowledge has forced the scientific community to look for better analytical techniques to understand silica interactions with biomolecules in both solution and solid state. As an example of the approach, Sarikaya and co-workers reported a peptide-enabled co-assembly strategy for developing hierarchical multimaterial nanosurfaces such as quantum dot arrays (QD) and further monitored their specific binding affinities using surface plasmon resonance (SPR), quartz crystal microbalance (QCM) and atomic force microscopy (AFM)<sup>42,43,319,388–390</sup>. Further, in a simultaneous assembly of material binding peptides to a gold-silica substrate, a quartz silica binding QBP1 (PPPWLPYMPPWS) and a gold binding AuBP2 (WALRRSIRRQSY) peptide showed high affinity to their specific material surfaces as measured by SPR (i.e. SBPs-silica and AuBPs-gold)<sup>167</sup>. Moreover, QCM was used to measure the thickness of the very thin silica film coating (~ 5nm) onto the Au substrate, and AFM showed specific morphologies of the final material depending on the peptides used.

This study further showed that the combination of both materials permitted the design of biologically viable probe specific materials<sup>167</sup>.

Other groups have reported the ability of SPR technique to detect silica or silver coated plasmonic nanostructures tagged with immunoglobulin G (IgG) which further helped in recognising early cancer stages and related biomolecules even at low level analyte concentrations<sup>391</sup>. It should be noted that thermodynamic studies of peptide adsorption on silica is little explored compared to studies on gold<sup>165</sup> or silver surfaces using SPR<sup>391</sup>. QCM is another technique that has been used to investigate binding kinetics, including energy dissipation and affinity interactions present between silica (sensor chip) and biomolecules passing over the sensor. The biomolecules reported on so far include amino acids<sup>392</sup>, small penta or hexa peptides<sup>145,393,394</sup>, longer peptides<sup>395</sup>, human IgG and the hexameric peptide ligand (HWRGWV). In this latter study, the short peptide ligand was immobilised on the surface of silica coated QCM sensors using polyethylene glycol as a solvent with a surface density of  $\sim 0.8$  chains  $\text{nm}^{-2}$  resulting in an increased surface accessibility and allowing a proper orientation of the peptide to IgG<sup>396</sup>.

Ozaki and co-workers have developed a site-specific process for precipitating silica using silica BPs combined with peptide nucleic acids (PNAs) in which the PNA sequence could act as a binding module for a complementary DNA sequence<sup>309</sup>. Here, AFM showed the formation of long chains and unique dumbbell shaped silica nanospheres as a result of site-specific silica biomineralisation on DNA sites. In addition, transmission electron microscope (TEM) and dynamic light scattering (DLS) analysis revealed that the control of nanoparticles depended on the number of silica binding peptide–PNA conjugates attached to the DNA molecule<sup>309</sup>.

A study by Bharti and co-workers reported the use of cryo-transmission electron microscopy (Cryo-TEM) and small-angle X-ray scattering (SAXS) as tools to study the structural properties of bridged silica aggregates directed by the electrostatic adsorption of the globular protein lysozyme as a function of pH ranging from 3-11. In this study, a theoretical/mathematical model was also used to explain the experimental findings of the interacting particles<sup>397</sup>. In another study, ultraviolet circular dichroism (UV-CD) and dynamic light scattering (DLS) has been used as tools to study the effect of surface properties of two different types of SiNPs synthesised either by pyrolytic or colloidal processes in water and in PBS at 7.4, respectively<sup>398</sup>. In this study, the surface hydrophobicity/ hydrophilicity



was found to affect the amount of BSA adsorbed onto the silica NPs and also gave evidence for the formation of protein hard corona (mono-layered or multi-layered) when bovine serum albumin was adsorbed<sup>398</sup>.

Fluorescence based assays using fluorophores and dyes have been used to quantify peptide concentrations in solution. For example, fluorescence is commonly employed to quantify the amount of peptide adsorbed on amorphous silica NPs of different size and/or functionalities<sup>4,10,107</sup>. Fluorescamine assays have shown that simply by changing the silica surface properties and solution pH, the peptide adsorption mechanism can be modified<sup>4,107</sup>. In this latter study, the adsorption isotherms of peptides KLPGWSG (positively charged), AFILPTG (neutral) and LDHSLHS (negatively charged) showed the role of electrostatic/hydrophobic interactions and hydrogen bonding at the aqueous silica interface. Fluorescence based assays have also been used to study the biosilicification process using the fluorescent dye PDMPO<sup>117,399,400</sup>. The response of the 'silicaphilic' fluorescence to different environments such as solvent and pH has been recently probed using fluorescence spectroscopy as well as UV-vis, further supported by computational data, dynamic light scattering and zeta potential measurements to understand the PDMPO-silica interaction. The data show that pH affects charged states of the molecule, particularly in the presence of silica, and modified the mode of attachment, with both single point (low anisotropy) or multipoint modes (high anisotropy) modes of attachment being possible<sup>117</sup>.

Raman based spectroscopic tools have attracted much attention in the last decade for the characterisation of biomolecules (i.e. peptides, proteins, DNA) and metal-based compounds such as silica and gold<sup>358,401,402</sup>. Moreover, these techniques have been extended from probing inorganic material-peptide/protein interactions<sup>358</sup> to study catalytic reactions<sup>402</sup> or chemical imaging of live cells<sup>401</sup>. Note that, since surface-enhanced Raman spectroscopy (SERS) enhancement is based on the oscillation frequency of the electron plasma, only plasmonic nanostructures (i.e. VO, Mo, Au etc.) are suitable. Therefore, Raman based spectroscopic techniques have not been yet considered as potential tools to study biomolecule interactions on a silica surface itself but for example on a metallic surface such as Au with a thin silica coating layer<sup>401</sup>.

Although *in vitro* tools have been employed to study silica-biomolecule interfaces, understanding specific molecular recognition and mineral assembly is still challenging using current technologies. Therefore, computational studies have been used to generate better

engineering of silica-based materials as they are able to provide atomic level information including binding free energies, nuclear magnetic resonance (NMR) chemical shifts, vibrational frequencies, and electrostatic potentials maps. For example, molecular recognition of a solid by a peptide has been studied combining bioinformatics and molecular simulations. Oren and co-workers, showed that strong quartz SiO<sub>2</sub>-BPs always had at least one of Pro, Leu, and Trp residues in direct surface contact<sup>42,43</sup>. Rimola *et al.* demonstrated by computed adsorption energies that amino acids containing side chains with either polar or large aliphatic groups have the most favourable interaction energies towards hydroxylated amorphous silica and suggested hydrogen bonds and London dispersive interactions as the main driving force<sup>40,3</sup>. Recent computational studies using molecular dynamics simulations with the CHARMM-INTERFACE force field showed that adsorption of charged peptides (i.e. KLPGWSG and LDHSLHS) is highly influenced by the working pH<sup>44,124</sup>. In contrast, no significant difference was observed for neutral peptides (i.e. AFILPTG) which were more weakly attached by hydrogen bonds and hydrophobic interactions<sup>44,124</sup>. Moreover, the amount of peptide adsorbed onto the silica surface was shown to be influenced by the particle size, being higher for larger particles due to the larger silica surface ionization<sup>10,124</sup>. These quantitative predictions of peptide-silica binding as a function of pH and particle size were comparable and in accordance with experimental measurements (i.e. fluorescamine assay)<sup>10,124</sup>. Although great advances have been made in the mechanisms concerning silica-biomolecule interactions, the control of selective recognition of biomolecules is still unclear and is a challenge for applications including the fabrication of drug delivery systems and new catalysts, amongst others. Furthermore, much scientific attention is needed to increase our limited fundamental understanding of silica-biomolecule interactions as opposed to focussing on an application-oriented approaches.

In this chapter, three peptide sequences (YSLKQYQ, ADIRHIK and HYIDFRW) identified by phage display were chosen to examine the binding of phage and/ or synthetically synthesised peptides with silica using the fluorescamine assay and TEM. These sequences were selected based on results obtained from experimental phage display, relative binding assay, physico-chemical properties and bioinformatics analysis (Table 5.1). Further, these peptides have been synthesized to primarily test the experimental phage display process, including peptide selection process and to understand the peptide binding mechanism on the surface of hydrophilic silica nanoparticles at pH-7.5. Moreover, the peptides have been used to investigate the effect of functionalising the C-terminal end either with acid (COOH) or amide

(CONH<sub>2</sub>) groups and how that small change can affect the binding process. Additionally, TEM has been used to for checking phage-silica binding patterns.

## **5.2 Materials and Methods**

### **5.2.1 Materials**

Chapter 2, section 2.1.1 provides details of materials used for adsorption studies.

### **5.2.2 Methods**

#### **5.2.2.1 Fluorescamine protein quantification assay**

The synthesized and characterized peptides YSLKQYQ, ADIRHIK, HYIDFRW and GASESYL isolated by phage display were selected for this protein quantification assay. Moreover, the same peptides chemically modified by functionalising the C-terminal end group with amide (YSLKQYQ-NH<sub>2</sub>, ADIRHIK-NH<sub>2</sub> and HYIDFRW-NH<sub>2</sub>) were also used for this analysis. The procedures including the protocol and materials used for this assay are described in chapter 2, section 2.1.2.7.1. Calibration data for all the peptides were prepared and are presented in (Appendix 5.1).

#### **5.2.2.2 TEM to visualise the binding of phage peptides to silica**

The individual phage clones displaying the peptide sequences YSLKQYQ, ADIRHIK and HYIDFRW were selected for probing phage-silica binding studies using TEM. The process by which these phage clones were prepared is described in section 2.1.2.5, Chapter 2 under the subheading 'selection of single phage clones for binding studies'. The sampling process and protocol including materials used for TEM binding studies is described in Chapter 2, section 2.1.2.7.3.

## 5.3 Results and Discussion

### 5.3.1 Selection of SiBPs for experimental binding studies

It is a critical step to identify which peptides to choose (eg. few peptide sequences out of many binders isolated from phage display) for binding studies to verify them experimentally *in vitro*. For peptide-inorganic material binding studies, one can select peptide in different ways including the results from the phage display<sup>10</sup>, affinity binding assays<sup>322,323</sup> and based on previous knowledge of their binding mechanism to the target material and by rational design<sup>43,44,129,319</sup>. Although, it is common to select inorganic binding peptides merely relying on their experimental phage display results (i.e most frequently occurring peptides as the main binder)<sup>4,10,404</sup>; these peptides synthesised were shown to display dissimilar binding behaviour with nanoparticles *in vitro* even after maintaining similar conditions to those which were identified earlier by the phage display process<sup>10,13,60,404</sup>. This binding variations is believed to be due to the complex surface chemistry of the nanoparticles<sup>4,10,44,107</sup> and dependent on number of binding parameters such as the materials surface chemistry including their physico-chemical properties and the binding environment<sup>4,7,357,9,10,13,44,129,234,355,356</sup>. Also, it has been an recognized way to predict the likely type of interactions through which the peptides bind to silica nanoparticles by analysing the physico-chemical properties such as the charge, pI and functional amino acid groups of the isolated peptides from phage display<sup>124,328</sup>.

For this study, three peptides were chosen for *in vitro* silica binding studies. These peptides are YSLKQYQ, ADIRHIK and HYIDFRW. Also, the same peptide GASESYL that was considered as a control in Chapter 3 is included here for comparison. These peptides were selected based on the biopanning method through which they were identified, alongside considering relative binding results, pI values, net charge at pH 7 and the functional amino acid groups present as shown in Table 5.1. In addition, the bioinformatics analysis (possibility of binding to target or unrelated targets) carried out in the Chapter 4 was also considered for peptide selection. It is anticipated that these peptides might show better binding behaviour with silica nanoparticles under *in vitro* conditions than those selected only based on a single criterion (i.e. relying on experimental phage display data) as in Chapter 3. The above parameters considered while selecting the peptides for this adsorption studies were grouped as three different criteria; i) Experimental phage display results (Table 5.1, 1-

4) ii) Physico-chemical properties (Table 5.1, 5-9) and iii) Bioinformatics results (Table 5.1, 10-11).

**Table 5.1. Selection of peptides based on experimental phage display results (1-4), physico-chemical properties (5-9) and bioinformatics analysis (10-11).**

Experimental phage display results (1-3) taken into consideration include the type of library lot used and biopanning approach through which they were identified, alongside their appearance (i.e most frequently repeated sequences within the small number of sequences analysed) at different phage display experiments and rounds. Physico-chemical properties (5-9) of the peptides taken into consideration anticipating their binding behaviour to silica include the pI, hydrophilicity and net charge of peptide at pH7; Bioinformatics analysis (10-11) MimoDB analysis results to check the authenticity of their binding to target. According to probability prediction analysis, any peptide value that is less than 0.5 should be considered a true target binder not a target unrelated peptide (described in section 4.3.4). MimoDB search results refers to the sequences that were reported to bind to other materials (based on published data) other than to silica (in this study).

No	Criteria for peptide selection	HYIDFRW*	ADIRHIK*	YSLKQYQ*	GASESYL
1	Identified from library lot	Lot 1 (0211212)	Lot 2 (0221501)	Lot 1 (0211212)	Lot 1 (0211212)
2	Biopanning method used	Repanning	Optimised biopanning	Repanning	Initial bioapnning
3	Frequency repeated	Yes	Yes	Yes	No
4	Relative binding result	High affinity binder	High affinity binder	High affinity binder	Weak binder
5	pI value	7.76	10.18	9.3	3.3
6	Net charge @7	0.1	+1.1	+1	-1
7	C-terminal with amine side chain containing group in a peptide	W	K	Q	-
8	Ratio of hydrophilic residues / total number of residues	29%	43%	57%	43%
9	pI value	7.76	10.18	9.3	3.3
10	MimoDB probability of target binder	Target binder (0.23)	Target binder (0.34)	Target binder (0.32)	Target binder (0.41)
11	MimoDB search results (reported to have affinity for)	Fe <sub>3</sub> O <sub>4</sub> NPs	No hit	No hit	Sera of peanut allergic patient

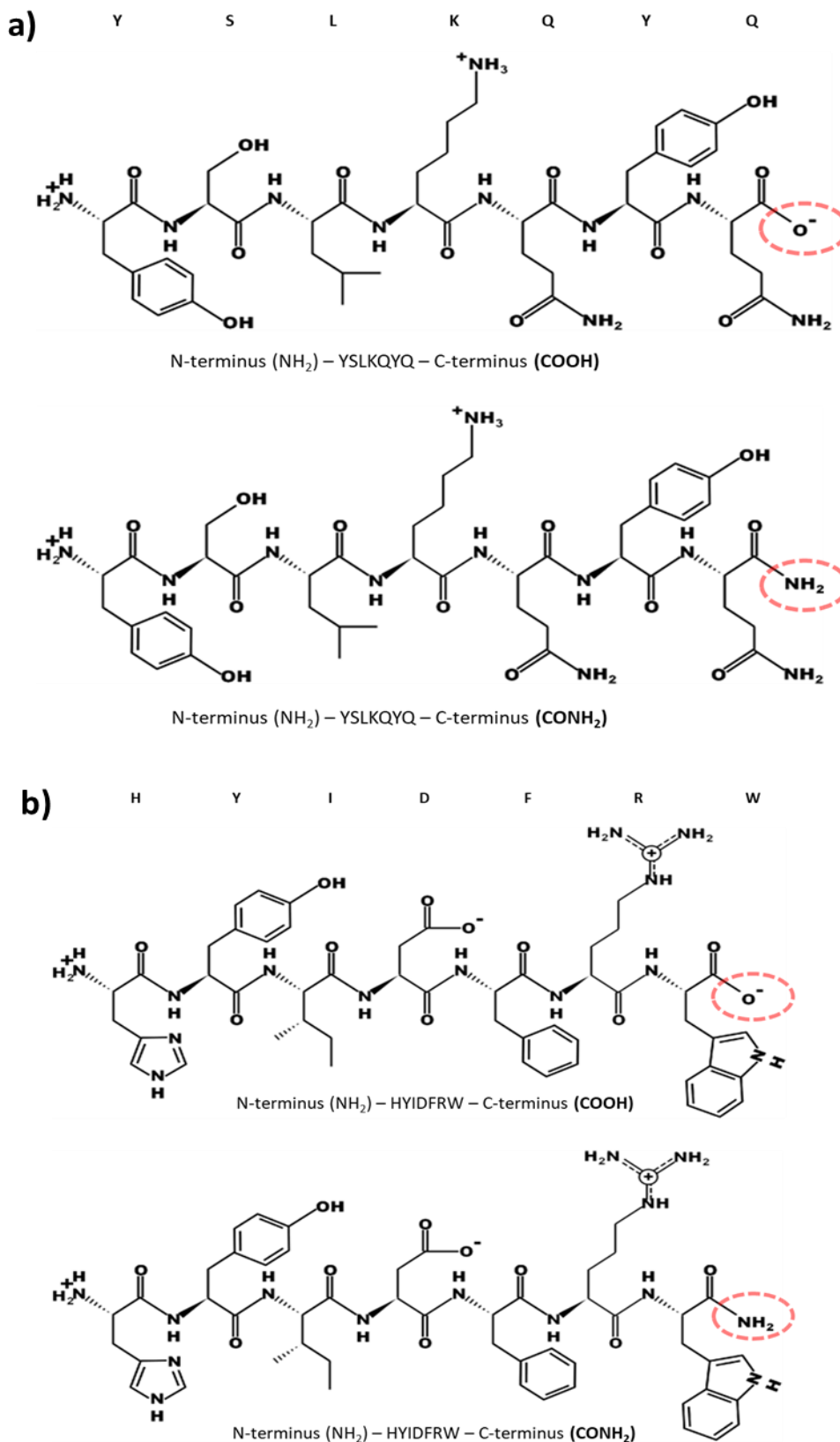


**Figure 5.1. Primary structure of silica binding peptides a) YSLKQYQ b) HYIDFRW depicting the modified C-terminal group end.** Peptide primary structure generated using the online tool PepDraw (<http://pepdraw.com/>). Highlighted in red coloured ring showing the C-terminal group (Gln, Q) acid (COOH) modified with amide (CONH<sub>2</sub>).



$\mu\text{m}$  Proteo 90 Å C12) was used to detect the purity of lyophilized (VirTis® 110 freeze dryer) peptides as detailed in section 2.1.2.6.2, Chapter 2. Further, Chromeleon® software was used for processing the data peaks thereby analysing the purity of the peptide samples. The purity of synthesized peptides YSLKQYQ-OH, YSLKQYQ-NH<sub>2</sub>, ADIRHIK-OH, ADIRHIK-NH<sub>2</sub>, HYIDFRW-OH and HYIDFRW-NH<sub>2</sub> was measured as 93.8%, 92.9%, 94.1%, 97.7%, 77.3% and 72.9% respectively (Appendix 2.2).

### 5.3.2 Fluorometric quantification of peptide adsorbed to silica by fluorescamine

A fluorometric method, based on the use of fluorescamine<sup>4,10,271,272,354</sup> was performed to test the peptide sequences obtained from the experimental phage display processes including the peptide selection process and to study the events happening at peptide-silica aqueous interface. The fluorescamine assay working principle and procedure including the materials used for this assay is described in Chapter 2, section 2.1.2.7.1. These three peptides YSLKQYQ, ADIRHIK and HYIDFRW selected based on experimental and bioinformatics results besides considering varied physico-chemical properties as shown in Table 5.2. The peptide GASESYL was chosen as a control peptide for this binding study, as described earlier in Chapter 3.

**Table 5.2. Physico-chemical properties of selected phage displayed silica binding peptides.** <sup>a</sup>Physico-chemical properties of all the sequences were obtained from Innovagen (<https://pepcalc.com/>) and Bachem (<http://www.bachem.com/service-support/peptide-calculator/>) peptide property calculator. The side chain amino acid groups (R-CO-N) or (R-OH) that are likely responsible for hydrogen bonding are shown separately as hydroxyl (Ser, Thr and Tyr) and amine side chain (Asn, Gln) containing groups.

Peptide sequence	pI <sup>a</sup>	Net charge @pH 7 <sup>a</sup>	Functional amino acid residues							Average Hydrophilicity <sup>a</sup>
			Acidic - (D, E)	Basic + (R, K, H)	Polar Unchar -ged	Hydrop -hobic	Hydroxyl side chain (S, T, Y)	Amino side chain (N,Q,P, W)	C-terminal group	
YSLKQYQ	9.3	+1	0	1	5	1	3	2	Q	-0.4
ADIRHIK	10.2	+1.1	1	3	0	3	0	0	K	0.6
HYIDFRW	7.8	0.1	1	2	1	3	1	0	W	-0.6
GASESYL	3.3	-1	1	0	2	3	3	0	L	-0.1



All three peptides showed nearly similar binding to silica nanoparticles (Figure 5.3), unlike peptides selected on the basis of experimental phage display results (Figure 3.4). However, the peptide GASESYL with low pI (3.3) and net negative charge (-1), which was selected as a control for this adsorption investigation showed least binding to negatively charged silica nanoparticles at pH-7.5. Interestingly, the peptide HYIDFRW with pI value 7.8 and net neutral or slightly positive charge (0.1) displayed more binding to silica than ADIRHIK and YSLKQYQ both having higher pI values (10.2 and 9.3) and net positive charge (+1.1 and +1). The binding order observed was HYIDFRW > ADIRHIK > YSLKQYQ > GASESYL. Also, the uptake in binding of peptides HYIDFRW, ADIRHIK and YSLKQYQ to silica was high at low concentrations until 0.4 mM and eventually becoming steady at higher peptide concentrations (0.4 mM to 1.6 mM), probably due to the formation of multi-layers on the surface of silica nanoparticles (Figure 5.4)<sup>4</sup>. However, the control peptide GASESYL showed little uptake in binding at low concentrations, while at higher concentrations there was a gradual increase in uptake.

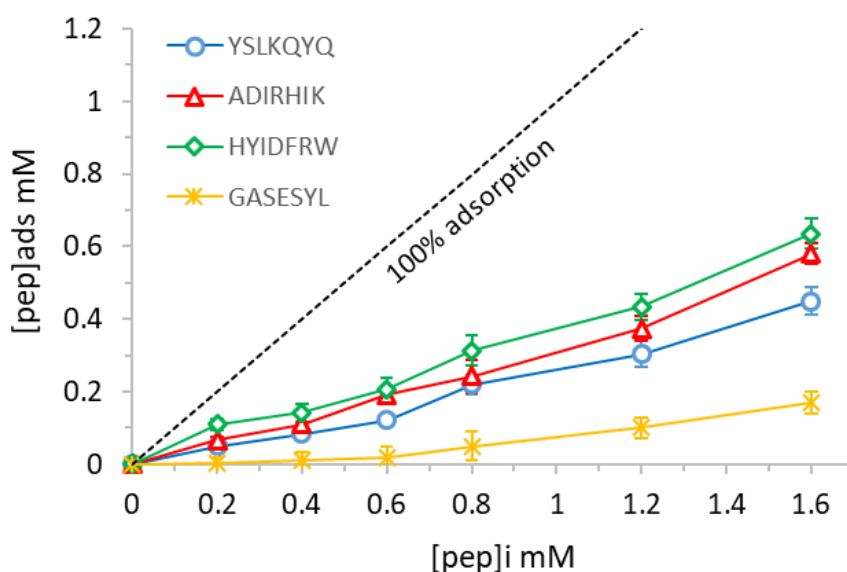


**Figure 5.3: Adsorption behaviour of selected phage displayed peptides on the surface of 82 nm sized silica nanoparticles at pH-7.5 (PBS buffer).** The y-axis represents the amount of peptide adsorbed to silica in mM, while the x-axis shows the initial peptide concentration or peptide added in mM. The theoretical 100% peptide adsorption is shown in black dotted line. The error bars represent the standard deviation error calculated as a result of the assay being repeated in triplicate. Based on the above data, the binding order of the peptides was ranked as HYIDFRW > ADIRHIK > YSLKQYQ > GASESYL.

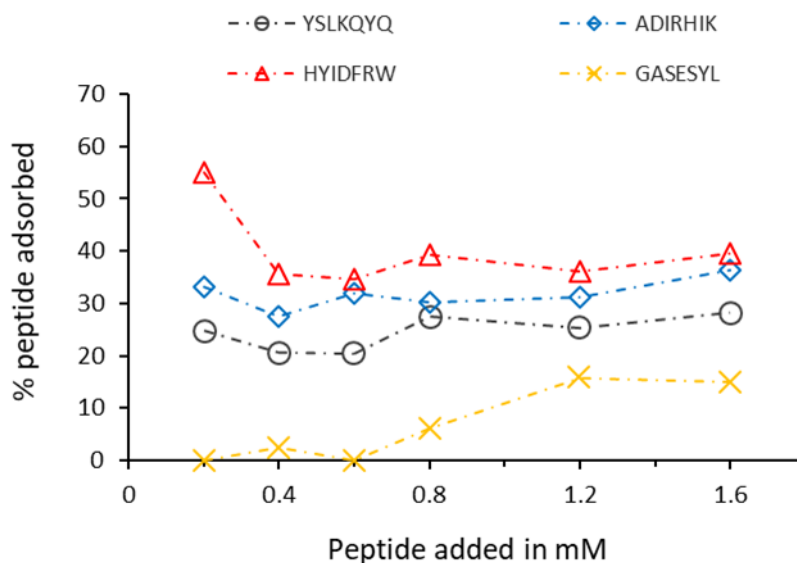


**Figure 5.4. Analysis of the above peptides displayed in Figure 5.3.** The graph showing the peptides and their binding (%) amounts to silica at six different peptide concentrations. The y-axis represents the percentage of peptide adsorbed to silica, while the x-axis shows the peptide added in mM.

The high binding of peptide HYIDFRW to a silica surface is interesting and might be because of the involvement of more than one type of interactions including electrostatic, hydrophobic and hydrogen bonding<sup>4,10,107</sup>. The electrostatic interactions between HYIDFRW and silica likely arise due to the presence of individual basic amino acids (Histidine at N-terminus and Arginine at 6<sup>th</sup> position) and amine side chain at C-terminal aromatic residue (Tryptophan). Thus, increasing the percentage of functional amine groups present at two sites (N-terminal and active side chain of amino acids) in the peptide encouraging ionic interactions. The polar uncharged amino acid Tyr (Y) present at 2<sup>nd</sup> position along with other charged polar residues including His (H) and Arg (R) are likely responsible for initiating hydrogen bonding resulting in multilayers connected by hydrogen bonds<sup>4</sup>. On the other hand, the possibility of hydrophobic interactions cannot be ruled out due to the occurrence of three hydrophobic residues (Isoleucine, aromatic Phenylalanine and Tryptophan) at 3<sup>rd</sup>, 5<sup>th</sup> and 7<sup>th</sup> positions of the sequence resulting in likely increase in the hydrophobic character, hence dominating the overall hydrophobicity in the system leading to hydrophobic interactions at peptide-silica surface<sup>4</sup>. Consequently, this type of binding behaviour of peptide HYIDFRW to negatively charged silica at pH-7.5, is likely due to the participation of more than one type of interactions.

**Table 5.3. Likely type of interactions that might be responsible for adsorption of peptides and the likely effect of increasing pH and particle size on binding to silica particles in PBS solution.** The asterisk (\*) represents the likely effect of increasing pH and particle size on binding to silica was estimated based on the previous studies where peptides of similar properties (eg. peptide length, net charge of peptide at pH-7 and same batch of silica nanoparticles) were investigated and assessed based on adsorption studies<sup>4,44,107</sup>. It has to be noted that the pH range and nanoparticle sizes considered for these studies include pH-3 to pH-8.5 and 28 nm, 82 nm and 210 nm.

Peptides	Likely type of interactions	Likely effect of increasing pH and particle size on binding*
YSLKQYQ	Electrostatic/ H-bonding	↑
ADIRHIK	Electrostatic/ Hydrophobic	↑
HYIDFRW	Electrostatic/ Hydrophobic/ H-bonding	↑

However, peptides ADIRHIK and YSLKQYQ showed slightly lower binding to silica in comparison to HYIDFRW peptide. This can likely be due to the presence of high pI (10.2 and 9.3), net positive charge (+1.1 and +1) values driving electrostatic interactions first. This type of electrostatic binding behaviour to silica is not new and likely arise due to the presence of basic positively charged groups (Arg, His and Lys at 4<sup>th</sup>, 5<sup>th</sup> and C-terminal positions for ADIRHIK; Lysine at 4<sup>th</sup> position for YSLKQYQ) and side chains containing functional amino groups (Gln at 5<sup>th</sup> and C-terminal position for YSLKQYQ); thus, giving the peptides a constant net positive charge (+1.1 and +1), resulting in the strongest possible ionic interactions. Also, it has been reported that biomolecules including peptides or proteins or even individual amino acids comprising of positively charged groups have been found to display high binding behaviour to negatively charged silica surfaces at neutral or high pH; due to the likely involvement of ion pairing mechanism<sup>4,44,65,107</sup> as discussed in Chapter 3. Nevertheless, ionic interactions are not the only force responsible for the ADIRHIK and YSLKQYQ adsorption; it can also be due to the existence of hydrophobic and H-bonding respectively. The hydrophobic interactions in the ADIRHIK peptide is highly driven by the non-polar groups (Isoleucine at 3<sup>rd</sup> and 6<sup>th</sup> position and Alanine at N-terminus of the peptide). The hydrogen bonding in YSLKQYQ is largely because of the polar uncharged groups (Tyr and Serine) and amino side chain functionalities from Lysine and Glutamine. However, the peptide GASESYL with low pI (3.3) and net negative charge (-1), which was selected as a

control for this adsorption studies showed least binding to silica nanoparticles. The possible reason that prevented binding of peptide GASESYL to silica might be due to the involvement of electrostatic repulsions between the negatively charged peptide and silica under these pH conditions<sup>4</sup>. Therefore, based on the available experimental evidence, the peptides would perhaps bind to silica surfaces by multiple interactions (ion-pairing and hydrogen bonding complemented by hydrophobic and van der Waals forces) as described in Chapter 3, binding studies.

#### **5.3.2.1 Effect of C-terminal group on binding to silica**

In order to test the influence of interactions (i.e more than one type) on binding to silica, further adsorption studies on the above peptides (YSLKQYQ, ADIRHIK and HYIDFRW) were carried out by substituting the C-terminal end carboxylic acid (R-COOH) with an amide group (R-CONH<sub>2</sub>). Encouraged by the above binding results, the same silica binders were synthesized by altering the peptide C-terminal end with an amide (NH<sub>2</sub>) group to understand the difference in binding behaviour and the effect of C-terminal group (negative charge) upon interaction with a silica surface. Therefore, C-terminal amide group silica binders YSLKQYQ-NH<sub>2</sub>, ADIRHIK-NH<sub>2</sub> and HYIDFRW-NH<sub>2</sub> have been investigated and compared with the corresponding C-terminal acid group peptides including YSLKQYQ-OH, ADIRHIK-OH, and HYIDFRW-OH. From the adsorption binding results, it was found that the peptides substituted with an amide group at the C-terminus end showed higher binding to negatively charged silica nanoparticles than corresponding carboxyl terminal acid group peptides (Figure 5.5).

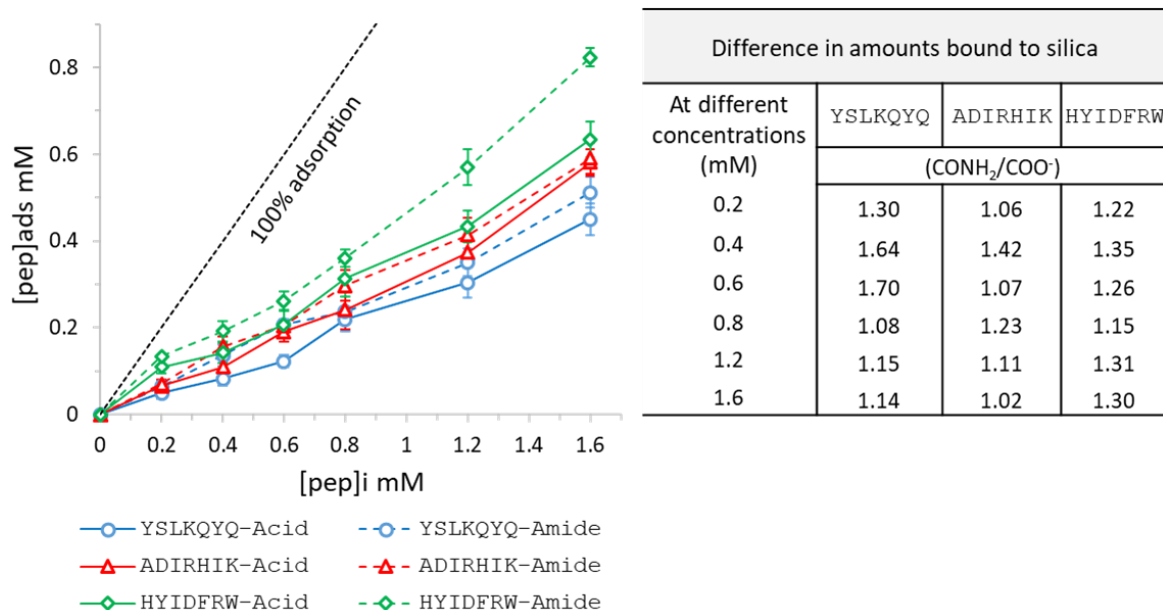


**Figure 5.5: Adsorption isotherms of peptides synthesized with either acid (COOH) or amide (CONH<sub>2</sub>) at C-terminal group of selected phage displayed peptides and their binding behaviour on the surface of hydrophilic silica nanoparticles at pH-7.5.** The y-axis represents the amount of peptide adsorbed to silica in mM, while the x-axis shows the initial peptide concentration or peptide added in mM. The error bars represent the standard deviation error calculated as a result of the assay being repeated in triplicate. The difference in ratio of peptides (CONH<sub>2</sub>/COO<sup>-</sup>) binding to silica at different concentrations (mM) are shown in the table on the right-hand side of the graphical plot.

**Table 5.4. Effect of C-terminal group on increasing the overall peptide net charge and/ or pI at pH-7.** <sup>a</sup>The change in the net charge or pI values of the peptides (either with acid or amide at C-terminal end group) were obtained from Bachem (<http://www.bachem.com/service-support/peptide-calculator/>) peptide property calculator.

Peptides	Effect of C-terminal functional group					
	Net charge @7 <sup>a</sup>			pI <sup>a</sup>		
	Acid	Amide	Difference	Acid	Amide	Difference
YSLKQYQ	1	2	1	9.6	10.1	0.5
ADIRHIK	1.1	2.1	1	10.1	11.5	1.4
HYIDFRW	0.1	1.1	1	7.8	9.9	2.1

This type of increase in binding activity to negatively charged silica (deprotonated silanols) by C-terminal amide groups is simply due to the increased activity of electrostatic and hydrogen bonding because of NH<sub>2</sub> (amide) group in the end. The electrostatic binding

behaviour of peptides at pH-7.5 was mainly due to an increase in overall charge by +1 and/or pI by 0.5 to 2.1 respectively (Table 5.4 and Figure 5.6). Thus, probably giving the peptides a constant net positive charge, resulting in the strongest possible ionic interactions. However, the same amide group attached to the C-terminal end (C=O H-N-H) acts as an hydrogen bond acceptor and donor<sup>405</sup>; hence, increasing the activity of hydrogen bonding either with the silica (i.e with silanol Si-OH groups present on the surface of negatively charged silica at pH-7.5) or peptide (by polar uncharged groups) forming peptide-peptide bonding resulting in multilayer formation or both under these conditions. Recently, it was evidenced that the change in surface functionalisation of silica with amino propyl/ amine groups lead to an increase in the binding activity at peptide-silica boundary<sup>124,406</sup>. In another study, where selective amino acids (Lys, Arg, His, Ser, Try) were shown to be mainly responsible for an increase in peptide binding to silica nanoparticles via electrostatic and H-bonding resulting in the precipitation of silica nanoparticles<sup>10</sup>.

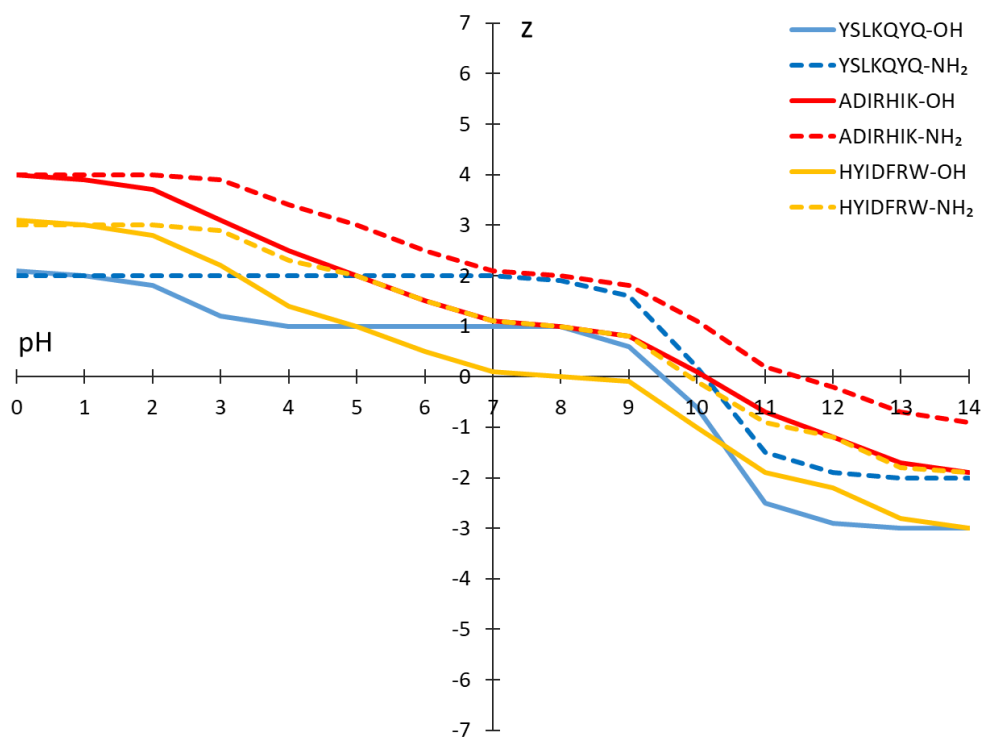


**Figure 5.6. Effect of C-terminal group as a function of pH v/s charge (z).** The x- axis and y-axis signifies the pH (0 to14) and charge (+7 to -7) range considered for plotting this graph. The change in the charge of the peptides at varied pH (either with acid or amide at C-terminal end group) was calculated from Bachem (<http://www.bachem.com/service-support/peptide-calculator/>) peptide property calculator.

Thus, providing the support that peptides containing amine functional groups depending on the position of amine group (i.e N or C- terminus or side chain) within the peptide backbone will likely help in either introducing electrostatic or hydrogen bonding on amorphous silica surface at pH-7. Also, depending on the experimental conditions (i.e pH), the silica surface would change (no charge at pH-2-3 and increase in negative charge with pH rise) resulting in the introduction or removal of an electrostatic binding and/ or repulsive interactions upon peptides binding to silica<sup>4,107</sup>. This study also revealed, the adsorption of peptide to silica was found to be sequence dependent and subject to the peptide charge<sup>4</sup>. Therefore, based on the available experimental evidence, the peptides would perhaps bind to silica surfaces by more than one type of interaction and could be influenced by experimental conditions.

Moreover, the above studies might provide a new dimension in the design of phage binding peptides to a minor coat protein pIII or major coat protein pVIII in M13 bacteriophage by either N-terminal and/ or C-terminal fusion to the target by mimicking the original phage constructs alongside using phage fused peptide as a template. From the previous studies, it was evident that by changing or modifying the N-terminus insert to coat protein pIII with the same peptide sequence screened from phage libraries but by changing the structure (i.e. by fusing the similar peptide sequence to coat protein III, one as constrained and another as linear fashion) showed different binding behaviour to zinc sulphide (ZnS) and cadmium sulphide (CdS) thereby affecting the size and structure of the crystals<sup>156</sup>.

In a recent review, site-specific phage functionalisation has been discussed in which a variety of synthetic chemical compounds and functional groups were incorporated into selected M13 phage proteins using chemical modification methods combined with genetic engineering for a range of biomedical applications<sup>407</sup>. To date, a wide variety of materials including RGDS peptide, PEG, biotin, fluorophores, fluorescein, enzymes and drugs have been used to target coat proteins (pIII and pVIII) by reacting them at specific N-terminal or C-terminal or other functional side chain groups including  $-SH$ <sup>408</sup>,  $-NH_2$ <sup>75,409-413</sup>,  $-COOH$ <sup>410</sup> and  $-OH$ <sup>414</sup> have been reported.

Another group have mimicked the phage structure by fusing the peptide ligands at C-terminus and constructed synthetic peptide dendrimers (divalent, tetravalent and pentavalent) by engineering the phage displayed peptide that have affinity for collagen, showed surface density dependent binding behaviour resulting in the increased efficiency of ligand mediated targeting<sup>415,416</sup>. Similar study has been reported, in which liposomes were

constructed by conjugating the brain binding peptide (isolated via phage display library) and a portion of coat protein pIII with GLA sequence, thus delivering the drug to the targeted brain tissue by further reducing the toxicity<sup>417,418</sup>. Consequently, these mimicked or engineered phage peptides had been shown to have potential applications as templates in the development of nanocarriers<sup>419</sup>, drug delivery vehicles<sup>417</sup>, constructing multi-valent or monovalent targeting systems<sup>415,416</sup> and in the synthesis of self-assembled hybrid nanomaterials<sup>88,156</sup>.

Therefore, from the above evidence, the peptides substituted with an amide group at the C-terminal end showed higher binding to negatively charged silica nanoparticles than corresponding carboxyl terminal acid group peptides at pH-7.5. Similarly, confirming the likely involvement of multiple interactions (electrostatic and non-electrostatic) upon peptides binding to hydrophilic amorphous silica nanoparticles. Moreover, this definite binding specificity to silica study by C-terminal amide groups could provide more insights possibly in the designing and engineering of silica targeted constructs including nanochips or nanomaterials, peptide phage libraries by targeting site specific proteins in M13 bacteriophage for a range of biomedical and nanotechnological applications.

### **5.3.3 TEM to probe silica- phage peptide interactions**

The phage clones displaying the peptide sequences YSLKQYQ, ADIRHIK and HYIDFRW were chosen and to observe how the phage binds to silica binding by TEM. The silica nanoparticles (82 nm) alone without EM stain 336 are shown in Figure 5.7, a, b. Just to make sure whether the EM stain 336 is binding to phage proteins or silica or both; initial experiments were performed by adding the EM stain 336 to freshly taken phages from M13 Ph.D.7 library and silica nanoparticles of size 82 nm. It can be seen from the TEM images that the EM stain 336 did not show any binding to silica nanoparticles (Figure 5.7, c, d). However, the M13 Ph.D.7 phage library stained with EM stain 336, appeared to be irregular thread like structures which are linked to each other (Figure 5.8). Besides, some unfamiliar shapes (irregular black agglomerations) are noticed which appear to be clump-like structures forming aggregates with the phage. It has been reported that the phage proteins (pIII or pVIII) or peptides affixed on the TEM grid and likely bound to the substrate by their tips, may then come in contact during the sample drying process forming agglomerations<sup>306,420,421</sup>.



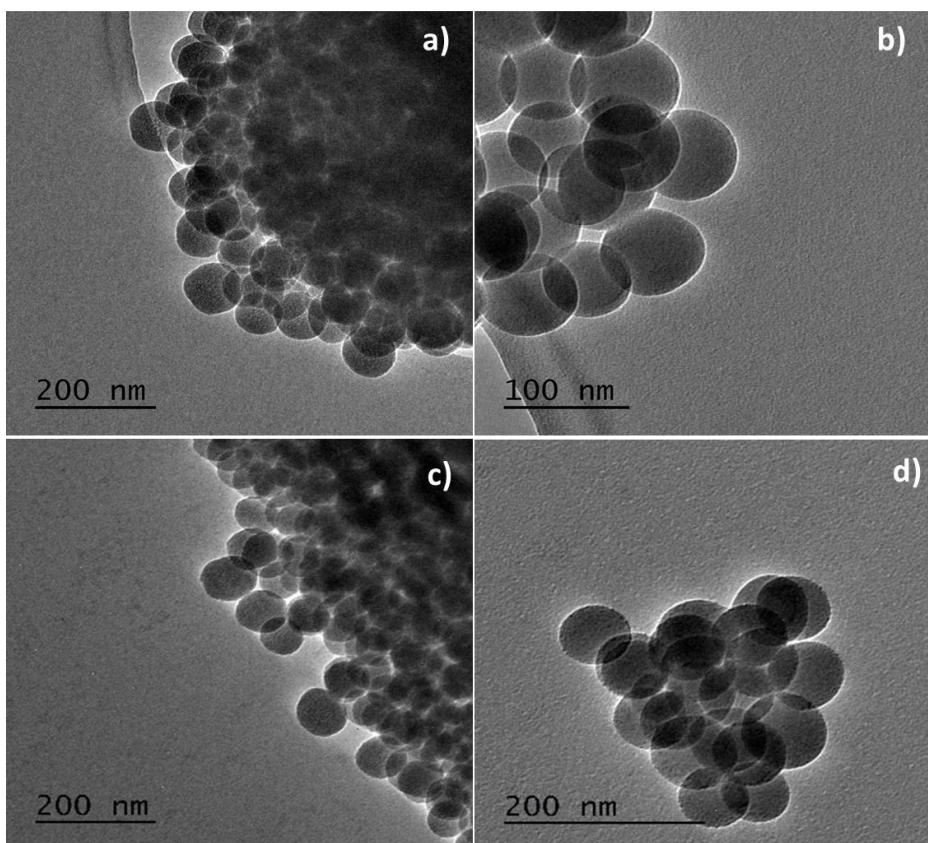


**Figure 5.7. TEM images of silica nanoparticles (82 nm) without EM stain 336 (a,b) and with EM stain 336 (c,d).**

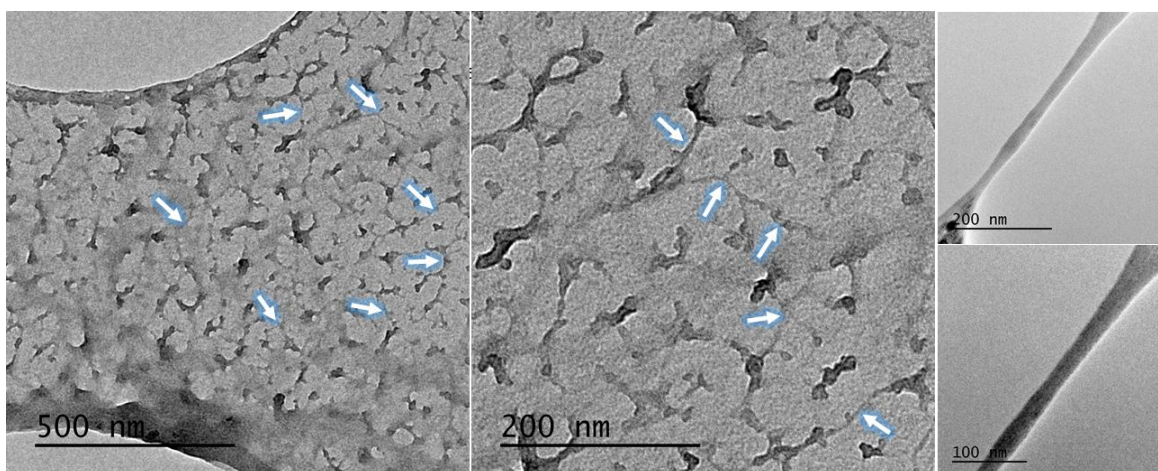


**Figure 5.8. TEM images of M13 Ph.D.7 phage library stained with EM stain 336.** The likely phage structures are indicated by white arrows. Alongside, some unusual shapes (irregular black bodies) are noticed which appear to be clump-like structures forming aggregates with the phage.

For an ideal TEM phage image, the phage structures should appear filamentous or thread like under the TEM. The length and diameter of the filamentous phage have been reported as roughly 880 nm and 6.5 nm respectively<sup>71,72,422</sup>. The other factors that might have affected

the proper binding of phage to silica possibly be due to i) improper binding of the EM stain 336 to phage ii) presence of low amounts of phage clones and PBS forming crystals during the sample storage process iii) changes occurring at the phage peptide-silica interface due to pH conditions<sup>74,281,423–426</sup>. Further, it is possible that the differences in structures observed arose because of the long storage period (in some cases ca. 2 years) between plaque isolation and microscopical investigation.

Though this experiment failed to identify clear controls (i.e control phage that do not display a putative silica binding peptide) and phage structures from the M13 Ph.D.7 library phage samples stained with EM stain 336 (Figure 5.8), further binding studies of phage displaying YSLKQYQ, ADIRHIK and HYIDFRW peptides on the surface of silica nanoparticles were carried out assuming some sort of binding patterns might be observed with these phage peptides. The binding of phage displaying YSLKQYQ, ADIRHIK and HYIDFRW peptides on the surface of silica nanoparticles can be seen in Figures 5.9, 5.10 and 5.11. In the images presented, the phage appears to be binding on the surface of silica by forming a thread like structures cross linking with the adjacent silica particles which can be seen indicated in white arrows. Further, some phage structures seem to be folded and lying on the surface of the silica particles, but this may be artefact of the sample preparation procedure.

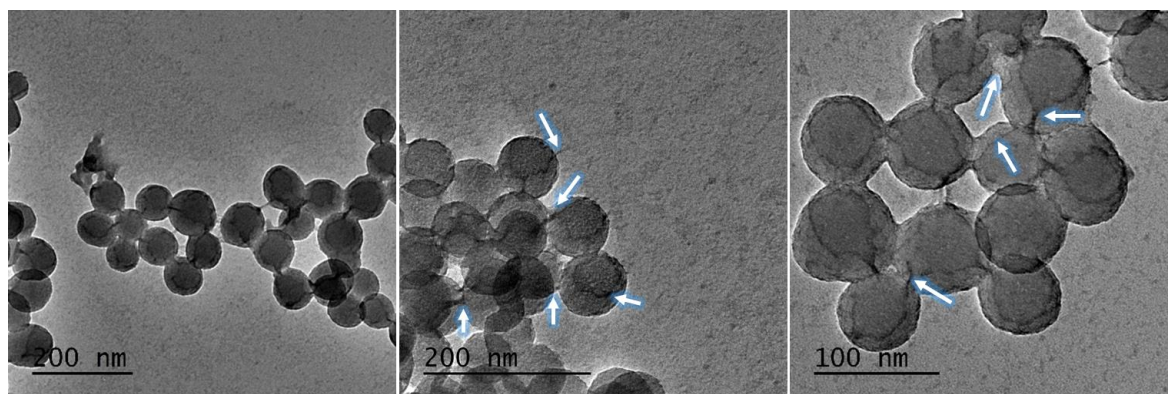


**Figure 5.9. TEM images of YSLKQYQ phage attached to silica NPs.** Phage structures thought to bind to silica are shown by white arrows.

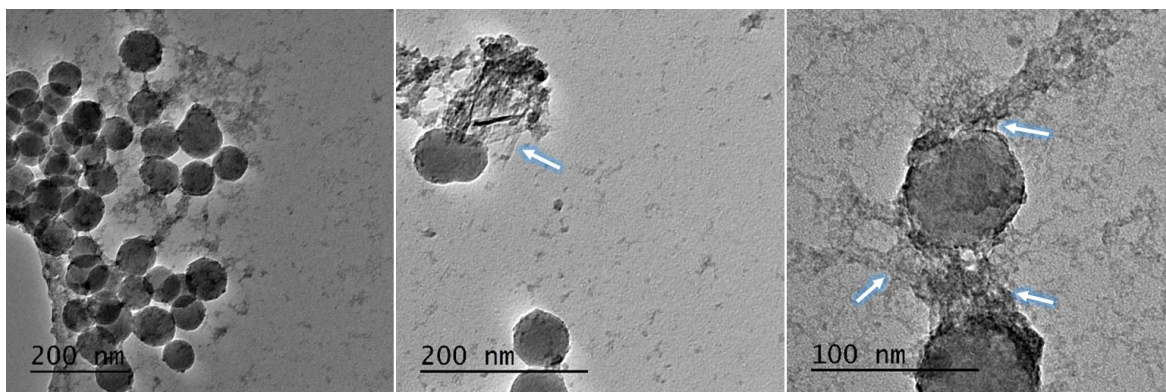


**Figure 5.10. TEM images of ADIRHIK phage attached to silica NPs.** Phage structures thought to bound to silica are indicated by white arrows.

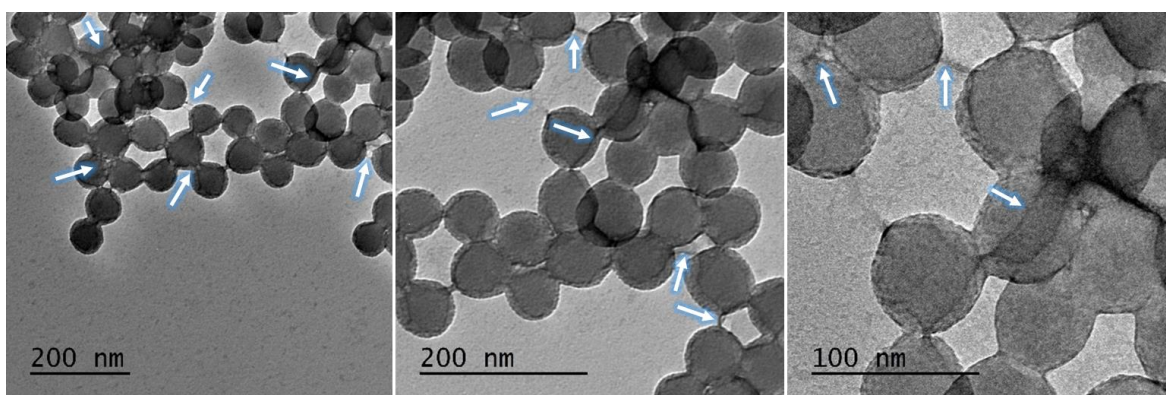


**Figure 5.11. TEM images of HYIDFRW phage attached to silica NPs.** Phage structures thought to bound to silica are pointed by white arrows.

A few relatively recent studies have demonstrated specific binding affinity of M13 phage displayed peptides to inorganic or organic surfaces using microscopy techniques such as SEM, TEM, AFM and fluorescence<sup>306,322,420,421</sup>. For example, the binding of M13 phage displaying the ASTLPKA peptide to thiamethoxam (TMX), an organic crystal was confirmed by electron microscopy (Figure 5.12, a and b)<sup>306</sup>. This study also reported high degree of specificity ( $1.47 \pm 0.80$  nN) between the bacteriophage and organic crystal surface using AFM<sup>306</sup>.

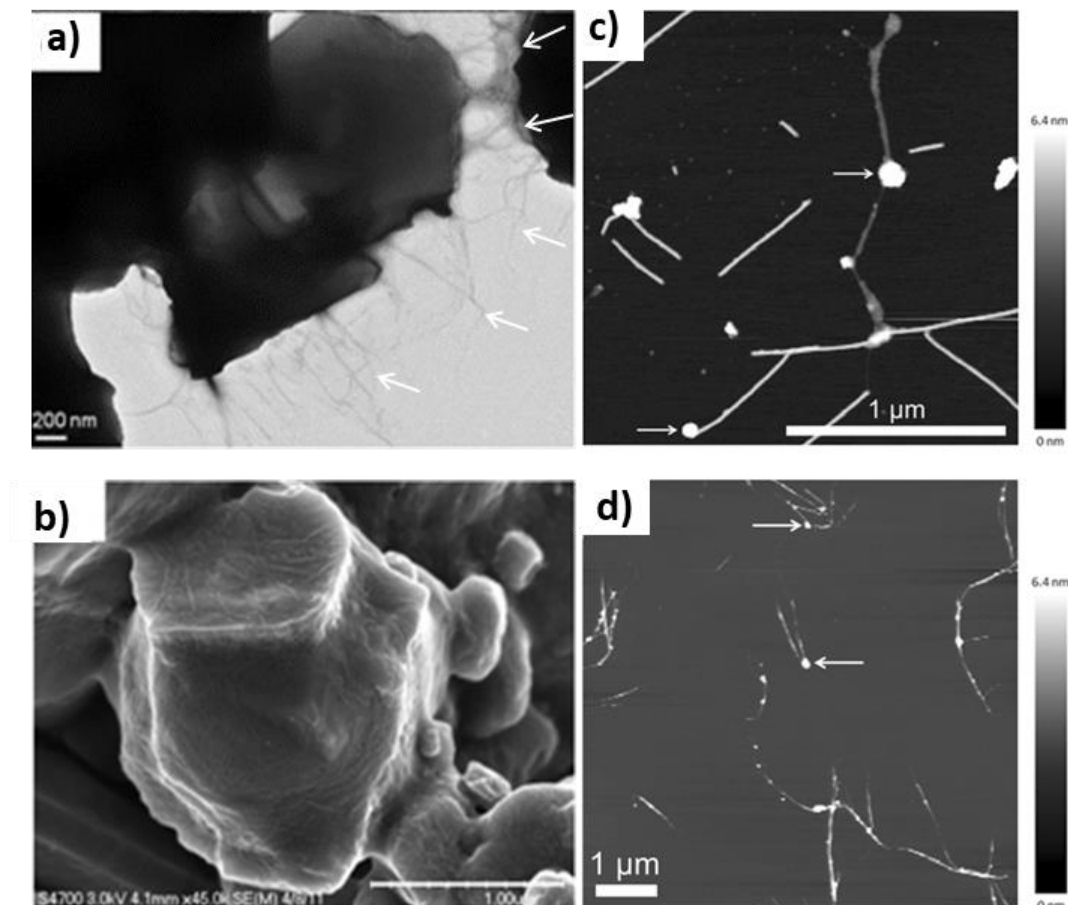


**Figure 5.12. Microscopy images showing specific binding affinity between M13 phage displayed peptides and organic<sup>306</sup> or inorganic surfaces<sup>322</sup>.** TEM and Field emission-scanning electron microscopy images of phage ASTLPKA bound to organic TMX crystal surfaces (a, b). The AFM images of the phage displaying the peptide LGFREKE on pIII showing their ends are attached to (c) amorphous and (d) crystalline nickel boride nanoparticles at the tip of pIII, which were shown by white arrows.

Another study in 2014 by Ploss *et al*, used fluorescence microscopy and AFM to measure the affinity of bound M13 phage (LGFREKE) to nickel boride (crystalline and amorphous) nanoparticles (Figure 5.12, c and d)<sup>322</sup>. The samples in the study were fluorescently tagged (fluorescein isothiocyanate) with anti-M13-monoclonal antibody against phage coat protein pVIII. The fluorescent intensity generated as result of phage attachment to nanoparticles measured by fluorescence spectroscopy<sup>322</sup>. In recent years, several studies have been reported using gold labelled anti-phage antibodies for determining and quantifying phage-substrate binding affinities via microscopy analysis<sup>167,323,432–435,340,364,420,427–431</sup>.

Therefore, although, this TEM study suggested some binding between the selected phage YSLKQYQ, ADIRHIK and HYIDFRW peptides and silica; more experiments are needed to

identify and understand the unanswered questions i) If only the phage displaying the peptide on the tip of the pIII is specifically interacting with silica ii) are there any phage-phage interactions (i.e one or the other end of the one phage being attached to other phage) iii) other possible non-specific interactions (i.e if any other part of the phage other than the peptide displaying end on pIII is bound to silica nanoparticle). The future experiments include, the repetition of the above phage-silica TEM binding studies but including more specific controls. Then, to visualize morphologically (i.e what are binding to silica, whether phage displaying the peptides or the phage itself or both) and measure their binding quantitatively using the above discussed microscopy techniques<sup>306,322,420,421</sup>.

## **5.4 Conclusions**

In summary, an alternate way of choosing material binding peptides for verification binding studies is introduced that considers a number of parameters including experimental phage display results, physico-chemical properties and bioinformatics analysis. All three peptides YSLKQYQ, ADIRHIK and HYIDFRW selected by this way exhibited steady and better binding (uniformity) to silica after reaching saturation unlike the peptides KIAVIST, LPVRLDW, NDLMNRA and GQSEKHL chosen by relying solely on their experimental phage display results. Also, the uptake in binding of peptides HYIDFRW, ADIRHIK and YSLKQYQ to silica was high at low concentration (0.2 mM) and eventually became steady at higher peptide concentrations (0.4 mM to 1.6 mM). Thus, indicating this behaviour could probably be due to the formation of multi-layers on the surface of silica nanoparticles.

The quantitative binding analysis of these peptides suggested that the peptide adsorption to silica surfaces would perhaps have more than one type of interaction (i.e. electrostatic, hydrophobic and H-bonding) and could be influenced by the experimental conditions; there by checking the experimental phage display process including the optimised elution approach. The peptide HYIDFRW with pI value 7.8 and net neutral or slightly positive charge (0.1) displayed slightly more binding to silica than ADIRHIK and YSLKQYQ both having higher pI values (10.2 and 9.3) and net positive charge (+1.1 and +1). This variation in binding to negatively charged silica at pH-7.5 in PBS buffer might be due to the participation of electrostatic (overall positive charge and individual positive groups His and Arg), hydrogen bonding and hydrophobic interactions (Ile, Phe and Trp). However, peptides ADIRHIK and YSLKQYQ showed slightly lower binding to silica in contrast to HYIDFRW

peptide. This can likely be due to the presence of basic positively charged groups (Arg, His and Lys at 4<sup>th</sup>, 5<sup>th</sup> and C-terminal positions for ADIRHIK; Lysine at 4<sup>th</sup> position for YSLKQYQ) and side chains containing functional amino groups (Gln at 5<sup>th</sup> and C-terminal position for YSLKQYQ); thus, giving the peptides a constant net positive charge (+1.1 and +1), resulting in the strongest possible ionic interactions. Nevertheless, electrostatic interactions might not be the only force responsible for the ADIRHIK and YSLKQYQ adsorption; it could also be due to the existence of hydrophobic and H-bonding respectively. The hydrophobic interactions in the ADIRHIK peptide is highly driven by the non-polar groups (Isoleucine at 3<sup>rd</sup> and 6<sup>th</sup> position and Alanine at N-terminus of the peptide). The hydrogen bonding in YSLKQYQ is largely because of the polar uncharged groups (Tyr and Serine) and amino side chain functionalities from Lysine and Glutamine. However, the peptide GASESYL with low pI (3.3) and net negative charge (-1), which was selected as a control for this adsorption studies showed least binding to silica nanoparticles. The possible reason that prevented binding of peptide GASESYL to silica might be due to the involvement of electrostatic repulsions between the negatively charged peptide and silica under these pH conditions<sup>4</sup>.

Moreover, an increase in binding activity to negatively charged silica nanoparticles was noticed for the peptides (YSLKQYQ, ADIRHIK and HYIDFRW) modified with amide (NH<sub>2</sub>) group opposed to carboxyl group at C-terminal end. This change in binding behaviour of peptides was possibly driven by an increase in overall charge and/ or pI. Also, with increase in the pH, the charge and pI of the peptides will change; resulting in the likely introduction or removal of an electrostatic binding and/ or repulsive interactions upon peptides binding to silica. Thus, providing the support that peptides containing amine functional groups depending on the position of amine group (i.e N or C- terminus or side chain) within the peptide backbone will likely help in either introducing electrostatic or hydrogen bonding on amorphous silica surface at pH-7.5. Also, depending on the experimental conditions (i.e pH), the silica surface would change (no charge at pH-2-3 and increase in negative charge with pH rise) resulting in the introduction or removal of an electrostatic binding and/ or repulsive interactions upon peptides binding to silica<sup>4,107</sup>.

Therefore, from the above evidence, it is clear that the peptides substituted with an amide group at the C-terminal end showed higher binding to negatively charged silica nanoparticles than corresponding carboxyl terminal acid group peptides at pH-7.5. Similarly, confirming

the likely contribution of multiple interactions (electrostatic and non-electrostatic) upon peptides binding to hydrophilic amorphous silica nanoparticles. Moreover, this definite binding specificity to silica study by C-terminal amide groups could provide more insights possibly in the designing and engineering of silica targeted constructs including nanochips or nanomaterials, peptide phage libraries by targeting site specific proteins in M13 bacteriophage for a range of biomedical and nanotechnological applications.

Furthermore, the TEM exposed some binding patterns between phage and silica surfaces. The binding of phage displaying YSLKQYQ, ADIRHIK and HYIDFRW peptides on the surface of silica nanoparticles appeared to be thread like structures cross linked with the adjacent silica particles. However, some phage structures seem to be broken, folded and lying on the surface of the silica particles but this may be an artefact of the sample preparation procedure. Although, this experiment failed to identify clear controls (i.e control phage that do not display a putative silica binding peptide) and phage structures from the M13 Ph.D.7 library phage samples, some exemplar studies were discussed indicating the possibility of microscopy techniques including TEM as a tool to be used for probing biomolecule-silica interaction studies. The insights gained from this TEM study, combined with knowledge obtained from the example studies gives a vision for future experiments. These include, the validation binding studies of phage to silica; and how the TEM and other microscopy techniques can effectively be used to visualize and measure their specific binding quantitatively; what are binding, whether the phage displaying the peptides or the phage itself or both and how are they binding to silica surfaces. In the end, by comparing the differences in binding to silica by phage displaying peptides verses artificially synthesised peptides, could help us in understanding the specific binding patterns. This information could perhaps provide more insights to understand the way phage is behaving during the biopanning process with substrates.

## Chapter 6: Overall conclusions and future work

### 6.1 Summary of the thesis

In summary, heptapeptides having affinity for amorphous silica nanoparticles (hydrophilic, 82 nm) have been isolated and identified by phage display technique using the M13 phage display library. To achieve this, three different chemical elution buffers (Gly-HCl, pH-2.2; MgCl<sub>2</sub>, pH-6.1; TEA, pH-11) with specific elution conditions have been used to remove unique heptapeptide binding phages from silica nanoparticles via disrupting the electrostatic and non-electrostatic interactions. These isolated silica binding peptides were further investigated by experimental and bioinformatics studies.

In this thesis, the silica binding sequences were eluted and identified in two different ways by using three different elution buffers mentioned above. The first way is by using traditional biopanning process and second one is optimised biopanning process (alternative sequential three step elution). The optimised biopanning approach differs from the traditional biopanning method as each mentioned buffer (Gly-HCl, pH-2.2; MgCl<sub>2</sub>, pH-6.1; TEA, pH-11) were used consecutively one after other in a single screening (biopanning) round, as appose to one specific buffer being used for all panning rounds including elution steps in traditional biopanning and repanning experiments.

The optimised biopanning method reported here, have eluted and recovered the phage clones that are bound to silica by hydrophobic, hydrogen bonding and electrostatic attractions or repulsions; as oppose to one specific buffer being used for all panning rounds including elution steps in traditional biopanning experiments. In addition, these three different elution buffers have eluted phage clones that may be interaction or charge specific subject to change in the elution buffer pH condition. Also, it was noticed that as the pH condition of the elution buffers increase in the elution steps, the net charge of the sequences being eluted from silica surface change from positive to negative. Hence, indicating the single elution buffer used for eluting the phage clones (Chapter 3) may have resulted in incomplete removal of all strong binders and resist detection to substrate silica. Hence, by using sequential three step elution process (optimised biopanning) varying elution buffers and pH condition in a single panning round, the phage clones that resist detection in single elution step may have eluted in the other successive elution steps, thereby recovering and improving the elution procedure for silica surfaces. Additionally, the low pH buffer that was used in the first elution step had eluted 63% of peptides with net positive charge, while the high salt and high pH buffers have



eluted 58% and 79% of peptides in the second and third elution steps displaying net neutral and negative charged sequences. Hence, suggesting the efficiency of the method to elute and isolate most of the silica binders in the early rounds of biopanning, removing the sequences that resist detection during traditional bioapnning method; thereby by reducing the number of biopanning rounds, saving time, cost and effort. In addition, these three different elution buffers could be used to remove interaction or charge specific peptides subject to change in elution and pH condition.

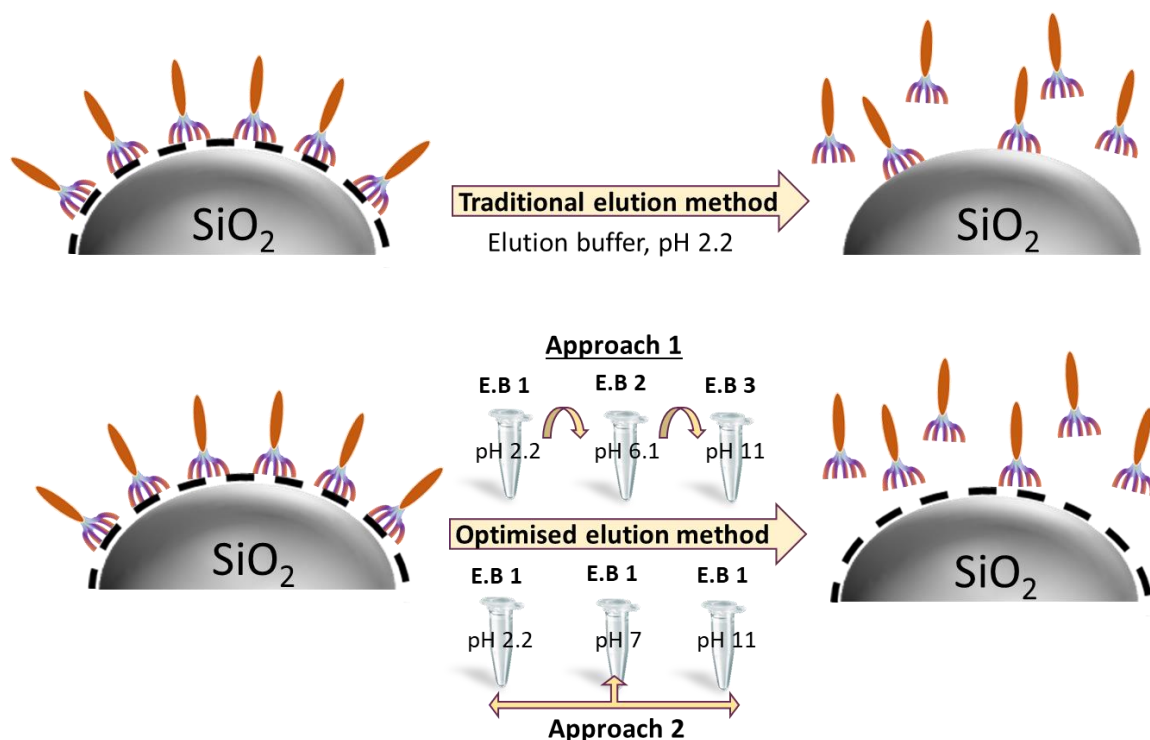


**Figure 6.1. Schematic representation of proposed adsorption and desorption mechanisms of phage clones upon interaction with silica at varied pH and the effectiveness of the three-step chemical elution approach (optimised biopanning) to that of traditional biopanning process.**

Therefore, based on the experimental evidence, we propose this three step chemical elution (optimised biopanning) process may be used to isolate interaction (polar or non-polar) or charge specific (positive, neutral or negative) peptide sequences from the silica surface subject to elution buffer and pH condition; thus, eluting and recovering the most silica binders including the sequences that may resist detection in traditional biopanning using one elution buffer (Figure 6.1).

Moreover, a repanning method has been reported to recheck the phage display process and verify silica binders by checking the reproducibility of the process. The repanning method may experimentally verify your own target binding results giving information about any possible non-specific binding due to panning limitation (amplification bias), thereby checking the direction of the ongoing phage display work. Thus, the repanning method reported for silica, appeared to be a straight forward approach to verify phage display experimental results by mixing phage clones from different biopanning experiments and rounds. Further the complementary bioinformatics suggesting that majority of the peptides isolated were target-related sequences and rather true silica binders without any human or pathogen or sample contamination, whereas the peptide sequences that were found to have exact or part of motif similarity for other targets indicate the possibility of promiscuous binding behaviour to multi-materials. Also, the results of sequences isolated from phage display experiments via two different batches of same library showed no identical sequences. However, in the comparative analysis, the two consensus sequences (ADLSVTS and VSTPLLA) and the frequency distribution of the amino acids (identified from separate lots) showed near similarities towards silica surfaces, thereby indicating the batch to batch library diversity.

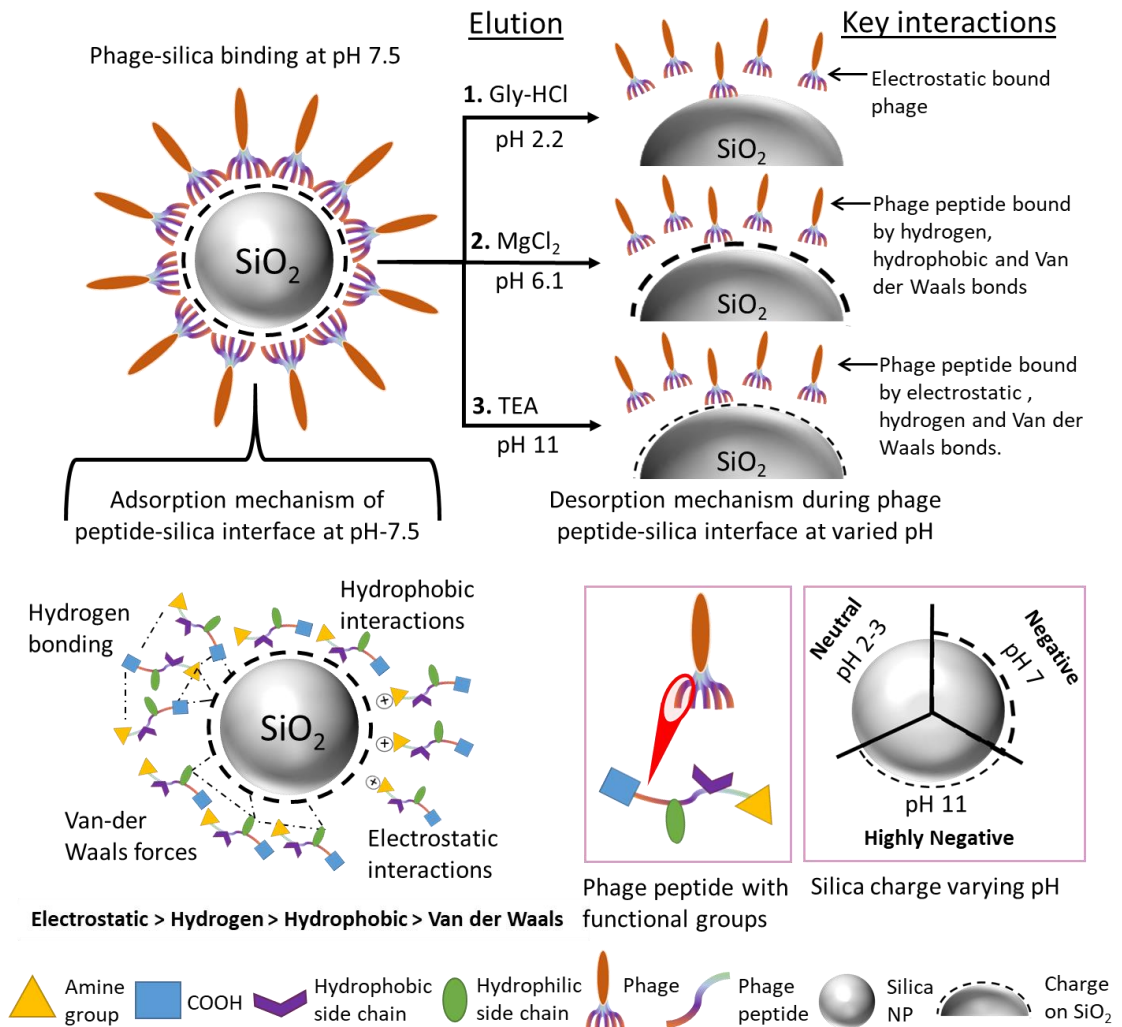


**Figure 6.2. Schematic representation of proposed adsorption and desorption mechanisms of phage /peptides upon interaction with silica at varied pH.**

To summarize, peptide sequences bound to silica via both electrostatic and non-electrostatic interactions have been identified by phage display technique using three different elution buffers (0.2 M Glycine-HCl, pH-2.2, 4 M MgCl<sub>2</sub>, pH-6.1 and 100 mM Triethylamine, pH-11) (Figure 6.2). From the results, it was found that the phage elution (desorption mechanism) process to silica was more selective to elution specific buffer and condition (low or high pH and salt) and is dependent on silica surface (pH 2-3, charge zero; pH-6, negative charge and pH-11, highly negative charge) subject to pH and charge change. The low pH elution buffer (0.2 M Glycine-HCl, pH-2.2) mostly eluted phage clones bound by strongest possible electrostatic attraction (positively charged peptides) and hydrophobic interactions

to silica. While the elution buffers with high salt (4 M MgCl<sub>2</sub>, pH-6.1) and high pH (100 mM Triethylamine, pH-11) typically eluted phage clones bound to negatively charged silica by hydrophobic or hydrogen bonding and electrostatic repulsion (negatively charged peptides) respectively.

Finally, the quantitative binding analysis of the selected peptides suggested that the peptide adsorption to silica surfaces would perhaps have more than one type of interaction (i.e. electrostatic, hydrophobic and H-bonding) and could be influenced by the experimental conditions. However, an increase in binding activity to negatively charged silica nanoparticles was noticed for the peptides modified with amide (NH<sub>2</sub>) group opposed to carboxyl group at C-terminal end. This change in binding behaviour of peptides was possibly driven by an increase in overall charge and/ or pI. Also, with increase in the pH, the charge and pI of the peptides will change; resulting in the likely introduction or removal of an electrostatic binding and/ or repulsive interactions upon peptides binding to silica. Thus, providing the support that peptides containing amine functional groups depending on the position of amine group (i.e N or C- terminus or side chain) within the peptide backbone will likely help in either introducing electrostatic or hydrogen bonding on amorphous silica surface at pH-7.5. Therefore, from the above evidence, it is clear that the peptides substituted with an amide group at the C-terminal end showed higher binding to negatively charged silica nanoparticles than corresponding carboxyl terminal acid group peptides at pH-7.5. Similarly, confirming the likely contribution of multiple interactions (electrostatic and non-electrostatic) upon peptides binding to hydrophilic amorphous silica nanoparticles.

## 6.2 Future directions

This project was able to investigate and propose the experimental and/ or bioinformatics methods for eluting and identifying silica specific peptides and their binding mechanisms using phage libraries. However, the assumptions of adsorption or desorption of phage or peptide studies was undoubtedly based on the amorphous hydrophilic silica nanosurfaces. Therefore, there is a need to investigate the hydrophobic or functionalised silica materials<sup>181,284</sup> to get a better picture and understanding of the vast and complex silica system<sup>94</sup>; thereby aiding in governing the biomolecule selection using phage display technique or *in vitro* binding studies<sup>4,10,24,319</sup>.

Although, the experiment to probe phage-silica binding studies using TEM failed to identify clear controls (i.e control phage that do not display a putative silica binding peptide), some exemplar studies were discussed indicating the possibility of microscopy techniques including TEM as a tool to be used for probing biomolecule-silica interaction studies. The insights gained from this TEM study, combined with knowledge obtained from the example studies gives a vision for future experiments. These include, the validation binding studies of phage to silica; and how the TEM and other microscopy techniques can effectively be used to visualize and measure their specific binding quantitatively; what are binding, whether the phage displaying the peptides or the phage itself or both and how are they binding to silica surfaces. In the end, by comparing the differences in binding to silica by phage displaying peptides verses artificially synthesised peptides, could help us in understanding the specific binding patterns.

In addition, look at the other reported studies to examine the binding affinity of the phage displaying peptide to silica. A few studies have been reported using ELISA and fluorescence microscopy. Andrea *et al.*, (2015) used alkaline phosphate linked phage ELISA to assay for magnetite nanoparticle binders, after three cycles of panning rounds. With each panning round an increase in intensity was detected, which indicated enriching of the phage pool with magnetite binding proteins. Results also indicated that a range of binding capabilities were present, with two domains groups for lower and higher affinity protein binders<sup>364</sup>. In another study, Serizawa *et al.*, (2005) used phage ELISA to successfully calculate binding affinities of selected phage on broad range of synthesis polymers, based on the assumption that deposition follows a Langmuir-type adsorption and that each phage concentration present identical surface concentration of binding sites. The Langmuir-type adoption model is not

suitable for substances with substances with high surface roughness. The binding affinities calculated were typically in the range of  $10^{10}$ - $10^{11}$  <sup>436</sup>. Studies have also shown that binding peptides and phages can also be assessed using fluorescently labelled primary or secondary antibodies, and can be analysed using fluorescence microscopy techniques<sup>437,438</sup>. As an example, Jaworski *et al.*, (2008) used Atto-425-streptavidin to conducted fluorometric assays to detect the extent of binding between, biotinylated DNT-binding peptides and its alanine-substituted derivatives<sup>437</sup>.

In this thesis, a few binding studies have been conducted to identify silica-binding peptides. However, these studies are not specific as it is unknown which specific residue or amino acids in a peptide, are responsible for specific interactions with silica nanoparticle. The instruments available currently provide little direct insight into binding mechanisms<sup>10</sup>. To understand adsorption mechanisms, some studies have performed binding assays for mutant peptide by making changes in the amino acid sequence. In a study by Patwardhan *et al.*, (2012) histidine motifs were replaced with alanine motifs, on a set of two mutants derived from pep1 (pep1\_6 and pep1\_11), to study the interactions and peptide-silica binding. Histidine is thought to frequently play a key role in *in vitro* and *in vivo* silica binding peptides and can form hydrogen bonding with specific functional groups (imidazole, siloxide and superficial silanol groups). The adoption of these mutants on the nanoparticle were assessed using fluorometric binding assay, changes in zeta potential, and by molecular dynamic simulation<sup>10</sup>. The insights gained from this point mutation study, will be useful in applying this knowledge to silica-binding peptide that were identified in this thesis. Few example silica binding peptides identified in this study include, LPVRLDW, KIAVIST, YSLKQYQ, ADIRHIK and HYIDFRW.

The SiBPs isolated in this study, were eluted using different elution buffers and conditions. This knowledge can be used to design and develop material specific elution buffers by careful understanding of the material and biomolecule chemistries<sup>107,124</sup>. Similarly, another important factor to consider is the limited fundamental understanding of peptide-material interactions which is a major bottle neck for generating peptide based inorganic nanomaterials with improved biostability/ compatibility, solubility and functionality and increased physico-chemical properties<sup>132</sup>. In advancing our understanding of peptide mineral

interactions a clear understanding of the solution behaviour of both the peptide and the material is needed before the interaction of the two can be understood.

Also, from the adsorption binding results, it was found that the peptides with an amide group at the C-terminus showed higher binding specificity to negatively charged silica nanoparticles than corresponding carboxyl terminal acid group peptides. This increase in amide (NH<sub>2</sub>) binding activity was mainly due to an increase in overall charge or pI of the peptide and is directly proportional to pH change<sup>124</sup>. Consequently, proving a new dimension to design and engineer material specific peptides or phage constructs as a function of charge or pI; by targeting the coat proteins pIII and pVIII of M13 bacteriophage either by N-terminal and/ or C-terminal fusion. This can help us to mimic the original phage structures for developing innovative and advanced biomimetic surfaces for promising applications in biomedical and bio-nanotechnology<sup>88,416,417,419,441</sup>.

Further, although, online databases are easily available for general organic and inorganic materials such as BDB<sup>217</sup> or Pep Bank<sup>326</sup>, no material specific databases have been designed for inorganic material binding peptides obtained from distinct classes of combinatorial display techniques combined with structural and bioinformatics data. We propose that such databases, with all the experimental and computational information relating to the different classes of nanomaterials and libraries should be built. These databases will find solutions for bias problems and improve our understanding of biomolecule-inorganic material interactions which will lead in turn to the development of smart nanomaterials and slowly reduce the sole dependence on *in vitro* display technologies to take this approach forward as is presently the case.

Appendices 1-8

Appendix 2.1

HPLC chromatograms of synthesized silica binding peptides for key binding studies

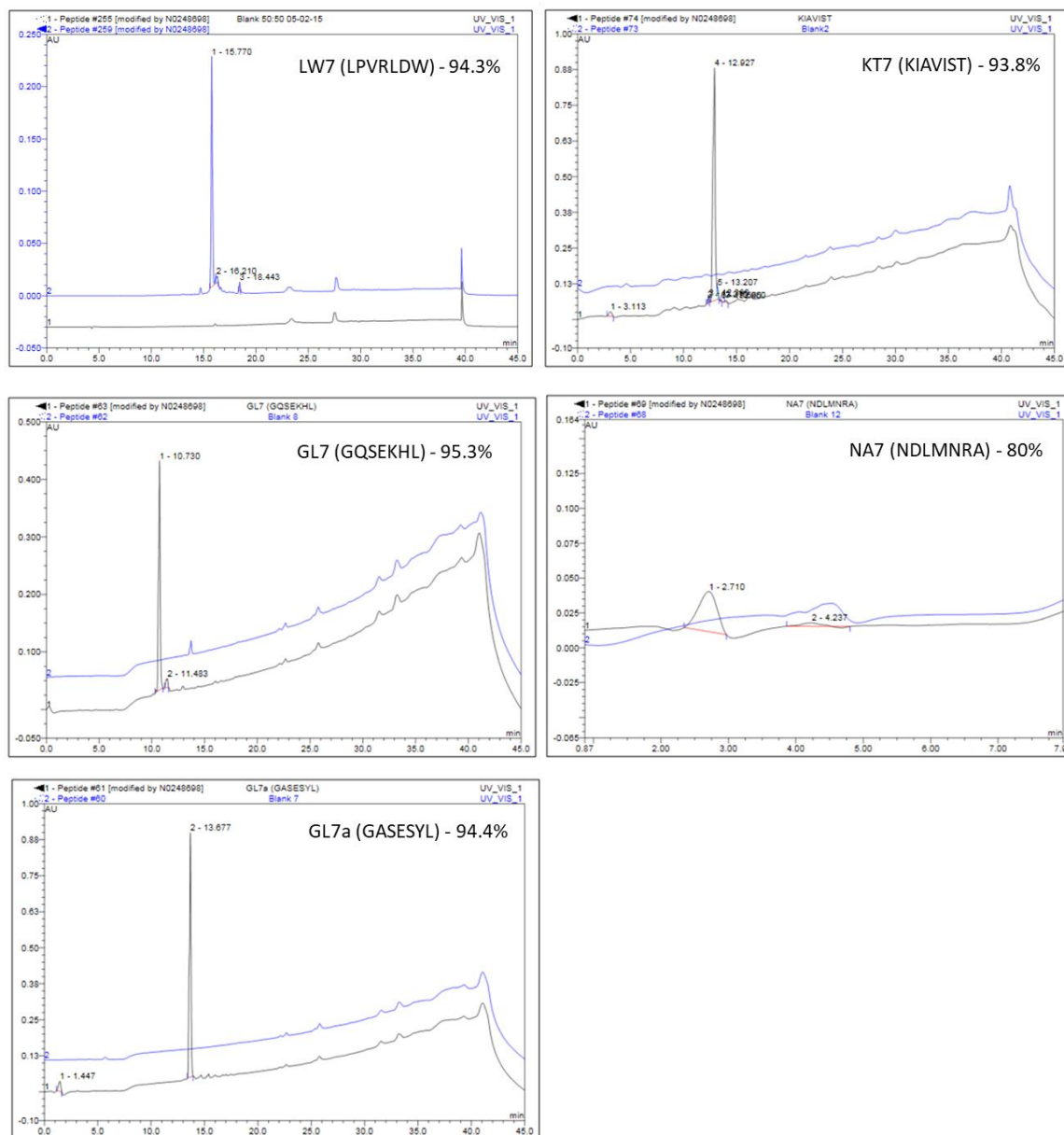


**Figure A1. HPLC chromatograms of synthesized silica binding peptides (identified from phage display work) used for binding studies.** The purity of LPVRLDW, KIAVIST, GQSEKHL, NDLMNRA and GASESYL peptides was determined as 94.3%, 93.8%, 95.3%, 80%, and 94.4% respectively.



**Appendix 2.2**

HPLC chromatograms of synthesized silica binding peptides for key binding studies

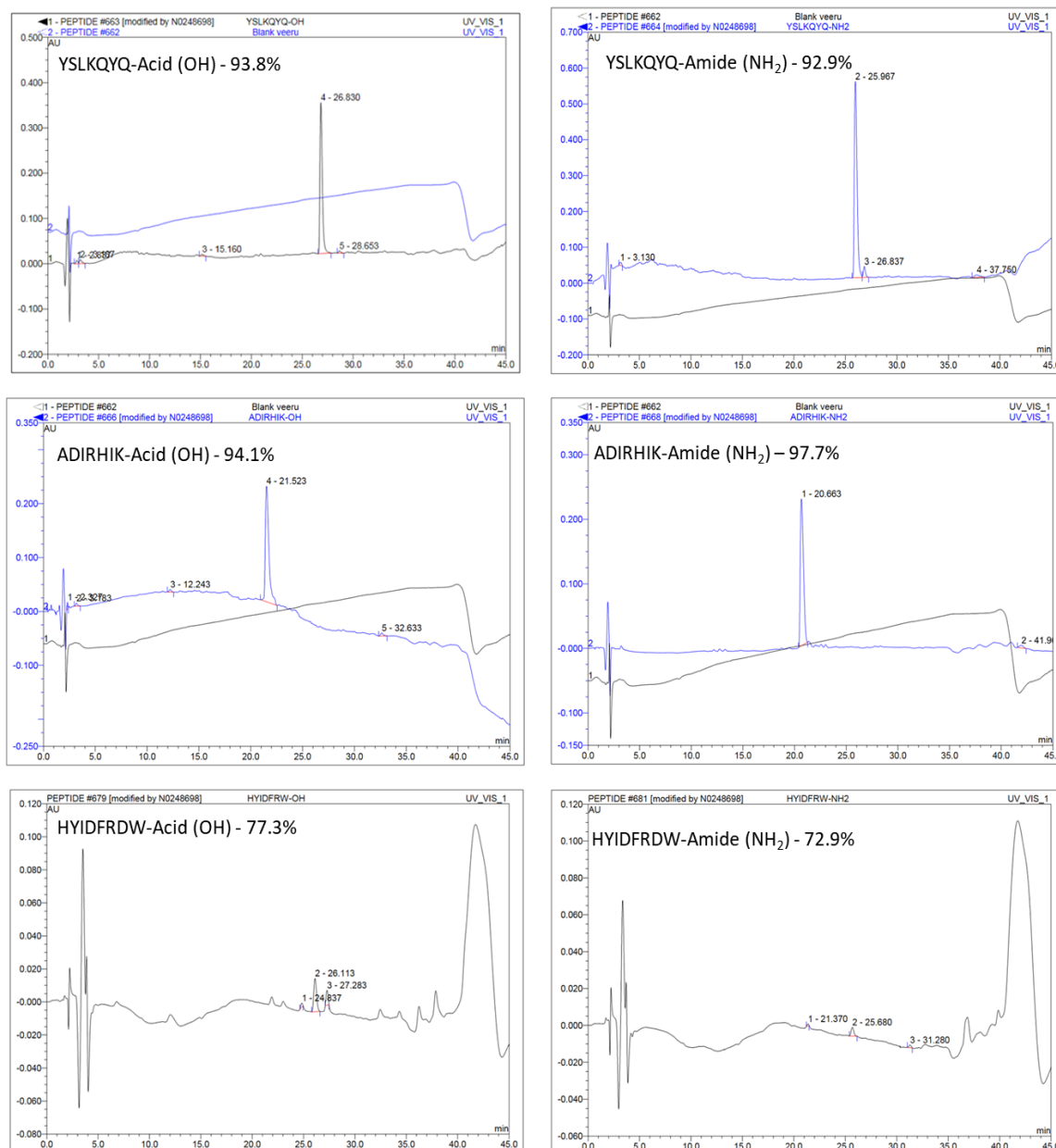


**Figure A2. HPLC chromatograms of synthesized silica binding peptides (identified from phage display work) used for binding studies.** The purity of YSLKQYQ-OH, YSLKQYQ-NH<sub>2</sub>, ADIRHIK-OH, ADIRHIK-NH<sub>2</sub>, HYIDFRW-OH and HYIDFRW-NH<sub>2</sub> peptides was determined as 93.8%, 92.9%, 94.1%, 97.7%, 77.3% and 72.9% respectively.

**Appendix 2.3**

Mass spectra (MALDI-TOF/TOF and MS/MS spectrums) of synthesized silica binding peptides identified from phage display work and used for key binding studies.

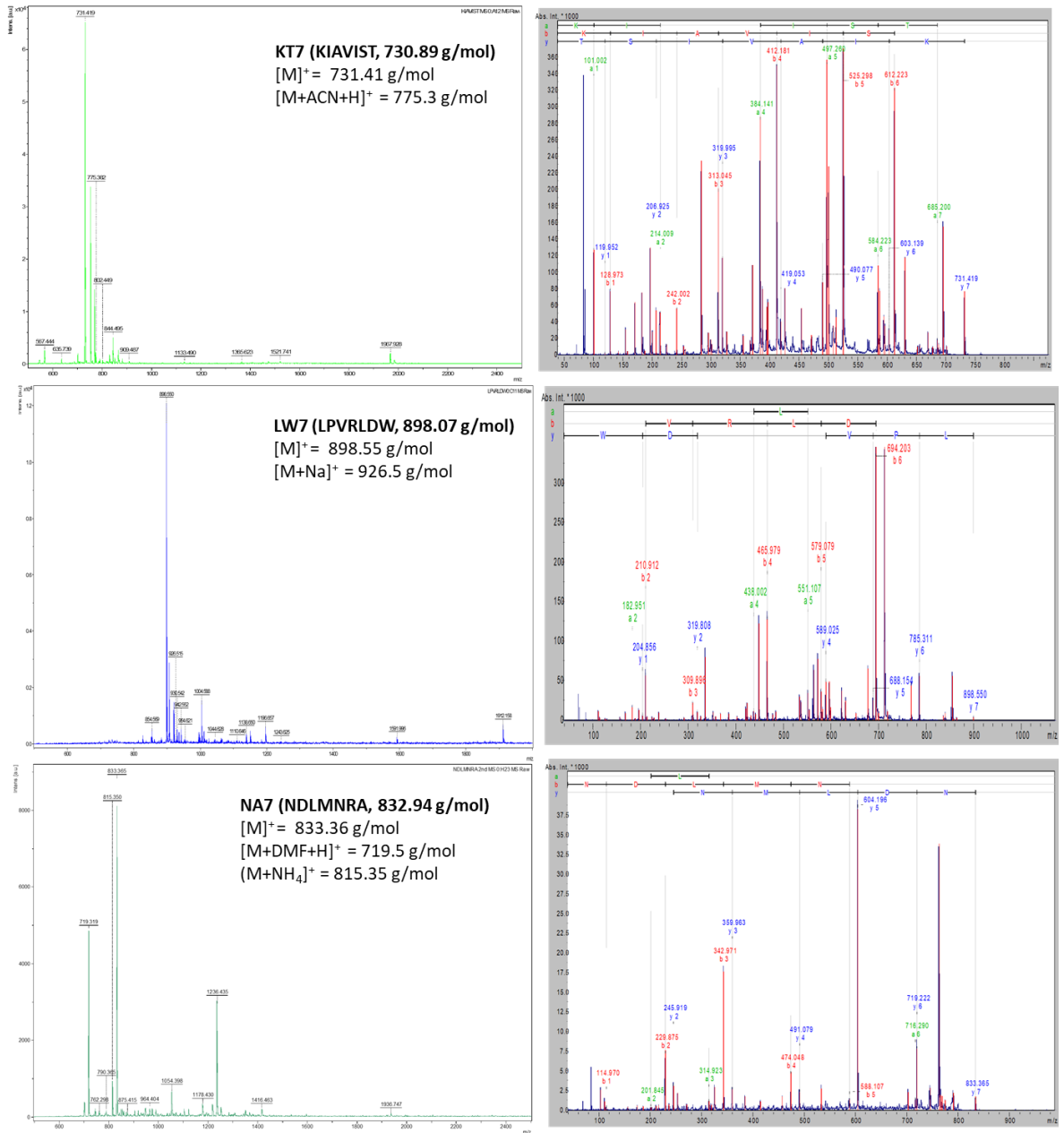


**Figure A3. Mass spectra of synthesized silica binding peptides (identified from phage display work) used for binding studies.** The molecular weight of the peptides KIAVIST, LPVRLDW and NDLMNRA was measured as 731.41 g/mol, 898.5 g/mol and 833.3 g/mol respectively.

## Appendices 1-8

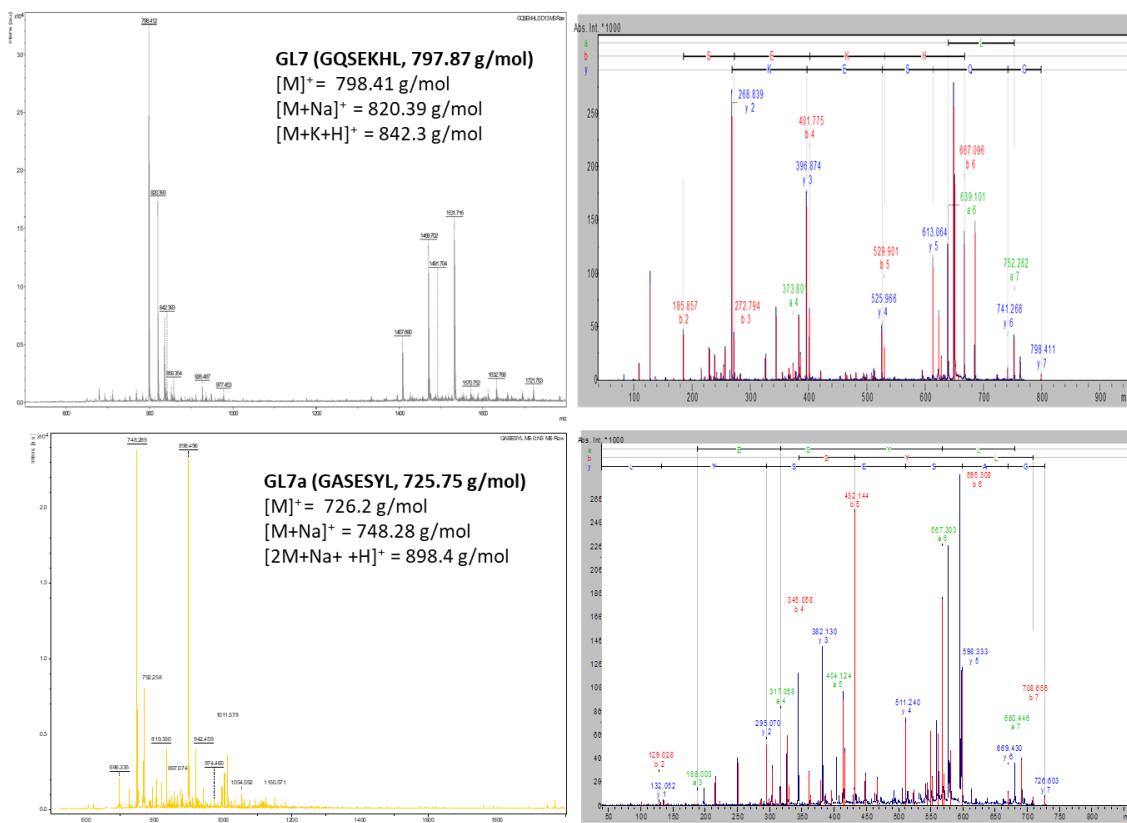


**Figure A3. Mass spectra of synthesized silica binding peptides (identified from phage display work) used for binding studies.** The molecular weight of the peptides GQSEKHL, and GASESYL was measured as 798.41 g/mol and 726.2 g/mol respectively.

**Appendix 3.1.****Table A4. Phage titer calculations for relative binding assay (1<sup>st</sup> time)**

	Number of plaques obtained <sup>a</sup>	vol of diluted phage solution <sup>b</sup> (ml)	Dilution factor <sup>c</sup>	bound phage <sup>d</sup> (pfu/ml) (d=a/b*c)	Input phage (pfu/ml)	Binding ratio (bound/input *100)
LPVRLDW	130	0.01	1.0E+04	1.3E+08	2.5E+10	0.52
GQSEKHL	54	0.01	1.0E+04	5.4E+07	2.5E+10	0.216
GASESYL	12	0.01	1.0E+04	12000000	2.5E+10	0.048
NDLMNRA	75	0.01	1.0E+04	7.5E+07	2.5E+10	0.3
VSRDTPQ	33	0.01	1.0E+04	3.3E+07	2.5E+10	0.132
KIAVIST	104	0.01	1.0E+04	1.0E+08	2.5E+10	0.416
HYIDFRW	126	0.01	1.0E+04	1.3E+08	2.5E+10	0.504
HVPRAMA	37	0.01	1.0E+04	3.7E+07	2.5E+10	0.148
ELTPLPL	77	0.01	1.0E+04	7.7E+07	2.5E+10	0.308
QQTNWSL	28	0.01	1.0E+04	2.8E+07	2.5E+10	0.112
QLAVAPS	19	0.01	1.0E+04	1.9E+07	2.5E+10	0.076
VGSYLG I	4	0.01	1.0E+04	4.0E+06	2.5E+10	0.016
GTGSQAS	9	0.01	1.0E+04	9.0E+06	2.5E+10	0.036
ETALIAA	2	0.01	1.0E+04	2.0E+06	2.5E+10	0.008
SQTFTSD	13	0.01	1.0E+04	13000000	2.5E+10	0.052
M13KE	23	0.01	1.0E+03	2300000	2.5E+10	0.0092

**Repeat (2<sup>nd</sup> time)**

	Number of plaques obtained <sup>a</sup>	vol of diluted phage <sup>b</sup> (ml)	Dilution factor <sup>c</sup>	bound phage <sup>d</sup> (pfu/ml) (d=a/b*c)	Input phage (pfu/ml)	Binding ratio	Average (1 <sup>st</sup> and 2 <sup>nd</sup> repeats)
LPVRLDW	123	0.01	1.0E+04	1.2E+08	2.5E+10	0.492	0.506
GQSEKHL	63	0.01	1.0E+04	6.3E+07	2.5E+10	0.252	0.234
GASESYL	14	0.01	1.0E+04	14000000	2.5E+10	0.056	0.052
NDLMNRA	89	0.01	1.0E+04	8.9E+07	2.5E+10	0.356	0.328
VSRDTPQ	27	0.01	1.0E+04	2.7E+07	2.5E+10	0.108	0.120
KIAVIST	111	0.01	1.0E+04	1.1E+08	2.5E+10	0.444	0.430
HYIDFRW	116	0.01	1.0E+04	1.2E+08	2.5E+10	0.464	0.484
HVPRAMA	46	0.01	1.0E+04	4.6E+07	2.5E+10	0.184	0.166
ELTPLPL	85	0.01	1.0E+04	8.5E+07	2.5E+10	0.34	0.324
QQTNWSL	39	0.01	1.0E+04	3.9E+07	2.5E+10	0.156	0.134
QLAVAPS	26	0.01	1.0E+04	2.6E+07	2.5E+10	0.104	0.090
VGSYLG I	13	0.01	1.0E+04	1.3E+07	2.5E+10	0.052	0.034
GTGSQAS	16	0.01	1.0E+04	1.6E+07	2.5E+10	0.064	0.050
ETALIAA	7	0.01	1.0E+04	7.0E+06	2.5E+10	0.028	0.018
SQTFTSD	17	0.01	1.0E+04	17000000	2.5E+10	0.068	0.060
M13KE	13	0.01	1.0E+03	1300000	2.5E+10	0.0052	0.0072

**Appendix 4.1****Table A5. Phage titer calculations for relative binding assay**

	Number of plaques obtained <sup>a</sup>	vol of diluted phage solution <sup>b</sup> (ml)	Dilution factor <sup>c</sup>	bound phage <sup>d</sup> (pfu/ml) (d=a/b*c)	Input phage (pfu/ml)	Binding ratio (bound/input *100)
SILPVTR	122	0.01	1.0E+04	1.2E+08	2.50E+10	0.492
ADIRHIK	151	0.01	1.0E+04	1.5E+08	2.50E+10	0.604
ADARYKS	67	0.01	1.0E+04	67000000	2.50E+10	0.268
HWNTVVS	55	0.01	1.0E+04	5.5E+07	2.50E+10	0.22
MPRLPPA	87	0.01	1.0E+04	8.7E+07	2.50E+10	0.348
YSLKQYQ	148	0.01	1.0E+04	1.5E+08	2.50E+10	0.592
YNGSANG	29	0.01	1.0E+04	2.9E+07	2.50E+10	0.116
ANPTFFS	76	0.01	1.0E+04	7.6E+07	2.50E+10	0.304
SPLHSNY	97	0.01	1.0E+04	9.7E+07	2.50E+10	0.388
ANEDTGT	79	0.01	1.0E+04	7.9E+07	2.50E+10	0.316
EGWIQTF	33	0.01	1.0E+04	3.3E+07	2.50E+10	0.132
LETVVSS	28	0.01	1.0E+04	2.8E+07	2.50E+10	0.112
ASMNQGG	22	0.01	1.0E+04	2.2E+07	2.50E+10	0.088
VDTSIFN	18	0.01	1.0E+04	1.8E+07	2.50E+10	0.072
M13KE	23	0.01	1.0E+03	2300000	2.5E+10	0.0092

**Repeat (2<sup>nd</sup> time)**

	Number of plaques obtained <sup>a</sup>	vol of diluted phage <sup>b</sup> (ml)	Dilution factor <sup>c</sup>	bound phage <sup>d</sup> (pfu/ml) (d=a/b*c)	Input phage (pfu/ml)	Binding ratio	Average (1 <sup>st</sup> and 2 <sup>nd</sup> repeats)
SILPVTR	135	0.01	1.0E+04	1.4E+08	2.50E+10	0.54	0.516
ADIRHIK	164	0.01	1.0E+04	1.6E+08	2.50E+10	0.656	0.630
ADARYKS	61	0.01	1.0E+04	61000000	2.50E+10	0.244	0.256
HWNTVVS	43	0.01	1.0E+04	4.3E+07	2.50E+10	0.172	0.196
MPRLPPA	92	0.01	1.0E+04	9.2E+07	2.50E+10	0.368	0.358
YSLKQYQ	136	0.01	1.0E+04	1.4E+08	2.50E+10	0.544	0.568
YNGSANG	23	0.01	1.0E+04	2.3E+07	2.50E+10	0.092	0.104
ANPTFFS	66	0.01	1.0E+04	6.6E+07	2.50E+10	0.264	0.284
SPLHSNY	85	0.01	1.0E+04	8.5E+07	2.50E+10	0.34	0.364
ANEDTGT	91	0.01	1.0E+04	9.1E+07	2.50E+10	0.364	0.340
EGWIQTF	26	0.01	1.0E+04	2.6E+07	2.50E+10	0.104	0.118
LETVVSS	23	0.01	1.0E+04	2.3E+07	2.50E+10	0.092	0.102
ASMNQGG	28	0.01	1.0E+04	2.8E+07	2.50E+10	0.112	0.100
VDTSIFN	14	0.01	1.0E+04	1.4E+07	2.50E+10	0.056	0.064
M13KE	13	0.01	1.0E+03	1300000	2.5E+10	0.0052	0.0072

**Appendix 4.2**

Table A6: Repanning experimental results to check the optimised biopanning approach and reproducibility. Selected silica binders (most frequently observed) were shown in the chapter 4 and full list of sequences including the additional sequences isolated from Elution strategy 1 were shown here.

<b>Gly-HCl pH-2.2</b>	<b>Freq</b>	<b>MgCl2 pH-6.1</b>	<b>Freq</b>	<b>TEA pH-11.1</b>	<b>Freq</b>	<b>TEA pH- 11.1 (Repeat)</b>	<b>Freq</b>
<b>Most frequently identified silica binders</b>							
TVNFKLY	<b>8/30</b>	VSRDTPQ	<b>12/30</b>	YSLKQYQ	<b>8/30</b>	YSLKQYQ	<b>12/30</b>
VSRDTPQ	3/30	-	-	-	-	-	-
GQSEKHL	2/30	GQSEKHL	6/30	-	-	-	-
LPVRLDW	1/30	-	-	-	-	-	-
GTGSQAS	1/30	-	-	-	-	-	-
		TVNFKLY	1/30	-	-	-	-
		ELTPLPL	1/30	-	-	-	-
VENVHVR	(2/30)	GISDLPS	(1/30)	YSFKQYQ	(4/30)	YSFKQYQ	(5/30)
YSLKQYQ	(2/30)	SPFNRYQ	(1/30)	SLSKWSF	(2/30)	YNGSANQ	(3/30)
YNGSANQ	(2/30)	ISETRSL	(1/30)	GSCSQSQ	(1/30)	VENVHVR	(1/30)
FASRSDT	(2/30)	YNGSPYQ	(1/30)	GLKYTMP	(1/30)	SFPLSKY	(1/30)
AIDFARN	(1/30)	QSMPQSR	(1/30)	TSFEHQP	(1/30)	VAPFRLI	
NTADDRK	(1/30)	VAPPRFI	(1/30)			VHLDSWT	
VPASPWT	(1/30)					TQVLTEA	
IDNSHTH	(1/30)					GQGLSLP	
VPNLNMR	(1/30)						
Nil	(2/30)	Nil	(4/30)	Nil	(13/30)	Nil	(4/30)

**Appendix 4.3**

Table A7: Repanning experimental results to check the optimised biopanning approach and reproducibility. Selected silica binders (most frequently observed) were shown in the chapter 4 and full list of sequences including the additional sequences isolated from Elution strategy 1 were shown here of sequences isolated from Elution strategy 2.

<b>Gly-HCl pH-2.2</b>	<b>Freq</b>	<b>Gly-HCl pH-7</b>	<b>Freq</b>	<b>Gly-HCl pH-11</b>	<b>Freq</b>
<b>Most frequently identified silica binders</b>					
VSRDTPQ	<b>5/30</b>	VSRDTPQ	<b>6/30</b>	VSRDTPQ	<b>6/30</b>
TVNFKLY	<b>4/30</b>	TVNFKLY	<b>3/30</b>	TVNFKLY	<b>3/30</b>
KIAVIST	<b>2/30</b>	-	-	-	-
HGGVRLY	<b>2/30</b>	-	-	-	-
GQSEKHL	<b>1/30</b>	GQSEKHL	<b>3/30</b>	GQSEKHL	<b>1/30</b>
-	-	YSLKQYQ	<b>3/30</b>	YSLKQYQ	<b>1/30</b>
-	-	ELTPLTL	<b>2/30</b>	ELTPLTL	<b>1/30</b>
LPVRLDW	<b>1/30</b>	LPVRLDW	<b>1/30</b>	-	-
WSLSELH	<b>1/30</b>	-	-	WSLSELH	<b>1/30</b>
-	-	NGLMNRA	<b>1/30</b>	-	-
QQTNWSL	<b>2/30</b>	QQTNWSL	<b>1/30</b>	-	-
FASRSDT	<b>1/30</b>	-	-	FASRSDT	<b>1/30</b>
		YNGSANQ	<b>1/30</b>		
		TTQVLEA	<b>1/30</b>	TTQVLEA	<b>1/30</b>
		VKMESPL	<b>1/30</b>	VKMESPL	<b>1/30</b>
		SWTALGP	<b>1/30</b>		
		QMHREPA	<b>1/30</b>	QMHREPA	<b>1/30</b>
QSMPQAR	<b>(1/30)</b>	-	-	ENHVHVR	<b>(1/30)</b>
NQIYSAN	<b>(1/30)</b>	-	-	VENVHVR	<b>(1/30)</b>
STPATLI	<b>(1/30)</b>	-	-	VASHSKP	<b>(1/30)</b>
NAPYRAM	<b>(1/30)</b>	-	-	VAPPRLI	<b>(1/30)</b>
WTTSVGT	<b>(1/30)</b>	-	-	GQGQTIP	<b>(1/30)</b>
TNLSHVP	<b>(1/30)</b>	-	-	DSMSLLQ	<b>(1/30)</b>
VHRDSWT	<b>(1/30)</b>	-	-	AHINVPS	<b>(1/30)</b>
-	-	VVTPKTA	<b>(1/30)</b>	SFNPLAY	<b>(1/30)</b>
Nil	<b>(6/30)</b>	Nil	<b>(4/30)</b>	Nil	<b>(7/30)</b>

Appendix 5.1

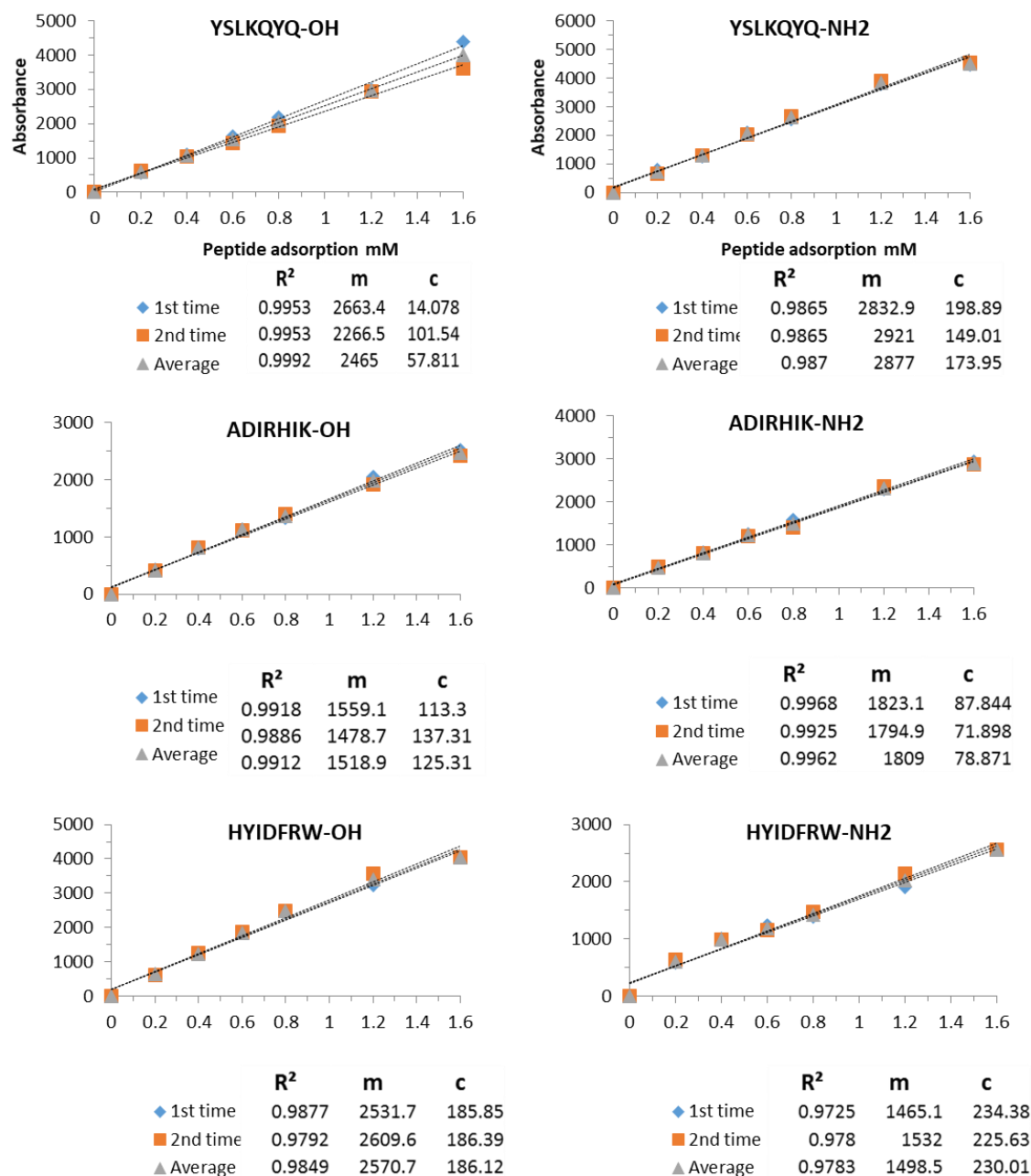


**Figure A8: Peptide calibrations from two different sets of experimental repeats.**

The calibration data plotted for peptides include YSLKQYQ-OH, YSLKQYQ-NH<sub>2</sub>, ADIRHIK-OH, ADIRHIK-NH<sub>2</sub>, HYIDFRW-OH and HYIDFRW-NH<sub>2</sub> at varying known peptide concentrations (0.2-1.6 mM) in PBS at pH-7.5. The x-axis represents the known amounts of peptide added (mM) and the measured absorbance reading was shown in Y-axis. The average R<sup>2</sup> (correlation coefficient) error (from two different sets of experimental repeats) considered for plotting the peptide adsorption isotherms (chapter 5) are shown here. Also, the c and m values used to find the R<sup>2</sup> values via the equation Y=mx+C are also shown.



## Publications

### Published works

- 1) Thota, V. & Perry, C. C. A Review on Recent Patents and Applications of Inorganic Material Binding Peptides. *Recent Pat Nanotechnol* **11**, 168–180 (2017).
- 2) Limo, M. J. *et al.* Interactions between Metal Oxides and Biomolecules: from Fundamental Understanding to Applications. *Chem. Rev.* **118**, 11118–11193 (2018).

## A Review on Recent Patents and Applications of Inorganic Material Binding Peptides

Veeranjaneyulu Thota and Carole C Perry\*

*Biomolecular and Materials Interface Research Group, Interdisciplinary Biomedical Research Centre, Nottingham Trent University, Clifton Lane, Nottingham NG11 8NS, United Kingdom*

**Abstract:** Over the past decade, significant progress has been made in the identification of novel material binding peptides having affinity to a wide range of target materials and their use in nanobiotechnological innovations. These material binding peptides (MBPs), also known as solid/ substance binding peptides (SBPs) can be isolated using combinatorial display technologies such as phage display (PD), surface display (cell, bacterial, yeast, mRNA) exhibit material specific selectivity and affinity towards a range of inorganic and organic nanomaterial surfaces including metals, metal oxides, minerals, semiconductors and biomolecules. MBPs serve as mediators in bringing nanotechnology and biotechnology under one umbrella by linking solid nanoparticles with biomolecules including proteins, bioactive peptide motifs, bifunctional binding peptides, enzymes, antigens and antibody fragments. As the utilization and application of these inorganic binding peptides as molecular connectors, molecular assemblers and material specific synthesizers in nanotechnology has been expanding rapidly, so too has growing commercial interest in patenting such innovations. In this review, we present the past, current and future developments and applications of inorganic MBPs specific to nanomaterials and their applications.

**Keywords:** Affinity, application, biomolecule, combinatorial peptide display, material binding peptide, mediator, nanotechnology, selectivity.

### 1. INTRODUCTION

MBPs have attracted considerable interest in the development of innovative nanostructured materials in particular because of their promising and growing applications in nanotechnology. These MBPs are also called inorganic binding peptides (IOBPs) or substrate binding peptides (SUBPs) or solid binding peptides (SBPs) or genetically engineered peptides for inorganics (GEPs). MBPs are short amino acid peptide sequences that are genetically constructed and show specific affinity to a target material through combinatorial display approaches which include phage display [1-6], cell surface display [7-10], ribosome display [11-14] and mRNA display [15-18] technologies. Although nanomaterials have been designed and produced decades ago, their utilization in nano- or biotechnology is limited due to poor solubility and biocompatibility issues. However, several strategies have been developed to overcome the potential safety concerns and eventually, peptide display technologies came into existence by managing greater control over the nanomaterials without compromising their physical, chemical and functional properties.

G.P Smith, for the first time used phage display technology as a powerful tool to identify ligands for numerous targets in 1985 [1]. From there on, phage or cell surface displayed (7-15mers) libraries have become ubiquitous in selecting and screening peptides having strong

affinity towards a range of inorganic material surfaces such as metals (Ag [19-21], Au [22, 23], Pt [24], Pd [25]), metal oxides (SiO<sub>2</sub> [26-30], ZnO [31, 32], TiO<sub>2</sub> [33-35], Fe<sub>2</sub>O<sub>3</sub> [36, 37], IrO<sub>2</sub> [38], Al<sub>2</sub>O<sub>3</sub> [24, 39], Cu<sub>2</sub>O [31]), minerals (calcite, hydroxyapatite, graphite, mica, sapphire) [40-42], semiconductors (CdS, GaN, GaAs and ZnS) [43-45], carbon materials (graphene, carbon nanotubes) [46, 47] and polymer materials [48, 49]. These isolated peptides have many practical applications in biomineralization [32, 50, 51], synthesis and fabrication of inorganic nanomaterials [40, 52-58], immobilization of nanoparticles onto inorganic or organic surfaces and surface functionalization [34, 38, 59-61]. Now, it is starting to be possible to create novel materials using biological linkers to join more than one type of material generating hybrids with unique electronic, mechanical, magnetic or photonic properties [26, 27].

The aim of this paper is to summarize and discuss recent progress in patents on MBPs specifically exploring inorganic nano surfaces like metals, metal oxides, minerals, carbon based materials, polymer based materials, magnetic materials and semiconductors by peptide display strategies and their utilization in the generation of advanced nanomaterials.

In order to get a clear picture on the number of patents present to date relevant to MBPs and their applications, a thorough online search was conducted using the available free national and worldwide databases which include EPO Espacenet, WIPO patent scope, USPTO, Google patent search, Patent lens etc. along with commercial databases including Derwent and Patbase. The key words used to find all the relevant patents were combinatorial/ phage displayed

\*Address correspondence to this author at the Interdisciplinary Biomedical Research Centre, Nottingham Trent University, Clifton Lane, NG11 8NS, Nottingham, UK; Tel: +44-115-8486695; E-mail: [Carole.Perry@ntu.ac.uk](mailto:Carole.Perry@ntu.ac.uk)

This is an open access article published under a Creative Commons Attribution (CC-BY) License, which permits unrestricted use, distribution and reproduction in any medium, provided the author and source are cited.



# CHEMICAL REVIEWS

Cite This: *Chem. Rev.* 2018, 118, 11118–11193

Review

pubs.acs.org/CR

## Interactions between Metal Oxides and Biomolecules: from Fundamental Understanding to Applications

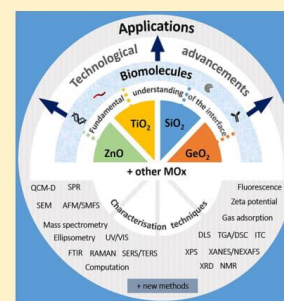
Marion J. Limo,<sup>||,†,‡</sup> Anna Sola-Rabada,<sup>||,†</sup> Estefania Boix,<sup>||,†,§</sup> Veeranjaneyulu Thota,<sup>†</sup> Zayd C. Westcott,<sup>†</sup> Valeria Puddu,<sup>†</sup> and Carole C. Perry<sup>\*,†,§</sup>

<sup>†</sup>Interdisciplinary Biomedical Research Centre, School of Science and Technology, Nottingham Trent University, Clifton Lane, Nottingham NG11 8NS, United Kingdom

<sup>‡</sup>Interface and Surface Analysis Centre, School of Pharmacy, University of Nottingham, University Park, Nottingham NG7 2RD, United Kingdom

<sup>§</sup>Department of Bioproducts and Biosystems, Aalto University, P.O. Box 16100, FI-00076 Aalto, Finland

**ABSTRACT:** Metallo-oxide (MO)-based bioinorganic nanocomposites promise unique structures, physicochemical properties, and novel biochemical functionalities, and within the past decade, investment in research on materials such as ZnO, TiO<sub>2</sub>, SiO<sub>2</sub>, and GeO<sub>2</sub> has significantly increased. Besides traditional approaches, the synthesis, shaping, structural patterning, and postprocessing chemical functionalization of the materials surface is inspired by strategies which mimic processes in nature. Would such materials deliver new technologies? Answering this question requires the merging of historical knowledge and current research from different fields of science. Practically, we need an effective defragmentation of the research area. From our perspective, the superficial accounting of material properties, chemistry of the surfaces, and the behavior of biomolecules next to such surfaces is a problem. This is particularly of concern when we wish to bridge between technologies in vitro and biotechnologies in vivo. Further, besides the potential practical technological efficiency and advantages such materials might exhibit, we have to consider the wider long-term implications of material stability and toxicity. In this contribution, we present a critical review of recent advances in the chemistry and engineering of MO-based biocomposites, highlighting the role of interactions at the interface and the techniques by which these can be studied. At the end of the article, we outline the challenges which hamper progress in research and extrapolate to developing and promising directions including additive manufacturing and synthetic biology that could benefit from molecular level understanding of interactions occurring between inanimate (abiotic) and living (biotic) materials.



### CONTENTS

1. Introduction	11119	2.6. Techniques Directly Probing SiO <sub>2</sub> -Biomolecules Interactions	11131
1.1. Approaches Used in the Study of MO-Biomolecule Interactions	11120	2.6.1. Experimental Techniques for the Study of Silica-Biomolecule Interactions	11131
1.2. Choice of Metal (Metalloid) Oxide Systems	11121	2.6.2. Computational Techniques for the Study of Silica-Biomolecule Interactions	11133
2. SiO <sub>2</sub>	11123	2.7. Toxicology of SiO <sub>2</sub>	11134
2.1. Introduction to SiO <sub>2</sub> as a Material	11123	3. TiO <sub>2</sub>	11135
2.2. Silica Structure and Synthesis Methods	11123	3.1. Overview of TiO <sub>2</sub>	11135
2.3. Silica Surface Chemistry	11124	3.2. TiO <sub>2</sub> Properties and Traditional Synthetic Methods	11135
2.3.1. Surface Speciation and Associated Properties	11124	3.3. Surface Chemistry of TiO <sub>2</sub>	11136
2.3.2. Issue of Surface Contamination	11125	3.3.1. Bulk and Surface Structures	11136
2.4. Modifying the Functionality of Silicas	11125	3.3.2. Surface Hydroxylation and Charge	11136
2.5. SiO <sub>2</sub> -Biomolecule Interactions and Applications	11127	3.3.3. Water/Inorganic Interface	11137
2.5.1. Silica Formed in Nature	11127	3.3.4. Outlook for Application at the Bioinorganic Interface	11137
2.5.2. Mimetic Studies to Understand Biosilicification	11127		
2.5.3. Interaction of Biomolecules with Silica	11129		
2.5.4. Applications of Silica-Biomolecule Interactions	11130		

Received: November 1, 2017

Published: October 26, 2018



© 2018 American Chemical Society

11118

DOI: 10.1021/acs.chemrev.7b00660  
*Chem. Rev.* 2018, 118, 11118–11193

## References

1. Vodnik, M., Zager, U., Strukelj, B. & Lunder, M. Phage Display: Selecting Straws Instead of a Needle from a Haystack. *Molecules* **16**, 790–817 (2011).
2. Matochko, W. L., Cory Li, S., Tang, S. K. Y. & Derda, R. Prospective identification of parasitic sequences in phage display screens. *Nucleic Acids Res.* **42**, 1784–1798 (2014).
3. Umlauf, B. J., McGuire, M. J. & Brown, K. C. Introduction of plasmid encoding for rare tRNAs reduces amplification bias in phage display biopanning. *Biotechniques* **58**, 81–84 (2015).
4. Puddu, V. & Perry, C. C. Peptide adsorption on silica nanoparticles: Evidence of hydrophobic interactions. *ACS Nano* **6**, 6356–6363 (2012).
5. Dickerson, M. B., Sandhage, K. H. & Naik, R. R. Protein- and peptide-directed syntheses of inorganic materials. *Chem. Rev.* **108**, 4935–4978 (2008).
6. Sanghvi, A. B., Miller, K. P.-H., Belcher, A. M. & Schmidt, C. E. Biomaterials functionalization using a novel peptide that selectively binds to a conducting polymer. *Nat. Mater.* **4**, 496–502 (2005).
7. Hnilova, M. *et al.* Effect of molecular conformations on the adsorption behavior of gold-binding peptides. *Langmuir* **24**, 12440–12445 (2008).
8. Khatayevich, D. *et al.* Biofunctionalization of materials for implants using engineered peptides. *Acta Biomater.* **6**, 4634–4641 (2010).
9. Slocik, J. M. *et al.* Probing peptide–nanomaterial interactions. *Chem. Soc. Rev.* **39**, 3454 (2010).
10. Patwardhan, S. V. *et al.* Chemistry of aqueous silica nanoparticle surfaces and the mechanism of selective peptide adsorption. *J. Am. Chem. Soc.* **134**, 6244–6256 (2012).
11. Care, A., Bergquist, P. L. & Sunna, A. Solid-binding peptides: Smart tools for nanobiotechnology. *Trends Biotechnol.* **33**, 259–268 (2015).
12. Thota, V. & Perry, C. C. A Review on Recent Patents and Applications of Inorganic Material Binding Peptides. *Recent Pat Nanotechnol* **11**, 168–180 (2017).
13. Belcher, A. Molecular recognition of materials. (2003).
14. Ku, J. & Schultz, P. G. Alternate protein frameworks for molecular recognition. *Proc. Natl. Acad. Sci. U. S. A.* **92**, 6552–6556 (1995).
15. Schneider, G. & Wrede, P. Artificial neural networks for computer-based molecular design. *Progress in Biophysics and Molecular Biology* **70**, 175–222 (1998).
16. Paine, M. L. & Snead, M. L. Protein interactions during assembly of the enamel organic extracellular matrix. *J. Bone Miner. Res.* **12**, 221–227 (1997).
17. Kröger, N. Polycationic Peptides from Diatom Biosilica That Direct Silica Nanosphere Formation. *Science (80-. )*. **286**, 1129–1132 (1999).

## References

18. Liou, Y.-C., Tocilj, A., Davies, P. L. & Jia, Z. Mimicry of ice structure by surface hydroxyls and water of a  $\beta$ -helix antifreeze protein. *Nature* **406**, 322–324 (2000).
19. Brown, S. Metal-recognition by repeating polypeptides. *Nat. Biotechnol.* **15**, 269–272 (1997).
20. Giver, L. & Arnold, F. H. Combinatorial protein design by in vitro recombination. *Curr. Opin. Chem. Biol.* **2**, 335–338 (1998).
21. Schembri, M. A., Kjærgaard, K. & Klemm, P. Bioaccumulation of heavy metals by fimbrial designer adhesins. *FEMS Microbiol. Lett.* **170**, 363–371 (1999).
22. Brown, S., Sarikaya, M. & Johnson, E. A genetic analysis of crystal growth. *J. Mol. Biol.* **299**, 725–735 (2000).
23. Whaley, S. R., English, D. S., Hu, E. L., Barbara, P. F. & Belcher, A. M. Selection of peptides with semiconductor binding specificity for directed nanocrystal assembly. *Nature* **405**, 665–8 (2000).
24. Naik, R. R., Brott, L. L., Clarson, S. J. & Stone, M. O. Silica-precipitating peptides isolated from a combinatorial phage display peptide library. *J. Nanosci. Nanotechnol.* **2**, 95–100 (2002).
25. Smith, G. P. Filamentous fusion phage: novel expression vectors that display cloned antigens on the virion surface. *Science (80-. )*. **228**, 1315–1317 (1985).
26. Winter, G., Griffiths, A. D., Hawkins, R. E. & Hoogenboom, H. R. Making antibodies by phage display technology. *Annu. Rev. Immunol.* **12**, 433–55 (1994).
27. Hoogenboom, H. R. *et al.* Antibody phage display technology and its applications. *Immunotechnology* **4**, 1–20 (1998).
28. Azzazy, H. M. E. & Highsmith, W. E. Phage display technology: Clinical applications and recent innovations. *Clin. Biochem.* **35**, 425–445 (2002).
29. Petrenko, V. Evolution of phage display: from bioactive peptides to bioselective nanomaterials. *Expert Opin. Drug Deliv.* **5**, 825–836 (2008).
30. Ullman, C. G., Frigotto, L. & Cooley, R. N. In vitro methods for peptide display and their applications. *Brief. Funct. Genomics* **10**, 125–134 (2011).
31. Kieke, M. C. *et al.* Selection of functional T cell receptor mutants from a yeast surface-display library. *Proc. Natl. Acad. Sci.* **96**, 5651–5656 (1999).
32. Feldhaus, M. J. & Siegel, R. W. Yeast display of antibody fragments: A discovery and characterization platform. *J. Immunol. Methods* **290**, 69–80 (2004).
33. Kondo, A. & Ueda, M. Yeast cell-surface display - Applications of molecular display. *Appl. Microbiol. Biotechnol.* **64**, 28–40 (2004).
34. Pepper, L. R., Cho, Y. K., Boder, E. T. & Shusta, E. V. A decade of yeast surface display technology: Where are we now? *Comb. Chem. High Throughput Screen.* **11**, 127–134 (2008).
35. Schaffitzel, C., Hanes, J., Jermutus, L. & Plückthun, A. Ribosome display: An in vitro method for selection and evolution of antibodies from libraries. *J. Immunol. Methods* **231**, 119–135 (1999).

## References

36. Yan, X. & Xu, Z. Ribosome-display technology: applications for directed evolution of functional proteins. *Drug Discov. Today* **11**, 911–916 (2006).
37. Zahnd, C., Amstutz, P. & Plückthun, A. Ribosome display: selecting and evolving proteins in vitro that specifically bind to a target. *Nat. Methods* **4**, 269–279 (2007).
38. Xu, L. *et al.* Directed evolution of high-affinity antibody mimics using mRNA display. *Chem. Biol.* **9**, 933–942 (2002).
39. Takahashi, T. T., Austin, R. J. & Roberts, R. W. mRNA display: ligand discovery, interaction analysis and beyond. *Trends Biochem. Sci.* **28**, 159–165 (2003).
40. Lipovsek, D. & Plückthun, A. In-vitro protein evolution by ribosome display and mRNA display. *J. Immunol. Methods* **290**, 51–67 (2004).
41. Fukuda, I. *et al.* In vitro evolution of single-chain antibodies using mRNA display. *Nucleic Acids Res.* **34**, 127 (2006).
42. Oren, E. E. *et al.* A novel knowledge-based approach to design inorganic-binding peptides. *Bioinformatics* **23**, 2816–2822 (2007).
43. Oren, E. E. *et al.* Probing the molecular mechanisms of quartz-binding peptides. *Langmuir* **26**, 11003–11009 (2010).
44. Emami, F. S. *et al.* Force field and a surface model database for silica to simulate interfacial properties in atomic resolution. *Chem. Mater.* **26**, 2647–2658 (2014).
45. Hoess, R. H. Protein Design and Phage Display. *Chem. Rev.* **101**, 3205–3218 (2001).
46. Wittrup, K. D. Protein engineering by cell-surface display. *Curr. Opin. Biotechnol.* **12**, 395–399 (2001).
47. Smith, G. P. & Petrenko, V. A. Phage Display. *Chem. Rev.* **97**, 391–410 (1997).
48. Rosander, A., Bjerketorp, J., Frykberg, L. & Jacobsson, K. Phage display as a novel screening method to identify extracellular proteins. *J. Microbiol. Methods* **51**, 43–55 (2002).
49. Benhar, I. Biotechnological applications of phage and cell display. *Biotechnol. Adv.* **19**, 1–33 (2001).
50. Amstutz, P., Forrer, P., Zahnd, C. & Plückthun, A. In vitro display technologies: novel developments and applications. *Curr. Opin. Biotechnol.* **12**, 400–405 (2001).
51. Sladek, J., Sladek, V. & Zhang, C. Application of meshless local Petrov-Galerkin (MLPG) method to elastodynamic problems in continuously nonhomogeneous solids. *C. - Comput. Model. Eng. Sci.* **4**, 637–647 (2003).
52. Devlin, J. J., Panganiban, L. C. & Devlin, P. E. Random peptide libraries: A source of specific protein binding molecules. *Science (80-. )*. **249**, 404–406 (1990).
53. He, M. & Khan, F. Ribosome display: next-generation display technologies for production of antibodies in vitro. *Expert Rev. Proteomics* **2**, 421–430 (2005).
54. Dower, W. J. & Mattheakis, L. C. In vitro selection as a powerful tool for the applied evolution of proteins and peptides. *Curr. Opin. Chem. Biol.* **6**, 390–398 (2002).

## References

55. Huang, J., Ru, B. & Dai, P. Bioinformatics resources and tools for phage display. *Molecules* **16**, 694–709 (2011).
56. Clark, J. R. & March, J. B. Bacteriophages and biotechnology: vaccines, gene therapy and antibacterials. *Trends Biotechnol.* **24**, 212–218 (2006).
57. Krumpe, L. R. H. & Mori, T. The use of phage-displayed peptide libraries to develop tumor-targeting drugs. *Int. J. Pept. Res. Ther.* **12**, 79–91 (2006).
58. Sergeeva, A., Kolonin, M. G., Mollrem, J. J., Pasqualini, R. & Arap, W. Display technologies: Application for the discovery of drug and gene delivery agents. *Adv. Drug Deliv. Rev.* **58**, 1622–1654 (2006).
59. Patwardhan, S. V., Patwardhan, G. & Perry, C. C. Interactions of biomolecules with inorganic materials: Principles, applications and future prospects. *J. Mater. Chem.* **17**, 2875–2884 (2007).
60. Tamerler, C. & Sarikaya, M. Molecular biomimetics: nanotechnology and bionanotechnology using genetically engineered peptides. *Philos. Trans. R. Soc. A Math. Phys. Eng. Sci.* **367**, 1705–1726 (2009).
61. Pande, J., Szewczyk, M. M. & Grover, A. K. Phage display: Concept, innovations, applications and future. *Biotechnol. Adv.* **28**, 849–858 (2010).
62. Castel, G., Chtéoui, M., Heyd, B. & Tordo, N. Phage display of combinatorial peptide libraries: Application to antiviral research. *Molecules* **16**, 3499–3518 (2011).
63. Hairul Bahara, N. H. *et al.* Phage display antibodies for diagnostic applications. *Biologicals* **41**, 209–216 (2013).
64. Hoang, V. Van & Ganguli, D. Amorphous nanoparticles - Experiments and computer simulations. *Phys. Rep.* **518**, 81–140 (2012).
65. Eteshola, E., Brillson, L. J. & Lee, S. C. Selection and characteristics of peptides that bind thermally grown silicon dioxide films. *Biomol. Eng.* **22**, 201–204 (2005).
66. Sarikaya, M., Tamerler, C., Jen, A. K. Y.-Y., Schulten, K. & Baneyx, F. Molecular biomimetics: nanotechnology through biology. *Nat. Mater.* **2**, 577–585 (2003).
67. Grönwall, C. & Ståhl, S. Engineered affinity proteins-Generation and applications. *Journal of Biotechnology* (2009). doi:10.1016/j.jbiotec.2009.01.014
68. Lunder, M., Bratkovič, T., Urleb, U., Kreft, S. & Štrukelj, B. Ultrasound in phage display: A new approach to nonspecific elution. *Biotechniques* **44**, 893–900 (2008).
69. Donatan, S. *et al.* Physical elution in phage display selection of inorganic-binding peptides. *Mater. Sci. Eng. C* **29**, 14–19 (2009).
70. Bazan, J., Całkosinski, I. & Gamian, A. Phage display—A powerful technique for immunotherapy. *Hum. Vaccin. Immunother.* **8**, 1817–1828 (2012).
71. Wang, Y. A. *et al.* The Structure of a Filamentous Bacteriophage. *J. Mol. Biol.* **361**, 209–215 (2006).
72. Rakonjac, J., Bennett, N. J., Spagnuolo, J., Gagic, D. & Russel, M. Filamentous bacteriophage: biology, phage display and nanotechnology applications. *Curr.*

## References

- Issues Mol. Biol.* **13**, 51–76 (2011).
73. Webster, R. Filamentous Phage Biology. *Phage Disp. Pept. Proteins A Lab. Man.* (1996).
  74. Moghimian, P., Srot, V., Pichon, B. P., Facey, S. J. & Aken, P. A. van. Stability of M13 Phage in Organic Solvents. *J. Biomater. Nanobiotechnol.* **07**, 72–77 (2016).
  75. Li, K. *et al.* Chemical modification of M13 bacteriophage and its application in cancer cell imaging. *Bioconjug. Chem.* **21**, 1369–1377 (2010).
  76. Hamzeh-Mivehroud, M., Alizadeh, A. A., Morris, M. B., Bret Church, W. & Dastmalchi, S. Phage display as a technology delivering on the promise of peptide drug discovery. *Drug Discov. Today* **18**, 1144–1157 (2013).
  77. Endemann, H. & Model, P. Location of filamentous phage minor coat proteins in phage and in infected cells. *J. Mol. Biol.* (1995). doi:10.1006/jmbi.1995.0393
  78. Gao, C. *et al.* Making artificial antibodies: a format for phage display of combinatorial heterodimeric arrays. *Proc. Natl. Acad. Sci. U. S. A.* (1999). doi:10.1073/pnas.96.11.6025
  79. Løset, G. Å. Å., Bogen, B. & Sandlie, I. Expanding the versatility of phage display I: Efficient display of peptide-tags on protein VII of the filamentous phage. *PLoS One* (2011). doi:10.1371/journal.pone.0014702
  80. Min, N. S. and L. Phage Display Technologies. in *Encyclopedia of Life Sciences* (2001). doi:10.1038/npg.els.0000982
  81. Russel, M., Lowman, H. B. & Clackson, T. Introduction to phage biology and phage display. *Phage Disp. A Pract. Approach* (2004). doi:10.1097/00002820-200511000-00012
  82. Bratkovič, T. Progress in phage display: Evolution of the technique and its applications. *Cellular and Molecular Life Sciences* (2010). doi:10.1007/s00018-009-0192-2
  83. Makowski, L. Phage display: structure, assembly and engineering of filamentous bacteriophage M13. *Curr. Opin. Struct. Biol.* (1994). doi:10.1016/S0959-440X(94)90312-3
  84. Blaber, M. BCH5425 Molecular Biology and Biotechnology. *Spring* 1–9 (1998). Available at: <http://www.mikeblaber.org/oldwine/bch5425/lect33/lect33.htm>. (Accessed: 11th December 2017)
  85. Qi, H., Lu, H., Qiu, H. J., Petrenko, V. & Liu, A. Phagemid vectors for phage display: Properties, characteristics and construction. *J. Mol. Biol.* **417**, 129–143 (2012).
  86. Lee, S.-W. Ordering of Quantum Dots Using Genetically Engineered Viruses. *Science* (80-. ). **296**, 892–895 (2002).
  87. Lubkowski, J., Hennecke, F., Plückthun, A. & Wlodawer, A. Filamentous phage infection: Crystal structure of g3p in complex with its coreceptor, the C-terminal domain of TolA. *Structure* **7**, 711–722 (1999).
  88. Merzlyak, A. & Lee, S. W. Phage as templates for hybrid materials and mediators for nanomaterial synthesis. *Curr. Opin. Chem. Biol.* **10**, 246–252 (2006).



## References

89. Konthur, Z. & Cramer, R. High-throughput applications of phage display in proteomic analyses. *Targets* (2003). doi:10.1016/S1477-3627(03)02383-3
90. Seker, U. O. S. & Demir, H. V. Material binding peptides for nanotechnology. *Molecules* **16**, 1426–1451 (2011).
91. Huang, Y., Wiedmann, M. M. M. & Suga, H. RNA Display Methods for the Discovery of Bioactive Macrocycles. *Chem. Rev.* acs.chemrev.8b00430 (2018). doi:10.1021/acs.chemrev.8b00430
92. Yeh, Y.-W. Phage Display Techniques for Selection of Inorganic Binding Peptides with Electroactive Properties for Biosensor Applications. (University of Florida, USA, 2013).
93. Sarikaya, M., Tamerler, C., Schwartz, D. T. & Baneyx, F. Materials assembly and formation using engineered polypeptides. *Annu. Rev. Mater. Res.* **34**, 373–408 (2004).
94. Belton, D. J., Deschaume, O. & Perry, C. C. An overview of the fundamentals of the chemistry of silica with relevance to biosilicification and technological advances. *FEBS J.* **279**, 1710–1720 (2012).
95. Currie, H. A. & Perry, C. C. Silica in Plants: Biological, Biochemical and Chemical Studies. *Ann. Bot.* **100**, 1383–1389 (2007).
96. Perry, C. C. & Keeling-Tucker, T. Biosilicification: The role of the organic matrix in structure control. *J. Biol. Inorg. Chem.* **5**, 537–550 (2000).
97. Poulsen, N., Sumper, M. & Kroger, N. Biosilica formation in diatoms: Characterization of native silaffin-2 and its role in silica morphogenesis. *Proc. Natl. Acad. Sci.* **100**, 12075–12080 (2003).
98. Otzen, D. The Role of Proteins in Biosilicification. *Scientifica (Cairo)*. **2012**, 1–22 (2012).
99. Mieszawska, A. J. *et al.* Osteoinductive silk-silica composite biomaterials for bone regeneration. *Biomaterials* **31**, 8902–8910 (2010).
100. Plowright, R. *et al.* Influence of silk-silica fusion protein design on silica condensation in vitro and cellular calcification. *RSC Adv.* **6**, 21776–21788 (2016).
101. Cha, J. N. *et al.* Silicatein filaments and subunits from a marine sponge direct the polymerization of silica and silicones in vitro. *Proc. Natl. Acad. Sci. U. S. A.* **96**, 361–365 (1999).
102. Rai, A. & Perry, C. C. Facile fabrication of uniform silica films with tunable physical properties using silicatein protein from sponges. *Langmuir* **26**, 4152–4159 (2010).
103. Patwardhan, S. V. *et al.* Bioinspired synthesis of new silica structures Electronic supplementary information (ESI) available: Methods, EDS for specimens in Fig. 2c and Fig. 2b; additional SEM and TEM of silica. See <http://www.rsc.org/suppdata/cc/b3/b302056h/>. *Chem. Commun.* **365**, 1122–1123 (2003).
104. Perry, C. C. Silicification: The processes by which organisms capture and mineralize silica. *Rev. Mineral. Geochemistry* **54**, 291–327 (2003).

## References

105. Sumper, M. & Kröger, N. Silica formation in diatoms: the function of long-chain polyamines and silaffins. *J. Mater. Chem.* **14**, 2059–2065 (2004).
106. Kröger, N. & Sandhage, K. H. From Diatom Biomolecules to Bioinspired Syntheses of Silica- and Titania-Based Materials. *MRS Bull.* **35**, 122–126 (2010).
107. Puddu, V. & Perry, C. C. Interactions at the silica-peptide interface: The influence of particle size and surface functionality. *Langmuir* **30**, 227–233 (2014).
108. Rahman, I. A. & Padavettan, V. Synthesis of Silica Nanoparticles by Sol-Gel: Size-Dependent Properties, Surface Modification, and Applications in Silica-Polymer Nanocomposites—A Review. *J. Nanomater.* **2012**, 1–15 (2012).
109. Van Blaaderen, A., Van Geest, J. & Vrij, A. Monodisperse colloidal silica spheres from tetraalkoxysilanes: Particle formation and growth mechanism. *J. Colloid Interface Sci.* **154**, 481–501 (1992).
110. Stöber, W., Fink, A. & Bohn, E. Controlled growth of monodisperse silica spheres in the micron size range. *J. Colloid Interface Sci.* **26**, 62–69 (1968).
111. De, G., Karmakar, B. & Ganguli, D. Hydrolysis-condensation reactions of TEOS in the presence of acetic acid leading to the generation of glass-like silica microspheres in solution at room temperature. *J. Mater. Chem.* **10**, 2289–2293 (2000).
112. Izutsu, H., Nair, P. K., Maeda, K., Kiyozumi, Y. & Mizukami, F. Structure and properties of TiO<sub>2</sub>-SiO<sub>2</sub> prepared by sol-gel method in the presence of tartaric acid. *Mater. Res. Bull.* **32**, 1303–1311 (1997).
113. Kawaguchi, T. & Ono, K. Spherical silica gels precipitated from acid catalyzed TEOS solutions. *J. Non. Cryst. Solids* **121**, 383–388 (1990).
114. Lovingood, D. D., Owens, J. R., Seeber, M., Kornev, K. G. & Luzinov, I. Preparation of Silica Nanoparticles Through Microwave-assisted Acid-catalysis. *J. Vis. Exp.* e51022 (2013). doi:10.3791/51022
115. Perry, C. C. & Keeling-Tucker, T. Model studies of colloidal silica precipitation using biosilica extracts from *Equisetum telmateia*. *Colloid Polym. Sci.* **281**, 652–664 (2003).
116. Villa, M., Ortiz, M. I. & Parra, J. E. Validación de la técnica de digestibilidad total en cerdos como método de determinación de la digestibilidad posruminal de la proteína en bovinos. *Livest. Res. Rural Dev.* **22**, 57–93 (2010).
117. Parambath, M. *et al.* The nature of the silicophilic fluorescence of PDMPO. *Phys. Chem. Chem. Phys.* **18**, 5938–5948 (2016).
118. Ewing, C. S. S., Bhavsar, S., Vesper, G., McCarthy, J. J. J. & Johnson, J. K. K. Accurate amorphous silica surface models from first-principles thermodynamics of surface dehydroxylation. *Langmuir* (2014). doi:10.1021/la500422p
119. Zhuravlev, L. T. The surface chemistry of amorphous silica. Zhuravlev model. *Colloids Surfaces A Physicochem. Eng. Asp.* **173**, 1–38 (2000).
120. Hickman, G. J., Rai, A., Boocock, D. J., Rees, R. C. & Perry, C. C. Fabrication, characterisation and performance of hydrophilic and super-hydrophilic silica as cell culture surfaces. *J. Mater. Chem.* **22**, 12141 (2012).

## References

121. Hickman, G. J., Rees, R. C., Boocock, D. J., Pockley, A. G. & Perry, C. C. Controlling the dynamics of cell transition in heterogeneous cultures using surface chemistry. *Adv. Healthc. Mater.* **4**, 593–601 (2015).
122. Nicklin, M., Rees, R. C., Pockley, A. G. & Perry, C. C. Development of an hydrophobic fluoro-silica surface for studying homotypic cancer cell aggregation-disaggregation as a single dynamic process in vitro. *Biomater. Sci.* **2**, 1486–1496 (2014).
123. Zhou, Y., Shimizu, K., Cha, J. N., Stucky, G. D. & Morse, D. E. Efficient Catalysis of Polysiloxane Synthesis. *Angew. Chem. Int. Ed. Engl.* **38**, 779–782 (1999).
124. Emami, F. S. *et al.* Prediction of specific biomolecule adsorption on silica surfaces as a function of pH and particle size. *Chem. Mater.* **26**, 5725–5734 (2014).
125. Limo, M. J., Ramasamy, R. & Perry, C. C. ZnO binding peptides: Smart versatile tools for controlled modification of ZnO growth mechanism and morphology. *Chem. Mater.* **27**, 1950–1960 (2015).
126. Liang, M. K., Limo, M. J., Sola-Rabada, A., Roe, M. J. & Perry, C. C. New insights into the mechanism of zno formation from aqueous solutions of zinc acetate and zinc nitrate. *Chem. Mater.* **26**, 4119–4129 (2014).
127. Sola-Rabada, A., Liang, M. K., Roe, M. J. & Perry, C. C. Peptide-directed crystal growth modification in the formation of ZnO. *J. Mater. Chem. B* **3**, 3777–3788 (2015).
128. Lambert, J. F. Adsorption and polymerization of amino acids on mineral surfaces: A review. *Orig. Life Evol. Biosph.* **38**, 211–242 (2008).
129. Rimola, A., Costa, D., Sodupe, M., Lambert, J. F. & Ugliengo, P. Silica surface features and their role in the adsorption of biomolecules: Computational modeling and experiments. *Chem. Rev.* **113**, 4216–4313 (2013).
130. Heinz, H. & Ramezani-Dakhel, H. Simulations of inorganic–bioorganic interfaces to discover new materials: insights, comparisons to experiment, challenges, and opportunities. *Chem. Soc. Rev.* **45**, 412–448 (2016).
131. Costa, D., Garrain, P. A. & Baaden, M. Understanding small biomolecule-biomaterial interactions: A review of fundamental theoretical and experimental approaches for biomolecule interactions with inorganic surfaces. *J. Biomed. Mater. Res. - Part A* **101 A**, 1210–1222 (2013).
132. Limo, M. J. *et al.* Interactions between Metal Oxides and Biomolecules: from Fundamental Understanding to Applications. *Chem. Rev.* **118**, 11118–11193 (2018).
133. Tang, F., Li, L. & Chen, D. Mesoporous silica nanoparticles: Synthesis, biocompatibility and drug delivery. *Adv. Mater.* **24**, 1504–1534 (2012).
134. Altintoprak, K. *et al.* Peptide-equipped tobacco mosaic virus templates for selective and controllable biomineral deposition. *Beilstein J. Nanotechnol.* **6**, 1399–1412 (2015).
135. Jin, C., Han, L. & Che, S. Synthesis of a DNA-silica complex with rare two-dimensional square p4mm symmetry. *Angew. Chemie - Int. Ed.* **48**, 9268–9272 (2009).

## References

136. Luckarift, H. R., Johnson, G. R. & Spain, J. C. Silica-immobilized enzyme reactors; application to cholinesterase-inhibition studies. *J. Chromatogr. B Anal. Technol. Biomed. Life Sci.* **843**, 310–316 (2006).
137. Bazylnski, D. A. *et al.* Controlled biomineralization of magnetite (Fe<sub>3</sub>O<sub>4</sub>) and greigite (Fe<sub>3</sub>S<sub>4</sub>) in a magnetotactic bacterium. *Appl. Environ. Microbiol.* **61**, 3232–3239 (1995).
138. Yan, L. *et al.* Magnetotactic bacteria, magnetosomes and their application. *Microbiol. Res.* **167**, 507–519 (2012).
139. Arakaki, A., Yamagishi, A., Fukuyo, A., Tanaka, M. & Matsunaga, T. Co-ordinated functions of Mms proteins define the surface structure of cubo-octahedral magnetite crystals in magnetotactic bacteria. *Mol. Microbiol.* **93**, 554–567 (2014).
140. Addadi, L., Joester, D., Nudelman, F. & Weiner, S. Mollusk shell formation: A source of new concepts for understanding biomineralization processes. *Chem. - A Eur. J.* **12**, 980–987 (2006).
141. Hanes, J. & Pluckthun, A. In vitro selection and evolution of functional proteins by using ribosome display. *Proc. Natl. Acad. Sci.* **94**, 4937–4942 (1997).
142. Pacardo, D. B., Sethi, M., Jones, S. E., Naik, R. R. & Knecht, M. R. Biomimetic synthesis of pd nanocatalysts for the stille coupling reaction. *ACS Nano* **3**, 1288–1296 (2009).
143. Chan, P., Phan, T., Kao, M. C., Dolan, C. & Tok, J. B. H. Generating short peptidic ligands for silver nanowires from phage display random libraries. *Bioorganic Med. Chem. Lett.* **16**, 5261–5264 (2006).
144. Currie, H. A., Deschaume, O., Naik, R. R., Perry, C. C. & Kaplan, D. L. Genetically engineered chimeric silk-silver binding proteins. *Adv. Funct. Mater.* **21**, 2889–2895 (2011).
145. Chen, H., Su, X., Neoh, K. G. & Choe, W. S. QCM-D analysis of binding mechanism of phage particles displaying a constrained heptapeptide with specific affinity to SiO<sub>2</sub> and TiO<sub>2</sub>. *Anal. Chem.* **78**, 4872–4879 (2006).
146. Thai, C. K. *et al.* Identification and characterization of Cu<sub>2</sub>O- and ZnO-binding polypeptides by escherichia coli cell surface display: Toward an understanding of metal oxide binding. *Biotechnol. Bioeng.* **87**, 129–137 (2004).
147. Umetsu, M. *et al.* Bioassisted room-temperature immobilization and mineralization of zinc oxide - The structural ordering of ZnO nanoparticles into a flower-type morphology. *Adv. Mater.* **17**, 2571–2575 (2005).
148. Sultan, A. M. *et al.* Aqueous Peptide-TiO<sub>2</sub> Interfaces: Isoenergetic Binding via Either Entropically or Enthalpically Driven Mechanisms. *ACS Appl. Mater. Interfaces* **8**, 18620–18630 (2016).
149. Brown, S. Engineered iron oxide-adhesion mutants of the Escherichia coli phage lambda receptor. *Proc. Natl. Acad. Sci.* **89**, 8651–8655 (1992).
150. Lower, B. H. *et al.* In vitro evolution of a peptide with a hematite binding motif that may constitute a natural metal-oxide binding archetype. *Environ. Sci. Technol.* **42**, 3821–3827 (2008).

## References

151. Nam, Y. S. *et al.* Biologically templated photocatalytic nanostructures for sustained light-driven water oxidation. *Nat. Nanotechnol.* **5**, 340–344 (2010).
152. Zuo, R., Örneke, D. & Wood, T. K. Aluminum- and mild steel-binding peptides from phage display. *Appl. Microbiol. Biotechnol.* **68**, 505–509 (2005).
153. Naik, R. R. *et al.* Peptide Templates for Nanoparticle Synthesis Derived from Polymerase Chain Reaction-Driven Phage Display. *Adv. Funct. Mater.* **14**, 25–30 (2004).
154. Roy, M. D., Stanley, S. K., Amis, E. J. & Becker, M. L. Identification of a highly specific hydroxyapatite-binding peptide using phage display. *Adv. Mater.* **20**, 1830–1836 (2008).
155. Chung, W. J., Kwon, K. Y., Song, J. & Lee, S. W. Evolutionary screening of collagen-like peptides that nucleate hydroxyapatite crystals. *Langmuir* **27**, 7620–7628 (2011).
156. Flynn, C. E. *et al.* Synthesis and organization of nanoscale II–VI semiconductor materials using evolved peptide specificity and viral capsid assembly. *J. Mater. Chem.* **13**, 2414–2421 (2003).
157. Kase, D. *et al.* Affinity selection of peptide phage libraries against single-wall carbon nanohorns identifies a peptide aptamer with conformational variability. *Langmuir* **20**, 8939–8941 (2004).
158. Pender, M. J., Sowards, L. A., Hartgerink, J. D., Stone, M. O. & Naik, R. R. Peptide-mediated formation of single-wall carbon nanotube composites. *Nano Lett.* **6**, 40–44 (2006).
159. Serizawa, T., Sawada, T. & Matsuno, H. Highly specific affinities of short peptides against synthetic polymers. *Langmuir* **23**, 11127–11133 (2007).
160. Matsuno, H., Sekine, J., Yajima, H. & Serizawa, T. Biological selection of peptides for poly(L-lactide) substrates. *Langmuir* **24**, 6399–6403 (2008).
161. Nel, A. E. *et al.* Understanding biophysicochemical interactions at the nano-bio interface. *Nature Materials* (2009). doi:10.1038/nmat2442
162. Zhang, Y. *et al.* Tuning the autophagy-inducing activity of lanthanide-based nanocrystals through specific surface-coating peptides. *Nat. Mater.* (2012). doi:10.1038/nmat3363
163. Adigun, O. O. O. *et al.* BSMV as a Biotemplate for Palladium Nanomaterial Synthesis. *Langmuir* **33**, 1716–1724 (2017).
164. Tao, F. & Bernasek, S. L. L. Self-Assembled Monolayers. in *Comprehensive Nanoscience and Technology* (2010). doi:10.1016/B978-0-12-374396-1.00050-7
165. Wei, Y. & Latour, R. A. Determination of the adsorption free energy for peptide-surface interactions by SPR spectroscopy. *Langmuir* **24**, 6721–6729 (2008).
166. Wink, T., Van Zuilen, S. J. J., Bult, A. & Van Bennekom, W. P. P. Self-assembled monolayers for biosensors. *Analyst* (1997). doi:10.1039/a606964i
167. Hnilova, M. *et al.* Peptide-directed co-assembly of nanoprobe on multimaterial patterned solid surfaces. *Soft Matter* **8**, 4327 (2012).

## References

168. Kacar, T. *et al.* Quartz binding peptides as molecular linkers towards fabricating multifunctional micropatterned substrates. *Adv. Mater.* **21**, 295–299 (2009).
169. Niemeyer, C. M. Nanoparticles, Proteins, and Nucleic Acids: Biotechnology Meets Materials Science. *Angew. Chemie Int. Ed.* **40**, 4128–4158 (2001).
170. Kim, J., Grate, J. W. & Wang, P. Nanobiocatalysis and its potential applications. *Trends Biotechnol.* **26**, 639–646 (2008).
171. Puri, M., Barrow, C. J. & Verma, M. L. Enzyme immobilization on nanomaterials for biofuel production. *Trends in Biotechnology* **31**, 215–216 (2013).
172. Mateo, C., Palomo, J. M., Fernandez-Lorente, G., Guisan, J. M. & Fernandez-Lafuente, R. Improvement of enzyme activity, stability and selectivity via immobilization techniques. *Enzyme and Microbial Technology* **40**, 1451–1463 (2007).
173. Yang, M. *et al.* Site-specific immobilization of gold binding polypeptide on gold nanoparticle-coated graphene sheet for biosensor application. *Nanoscale* **3**, 2950 (2011).
174. Care, A., Nevalainen, H., Bergquist, P. L. & Sunna, A. Effect of *Trichoderma reesei* Proteinases on the Affinity of an Inorganic-Binding Peptide. *Appl. Biochem. Biotechnol.* **173**, 2225–2240 (2014).
175. Hattori, T. *et al.* A high-affinity gold-binding camel antibody: Antibody engineering for one-pot functionalization of gold nanoparticles as biointerface molecules. *Bioconjug. Chem.* **23**, 1934–1944 (2012).
176. de Juan-Franco, E., Caruz, A., Pedrajas, J. R. & Lechuga, L. M. Site-directed antibody immobilization using a protein A–gold binding domain fusion protein for enhanced SPR immunosensing. *Analyst* **138**, 2023 (2013).
177. Sunna, A., Chi, F. & Bergquist, P. L. A linker peptide with high affinity towards silica-containing materials. *N. Biotechnol.* **30**, 485–492 (2013).
178. Cho, N.-H. *et al.* A multifunctional core–shell nanoparticle for dendritic cell-based cancer immunotherapy. *Nat. Nanotechnol.* **6**, 675–682 (2011).
179. Seker, U. O. S., Sharma, V. K., Akhavan, S. & Demir, H. V. Engineered peptides for nanohybrid assemblies. *Langmuir* **30**, 2137–2143 (2014).
180. Nochomovitz, R., Amit, M., Matmor, M. & Ashkenasy, N. Bioassisted multi-nanoparticle patterning using single-layer peptide templates. *Nanotechnology* **21**, 145305 (2010).
181. Cui, Y. *et al.* Chemical functionalization of graphene enabled by phage displayed peptides. *Nano Lett.* **10**, 4559–4565 (2010).
182. Park, T. J., Zheng, S., Kang, Y. J. & Lee, S. Y. Development of a whole-cell biosensor by cell surface display of a gold-binding polypeptide on the gold surface. *FEMS Microbiol. Lett.* **293**, 141–7 (2009).
183. Huang, Y. *et al.* Programmable assembly of nanoarchitectures using genetically engineered viruses. *Nano Lett.* **5**, 1429–1434 (2005).
184. Slocik, J. M., Stone, M. O. & Naik, R. R. Synthesis of gold nanoparticles using multifunctional peptides. *Small* **1**, 1048–1052 (2005).

## References

185. Naik, R. R., Stringer, S. J., Agarwal, G., Jones, S. E. & Stone, M. O. Biomimetic synthesis and patterning of silver nanoparticles. *Nat. Mater.* **1**, 169–172 (2002).
186. Kim, J. *et al.* Peptide-mediated shape-and size-tunable synthesis of gold nanostructures. *Acta Biomater.* **6**, 2681–2689 (2010).
187. Liu, Y., Mao, J., Zhou, B., Wei, W. & Gong, S. Peptide aptamers against titanium-based implants identified through phage display. *J. Mater. Sci. Mater. Med.* **21**, 1103–1107 (2010).
188. Inoue, I. *et al.* Biological Construction of Single-Walled Carbon Nanotube Electron Transfer Pathways in Dye-Sensitized Solar Cells. *ChemSusChem* **7**, 2805–2810 (2014).
189. Tamerler, C., Kacar, T., Sahin, D., Fong, H. & Sarikaya, M. Genetically engineered polypeptides for inorganics: A utility in biological materials science and engineering. *Mater. Sci. Eng. C* **27**, 558–564 (2007).
190. Löbmann, P. Transparent Conducting Oxides. in *Chemical Solution Deposition of Functional Oxide Thin Films* **9783211993**, 655–672 (Springer Vienna, 2013).
191. He, R. & Tsuzuki, T. Low-temperature solvothermal synthesis of ZnO quantum dots. *J. Am. Ceram. Soc.* (2010). doi:10.1111/j.1551-2916.2010.03746.x
192. Care, A., Chi, F., Bergquist, P. L. & Sunna, A. Biofunctionalization of silica-coated magnetic particles mediated by a peptide. *J. Nanoparticle Res.* **16**, 2543 (2014).
193. Wu, C.-H., Liu, I.-J., Lu, R.-M. & Wu, H.-C. Advancement and applications of peptide phage display technology in biomedical science. *J. Biomed. Sci.* **23**, 8 (2016).
194. He, B. *et al.* Epitope Mapping of Metuximab on CD147 Using Phage Display and Molecular Docking. *Comput. Math. Methods Med.* **2013**, 1–6 (2013).
195. Larimer, B. M. & Deutscher, S. L. Development of a peptide by phage display for SPECT imaging of resistance-susceptible breast cancer. *Am. J. Nucl. Med. Mol. Imaging* **4**, 435–447 (2014).
196. Stewart, L. D., Foddai, A., Elliott, C. T. & Grant, I. R. Development of a novel phage-mediated immunoassay for the rapid detection of viable *Mycobacterium avium* subsp. paratuberculosis. *J. Appl. Microbiol.* **115**, 808–817 (2013).
197. Vodnik, M., Molek, P., Štrukelj, B. & Lunder, M. Peptides binding to the hunger hormone ghrelin. *Horm. Metab. Res.* **45**, 372–377 (2013).
198. Yang, M. *et al.* Phage-display library biopanning and bioinformatic analysis yielded a high-affinity peptide to inflamed vascular endothelium both in vitro and in vivo. *J. Control. Release* **174**, 72–80 (2014).
199. Bachler, B. C. *et al.* Novel Biopanning Strategy To Identify Epitopes Associated with Vaccine Protection. *J. Virol.* **87**, 4403–4416 (2013).
200. Bedford, R. *et al.* Alternative reagents to antibodies in imaging applications. *Biophys. Rev.* **9**, 299–308 (2017).
201. Hammers, Christoph, M. & Stanley, J. R. Antibody Phage Display: Technique and Applications. *J Invest Dermatol.* (2014).

## References

- doi:10.1038/jid.2013.521.Antibody
202. Sambrook, J., Fritsch, E. F. & Maniatis, T. Molecular Cloning: A Laboratory Manual. in *Cold Spring Harbor Laboratory Press* 931–957 (1989). doi:10.1096/fj.201600781R
  203. Sigma Aldrich. Introduction to Blue – white screening. *Molecular Biology Handbook* 1–7 (2017). Available at: <http://www.sigmaaldrich.com>. (Accessed: 4th December 2017)
  204. Becker, D. M. & Lundblad, V. Introduction of DNA into Yeast Cells. in *Current Protocols in Molecular Biology* 336 (John Wiley & Sons, Inc., 2001). doi:10.1002/0471142727.mb1307s27
  205. Matlock, B. *Assessment of Nucleic Acid Purity. Technical Note 52646* (2012).
  206. Desjardins, P. & Conklin, D. NanoDrop Microvolume Quantitation of Nucleic Acids. *J. Vis. Exp.* 1–4 (2010). doi:10.3791/2565
  207. Wallis, Y. & Morrell, N. Automated DNA Sequencing. in *Methods in molecular biology (Clifton, N.J.)* **688**, 173–185 (2011).
  208. Slatko, B. & Kieleczawa, J. “First Generation” Automated DNA Sequencing Technology. *Curr. Protoc. Mol. Biol.* **Chapter 7**, 1–7 (2011).
  209. Shendure, J., Mitra, R. D., Varma, C. & Church, G. M. Advanced sequencing technologies: methods and goals. *Nat. Rev. Genet.* **5**, 335–344 (2004).
  210. Applied Biosystems. *Chemistry Guide DNA Sequencing by Capillary Electrophoresis Applied Biosystems Chemistry Guide | Second Edition.* **2**, (2017).
  211. INNOVAGEN. Peptide calculator. 1 (2014). Available at: <http://pepcalc.com/>. (Accessed: 8th December 2017)
  212. Bachem. Bachem - Peptide Calculator. *Bachem* (2017). Available at: <http://www.bachem.com/service-support/peptide-calculator/>. (Accessed: 8th December 2017)
  213. Yachdav, G. *et al.* MSAViewer: interactive JavaScript visualization of multiple sequence alignments. *Bioinformatics* **32**, btw474 (2016).
  214. in-silico.net. Sequence conversion. (2016). Available at: [http://in-silico.net/tools/biology/sequence\\_conversion](http://in-silico.net/tools/biology/sequence_conversion). (Accessed: 5th December 2017)
  215. He, B. *et al.* Biopanning data bank 2018: hugging next generation phage display. *Database* **2018**, 1–8 (2018).
  216. Huang, J. *et al.* MimoDB 2.0: a mimotope database and beyond. *Nucleic Acids Res.* **40**, D271–D277 (2012).
  217. He, B. *et al.* BDB: Biopanning data bank. *Nucleic Acids Res.* **44**, D1127–D1132 (2016).
  218. McGinnis, S. & Madden, T. L. BLAST: at the core of a powerful and diverse set of sequence analysis tools. *Nucleic Acids Res.* **32**, W20–W25 (2004).
  219. RU, B. *et al.* PhD7FASTER: PREDICTING CLONES PROPAGATING FASTER FROM THE Ph.D.-7 PHAGE DISPLAY PEPTIDE LIBRARY. *J. Bioinform.*



## References

- Comput. Biol.* **12**, 1450005 (2014).
220. Adey, N. B., Mataragnon, A. H., Rider, J. E., Carter, J. M. M. & Kay, B. K. Characterization of phage that bind plastic from phage-displayed random peptide libraries. *Gene* **156**, 27–31 (1995).
221. Gebhardt, K., Lauvrak, V., Babaie, E., Eijsink, V. & Lindqvist, B. H. Adhesive peptides selected by phage display: characterization, applications and similarities with fibrinogen. *Pept. Res.* **9**, 269–278 (1996).
222. Caparon, M. H., De Ciechi, P. A., Devine, C. S., Olins, P. O. & Lee, S. C. Analysis of novel streptavidin-binding peptides, identified using a phage display library, shows that amino acids external to a perfectly conserved consensus sequence and to the presented peptides contribute to binding. *Mol. Divers.* **1**, 241–246 (1996).
223. Anni, H., Nikolaeva, O. & Israel, Y. Selection of phage-display library peptides recognizing ethanol targets on proteins. *Alcohol* **25**, 201–209 (2001).
224. Hoffman, J. A. *et al.* Progressive vascular changes in a transgenic mouse model of squamous cell carcinoma. *Cancer Cell* **4**, 383–391 (2003).
225. Sakiyama, T., Ueno, S., Imamura, K. & Nakanishi, K. Use of a novel affinity tag selected with a bacterial random peptide library for improving activity retention of glutathione S-transferase adsorbed on a polystyrene surface. *J. Mol. Catal. B Enzym.* **28**, 207–214 (2004).
226. Menendez, A. & Scott, J. K. The nature of target-unrelated peptides recovered in the screening of phage-displayed random peptide libraries with antibodies. *Anal. Biochem.* **336**, 145–157 (2005).
227. Kenan, D. J. *et al.* Peptide-PEG Amphiphiles as Cytophobic Coatings for Mammalian and Bacterial Cells. *Chem. Biol.* **13**, 695–700 (2006).
228. Kumada, Y. *et al.* Screening and characterization of affinity peptide tags specific to polystyrene supports for the orientated immobilization of proteins. *Biotechnol. Prog.* **22**, 401–405 (2006).
229. Serizawa, T., Techawanitchai, P. & Matsuno, H. Isolation of peptides that can recognize syndiotactic polystyrene. *ChemBioChem* **8**, 989–993 (2007).
230. Feng, B. *et al.* A novel affinity ligand for polystyrene surface from a phage display random library and its application in anti-HIV-1 ELISA system. *Biologicals* **37**, 48–54 (2009).
231. Vodnik, M., Štrukelj, B. & Lunder, M. HWGMWSY, an unanticipated polystyrene binding peptide from random phage display libraries. *Anal. Biochem.* **424**, 83–86 (2012).
232. Bakhshinejad, B. & Sadeghizadeh, M. A polystyrene binding target-unrelated peptide isolated in the screening of phage display library. *Anal. Biochem.* **512**, 120–128 (2016).
233. Qiang, X. *et al.* Discovery of a polystyrene binding peptide isolated from phage display library and its application in peptide immobilization. *Sci. Rep.* **7**, 2673 (2017).
234. Roach, P., Farrar, D. & Perry, C. C. Interpretation of protein adsorption: Surface-

## References

- induced conformational changes. *J. Am. Chem. Soc.* **127**, 8168–8173 (2005).
235. Merrifield, R. B. Solid Phase Peptide Synthesis. I. The Synthesis of a Tetrapeptide. *J. Am. Chem. Soc.* **85**, 2149–2154 (1963).
236. Amblard, M., Fehrentz, J.-A., Martinez, J. & Subra, G. Methods and Protocols of Modern Solid Phase Peptide Synthesis. *Mol. Biotechnol.* **33**, 239–254 (2006).
237. Sigma Aldrich. *Solid Phase Synthesis. technical documents* (2017).
238. Mäde, V., Els-Heindl, S. & Beck-Sickinger, A. G. Automated solid-phase peptide synthesis to obtain therapeutic peptides. *Beilstein J. Org. Chem.* **10**, 1197–1212 (2014).
239. Stawikowski, M. & Fields, G. B. Introduction to peptide synthesis. *Curr. Protoc. Protein Sci.* **1**, 1–18 (2012).
240. Jensen, K. J. *Solid-Phase Peptide Synthesis: An Introduction. Peptide Synthesis and Applications* 1–21 (2013). doi:10.1007/978-1-62703-544-6\_1
241. Behrendt, R., White, P. & Offer, J. Advances in Fmoc solid-phase peptide synthesis. *J. Pept. Sci.* **22**, 4–27 (2016).
242. Schnölzer, M., Alewood, P., Jones, A., Alewood, D. & Kent, S. B. H. In situ neutralization in boc-chemistry solid phase peptide synthesis: Rapid, high yield assembly of difficult sequences. *Int. J. Pept. Res. Ther.* **13**, 31–44 (2007).
243. Palomo, J. M. Solid-phase peptide synthesis: an overview focused on the preparation of biologically relevant peptides. *RSC Adv.* **4**, 32658–32672 (2014).
244. Pedersen, S. L., Tofteng, A. P., Malik, L. & Jensen, K. J. Microwave heating in solid-phase peptide synthesis. *Chem. Soc. Rev.* **41**, 1826–1844 (2012).
245. Mccarthy, P. Principles and practice of chromatography. *Complement. Ther. Med.* **1**, 108–109 (1993).
246. Ettre, L. S. & Sakodynskii, K. I. M.S. Tswett and the discovery of chromatography. I: Early work (1899-1903). *Chromatographia* **35**, 223–231 (1993).
247. Berezkin, V. G. M.S. Tswett's intellectual heritage and modern chromatography. *J. Anal. Chem.* **56**, 587–592 (2001).
248. Snyder, L. R., Kirkland, J. J. & Dolan, J. W. Introduction to modern liquid chromatography. *Mater. Technol.* **1**, 1–881 (1979).
249. Ardrey, R. E. Liquid Chromatography. in *Liquid Chromatography – Mass Spectrometry: An Introduction* (ed. Dartford, Kent, U.) **1**, 7–31 (John Wiley & Sons, Ltd, 2003).
250. Hamilton, R. J. & Sewell, P. A. Introduction to high performance liquid chromatography. in *Introduction to high performance liquid chromatography* (eds. Hamilton, R. J. & Sewell, P. A.) 1–12 (Springer Netherlands, 1982). doi:10.1007/978-94-009-5938-5\_1
251. Mitulovic, G. & Mechtler, K. HPLC techniques for proteomics analysis--a short overview of latest developments. *Briefings Funct. Genomics Proteomics* **5**, 249–260 (2006).

## References

252. Hoffmann, E. De & Stroobant, V. *Mass Spectrometry - Principles and Applications. Mass spectrometry reviews* **29**, (2007).
253. Fenn, J. B., Mann, M., Meng, C. K., Wong, S. F. & Whitehouse, C. M. Electrospray ionization—principles and practice. *Mass Spectrom. Rev.* **9**, 37–70 (1990).
254. Guilhaus, M. Special feature: Tutorial. Principles and instrumentation in time-of-flight mass spectrometry. Physical and instrumental concepts. *J. Mass Spectrom.* **30**, 1519–1532 (1995).
255. Ho, C. S. *et al.* Electrospray ionisation mass spectrometry: principles and clinical applications. *Clin. Biochem.* **24**, 3–12 (2003).
256. Yates, J. R., Ruse, C. I. & Nakorchevsky, A. Proteomics by Mass Spectrometry: Approaches, Advances, and Applications. *Annu. Rev. Biomed. Eng.* **11**, 49–79 (2009).
257. Aebersold, R. & Mann, M. Mass spectrometry-based proteomics. *Nature* **422**, 198–207 (2003).
258. Bucknall, M., Fung, K. Y. C. & Duncan, M. W. Practical quantitative biomedical applications of MALDI-TOF mass spectrometry. *J. Am. Soc. Mass Spectrom.* **13**, 1015–1027 (2002).
259. Lay, J. O. MALDI-TOF mass spectrometry of bacteria. *Mass Spectrom. Rev.* **20**, 172–194 (2001).
260. Seng, P. *et al.* MALDI-TOF-mass spectrometry applications in clinical microbiology. *Future Microbiol.* **5**, 1733–1754 (2010).
261. Fenselau, C. Peer Reviewed: MALDI MS and Strategies for Protein Analysis. *Anal. Chem.* **69**, 661A–665A (1997).
262. Karas, M., Bachmann, D. & Hillenkamp, F. Influence of the Wavelength in High-Irradiance Ultraviolet Laser Desorption Mass Spectrometry of Organic Molecules. *Anal. Chem.* **57**, 2935–2939 (1985).
263. Jurinke, C., Oeth, P. & van den Boom, D. MALDI-TOF Mass Spectrometry: A Versatile Tool for High-Performance DNA Analysis. *Mol. Biotechnol.* **26**, 147–164 (2004).
264. Melville, J., Cooper, R. & Mortensen, D. Matrix-Assisted Laser Desorption/Ionization (MALDI). *Instrum. Methods Anal. Chem.* 1–16 (2014).
265. Karas, M. & Krüger, R. Ion formation in MALDI: The cluster ionization mechanism. *Chem. Rev.* **103**, 427–439 (2003).
266. Lakowicz, J. R. *Principles of Fluorescence Spectroscopy. Principles of fluorescence spectroscopy, Springer, New York, USA, 3rd edn, 2006.* (Springer US, 2006). doi:10.1007/978-0-387-46312-4
267. JABŁOŃSKI, A. Efficiency of Anti-Stokes Fluorescence in Dyes. *Nature* **131**, 839–840 (1933).
268. Held, P. B. I. Fluorimetric Quantitation of Protein using the Reactive Compound Fluorescamine. *Nat. Methods/ Appl. Notes* **1**, 1–5 (2006).

## References

269. Udenfriend, S. *et al.* Fluorescamine: A reagent for assay of amino acids, peptides, proteins, and primary amines in the picomole range. *Science* (80-. ). (1972). doi:10.1126/science.178.4063.871
270. Nakamura, H. & Tamura, Z. Fluorometric determination of secondary amines based on their reaction with fluorescamine. *Anal. Chem.* **52**, 2087–2092 (1980).
271. Held, P. Fluorimetric Quantitation of Protein using the Reactive Compound Fluorescamine. *Nat. Methods / Appl. Notes* **1**, 1–5 (2006).
272. Nakamura, H. & Pisano, J. J. Sensitive fluorometric assay for proteins: Use of fluorescamine and membrane filters. *Arch. Biochem. Biophys.* **172**, 102–105 (1976).
273. Ashby, J., Duan, Y., Ligans, E., Tamsi, M. & Zhong, W. High-throughput profiling of nanoparticle-protein interactions by fluorescamine labeling. *Anal. Chem.* **87**, 2213–2219 (2015).
274. Zhu, G., Zhu, X., Fan, Q. & Wan, X. Raman spectra of amino acids and their aqueous solutions. *Spectrochim. Acta - Part A Mol. Biomol. Spectrosc.* **78**, 1187–1195 (2011).
275. Rygula, A. *et al.* Raman spectroscopy of proteins: A review. *J. Raman Spectrosc.* **44**, 1061–1076 (2013).
276. Lefèvre, T., Boudreault, S., Cloutier, C. & Pézolet, M. Diversity of molecular transformations involved in the formation of spider silks. *J. Mol. Biol.* **405**, 238–253 (2011).
277. Jenkins, A. L., Larsen, R. A. & Williams, T. B. Characterization of amino acids using Raman spectroscopy. *Spectrochim. Acta - Part A Mol. Biomol. Spectrosc.* **61**, 1585–1594 (2005).
278. David, C. HORIBA webinar proteins; Raman Spectroscopy for proteins. *Raman Spectroscopy* 1–53 (2012). Available at: [http://www.horiba.com/fileadmin/uploads/Scientific/Documents/Raman/HORIBA\\_webinar\\_proteins.pdf](http://www.horiba.com/fileadmin/uploads/Scientific/Documents/Raman/HORIBA_webinar_proteins.pdf). (Accessed: 17th December 2015)
279. Raza, G. *Principle & Applications of Transmission Electron Microscopy (TEM) & High Resolution TEM.* (2016).
280. Flannigan, D. J. & Zewail, A. H. 4D electron microscopy: Principles and applications. *Acc. Chem. Res.* (2012). doi:10.1021/ar3001684
281. Cao, B., Xu, H. & Mao, C. Transmission electron microscopy as a tool to image bioinorganic nanohybrids: The case of phage-gold nanocomposites. *Microsc. Res. Tech.* **74**, 627–635 (2011).
282. Atomic world. Basic principle of transmission electron microscopy. 1–6 (2000). Available at: [http://www.hk-phy.org/atomic\\_world/tem/tem02\\_e.html](http://www.hk-phy.org/atomic_world/tem/tem02_e.html). (Accessed: 8th December 2017)
283. Belton, D. J., Deschaume, O. & Perry, C. C. An overview of the fundamentals of the chemistry of silica with relevance to biosilicification and technological advances. *FEBS J.* **279**, 1710–1720 (2012).
284. Liberman, A., Mendez, N., Trogler, W. C. & Kummel, A. C. Synthesis and surface functionalization of silica nanoparticles for nanomedicine. *Surf. Sci. Rep.* **69**, 132–

## References

- 158 (2014).
285. Bitar, A., Ahmad, N. M., Fessi, H. & Elaissari, A. Silica-based nanoparticles for biomedical applications. *Drug Discov. Today* **17**, 1147–1154 (2012).
286. Tang, L. & Cheng, J. Nonporous silica nanoparticles for nanomedicine application. *Nano Today* **8**, 290–312 (2013).
287. Kim, I. Y., Joachim, E., Choi, H. & Kim, K. Toxicity of silica nanoparticles depends on size, dose, and cell type. *Nanomedicine Nanotechnology, Biol. Med.* **11**, 1407–1416 (2015).
288. Barnes, C. A. *et al.* Reproducible cornet assay of amorphous silica nanoparticles detects no genotoxicity. *Nano Lett.* **8**, 3069–3074 (2008).
289. Rancan, F. *et al.* Skin penetration and cellular uptake of amorphous silica nanoparticles with variable size, surface functionalization, and colloidal stability. *ACS Nano* **6**, 6829–6842 (2012).
290. Zhang, H. *et al.* Processing pathway dependence of amorphous silica nanoparticle toxicity: Colloidal vs pyrolytic. *J. Am. Chem. Soc.* **134**, 15790–15804 (2012).
291. Yu, K. O. *et al.* Toxicity of amorphous silica nanoparticles in mouse keratinocytes. *J. Nanoparticle Res.* **11**, 15–24 (2009).
292. Napierska, D. *et al.* Size-Dependent Cytotoxicity of Monodisperse Silica Nanoparticles in Human Endothelial Cells. *Small* **5**, 846–853 (2009).
293. Lin, W., Huang, Y., Zhou, X.-D. & Ma, Y. In vitro toxicity of silica nanoparticles in human lung cancer cells. *Toxicol. Appl. Pharmacol.* **217**, 252–259 (2006).
294. Chang, J. S., Chang, K. L. B., Hwang, D. F. & Kong, Z. L. In vitro cytotoxicity of silica nanoparticles at high concentrations strongly depends on the metabolic activity type of the cell line. *Environ. Sci. Technol.* **41**, 2064–2068 (2007).
295. An, Y., Chen, M., Xue, Q. & Liu, W. Preparation and self-assembly of carboxylic acid-functionalized silica. *J. Colloid Interface Sci.* **311**, 507–513 (2007).
296. Smith, E. A. & Chen, W. How to prevent the loss of surface functionality derived from aminosilanes. *Langmuir* **24**, 12405–12409 (2008).
297. Luechinger, M., Prins, R. & Pirngruber, G. D. Functionalization of silica surfaces with mixtures of 3-aminopropyl and methyl groups. *Microporous Mesoporous Mater.* **85**, 111–118 (2005).
298. Wu, Z., Xiang, H., Kim, T., Chun, M.-S. & Lee, K. Surface properties of submicrometer silica spheres modified with aminopropyltriethoxysilane and phenyltriethoxysilane. *J. Colloid Interface Sci.* **304**, 119–124 (2006).
299. Yang, P., Gai, S. & Lin, J. Functionalized mesoporous silica materials for controlled drug delivery. *Chem. Soc. Rev.* **41**, 3679 (2012).
300. Bringley, J. F. *et al.* Silica nanoparticles encapsulating near-infrared emissive cyanine dyes. *J. Colloid Interface Sci.* (2008). doi:10.1016/j.jcis.2007.09.006
301. Knopp, D., Tang, D. & Niessner, R. Review: Bioanalytical applications of biomolecule-functionalized nanometer-sized doped silica particles. *Anal. Chim. Acta* **647**, 14–30 (2009).

## References

302. Ha, S.-W., Camalier, C. E., Beck Jr., G. R. & Lee, J.-K. New method to prepare very stable and biocompatible fluorescent silica nanoparticles. *Chem. Commun.* 2881 (2009). doi:10.1039/b902195g
303. Johnson, A. K., Zawadzka, A. M., Deobald, L. A., Crawford, R. L. & Paszczynski, A. J. Novel method for immobilization of enzymes to magnetic nanoparticles. *J. Nanoparticle Res.* **10**, 1009–1025 (2008).
304. Wolny, P. M., Spatz, J. P. & Richter, R. P. On the adsorption behavior of biotin-binding proteins on gold and silica. *Langmuir* **26**, 1029–1034 (2010).
305. Chang, R. H.-Y., Jang, J. & Wu, K. C.-W. Cellulase immobilized mesoporous silica nanocatalysts for efficient cellulose-to-glucose conversion. *Green Chem.* **13**, 2844 (2011).
306. Cho, W., Fowler, J. D. & Furst, E. M. Targeted binding of the M13 bacteriophage to thiamethoxam organic crystals. *Langmuir* **28**, 6013–6020 (2012).
307. Royston, E., Lee, S. Y., Culver, J. N. & Harris, M. T. Characterization of silica-coated tobacco mosaic virus. *J. Colloid Interface Sci.* **298**, 706–712 (2006).
308. Abdelhamid, M. A. A. *et al.* Affinity purification of recombinant proteins using a novel silica-binding peptide as a fusion tag. *Appl. Microbiol. Biotechnol.* **98**, 5677–5684 (2014).
309. Ozaki, M. *et al.* Site-specific control of silica mineralization on DNA using a designed peptide. *Chem. Commun.* **52**, 4010–4013 (2015).
310. Shiba, K. Natural and artificial peptide motifs: their origins and the application of motif-programming. *Chem. Soc. Rev.* **39**, 117–126 (2010).
311. Ikeda, T. *et al.* The silica-binding Si-tag functions as an affinity tag even under denaturing conditions. *Protein Expr. Purif.* **77**, 173–177 (2011).
312. Gungormus, M. *et al.* Regulation of in vitro calcium phosphate mineralization by combinatorially selected hydroxyapatite-binding peptides. *Biomacromolecules* **9**, 966–973 (2008).
313. Chiu, D. *et al.* Biom mineralization and size control of stable calcium phosphate core-protein shell nanoparticles: Potential for vaccine applications. *Bioconjug. Chem.* **23**, 610–617 (2012).
314. Nam, K. T. Virus-Enabled Synthesis and Assembly of Nanowires for Lithium Ion Battery Electrodes. *Science (80-. )*. **312**, 885–888 (2006).
315. Li, Y. & Huang, Y. Morphology-controlled synthesis of platinum nanocrystals with specific peptides. *Adv. Mater.* **22**, 1921–1925 (2010).
316. Tomczak, M. M., Gupta, M. K., Drummy, L. F., Rozenzhak, S. M. & Naik, R. R. Morphological control and assembly of zinc oxide using a biotemplate. *Acta Biomater.* **5**, 876–882 (2009).
317. Estephan, E. *et al.* Peptides for functionalization of InP semiconductors. *J. Colloid Interface Sci.* **337**, 358–363 (2009).
318. Sinensky, A. K. & Belcher, A. M. Biomolecular recognition of crystal defects: A diffuse-selection approach. *Adv. Mater.* **18**, 991–996 (2006).

## References

319. Tamerler, C. & Sarikaya, M. Molecular biomimetics: Utilizing nature's molecular ways in practical engineering. *Acta Biomater.* **3**, 289–299 (2007).
320. Swaminathan, S., Bullough, M., Li, Q., Zhou, A. & Cui, Y. Non-lithographic patterning of phage-displayed peptides with wrinkled elastomers. *J. R. Soc. Interface* **11**, 20130893–20130893 (2013).
321. Müller, W. E. G. *et al.* The silicatein propeptide acts as inhibitor/modulator of self-organization during spicule axial filament formation. *FEBS J.* **280**, 1693–1708 (2013).
322. Ploss, M. *et al.* Selection of peptides binding to metallic borides by screening M13 phage display libraries. *BMC Biotechnol.* **14**, 1–14 (2014).
323. You, F. *et al.* Biopanning and characterization of peptides with Fe<sub>3</sub>O<sub>4</sub> nanoparticles-binding capability via phage display random peptide library technique. *Colloids Surfaces B Biointerfaces* **141**, 537–545 (2016).
324. Derda, R. *et al.* Diversity of phage-displayed libraries of peptides during panning and amplification. *Molecules* **16**, 1776–803 (2011).
325. T Hoen, P. A. C. *et al.* Phage display screening without repetitious selection rounds. *Anal. Biochem.* **421**, 622–631 (2012).
326. Shtatland, T., Guettler, D., Kossodo, M., Pivovarov, M. & Weissleder, R. PepBank - A database of peptides based on sequence text mining and public peptide data sources. *BMC Bioinformatics* **8**, 280 (2007).
327. Huang, J., Ru, B., Li, S., Lin, H. & Guo, F.-B. SAROTUP: Scanner and Reporter of Target-Unrelated Peptides. *J. Biomed. Biotechnol.* **2010**, 1–7 (2010).
328. Limo, M. J. Towards an Understanding of Peptide - Inorganic Interactions. (2013).
329. Bashari, O. *et al.* Discovery of peptide drug carrier candidates for targeted multi-drug delivery into prostate cancer cells. *Cancer Lett.* **408**, 164–173 (2017).
330. Christiansen, A. *et al.* High-throughput sequencing [SI] enhanced phage display enables the identification of patient-specific epitope motifs in serum. *Sci. Rep.* **5**, 1–13 (2015).
331. Yang, Y. *et al.* Identification of triosephosphate isomerase as a novel allergen in *Octopus fangsiao*. *Mol. Immunol.* **85**, 35–46 (2017).
332. Reiss, B. D. *et al.* Biological routes to metal alloy ferromagnetic nanostructures. *Nano Lett.* **4**, 1127–1132 (2004).
333. Dickerson, M. B. *et al.* Identification and design of peptides for the rapid, high-yield formation of nanoparticulate TiO<sub>2</sub> from aqueous solutions at room temperature. *Chem. Mater.* **20**, 1578–1584 (2008).
334. Zhu, Y., Ho, B. & Ding, J. L. Sequence and structural diversity in endotoxin-binding dodecapeptides. *Biochim. Biophys. Acta - Biomembr.* **1611**, 234–242 (2003).
335. Lin, H., Ma, Z., Hou, X., Chen, L. & Fan, H. Construction and immunogenicity of a recombinant swinepox virus expressing a multi-epitope peptide for porcine reproductive and respiratory syndrome virus. *Sci. Rep.* **7**, 43990 (2017).

## References

336. Warren, J. G., Kasun, G. W., Leonard, T. & Kirkpatrick, B. C. A phage display-selected peptide inhibitor of *Agrobacterium vitis* polygalacturonase. *Mol. Plant Pathol.* **17**, 480–486 (2016).
337. Burch, L., Shimizu, H., Smith, A., Patterson, C. & Hupp, T. R. Expansion of Protein Interaction Maps by Phage Peptide Display Using MDM2 as a Prototypical Conformationally Flexible Target Protein. *J. Mol. Biol.* **337**, 129–145 (2004).
338. Fan, X. *et al.* An in vivo approach to structure activity relationship analysis of peptide ligands. *Pharm. Res.* **24**, 868–879 (2007).
339. Fang, Y. *et al.* Identification of peptides capable of inducing the formation of titania but not silica via a subtractive bacteriophage display approach. *J. Mater. Chem.* **18**, 3871–3875 (2008).
340. So, C. R., Tamerler, C. & Sarikaya, M. Adsorption, diffusion, and self-assembly of an engineered goldbinding peptide on Au(111) investigated by atomic force microscopy. *Angew. Chemie - Int. Ed.* **48**, 5174–5177 (2009).
341. Lopata, A. *et al.* Affimer proteins for F-actin: novel affinity reagents that label F-actin in live and fixed cells. *Sci. Rep.* **8**, 6572 (2018).
342. Koutsoumpeli, E. *et al.* Antibody Mimetics for the Detection of Small Organic Compounds Using a Quartz Crystal Microbalance. *Anal. Chem.* **89**, 3051–3058 (2017).
343. Schlichthaerle, T. *et al.* Site-Specific Labeling of Affimers for DNA-PAINT Microscopy. *Angew. Chemie - Int. Ed.* **57**, 11060–11063 (2018).
344. Tiede, C. *et al.* Affimer proteins are versatile and renewable affinity reagents. *Elife* **6**, (2017).
345. Tiede, C. *et al.* Adhiron: a stable and versatile peptide display scaffold for molecular recognition applications. *Protein Eng. Des. Sel.* **27**, 145–155 (2014).
346. King, R. *et al.* Inhibition of complement C3 and fibrinogen interaction: a potential novel therapeutic target to reduce cardiovascular disease in diabetes. *Lancet* **385**, S57 (2015).
347. Hughes, D. J. *et al.* Affimer/Adhiron technology produces inhibitors of SUMO1-mediated or of SUMO2/3-mediated protein-protein interactions. *Sci. Signal.* (2017).
348. Kyle, H. F. *et al.* Exploration of the HIF-1 $\alpha$ /p300 interface using peptide and Adhiron phage display technologies. *Mol. Biosyst.* **11**, 2738–2749 (2015).
349. Li, W. & Caberoy, N. B. New perspective for phage display as an efficient and versatile technology of functional proteomics. *Appl. Microbiol. Biotechnol.* **85**, 909–919 (2010).
350. Kuzmicheva, G. A., Jayanna, P. K., Sorokulova, I. B. & Petrenko, V. A. Diversity and censoring of landscape phage libraries. *Protein Eng. Des. Sel.* **22**, 9–18 (2009).
351. Thomas, W. D., Golomb, M. & Smith, G. P. Corruption of phage display libraries by target-unrelated clones: Diagnosis and countermeasures. *Anal. Biochem.* **407**, 237–240 (2010).
352. Kairdolf, B. A., Mancini, M. C., Smith, A. M. & Nie, S. Minimizing nonspecific



## References

- cellular binding of quantum dots with hydroxyl-derivatized surface coatings. *Anal. Chem.* **80**, 3029–3034 (2008).
353. Hammoudeh, D. I., Follis, A. V., Prochownik, E. V. & Metallo, S. J. Multiple independent binding sites for small-molecule inhibitors on the oncoprotein c-Myc. *J. Am. Chem. Soc.* **131**, 7390–7401 (2009).
354. Noble, J. E., Knight, A. E., Reason, A. J., Di Matola, A. & Bailey, M. J. A. A comparison of protein quantitation assays for biopharmaceutical applications. *Mol. Biotechnol.* **37**, 99–111 (2007).
355. Gray, J. J. The interaction of proteins with solid surfaces. *Curr. Opin. Struct. Biol.* **14**, 110–115 (2004).
356. Vallee, A., Humblot, V. & Pradier, C.-M. Peptide interactions with metal and oxide surfaces. *Acc. Chem. Res.* **43**, 1297–1306 (2010).
357. Rabe, M., Verdes, D. & Seeger, S. Understanding protein adsorption phenomena at solid surfaces. *Adv. Colloid Interface Sci.* **162**, 87–106 (2011).
358. Wei, F., Zhang, D., Halas, N. J. & Hartgerink, J. D. Aromatic amino acids providing characteristic motifs in the raman and SERS spectroscopy of peptides. *J. Phys. Chem. B* **112**, 9158–9164 (2008).
359. Yu, H., Dong, X. Y. & Sun, Y. An alternating elution strategy for screening high affinity peptides from a phage display peptide library. *Biochem. Eng. J.* **18**, 169–175 (2004).
360. Cwirla, S. E., Peters, E. A., Barrett, R. W. & Dower, W. J. Peptides on phage: a vast library of peptides for identifying ligands. *Proc. Natl. Acad. Sci.* **87**, 6378–6382 (1990).
361. D’Mello, F. & Howard, C. R. An improved selection procedure for the screening of phage display peptide libraries. *J. Immunol. Methods* **247**, 191–203 (2001).
362. Gaskin, D. J. H., Starck, K., Turner, N. a. & Vulfson, E. N. Phage display combinatorial libraries of short peptides: ligand selection for protein purification. *Enzyme Microb. Technol.* **28**, 766–722 (2001).
363. Bruin, R. de, Spelt, K., Mol, J., Koes, R. & Quattrocchio, F. Selection of high-affinity phage antibodies from phage display libraries. *Nat. Biotechnol.* **17**, 397–399 (1999).
364. Rawlings, A. E. *et al.* Phage display selected magnetite interacting Adhirons for shape controlled nanoparticle synthesis. *Chem. Sci.* **6**, 5586–5594 (2015).
365. Shen, Y. *et al.* Generation and selection of immunized Fab phage display library against human B cell lymphoma. *Cell Res.* **17**, 650–660 (2007).
366. Keller, T. *et al.* Selection of scFv Antibody Fragments Binding to Human Blood versus Lymphatic Endothelial Surface Antigens by Direct Cell Phage Display. *PLoS One* **10**, e0127169 (2015).
367. Hoogenboom, H. R. *et al.* Selection-dominant and nonaccessible epitopes on cell-surface receptors revealed by cell-panning with a large phage antibody library. *Eur. J. Biochem.* (1999). doi:10.1046/j.1432-1327.1999.00214.x
368. Lipes, B. D. *et al.* An Entirely Cell-Based System to Generate Single-Chain

## References

- Antibodies against Cell Surface Receptors. *J. Mol. Biol.* (2008). doi:10.1016/j.jmb.2008.03.072
369. Giordano, R. J., Cardó-Vila, M., Lahdenranta, J., Pasqualini, R. & Arap, W. Biopanning and rapid analysis of selective interactive ligands. *Nat. Med.* **7**, 1249–1253 (2001).
370. Laakkonen, P., Porkka, K., Hoffman, J. A. & Ruoslahti, E. A tumor-homing peptide with a targeting specificity related to lymphatic vessels. *Nat. Med.* (2002). doi:10.1038/nm720
371. Michon, I. N. *et al.* Targeting of peptides to restenotic vascular smooth muscle cells using phage display in vitro and in vivo. *Biochim. Biophys. Acta - Mol. Cell Res.* **1591**, 87–97 (2002).
372. Liao, Chih-Wei;Gower, Laurie B; Wen, Y.-W. Electroactivated peptides and biosensors. 1–33 (2010).
373. Liao, C.-W. Inorganic Binding Peptides Designed by Phage Display Techniques for Biotechnology Applications. (University of Florida, USA, 2010).
374. Kristensen, P. & Winter, G. Proteolytic selection for protein folding using filamentous bacteriophages. *Fold. Des.* **3**, 321–328 (1998).
375. Ravn, P. *et al.* Identification of phage antibodies toward the Werner protein by selection on Western blots. *Electrophoresis* **21**, 509–516 (2000).
376. Duan, Z. & Siegmundfeldt, H. An Efficient Method for Isolating Antibody Fragments Against Small Peptides by Antibody Phage Display. *Comb. Chem. High Throughput Screen.* **13**, 818–828 (2010).
377. Hagemann, U. B. *et al.* Fully human antagonistic antibodies against CCR4 potently inhibit cell signaling and chemotaxis. *PLoS One* (2014). doi:10.1371/journal.pone.0103776
378. Meulemans, E. V., Nieland, L. J., Debie, W. H., Ramaekers, F. C. & van Eys, G. J. Phage displayed antibodies specific for a cytoskeletal antigen. Selection by competitive elution with a monoclonal antibody. *Hum. Antibodies* (1995). doi:10.3233/HAB-1995-6305
379. Meulemans, E. V, Slobbe, R., Wasterval, P., Ramaekers, F. C. & van, E. G. Selection of phage-displayed antibodies specific for a cytoskeletal antigen by competitive elution with a monoclonal antibody. *J Mol Biol* (1994). doi:10.1006/jmbi.1994.1735
380. Bassindale, A. R., Codina-Barrios, A., Frascione, N. & Taylor, P. G. An improved phage display methodology for inorganic nanoparticle fabrication. *Chem. Commun.* **12**, 2956–2958 (2007).
381. Tang, A. A. S., Tiede, C., Hughes, D. J., McPherson, M. & Tomlinson, D. C. Isolation of isoform-specific binding proteins (Affimers) by phage display using negative selection. *Sci. Signal.* (2017). doi:10.1126/scisignal.aan0868
382. Barrett, R. W. *et al.* Selective enrichment and characterization of high affinity ligands from collections of random peptides on filamentous phage. *Anal. Biochem.* **204**, 357–364 (1992).
383. Davies, J. M., O’Hehir, R. E. & Suphioglu, C. Use of phage display technology to

## References

- investigate allergen-antibody interactions. *J. Allergy Clin. Immunol.* (2000). doi:10.1067/mai.2000.107040
384. Barbas, C. F., Burton, D. R., Scott, J. K. & Silverman, G. J. *Phage Display: A Laboratory Manual. Analytical Biochemistry* (CSHL Press, 2004). doi:10.1016/j.jpuro.2007.09.001
385. NEB. Ph.D.-12<sup>TM</sup> Phage Display Peptide Library Kit. *NEB* (2002).
386. Bessette, P. H., Rice, J. J. & Daugherty, P. S. Rapid isolation of high-affinity protein binding peptides using bacterial display. *Protein Eng. Des. Sel.* **17**, 731–739 (2004).
387. Causa, F. *et al.* Evolutionary screening and adsorption behavior of engineered M13 bacteriophage and derived dodecapeptide for selective decoration of gold interfaces. *J. Colloid Interface Sci.* **389**, 220–229 (2013).
388. Seker, U. O. S., Zengin, G., Tamerler, C., Sarikaya, M. & Demir, H. V. Assembly kinetics of nanocrystals via peptide hybridization. *Langmuir* **27**, 4867–4872 (2011).
389. Seker, U. O. S., Wilson, B., Sahin, D., Tamerler, C. & Sarikaya, M. Quantitative affinity of genetically engineered repeating polypeptides to inorganic surfaces. *Biomacromolecules* **10**, 250–257 (2009).
390. Demir, H. V. *et al.* Spatially selective assembly of quantum dot light emitters in an LED using engineered peptides. *ACS Nano* **5**, 2735–2741 (2011).
391. Paul, S., Paul, D., Fern, G. R. & Ray, A. K. Surface plasmon resonance imaging detection of silver nanoparticle-tagged immunoglobulin. *J. R. Soc. Interface* **8**, 1204–11 (2011).
392. Holinga, G. J. *et al.* An SFG study of interfacial amino acids at the hydrophilic SiO<sub>2</sub> and hydrophobic deuterated polystyrene surfaces. *J. Am. Chem. Soc.* **133**, 6243–6253 (2011).
393. Phillips, D. C. *et al.* Side chain, chain length, and sequence effects on amphiphilic peptide adsorption at hydrophobic and hydrophilic surfaces studied by sum-frequency generation vibrational spectroscopy and quartz crystal microbalance. *J. Phys. Chem. C* **111**, 255–261 (2007).
394. Satriano, C. *et al.* Surface adsorption of fibronectin-derived peptide fragments: the influence of electrostatics and hydrophobicity for endothelial cells adhesion. *Soft Matter* **8**, 53 (2012).
395. Mermut, O. *et al.* In situ adsorption studies of a 14-amino acid leucine-lysine peptide onto hydrophobic polystyrene and hydrophilic silica surfaces using quartz crystal microbalance, atomic force microscopy, and sum frequency generation vibrational spectroscopy. *J. Am. Chem. Soc.* **128**, 3598–3607 (2006).
396. Shen, F., Rojas, O. J., Genzer, J., Gurgel, P. V. & Carbonell, R. G. Affinity interactions of human immunoglobulin G with short peptides: role of ligand spacer on binding, kinetics, and mass transfer. *Anal. Bioanal. Chem.* **408**, 1829–1841 (2016).
397. Bharti, B., Meissner, J. & Findenegg, G. H. Aggregation of silica nanoparticles directed by adsorption of lysozyme. *Langmuir* **27**, 9823–9833 (2011).

## References

398. Catalano, F., Alberto, G., Ivanchenko, P., Dovbeshko, G. & Martra, G. Effect of Silica Surface Properties on the Formation of Multilayer or Submonolayer Protein Hard Corona: Albumin Adsorption on Pyrolytic and Colloidal SiO<sub>2</sub> Nanoparticles. *J. Phys. Chem. C* **119**, 26493–26505 (2015).
399. Leblanc, K. & Hutchins, D. A. New applications of a biogenic silica deposition fluorophore in the study of oceanic diatoms. *Limnol. Oceanogr. Methods* **3**, 462–476 (2005).
400. Shimizu, K., Del Amo, Y., Brzezinski, M. A., Stucky, G. D. & Morse, D. E. A novel fluorescent silica tracer for biological silicification studies. *Chem. Biol.* **8**, 1051–1060 (2001).
401. Radziuk, D. & Moehwald, H. Prospects for plasmonic hot spots in single molecule SERS towards the chemical imaging of live cells. *Phys. Chem. Chem. Phys.* **17**, 21072–21093 (2015).
402. Kim, H., Kosuda, K. M., Van Duyne, R. P. & Stair, P. C. Resonance Raman and surface- and tip-enhanced Raman spectroscopy methods to study solid catalysts and heterogeneous catalytic reactions. *Chem. Soc. Rev.* **39**, 4820 (2010).
403. Rimola, A., Sodupe, M. & Ugliengo, P. Affinity scale for the interaction of amino acids with silica surfaces. *J. Phys. Chem. C* **113**, 5741–5750 (2009).
404. Naik, R., Stone, M. & Carter, D. Method of isolating binding peptides from a combinatorial phage display library and peptides produced thereby. (2006).
405. Yu, C. & Mosbach, K. Molecular Imprinting Utilizing an Amide Functional Group for Hydrogen Bonding Leading to Highly Efficient Polymers. *J. Org. Chem.* **62**, 4057–4064 (1997).
406. Sola-Rabada, A. *et al.* Interactions at the Silica-Peptide Interface: Influence of the Extent of Functionalization on the Conformational Ensemble. *Langmuir* **34**, 8255–8263 (2018).
407. Chung, W. J., Lee, D. Y. & Yoo, S. Y. Chemical modulation of m13 bacteriophage and its functional opportunities for nanomedicine. *Int. J. Nanomedicine* **9**, 5825–5836 (2014).
408. Hemminga, M. A. *et al.* Viruses: Incredible nanomachines. New advances with filamentous phages. *Eur. Biophys. J.* **39**, 541–550 (2010).
409. Rong, J. *et al.* Oriented cell growth on self-assembled bacteriophage M13 thin films. *Chem. Commun.* 5185 (2008). doi:10.1039/b811039e
410. Zhang, Z. *et al.* Charge reversal of the rodlike colloidal fd virus through surface chemical modification. *Langmuir* **26**, 10593–10599 (2010).
411. Carrico, Z. M. *et al.* N-terminal labeling of filamentous phage to create cancer marker imaging agents. *ACS Nano* **6**, 6675–6680 (2012).
412. Adhikari, M. *et al.* Functionalized viral nanoparticles as ultrasensitive reporters in lateral-flow assays. *Analyst* **138**, 5584 (2013).
413. Yacoby, I., Shamis, M., Bar, H., Shabat, D. & Benhar, I. Targeting antibacterial agents by using drug-carrying filamentous bacteriophages. *Antimicrob. Agents Chemother.* **50**, 2087–2097 (2006).

## References

414. Ng, S., Jafari, M. R., Matochko, W. L. & Derda, R. Quantitative synthesis of genetically encoded glycopeptide libraries displayed on M13 phage. *ACS Chem. Biol.* **7**, 1482–1487 (2012).
415. Helms, B. A. *et al.* High-affinity peptide-based collagen targeting using synthetic phage mimics: From phage display to dendrimer display. *J. Am. Chem. Soc.* **131**, 11683–11685 (2009).
416. Bastings, M. M. C. *et al.* From phage display to dendrimer display: Insights into multivalent binding. *J. Am. Chem. Soc.* **133**, 6636–6641 (2011).
417. Van Rooy, I., Hennink, W. E., Storm, G., Schiffelers, R. M. & Mastrobattista, E. Attaching the phage display-selected GLA peptide to liposomes: Factors influencing target binding. *Eur. J. Pharm. Sci.* **45**, 330–335 (2012).
418. Van Rooy, I. *et al.* In vivo methods to study uptake of nanoparticles into the brain. *Pharm. Res.* **28**, 456–471 (2011).
419. Wang, T., Kulkarni, N., DSouza, G. G. M., Petrenko, V. A. & Torchilin, V. P. On the mechanism of targeting of phage fusion protein-modified nanocarriers: Only the binding peptide sequence matters. *Mol. Pharm.* **8**, 1720–1728 (2011).
420. Drummy, L. F. *et al.* Bioassembled Layered Silicate-Metal Nanoparticle Hybrids. *ACS Appl. Mater. Interfaces* **2**, 1492–1498 (2010).
421. Scibilia, S. *et al.* Self-assembly of silver nanoparticles and bacteriophage. *Sens. Bio-Sensing Res.* **7**, 146–152 (2016).
422. Arap, M. A. Phage display technology - Applications and innovations. *Genet. Mol. Biol.* **28**, 1–9 (2005).
423. Zhao, F. Q. & Craig, R. Capturing time-resolved changes in molecular structure by negative staining. *J. Struct. Biol.* **141**, 43–52 (2003).
424. De Carlo, S. & Harris, J. R. Negative staining and cryo-negative staining of macromolecules and viruses for TEM. *Micron* **42**, 117–31 (2011).
425. Yazzie, M., Gamble, S. L., Civitello, E. R. & Stearns, D. M. Uranyl acetate causes DNA single strand breaks in vitro in the presence of ascorbate (vitamin C). *Chem. Res. Toxicol.* **16**, 524–530 (2003).
426. Cademartiri, R. *et al.* Immobilization of bacteriophages on modified silica particles. *Biomaterials* **31**, 1904–1910 (2010).
427. Zaman, M. S., Moon, C. H., Bozhilov, K. N. & Haberer, E. D. Phage-directed synthesis of copper sulfide: structural and optical characterization. *Nanotechnology* **24**, 325602 (2013).
428. Souza, G. R. *et al.* Networks of gold nanoparticles and bacteriophage as biological sensors and cell-targeting agents. *Proc. Natl. Acad. Sci.* **103**, 1215–1220 (2006).
429. Hutter, E. & Maysinger, D. Gold nanoparticles and quantum dots for bioimaging. *Microscopy Research and Technique* **74**, 592–604 (2011).
430. Abbineni, G., Safiejko-Mroccka, B. & Mao, C. Development of an optimized protocol for studying the interaction of filamentous bacteriophage with mammalian cells by fluorescence microscopy. *Microsc. Res. Tech.* **73**, 548–554 (2010).

## References

431. Mu, X. *et al.* An Electrochemiluminescence Immunosensor Based on Gold-Magnetic Nanoparticles and Phage Displayed Antibodies. *Sensors* **16**, 308 (2016).
432. Mikhailovskij, I. M. *et al.* Atomic structure of random grain boundaries in tungsten. *Mater. Lett.* **70**, 60–62 (2012).
433. Watanabe, H., Nakanishi, T., Umetsu, M. & Kumagai, I. Human anti-gold antibodies: Biofunctionalization of gold nanoparticles and surfaces with anti-gold antibodies. *J. Biol. Chem.* **283**, 36031–36038 (2008).
434. Kijanka, M. *et al.* A novel immuno-gold labeling protocol for nanobody-based detection of HER2 in breast cancer cells using immuno-electron microscopy. *J. Struct. Biol.* **199**, 1–11 (2017).
435. Barkhordarian, H., Emadi, S., Schulz, P. & Sierks, M. R. Isolating recombinant antibodies against specific protein morphologies using atomic force microscopy and phage display technologies. *Protein Eng. Des. Sel.* **19**, 497–502 (2006).
436. Serizawa, T., Sawada, T., Matsuno, H., Matsubara, T. & Sato, T. A Peptide Motif Recognizing a Polymer Stereoregularity. *J. Am. Chem. Soc.* **127**, 13780–13781 (2005).
437. Jaworski, J. W., Raorane, D., Huh, J. H., Majumdar, A. & Lee, S. W. Evolutionary screening of biomimetic coatings for selective detection of explosives. *Langmuir* (2008). doi:10.1021/la7035289
438. Cui, Y., Pattabiraman, A., Lisko, B., Collins, S. C. & McAlpine, M. C. Recognition of patterned molecular ink with phage displayed peptides. *J. Am. Chem. Soc.* (2010). doi:10.1021/ja9081809
439. Lundqvist, M. *et al.* Nanoparticle size and surface properties determine the protein corona with possible implications for biological impacts. *Proc. Natl. Acad. Sci.* **105**, 14265–14270 (2008).
440. Docter, D. *et al.* The nanoparticle biomolecule corona: lessons learned – challenge accepted? *Chem. Soc. Rev.* **44**, 6094–6121 (2015).
441. Flynn, C. E., Lee, S. W., Peelle, B. R. & Belcher, A. M. Viruses as vehicles for growth, organization and assembly of materials. *Acta Mater.* **51**, 5867–5880 (2003).